

Chapter 5
FUNDAMENTALS OF DESIGN

Table of Contents

	Page
VI-5-1. Introduction	VI-5-1
<i>a. Overview</i>	VI-5-1
<i>b. Wave/structure interaction</i>	VI-5-2
(1) Hydraulic response	VI-5-2
(2) Wave loadings and related structural response.....	VI-5-3
VI-5-2. Structure Hydraulic Response	VI-5-3
<i>a. Wave runup and rundown on structures</i>	VI-5-3
(1) Introduction	VI-5-3
(2) Surf similarity parameter	VI-5-5
(3) Wave runup and rundown on impermeable slopes	VI-5-7
(a) Smooth slope, irregular long-crested head-on waves	VI-5-8
(b) Rock armored slopes, irregular long-crested head-on waves	VI-5-15
(4) Wave runup and rundown on permeable slopes	VI-5-16
(a) Rock armored slopes, irregular long-crested head-on waves.....	VI-5-16
(b) Statistical distribution of runup	VI-5-18
<i>b. Wave overtopping of structures</i>	VI-5-19
(1) Admissible average overtopping discharge	VI-5-19
(2) Average overtopping discharge formulas	VI-5-21
(3) Overtopping volumes of individual waves	VI-5-31
<i>c. Wave reflection</i>	VI-5-33
(1) Introduction	VI-5-33
(2) Reflection from non-overtopped sloping structures	VI-5-33
(3) Reflection from vertical walls	VI-5-35
(4) Kinematics of reflected irregular waves	VI-5-36
<i>d. Wave transmission</i>	VI-5-43
(1) Introduction	VI-5-43
(2) Wave transmission through and over sloping structures	VI-5-44
(3) Wave transmission for vertical structures.....	VI-5-47
VI-5-3. Rubble-Mound Structure Loading and Response	VI-5-47
<i>a. Armor layer stability</i>	VI-5-47
(1) Introduction	VI-5-47
(2) Stability parameters and structure of stability formulae	VI-5-50
(3) Definition of armor layer damage.....	VI-5-55
(4) Armor layer damage progression.....	VI-5-58
(5) Practical formulae for hydraulic stability of armor layers	VI-5-61
(6) Structure head section stability	VI-5-80
(7) Riprap armor stability	VI-5-84
<i>b. Granulated filters and geotextile filter stability</i>	VI-5-84
(1) Filter layer functions.....	VI-5-84
(2) Granulated filter failure modes	VI-5-86

	Page
(3) Granulated filter design criteria	VI-5-86
(4) Granular filter construction aspects	VI-5-88
<i>c. Structural integrity of concrete armor units</i>	VI-5-88
(1) Introduction	VI-5-88
(2) Structural design formulae for dolosse and tetrapods.....	VI-5-89
(a) Stress determination.....	VI-5-90
(b) Reinforced dolos design	VI-5-90
(c) Prestressed dolos design	VI-5-96
(3) Ultimate impact velocities and equivalent drop height.....	VI-5-97
(4) Thermal stresses.....	VI-5-98
(5) Fatigue in concrete armor units	VI-5-99
<i>d. Toe stability and protection</i>	VI-5-99
(1) Introduction	VI-5-99
(2) Practical toe stability formulas for waves.....	VI-5-103
(3) Foot protection blocks	VI-5-105
(4) Toe stability in combined waves and currents.....	VI-5-111
<i>e. Design of structure cross section</i>	VI-5-112
(1) Introduction	VI-5-112
(2) Crest elevation and width	VI-5-115
(3) Concrete cap for rubble-mound structures.....	VI-5-118
(4) Thickness of armor layer and underlayers.....	VI-5-121
(5) Bottom elevation of primary cover layer.....	VI-5-122
(6) Toe berm for cover layer stability.....	VI-5-123
(7) Structure head and leeside cover layer	VI-5-123
(8) Secondary cover layer.....	VI-5-124
(9) Underlayers.....	VI-5-124
<i>f. Blanket stability in current fields</i>	VI-5-125
(1) Boundary layer shear stress	VI-5-125
(2) Incipient motion of stone blankets.....	VI-5-126
(3) Stone blanket stability design equation	VI-5-128
(4) Stone blanket gradation	VI-5-129
VI-5-4. Vertical-Front Structure Loading and Response	VI-5-129
<i>a. Wave forces on vertical walls</i>	VI-5-129
<i>b. Wave-generated forces on vertical walls and caissons</i>	VI-5-132
(1) Two-dimensional wave forces on vertical walls.....	VI-5-133
(2) Vertical wave barriers.....	VI-5-145
(3) Structure length and alignment effects on wave height	VI-5-148
(4) Horizontal wave force reduction for nonbreaking waves	VI-5-150
(5) Horizontal turning moment for nonbreaking waves	VI-4-152
(6) Horizontal wave force reduction for breaking waves.....	VI-5-153
(7) Broken wave forces	VI-5-154
<i>c. Wave-generated forces on concrete caps</i>	VI-5-156
<i>d. Stability of concrete caps and caissons against sliding and overturning</i>	VI-5-162
<i>e. Waves at structure convex and concave corners</i>	VI-5-163
(1) Waves at convex corners	VI-5-165
(a) Vertical structures with convex corners.....	VI-5-165
(b) Sloping structures with convex corners.....	VI-5-167
(2) Waves at concave corners.....	VI-5-167

	Page
(a) Vertical structures with concave corners	VI-5-167
(b) Sloping structures with concave corners	VI-5-168
<i>f. Uplift forces</i>	VI-5-168
(1) Submerged or partially submerged structure	VI-5-168
(2) Emergent structures	VI-5-170
VI-5-5. Foundation Loads	VI-5-172
<i>a. Introduction</i>	VI-5-172
<i>b. Soil and rock properties</i>	VI-5-173
(1) Grain sizes	VI-5-173
(2) Bulk density	VI-5-174
(3) Volume of voids	VI-5-174
(4) Relative density	VI-5-175
(5) Plasticity index	VI-5-175
(6) Total and effective stresses	VI-5-175
(7) Geostatic stress	VI-5-176
(8) Stresses within soil deposits	VI-5-176
(9) Stresses due to externally applied surface loads	VI-5-176
(10) Overconsolidation ratio	VI-5-177
(11) Deformation moduli	VI-5-177
(12) Damping ratio	VI-5-182
<i>c. Strength parameters</i>	VI-5-183
(1) Mohr-Coulomb failure criterion	VI-5-183
(2) Noncohesive soils	VI-5-184
(3) Dilatancy	VI-5-187
(4) Cohesive soils	VI-5-188
<i>d. Hydraulic gradient and flow forces in soils</i>	VI-5-190
(1) Hydraulic gradient	VI-5-190
(2) Permeability	VI-5-191
(3) Wave-induced internal setup	VI-5-193
(4) Pore pressure gradients in sloping rubble-mound structures	VI-5-194
<i>e. Cyclic loading of soils</i>	VI-5-194
(1) Time scale of drainage and consolidation	VI-5-194
(2) Wave load transmission to monolithic structure foundations	VI-5-196
(3) Noncohesive soil exposed to wave-induced cyclic loadings	VI-5-200
(4) Cohesive soil exposed to wave-induced cyclic loadings	VI-5-202
<i>f. Dynamic loading of soils under monolithic structures</i>	VI-5-206
<i>g. Slip surface and zone failures</i>	VI-5-208
<i>h. Settlement</i>	VI-5-224
VI-5-6. Scour and Scour Protection	VI-5-226
<i>a. Scour problems in coastal engineering</i>	VI-5-226
(1) Physical processes of scour	VI-5-226
(2) Common scour problems	VI-5-227
<i>b. Prediction of scour</i>	VI-5-230
(1) Scour at vertical walls.....	VI-5-230
(a) Nonbreaking waves.....	VI-5-230
(b) Breaking waves.....	VI-5-234
(2) Scour at sloping structures.....	VI-5-236

	Page
(a) Rules of thumb.....	VI-5-236
(b) Scour at head of sloping breakwater.....	VI-5-237
(3) Scour at piles	VI-5-238
(a) Scour at small diameter vertical piles	VI-5-238
(b) Scour at large diameter vertical piles.....	VI-5-241
(4) Scour at submerged pipelines	VI-5-242
(a) Pipeline scour by currents.....	VI-5-243
(b) Pipeline scour by waves	VI-5-243
(c) Pipeline scour by waves and currents	VI-5-244
(d) Pipelines in the nearshore	VI-5-244
(5) Other scour problems.....	VI-5-244
c. <i>Design of scour protection</i>	VI-5-244
(1) Scour protection for vertical walls.....	VI-5-245
(2) Scour protection for sloping structures.....	VI-5-246
(3) Scour protection for piles	VI-5-246
(4) Scour protection for submerged pipelines	VI-5-247
VI-5-7 Wave Forces on Slender Cylindrical Piles	VI-5-249
a. <i>Introduction</i>	VI-5-249
b. <i>Vertical cylindrical piles and nonbreaking waves</i>	VI-5-250
(1) Basic concepts	VI-5-250
(2) Calculation of forces and moments	VI-5-251
(a) Linear wave theory	VI-5-252
(b) Nonlinear wave theory.....	VI-5-254
(3) Transverse forces due to eddy shedding.....	VI-5-264
c. <i>Selection of hydrodynamic force coefficients C_D, C_M, and C_L</i>	VI-5-269
d. <i>Safety factors in pile design</i>	VI-5-273
e. <i>Other considerations related to forces on slender cylindrical piles</i>	VI-5-273
VI-5-8. Other Forces and Interactions	VI-5-274
a. <i>Impact forces</i>	VI-5-274
b. <i>Ice forces</i>	VI-5-275
(1) Horizontal ice forces.....	VI-5-275
(a) Solid ice forces.....	VI-5-275
(b) Localized ice crushing forces	VI-5-276
(c) Thermal ice forces.....	VI-5-278
(2) Ice forces on slopes.....	VI-5-278
(a) Ride-up of ice on slopes.....	VI-5-278
(b) Adfreeze loads	VI-5-280
(3) Vertical ice forces	VI-5-280
(a) Cylindrical piles.....	VI-5-280
(b) Vertical walls.....	VI-5-282
(c) Sloping structures	VI-5-283
(4) Aspects of slope protection design	VI-5-283
VI-5-9. References	VI-5-284
VI-5-10. Acknowledgements	VI-5-312
VI-5-11. Symbols	VI-5-313

List of Figures

	Page
Figure VI-5-1. Illustration of runup and rundown.....	VI-5-4
Figure VI-5-2. Typical velocity field for the porous flow in a breakwater. Numerical calculation	VI-5-5
Figure VI-5-3. $R_{i2\%}$ for head-on waves on smooth slopes.....	VI-5-8
Figure VI-5-4. R_{us} for head-on waves on smooth slopes	VI-5-9
Figure VI-5-5. R_{i2} percent for long-crested head-on waves on smooth slopes	VI-5-10
Figure VI-5-6. Parameters in berm test program at Delft Hydraulics	VI-5-11
Figure VI-5-7. Definition of α_{eq} and α in Equation VI-5-9.....	VI-5-12
Figure VI-5-8. Evaluation of the use of ξ_{eq} to account for the influence of a berm	VI-5-13
Figure VI-5-9. Test program for wave runup on smooth slopes conducted at Delft Hydraulics, de Waal and van der Meer (1992)	VI-5-14
Figure VI-5-10. Influence of angle of incidence β and directional spreading on runup on smooth slopes conducted at Delft Hydraulics; de Waal and van der Meer (1992)	VI-5-14
Figure VI-5-11. Notational permeability coefficients	VI-5-16
Figure VI-5-12. 2 percent and significant runup of irregular head-on waves on impermeable and permeable rock slopes.....	VI-5-17
Figure VI-5-13. Definition of crest freeboard, R_c	VI-5-19
Figure VI-5-14. Structure profile geometrical parameters related to overtopping	VI-5-21
Figure VI-5-15. Wave overtopping data as basis for Equations VI-5-24 and VI-5-25	VI-5-30
Figure VI-5-16. Vertical wall wave overtopping data plotted with $\gamma_s = 1.0$	VI-5-31
Figure VI-5-17. Vertical wall wave overtopping data with fitted mean and 95 percent confidence bands	VI-5-31
Figure VI-5-18. Reflection coefficients for concrete armor unit slopes.....	VI-5-35
Figure VI-5-19. Wave reflection coefficients for rock armored slope with berm at SWL.....	VI-5-36
Figure VI-5-20. Wave reflection coefficients for plain vertical breakwater on 1:50 seabed	VI-5-37

	Page
Figure VI-5-21. Wave reflection coefficients fro plain vertical breakwater on rubble-mound foundation	VI-5-38
Figure VI-5-22. Wave reflection coefficients for horizontal composite breakwaters with tetrapod slope 1:1.5	VI-5-39
Figure VI-5-23. Wave reflection coefficients for sloping top breakwaters	VI-5-40
Figure VI-5-24. Wave reflection coefficients for perforated caissons	VI-5-40
Figure VI-5-25. Wave reflection coefficients for single perforated screen	VI-5-41
Figure VI-5-26. Wave reflection coefficients for impermeable and permeable vertical breakwaters exposed to oblique, nonbreaking, short-crested waves	VI-5-42
Figure VI-5-27. Measured versus estimated u_{rms} near smooth, impermeable 1:2 slope	VI-5-44
Figure VI-5-28. Wave transmission diagram by Allsop (1983) and Powell and Allsop (1985)	VI-5-45
Figure VI-5-29. Example of total wave transmission coefficients, C_t , for conventional and reef type low-crested and submerged breakwaters, calculated from the van der Meer and d'Angremond (1991) formula given by Equation VI-5-54	VI-5-47
Figure VI-5-30. Wave transmission by overtopping of horizontal composite breakwaters armored with tetrapods	VI-5-50
Figure VI-5-31. Wave transmission by overtopping of sloping top structures	VI-5-51
Figure VI-5-32. Wave transmission through perforated single wall	VI-5-52
Figure VI-5-33. Typical armor layer failure modes	VI-5-53
Figure VI-5-34. Illustration of influence of slope angle on the stabilizing effects of gravitational force, interlocking and surface friction	VI-5-56
Figure VI-5-35. Damage parameters for structure armor layer	VI-5-61
Figure VI-5-36. Illustration of superstructure designs causing insignificant and significant reduction in front slope armor stability	VI-5-63
Figure VI-5-37. Illustration of critical areas for damage to armor layers in the round head	VI-5-80
Figure VI-5-38. Illustration of improvement of round head stability by change of geometry	VI-5-83
Figure VI-5-39. Convex and concave bends and corners	VI-5-83
Figure VI-5-40. Examples of concrete armor units	VI-5-89

	Page
Figure VI-5-41. Breakage formula for dolosse	VI-5-92
Figure VI-5-42. Breakage formula for tetrapods.....	VI-5-92
Figure VI-5-43. Wave height versus maximum flexural tensile stress for several dolos waist ratios	VI-5-95
Figure VI-5-44. Dolos mass versus maximum flexural tensile stress for several dolos waist ratios	VI-5-95
Figure VI-5-45. Example of calculation of thermal stresses and cracked regions in a 70-tonne cube 100 hr after casting	VI-5-98
Figure VI-5-46. Examples of temperature development during curing in 30-tonne modified cubes with and without a hole	VI-5-100
Figure VI-5-47. Typical toe and toe berm solutions in rubble-mound breakwater design.....	VI-5-102
Figure VI-5-48. Example of potential instability of the stones placed on rock seabed.....	VI-5-103
Figure VI-5-49. Support of the stones by a trench or anchor bolts	VI-5-103
Figure VI-5-50. Typical seawall to designs where scour is foreseen	VI-5-104
Figure VI-5-51. Illustration of foot protection blocks for vertical structures.....	VI-5-110
Figure VI-5-52. Example of Japanese foot protection block.....	VI-5-111
Figure VI-5-53. Design of foot protection blocks according to Japanese practice.....	VI-5-111
Figure VI-5-54. Rubble-mound section for seaward wave exposure with zero-to-moderate overtopping conditions.....	VI-5-115
Figure VI-5-55. Rubble-mound section for wave exposure on both sides with moderate overtopping conditions.....	VI-5-117
Figure VI-5-56. Logic diagram for preliminary design of rubble-mound structures	VI-5-119
Figure VI-5-57. Illustration of vertical wall wave forces from nonbreaking and breaking waves.....	VI-5-132
Figure VI-5-58. Identification of types of total horizontal wave loadins on vertical wall structure exposed to head-on long-crested irregular waves	VI-5-133
Figure VI-5-59. Pressure distributions for nonbreaking waves.....	VI-5-134
Figure VI-5-60. Pressure distributions on overtopped vertical wall.....	VI-5-135
Figure VI-5-61. Wave barrier definition sketch	VI-5-145

	Page
Figure VI-5-62. Best-fit to wave barrier force data.....	VI-5-146
Figure VI-5-63. Power curve exponents.....	VI-5-147
Figure VI-5-64. Comparison of Equation VI-5-139 to data used in empirical curve fits.....	VI-5-148
Figure VI-5-65. Variation of wave height along a semi-infinite, fully reflecting breakwater exposed to head-on, long-crested waves	VI-5-149
Figure VI-5-66. Peak-delay force reduction for oblique regular waves.....	VI-5-151
Figure VI-5-67. Numerical simulation of peak-delay reduction, long-crested waves. Example of uncertainty calculation for wave train with 500 waves	VI-5-151
Figure VI-5-68. Example of peak-delay force reduction for short-crested waves	VI-5-152
Figure VI-5-69. Nondimensional amplitude of horizontal turning moment around the center of the caisson exposed to oblique nonbreaking regular waves.....	VI-5-153
Figure VI-5-70. Example of force reduction from model tests with short-crested breaking waves.....	VI-5-153
Figure VI-5-71. Broken wave forces on wall seaward of shoreline	VI-5-154
Figure VI-5-72. Broken wave forces on wall landward of shoreline	VI-5-156
Figure VI-5-73. Illustration of forces on a superstructure.....	VI-5-157
Figure VI-5-74. Illustration of comparison between base plate pore pressure distributions (under quasi-static porous flow conditions) and the approximated linear distribution	VI-5-157
Figure VI-5-75. Impulsive pressure force caused by wave breaking on the wave wall.....	VI-5-158
Figure VI-5-76. Typical crown wall configurations.....	VI-5-158
Figure VI-5-77. Comparison of predictions to measurements using the methods in Table VI-5-61	VI-5-161
Figure VI-5-78. Convex and concave corners and bends at vertical walls.....	VI-5-165
Figure VI-5-79. Mach reflection at a vertical wall.....	VI-5-166
Figure VI-5-80. Total stresses in a soil element.....	VI-5-176
Figure VI-5-81. Illustration of shear modulus G and bulk modulus K for granular soils exposed to initial and repeated (cyclic) loadings	VI-5-179

	Page
Figure VI-5-82. In-situ secant values of shear modulus G for quasi static loaded saturated clays	VI-5-180
Figure VI-5-83. Static and secant cyclic shear modulus, g , for Drammen clay.....	VI-5-181
Figure VI-5-84. Values of G/G_{max} for sands and gravels	VI-5-183
Figure VI-5-85. Damping ratios for sands and saturated clays.....	VI-5-184
Figure VI-5-86. Mohr envelope for stresses of failure	VI-5-185
Figure VI-5-87. Illustration of straight-line approximations to curved Mohr envelopes corresponding to drained conditions.....	VI-5-185
Figure VI-5-88. Angle of friction in rock fill of different grading and porosity with maximum diameter in the range 70-200 mm.....	VI-5-186
Figure VI-5-89. Crude visualization of dilatancy and angle of dilation ψ	VI-5-187
Figure VI-5-90. Failure criterion for a water-saturated clay in undrained condition defined from Mohr envelope	VI-5-189
Figure VI-5-91. Representation of flow regimes for stationary porous flow based on a Forchheimer equation formulation	VI-5-191
Figure VI-5-92. Illustration of wave induced forces on caisson foundation and related stress variations in the subsoil	VI-5-198
Figure VI-5-93. Illustration of approximate cyclic wave loading and related cyclic shear stress variation in a subsoil element during a storm sequence.....	VI-5-199
Figure VI-5-94. Simplified stress conditions for some elements along a potential failure surface.....	VI-5-200
Figure VI-5-95. Illustration of (a) stabilization and pore pressure build-up, and (b) liquefaction undrained triaxial test on sand	VI-5-201
Figure VI-5-96. Illustration of effective stress paths for clay samples in undrained triaxial tests	VI-5-203
Figure VI-5-97. Stress strain behavior of Drammen clay under various cyclic loading conditions corresponding to $OCR = 4$	VI-5-204
Figure VI-5-98. Result of cyclic tests on normally consolidated Drammen clay with $OCR = 1$, and $I_p = 27$ percent	VI-5-205
Figure VI-5-99. Example of normalized diagrams for cyclic loading of Drammen clay with $OCR = 1$, in triaxial tests (a), and DSS tests (b)	VI-5-205

	Page
Figure VI-5-100. Cyclic shear strength of Drammen clay with OCR = 1	VI-5-206
Figure VI-5-101. Approximation to horizontal wave load history for waves breaking directly on vertical walls.....	VI-5-207
Figure VI-5-102. Definition of translatory and rotational motions and dimensions for caisson structure and parapet wave wall exposed to dynamic loading.....	VI-5-208
Figure VI-5-103. Amplification factors for translatory and rotational motions for caisson structure with square footing and triangular load shape	VI-5-209
Figure VI-5-104. Illustration of flow nets in a homogenous isotropic breakwater for two instantaneous wave load situations.....	VI-5-211
Figure VI-5-105. Illustration of instantaneous flow net in a homogeneous isotropic seabed under wave action.....	VI-5-214
Figure VI-5-106. Illustration of forces to be considered in slope stability analysis	VI-5-214
Figure VI-5-107. Illustration of logarithmic spiral	VI-5-215
Figure VI-5-108. Illustration of failure surface in case of weak stratum.....	VI-5-216
Figure VI-5-109. Illustration of forces on a soil slice in the method of slices slope stability analysis	VI-5-216
Figure VI-5-110. Illustration of safety factor F for three-dimensional slope failure.....	VI-5-218
Figure VI-5-111. Illustration of fictitious footing to replace real footing under eccentric loading conditions	VI-5-222
Figure VI-5-112. Simplified base and rear slope geometries to be applied in the general bearing capacity formula Table VI-5-86	VI-5-223
Figure VI-5-113. Illustration of passive earth pressure P to be included in the determination of the foundation load resultant R in place of the depth coefficients in Equations VI-5-248 and VI-5-250	VI-5-223
Figure VI-5-114. Coastal scour problems.....	VI-5-228
Figure VI-5-115. Regular and irregular wave-scoured profiles at a vertical-front structure	VI-5-231
Figure VI-5-116. Scour prediction for nonbreaking waves at vertical wall	VI-5-232
Figure VI-5-117. Scour due to breaking waves at a vertical seawall.....	VI-5-234
Figure VI-5-118. Relative scour depth as a function of relative depth at a vertical wall	VI-5-235

	Page
Figure VI-5-119. Correction factor, k_I , for pile/pier shape.....	VI-5-239
Figure VI-5-120. Wave-induced equilibrium scour depth at a vertical pile	VI-5-240
Figure VI-5-121. Wave and current scour around large vertical piles.....	VI-5-242
Figure VI-5-122. Pipeline scour and pipeline embedment	VI-5-242
Figure VI-5-123. Scour apron for vertical pile in a current.....	VI-5-247
Figure VI-5-124. Stone blanket scour protection for submerged pipelines	VI-5-248
Figure VI-5-125. Definition sketch of wave forces on a vertical cylinder	VI-5-249
Figure VI-5-126. K_m versus relative depth, d/gT^2	VI-5-255
Figure VI-5-127. K_{Dm} versus relative depth, d/gT^2	VI-5-256
Figure VI-5-128. Inertia force moment arm S_m versus relative depth, d/gT^2	VI-5-257
Figure VI-5-129. Drag force moment arm S_{Dm} versus relative depth, d/gT^2	VI-5-258
Figure VI-5-130. Breaking wave height and regions of validity of various wave theories	VI-5-259
Figure VI-5-131. Isolines of ϕ_m versus H/gT^2 and d/gT^2 ($W = 0.05$)	VI-5-260
Figure VI-5-132. Isolines of ϕ_m versus H/gT^2 and d/gT^2 ($W = 0.10$)	VI-5-261
Figure VI-5-133. Isolines of ϕ_m versus H/gT^2 and d/gT^2 ($W = 0.50$)	VI-5-262
Figure VI-5-134. Isolines of ϕ_m versus H/gT^2 and d/gT^2 ($W = 1.0$)	VI-5-263
Figure VI-5-135. Isolines of α_m versus H/gT^2 and d/gT^2 ($W = 0.05$).....	VI-5-265
Figure VI-5-136. Isolines of α_m versus H/gT^2 and d/gT^2 ($W = 0.10$).....	VI-5-266
Figure VI-5-137. Isolines of α_m versus H/gT^2 and d/gT^2 ($W = 0.5$).....	VI-5-267
Figure VI-5-138. Isolines of α_m versus H/gT^2 and d/gT^2 ($W = 1.0$).....	VI-5-268
Figure VI-5-139. Drag coefficient C_D as a function of KC and constant values of R_e or β for smooth cylinders	VI-5-270
Figure VI-5-140. Inertia coefficient C_M as a function of KC and constant values of R_e or β for smooth cylinders	VI-5-270
Figure VI-5-141. Lift coefficient C_L as a function of KC and constant values of R_e or β for smooth cylinders	VI-5-271

	Page
Figure VI-5-142. Drag coefficient C_D as a function of Reynolds number for rough cylinders	VI-5-271
Figure VI-5-143. Inertia coefficient C_M as a function of Reynolds number for rough cylinders	VI-5-272
Figure VI-5-144. Ice riding up on structure slope	VI-5-278
Figure VI-5-145. Vertical ice forces on a cylindrical pile	VI-5-281

List of Tables

	Page
Table VI-5-1. Types of Wave Breaking on Impermeable Slopes and Related ξ_o Values	VI-5-6
Table VI-5-2. Coefficients in Equation VI-5-3 for Runup of Long-Crested Irregular Waves on Smooth Impermeable Slopes.....	VI-5-9
Table VI-5-3. Surface Roughness Reduction Factor γ_r in Equation VI-3-5, Valid for $1 < \xi_{op} < 3-4$	VI-5-11
Table VI-5-4. Test Program.....	VI-5-15
Table VI-5-5. Coefficients in Equations VI-5-12 and VI-5-13 for Runup of Irregular Head-On Waves on Impermeable and Permeable Rock Armored Slopes	VI-5-17
Table VI-5-6. Critical Values of Average Overtopping Discharges.....	VI-5-20
Table VI-5-7. Models for Average Overtopping Discharge Formulae.....	VI-5-23
Table VI-5-8. Overtopping Formula by Owen (1980, 1982).....	VI-5-24
Table VI-5-9. Overtopping Formula by Bradbury and Allsop (1988).....	VI-5-25
Table VI-5-10. Coefficients by Aminti and Franco (1988) for Overtopping Formula by Bradbury and Allsop in Table VI-5-9.....	VI-5-26
Table VI-5-11. Overtopping Formula by van der Meer and Janssen (1995).....	VI-5-27
Table VI-5-12. Overtopping formula by Pedersen and Burcharth (1992), Pedersen (1996).....	VI-5-28
Table VI-5-13. Overtopping Formula by Franco and Franco (1999)	VI-5-29
Table VI-5-14. Wave Reflection Coefficients for Non-Overtopped Sloping Structures Based on Seelig (1983) Equation.....	VI-5-34
Table VI-5-15. Wave Transmission Formula by van der Meer and d'Angremond (1991) for Rock Armored Low-crested, Submerged, and Reef Breakwaters.....	VI-5-46
Table VI-5-16. Wave Transmission Formula by Goda (1969).....	VI-5-48
Table VI-5-17. Wave Transmission Formula by Takahashi (1996)	VI-5-49
Table VI-5-18. Parameters Influencing Hydraulic Stability of Armor Layers	VI-5-54
Table VI-5-19. Definition of Damage Parameters D , N_{od} and S	VI-5-57
Table VI-5-20. Examples of Experimentally Determined Relationships Between N_{od} and S	VI-5-59

	Page
Table VI-5-21. Damage Classification and Related Values of the Damage Parameters <i>D</i> , <i>N_{od}</i> and <i>S</i>	VI-5-60
Table VI-5-22. Rock, Two-Layer Armored Non-Overtopped Slopes (Hudson 1974).....	VI-5-64
Table VI-5-23. Rock, Two-Layer Armored Non-Overtopped Slopes (van der Meer 1988).....	VI-5-65
Table VI-5-24. Rock, Two-Layer Armored Overtopped, but Not Submerged, Low-Crested Slopes.....	VI-5-66
Table VI-5-25. Rock, Submerged Breakwaters with Two-Layer Armor on Front, Crest and Rear Slope (van der Meer 1991).....	VI-5-67
Table VI-5-26. Rock, Two-layer Armored Low-Crested and Submerged Breakwaters (Vidal et al. 1992).....	VI-5-68
Table VI-5-27. Rock, Low-Crested Reef Breakwaters Built Using Only One Class of Stone.....	VI-5-69
Table VI-5-28. Rock, Rear Slope Stability of Two-Layer Armored Breakwaters Without Superstructures (Jensen 1984).....	VI-5-70
Table VI-5-29. Concrete Cubes, Two-Layer Armored Non-Overtopped Slopes.....	VI-5-71
Table VI-5-30. Tetrapods, Two-Layer Armored Non-Overtopped Slopes.....	VI-5-72
Table VI-5-31. Dolos, Non-Overtopped Slopes (Burcharth and Liu 1992).....	VI-5-73
Table VI-5-32. ACCROPODE® (van der Meer 1988b).....	VI-5-75
Table VI-5-33. ACCROPODE®, Non-Overtopped or Marginally Overtopped Slopes (Burcharth et al. 1998).....	VI-5-76
Table VI-5-34. CORE-LOC®, Non or Marginally Overtopped Slopes (Melby and Turk 1994; Turk and Melby 1997).....	VI-5-77
Table VI-5-35. Tetrapods, Horizontally Composite Breakwaters (Hanzawa et al. 1996).....	VI-5-78
Table VI-5-36. Tribars, non-Overtopped or Minor Overtopped Slopes, Random and Uniform Placement.....	VI-5-79
Table VI-5-37. Rock and Dolos Breakwater Head Stability, No Overtopping (Carver and Heimbaugh 1989).....	VI-5-81
Table VI-5-38. Tetrapod and Tribar Breakwater Head Section Stability, No Overtopping.....	VI-5-82
Table VI-5-39. Types and Origins of Loads on Armor Units (Burcharth 1993b).....	VI-5-90
Table VI-5-40. Breakage Formula for Dolosse and Tetrapods.....	VI-5-91

	Page
Table VI-5-41. Stress Prediction Formulae for Dolosse.....	VI-5-93
Table VI-5-42. Approximate Values of Ultimate Rigid Body Impact Velocities For Concrete Armor Units	VI-5-97
Table VI-5-43. Drawbacks Related to Crack-Reducing Procedures	VI-5-99
Table VI-5-44. Fatigue for Conventional Unreinforced Concrete Exposed to Uniaxial and Flexural Stress Conditions With Zero Mean Stress	VI-5-101
Table VI-5-45. Stability of Toe Berm Tested in Regular Waves	VI-5-105
Table VI-5-46. Stability of Toe Berm Formed by 2 Layers of Stone Having Density 2.68 tonnes/m ³ . Variable Berm Width, and Sloping Structures.....	VI-5-106
Table VI-5-47. Stability of Toe Berm Formed by Two Layers of Stones or Parallelepiped Concrete Blocks	VI-5-108
Table VI-5-48. Stability of Toe Berm Formed by Two Layers of Stones in Front of Vertical Impermeable Wall Structure	VI-5-109
Table VI-5-49. Stability Under Combined Waves and Currents	VI-5-113
Table VI-5-50. Weight and Size Selection Dimensions of Quarrystone	VI-5-116
Table VI-5-51. Layer Coefficient and Porosity for Various Armor Units.....	VI-5-122
Table VI-5-52. The Sainflou Formula for Head-on, Fully Reflected, Standing Regular Waves	VI-5-136
Table VI-5-53. Goda Formula for Irregular Waves.....	VI-5-137
Table VI-5-54. Goda Formula Modified to Include Impulsive Forces from Head-on Breaking Waves	VI-5-138
Table VI-5-55. Resulting Wave Induced Forces and Moments, and Related Uncertainties and Bias When Calculated from Wave Load Equations by Goda and Takahashi	VI-5-139
Table VI-5-56. Wave Loads on Impermeable Inclined Walls	VI-5-140
Table VI-5-57. Wave Loads on Sloping Top Structures	VI-5-141
Table VI-5-58. Wave Loads on Vertical Walls Protected by a Rubble-Mound Structure	VI-5-142
Table VI-5-59. Wave Pressures from Regular Head-on Waves on Caissons with Vertical Slit Front Face and Open Wave Chamber	VI-5-143
Table VI-5-60. Horizontal Wave Force on Concrete Caps.....	VI-5-159

	Page
Table VI-5-61. Horizontal Wave Force, Uplift Wave Pressure and Turning Moment on Concrete Caps	VI-5-160
Table VI-5-62. Experimental Test Results of Friction Coefficient Conducted in Japan	VI-5-163
Table VI-5-63. Experimental Test Results of Friction Coefficient	VI-5-163
Table VI-5-64. Dynamic Friction Coefficient Between Caisson Bottom and Rubble-Mound.....	VI-5-164
Table VI-5-65. Fractional Limits of Grain Sizes According ISO/CEN.....	VI-5-173
Table VI-5-66. Typical Bulk Density Values	VI-5-174
Table VI-5-67. Typical Values of Void Ratio e and porosity n for Granular Soils.....	VI-5-174
Table VI-5-68. Density Characterization of Granular Soils	VI-5-175
Table VI-5-69. Deformation of Moduli for Elastic Material	VI-5-178
Table VI-5-70. Typical Values of Poisson's Ratio, ν	VI-5-178
Table VI-5-71. Example Values of Secant Young's Modulus E in MN/m^2 for sand	VI-5-179
Table VI-5-72. Typical Values of Secant Young's Modulus, E , for Clay	VI-5-180
Table VI-5-73. Typical Secant Values of Deformation-Moduli G , K and M for Quasi-Static Loaded Quartz Sand	VI-5-180
Table VI-5-74. Typical Values of Triaxial Test Friction Angle ϕ_s for Quartz Sand	VI-5-186
Table VI-5-75. Critical Value of Angle of Friction, ϕ'_{crit}	VI-5-188
Table VI-5-76. Typical Values of ψ_{max} for Quartz Sand and Quarried Granitic Gneiss.....	VI-5-188
Table VI-5-77. Classification of Clay According to Undrained Shear Strength, c_u	VI-5-189
Table VI-5-78. One-Dimensional Porous Flow Equation	VI-5-192
Table VI-5-79. Typical Values of Permeability, k , for Fine Materials.....	VI-5-192
Table VI-5-80. Typical Values of Permeability, k , for Stone Materials.....	VI-5-192
Table VI-5-81. Wave Induced Set-up in Sloping Rubble Mound Structures	VI-5-193
Table VI-5-82. Horizontal Wave Induced Pore Pressure Gradients in the Core Rubble-Mound Breakwaters	VI-5-195
Table VI-5-83. Classification of Loading and Soil Conditions	VI-5-196

	Page
Table VI-5-84. Example of Consolidation Times for Sand	VI-5-197
Table VI-5-85. Wave and Tide Induced Pore Pressures in Permeable Seabeds	VI-5-213
Table VI-5-86. Bearing Capacity Formula for Rectangular Concentrically Statically Loaded Horizontal Footings	VI-5-219
Table VI-5-87. Bearing Capacity Formula for Rectangular Statically Loaded Horizontal Footing	VI-5-220
Table VI-5-88. General Bearing Capacity Formula for Rectangular Statically Loaded Inclined Footing on Cohesionless Soil in Vicinity of Slope	VI-5-221
Table VI-5-89. Values of Skin Friction Coefficient, C_{sf}	VI-5-276
Table VI-5-90. Values of Effective Ice Crushing Strength, σ_c	VI-5-278

Chapter VI-5 Fundamentals of Design

VI-5-1. Introduction

a. Overview.

(1) Planning and design procedures for coastal projects are described in Part V-1, “Planning and Design Process.” The engineering design steps related to a specific type of coastal structure can be schematized as follows:

- (a.) Specification of functional requirements and structure service lifetime.
- (b.) Establishment of the statistics of local short-term and long-term sea states as well as estimation of possible geomorphological changes.
- (c.) Selection of design levels for the hydraulic responses: wave runup, overtopping, wave transmission, wave reflection (e.g., 20 percent probability of overtopping discharge exceeding $10^{-5} \text{ m}^3/\text{s} \cdot \text{m}$ during 1 hr in a 50-year period).
- (d.) Consideration of construction equipment and procedures, and of availability and durability of materials (e.g., only land based equipment operational and available at reasonable costs, rock of sufficient size easily available).
- (e.) Selection of alternative structure geometries to be further investigated (e.g., composite caisson structures, rubble structures with and without crown walls).
- (f.) Identification of all possible failure modes for the selected structures (e.g., armor layer displacement).
- (g.) Selection of design damage levels for the identified failure modes (e.g., 50 percent probability of displacement of 5 percent of the armor units within 50 years).
- (h.) Conceptual design of the structural parts based on the chosen design levels for failure mode damage and hydraulic responses (e.g., determination of armor layer block size and crest height for a breakwater).
- (i.) Evaluation of costs of the alternative structures and selection of preferred design(s) for more detailed analysis and optimization.
- (j.) Detailed design including economical optimization and evaluation of the overall safety of the structure. This stage will involve scale model tests and/or advanced computational analyses for non-standard and major structures.

(2) Items *c* and *g* are closely related to item *a*, and the failure modes mentioned in item *f* are dealt with in Part VI-2-4, “Failure Modes of Typical Structure Types.”

(3) The previous steps are a brief summary of the flow chart given as Figure V-1-2 in Part V-1-1. They are the steps most related to actual design of project structure elements. In all steps, the outlined design procedure should preferably involve a probabilistic approach which allows implementation of safety based on reliability assessments. The principles are explained in Part VI-6, "Reliability Based Design of Coastal Structures." The present Part VI-5 discusses the basic tools available for conceptual design related to wave-structure interactions (item *h* in the design process).

(4) Wave-structure interaction can be separated into hydraulic responses (such as wave runup, wave overtopping, wave transmission and wave reflection), and loads and response of structural parts. Each interaction is described by a formula, which in most cases is semiempirical in nature with the form based on physical considerations but the empirical constants determined by fitting to experimental data.

(5) The uncertainty and bias of the formula are given when known. Tables of available partial safety factors and the related design equations which show how the partial safety factors are implemented are given in Part VI-6, "Reliability Based Design of Coastal Structures."

b. Wave/structure interaction.

(1) Hydraulic response.

(a) Design conditions for coastal structures include acceptable levels of hydraulic responses in terms of wave runup, overtopping, wave transmission, and wave reflection. These topics are covered in Part VI-5-2, "Structure Hydraulic Response."

(b) The wave runup level is one of the most important factors affecting the design of coastal structures because it determines the design crest level of the structure in cases where no (or only marginal) overtopping is acceptable. Examples include dikes, revetments, and breakwaters with pedestrian traffic.

(c) Wave overtopping occurs when the structure crest height is smaller than the runup level. Overtopping discharge is a very important design parameter because it determines the crest level and the design of the upper part of the structure. Design levels of overtopping discharges frequently vary, from heavy overtopping of detached breakwaters and outer breakwaters without access roads, to very limited overtopping in cases where roads, storage areas, and moorings are close to the front of the structure.

(d) At impermeable structures, wave transmission takes place when the impact of overtopping water generates new waves at the rear side of the structure. With submerged structures, the incident waves will more or less pass over the structure while retaining much of the incident wave characteristics. Permeable structures like single stone size rubble mounds and slotted screens allow wave transmission as a result of wave penetration. Design levels of transmitted waves depend on the use of the protected area. Related to port engineering is the question of acceptable wave disturbance in harbor basins, which in turn is related to the movements of moored vessels. Where groins are included as part of a coastal protection scheme, it is desirable to ensure wave transmission (sediment transport) across the groins.

(e) Wave reflection from the boundary structures like quay walls and breakwaters determines to a large extent the wave disturbance in harbor basins. Also, maneuvering conditions at harbor entrances are highly affected by wave reflection from the breakwaters. Reflection causing steep waves and cross waves can be very dangerous to smaller vessels. Moreover, breakwaters and jetties can cause reflection of waves onto neighboring beaches and thereby increase wave impacts on beach processes.

(2) Wave loadings and related structural response.

(a) An important part of the design procedure for structures in general is the determination of the loads and the related stresses, deformations, and stability conditions of the structural members.

(b) In the case of rubble-mound structures exposed to waves, such procedures cannot be followed because the wave loading on single stones or blocks cannot be determined by theory, by normal scale model tests, or by prototype recordings. Instead a black box approach is used in which experiments are used to establish relationships between certain wave characteristics and the structural response, usually expressed in terms of armor movements. The related stresses, e.g., in concrete armor blocks, are known only for a few types of blocks for which special investigations have been performed. Rubble-mound structures are covered in Part VI-5-3, "Rubble-Mound Structure Loading and Response."

For vertical-front monolithic structures like breakwater caissons and seawalls it is possible either from theory or experiments to estimate the wave loadings and subsequently determine stresses, deformations, and stability. Vertical-front structures are covered in Part VI-5-4, "Vertical-Front Structure Loading and Response."

VI-5-2. Structure Hydraulic Response

a. Wave runup and rundown on structures.

(1) Introduction.

(a) Wind-generated waves have wave periods which trigger wave breaking on almost all sloping structures. The wave breaking causes runup, R_u , and rundown, R_d , defined as the maximum and minimum water-surface elevation measured vertically from the still-water level (SWL), see Figure VI-5-1a.

(b) R_u and R_d depend on the height and steepness of the incident wave and its interaction with the preceding reflected wave, as well as the slope angle, the surface roughness, and the permeability and porosity of the slope. Maximum values of flow velocities and values of R_u and R_d for a given sea state and slope angle are reached on smooth impermeable slopes.

(c) Figure VI-5-1a illustrates the variation of the flow velocity vectors along an impermeable slope over the course of a wave cycle. Figure VI-5-1b illustrates this variation for a permeable slope. Both the magnitude and direction of the velocity vectors are important for stability of the armor units. Generally, the most critical flow field occurs in a zone around and just below still-water level (swl) where down-rush normally produces the largest destabilizing forces. Exceptions are slopes flatter than approximately 1:3.5 in which cases up-rush is more vulnerable. The velocity vectors shown in Figure VI-5-1b explain why reshaping breakwaters attain S-profiles.

(d) Increase in permeability of the slope reduces the flow velocities along the slope surface because a larger proportion of the flow takes place inside the structure. The wave action will cause a rise of the internal water level (phreatic line) indicated in Figure VI-5-1c, leading to an increase in the mean pore pressures. The internal setup is due to a greater inflow surface area during wave runup than the outflow surface area during rundown. The mean flow path for inflow is also shorter than that for outflow. The rise of the phreatic line will continue until the outflow balances the inflow. The lower the permeability of the structure, the higher the setup as indicated on Figure VI-5-1c.

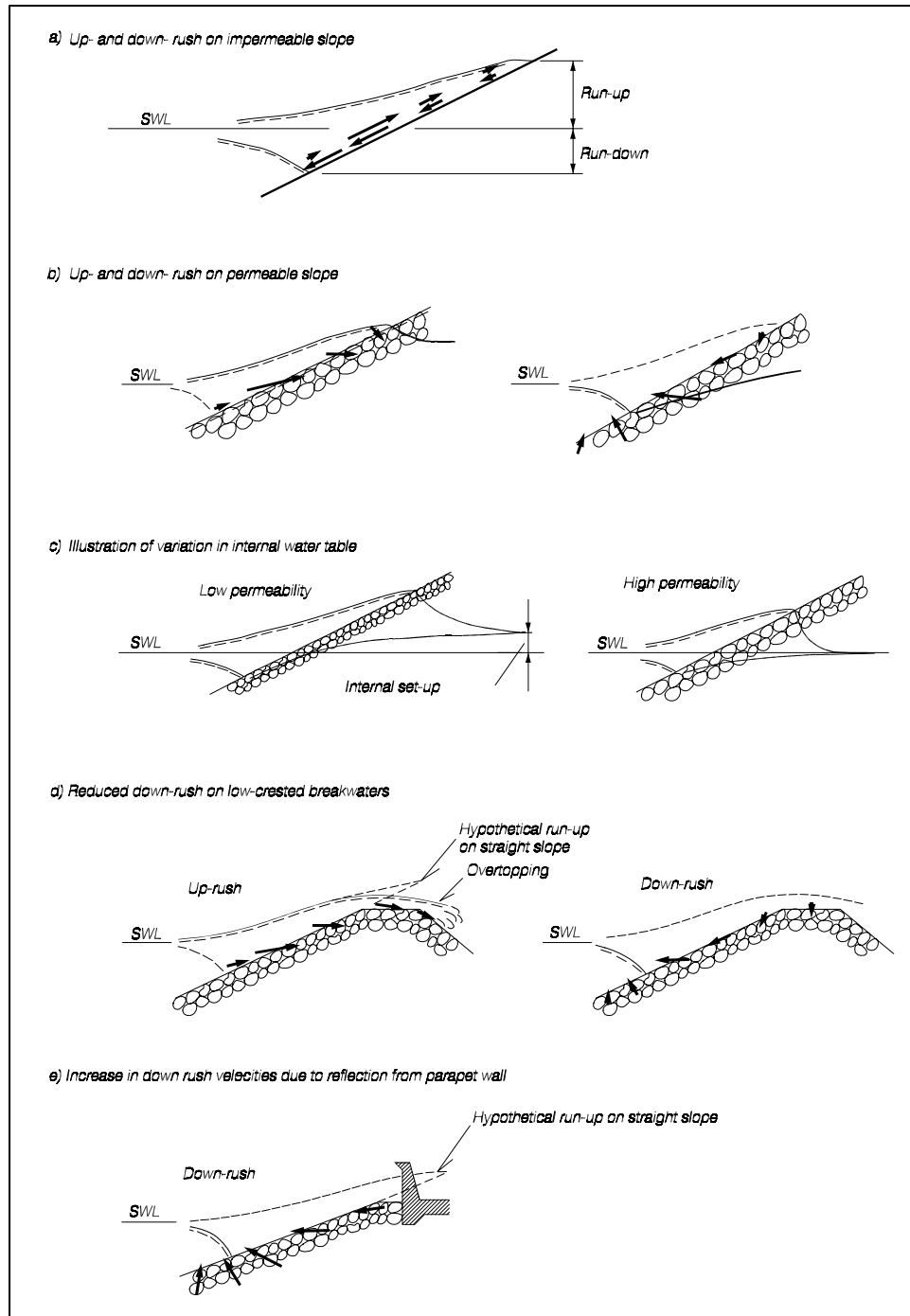


Figure VI-5-1. Illustration of runup and rundown (Burcharth 1993)

(e) Barends (1988) suggested practical formulae for calculation of the penetration length and the maximum average setup which occurs after several cycles. Two cases are considered: a conventional breakwater structure with open (permeable) rear side, and a structure with a closed (impermeable) rear side. The latter case causes the largest setup.

(f) An example of a numerical calculation of the internal flow patterns in a breakwater exposed to regular waves is shown in Figure VI-5-2. The strong outflow in the zone just below SWL when maximum rundown occurs is clearly seen.

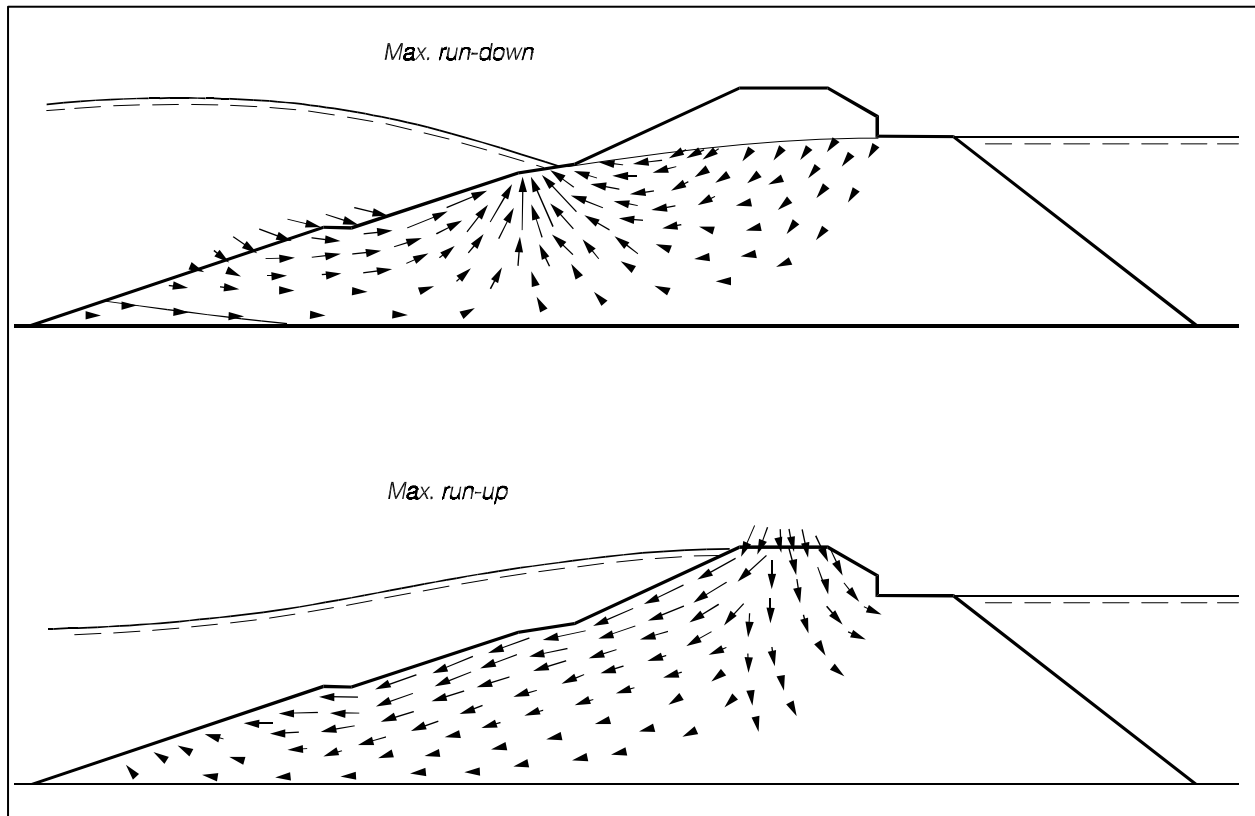


Figure VI-5-2. Typical velocity field for the porous flow in a breakwater. Numerical calculation (Barends et al. 1983)

(g) Increasing structure porosity also reduces the overflow velocities because a larger portion of the incoming water volume can be stored in the pores which then act as reservoirs. The destabilizing forces on armor units are thereby reduced. This positive reservoir effect is reduced in the case of a large internal setup of the water table.

(h) Breakwaters with crest levels lower than the runup level are called low-crested breakwaters. Although the runup velocities are almost unchanged compared to nonovertopped slopes, the rundown velocities are reduced due to the overtopping of some part of the incoming wave as seen in Figure VI-5-1d. Greater overtopping reduces rundown, and thus, lessens the destabilizing flow forces on the armor units. Parapet walls which cut off the hypothetical runup wedge (shown in Figure VI-5-1e) will increase the down-rush velocities and thereby increase the destabilizing flow forces on the armor units.

(2) Surf similarity parameter (Iribarren number).

(a) Wave runup and rundown on a structure depend on the type of wave breaking. Breaker types can be identified by the so-called surf-similarity parameter, ζ (Battjes 1974b). The parameter ζ is also referred to as the breaker parameter or Iribarren number. The surf-similarity parameter was originally defined for regular waves as

$$\xi_o = \frac{\tan \alpha}{\sqrt{s_o}} \quad (\text{VI-5-1})$$

where

α = slope angle

s_o = deepwater wave steepness ($= H_o / L_o$)

H_o = deepwater wave height

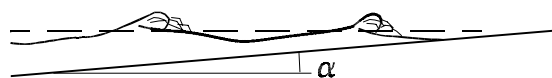
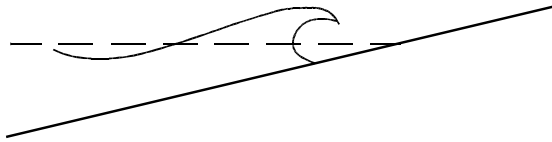
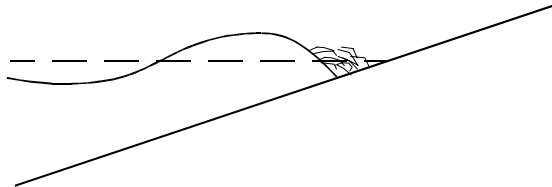
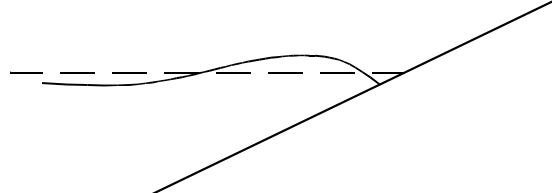
L_o = deepwater wavelength ($= gT^2/2\pi$)

T = wave period

g = acceleration due to gravity

(b) The wave height H_b at the breaking point is sometimes substituted for H_o in which case the parameter is denoted by ξ_b . Breaker types and related ranges of ξ_o -values are given for impermeable slopes in Table VI-5-1. The boundaries of transition from one type of breaker to another are approximate.

Table VI-5-1
Types of Wave Breaking on Impermeable Slopes and Related ξ_o -Values

	<p>SPILLING $\xi_o < 0.5$</p>
	<p>PLUNGING $0.5 < \xi_o < 3$</p>
	<p>COLLAPSING $\xi_o \approx 3 \text{ à } 3.5$</p>
	<p>SURGING $\xi_o > 3.5$</p>

(c) For irregular waves the surf-similarity parameter is defined as

$$\xi_{om} = \frac{\tan \alpha}{\sqrt{s_{om}}} \quad \text{or} \quad \xi_{op} = \frac{\tan \alpha}{\sqrt{s_{op}}} \quad (\text{VI-5-2})$$

where

$$s_{om} = \frac{H_s}{L_{om}} = \frac{2\pi H_s}{g T_m^2}$$

$$s_{op} = \frac{H_s}{L_{op}} = \frac{2\pi H_s}{g T_p^2}$$

and

H_s = significant wave height of incident waves at the toe of the structure

T_m = mean wave period

T_p = wave period corresponding to the peak of the wave spectrum

Note that s_{om} and s_{op} are fictitious wave steepnesses because they are ratios between a statistical wave height at the structure and representative deepwater wavelengths.

(d) The relative runup R_u/H is a function of ζ , the wave angle of incidence, and the slope geometry (profile, surface roughness, porosity). Differences in runup characteristics make it convenient to distinguish between impermeable and permeable slopes. Impermeable slopes belong to dikes, revetments, and breakwaters with either impermeable surfaces (e.g., asphalt, concrete) or rough surfaces (e.g., rubble stones, concrete ribs) on fine core materials. Permeable slopes belong typically to rubble-mound structures with secondary armor layers, filter layers, and quarryrun core.

(3) Wave runup and rundown on impermeable slopes. Runup on impermeable slopes can be formulated in a general expression for irregular waves having the form (Battjes 1974)

$$\frac{R_{ui\%}}{H_s} = (A\xi + C)\gamma_r\gamma_b\gamma_h\gamma_\beta \quad (\text{VI-5-3})$$

where

$R_{ui\%}$ = runup level exceeded by i percent of the incident waves

ζ = surf-similarity parameter, ζ_{om} or ζ_{op}

A, C = coefficients dependent on ζ and i but related to the reference case of a smooth, straight impermeable slope, long-crested head-on waves and Rayleigh-distributed wave heights

γ_r = reduction factor for influence of surface roughness ($\gamma_r = 1$ for smooth slopes)

γ_b = reduction factor for influence of a berm ($\gamma_b = 1$ for non-bermed profiles)

γ_h = reduction factor for influence of shallow-water conditions where the wave height distribution deviates from the Rayleigh distribution ($\gamma_h = 1$ for Rayleigh distributed waves)

γ_β = factor for influence of angle of incidence β of the waves ($\gamma_\beta = 1$ for head-on long-crested waves, i.e., $\beta = 0^\circ$). The influence of directional spreading in short-crested waves is included in γ_β as well

(a) Smooth slope, irregular long-crested head-on waves. Van Oorschot and d'Angremond (1968) tested slopes of 1:4 and 1:6 for $\xi_{op} < 1.2$. Ahrens (1981a) investigated slopes between 1:1 and 1:4 for $\xi_{op} > 1.2$. Figure VI-5-3 shows the range of test results and the fit of Equation VI-5-3 for $R_{u2\%}$. Considerable scatter is observed, most probably due to the fact that the runs for $\xi_{op} > 1.2$ contained only 100-200 waves. The coefficient of variation, $\sigma_{R_u} / \overline{R_u}$, seems to be approximately 0.15.

- The significant runup level $R_{us} = R_{u33\%}$ depicted in Figure VI-5-4 does not contain data for $\xi_{op} < 1.2$. The coefficient of variation appears to be approximately 0.1.
- The coefficients A and C together with estimates of the coefficient of variation for R_u are given in Table VI-5-2. It should be noted that data given in Allsop et al. (1985) showed runup levels considerably smaller than given here.

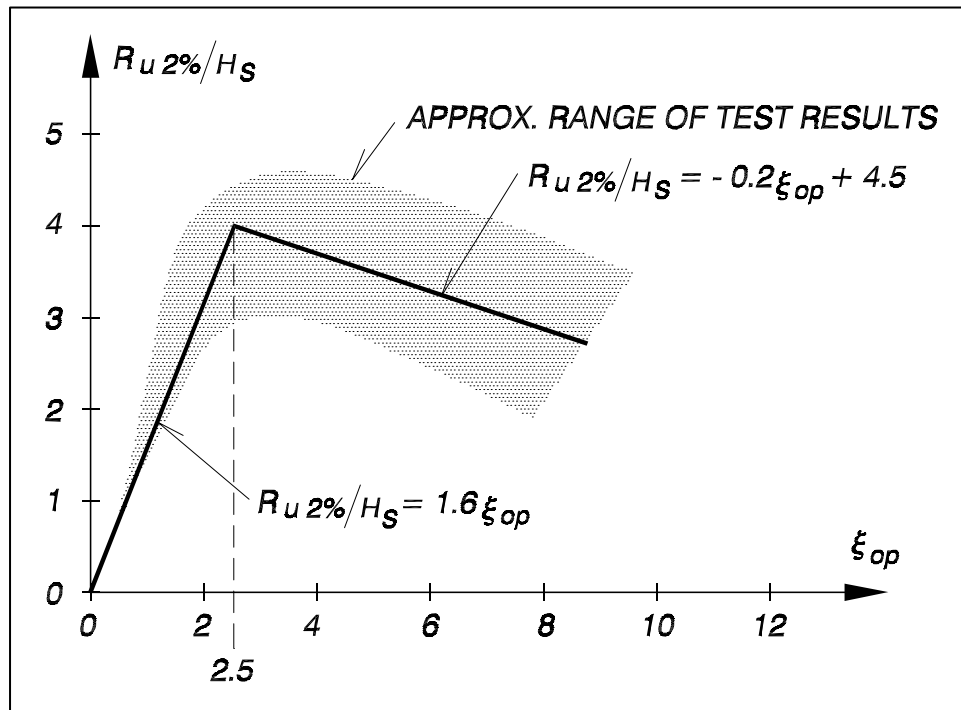


Figure VI-5-3. $R_{u2\%}$ for head-on waves on smooth slopes. Data by Ahrens (1981a) and Van Oorschot and d'Angremond (1968)

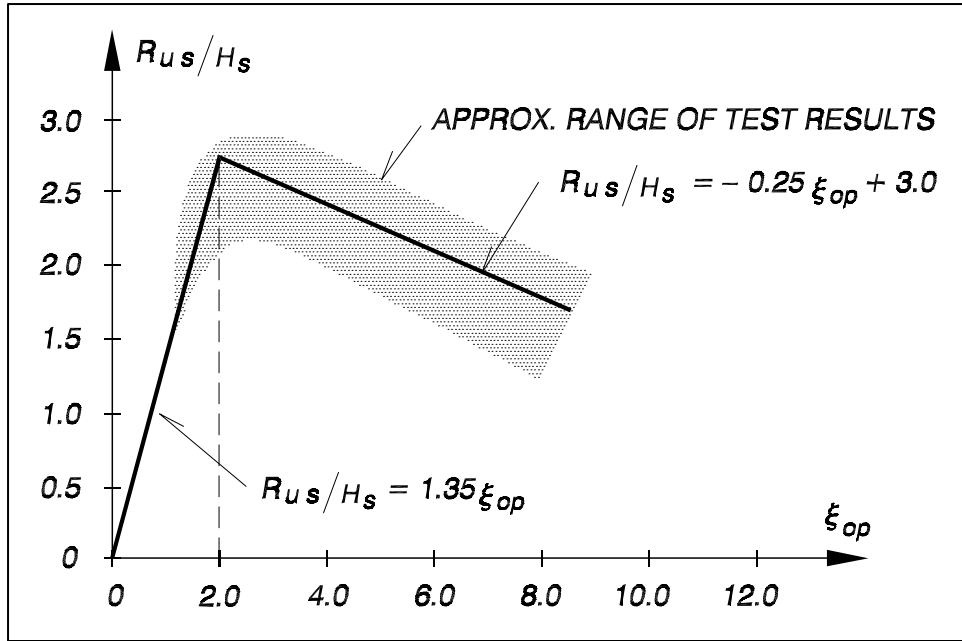


Figure VI-5-4. R_{us} for head-on waves on smooth slopes. Data by Ahrens (1981a)

Table VI-5-2
Coefficients in Equation VI-5-3 for Runup of Long-Crested Irregular Waves on Smooth Impermeable Slopes

ζ	R_u	ζ -Limits	A	C	σ_{R_u} / R_u
	$R_{u2\text{ percent}}$	$\zeta_p \leq 2.5$	1.6	0	≈ 0.15
		$2.5 < \zeta_p < 9$	-0.2	4.5	
ζ_{op}	R_{us}	$\zeta_p \leq 2.0$	1.35	0	≈ 0.10
		$2.0 < \zeta_p < 9$	-0.15	3.0	

- Generally less experimental data are available for rundown. Rundown corresponding to $R_{d2\text{ percent}}$ from long-crested irregular waves on a smooth impermeable slope can be estimated from

$$\frac{R_{d2\%}}{H_s} = \begin{cases} 0.33\zeta_{op} & \text{for } 0 < \zeta_{op} \leq 4 \\ 1.5 & \text{for } \zeta_{op} > 4 \end{cases} \quad (\text{VI-5-4})$$

- In the Dutch publication by Rijkswaterstaat Slope Revetments of Placed Blocks, 1990, the following expression was given for rundown on a smooth revetment of placed concrete block

$$\frac{R_{d2\%}}{H_s} = 0.5\zeta_{op} - 0.2 \quad (\text{VI-5-5})$$

- Another set of runup data for long-crested head-on waves on smooth slopes was presented by de Waal and van der Meer (1992). The data cover small scale tests for slopes 1:3, 1:4, 1:5, 1:6 and large scale tests for slopes 1:3, 1:6, 1:8. The surf-similarity parameter range for the small scale tests is $0.6 < \xi_{op} < 3.4$, and for the large scale tests $0.6 < \xi_{op} < 2.5$. The data are shown in Figure VI-5-5 and were used by de Waal and van der Meer (1992) and van der Meer and Janssen (1995) as the reference data for the evaluation of the γ -factors defined by Equation VI-5-3.

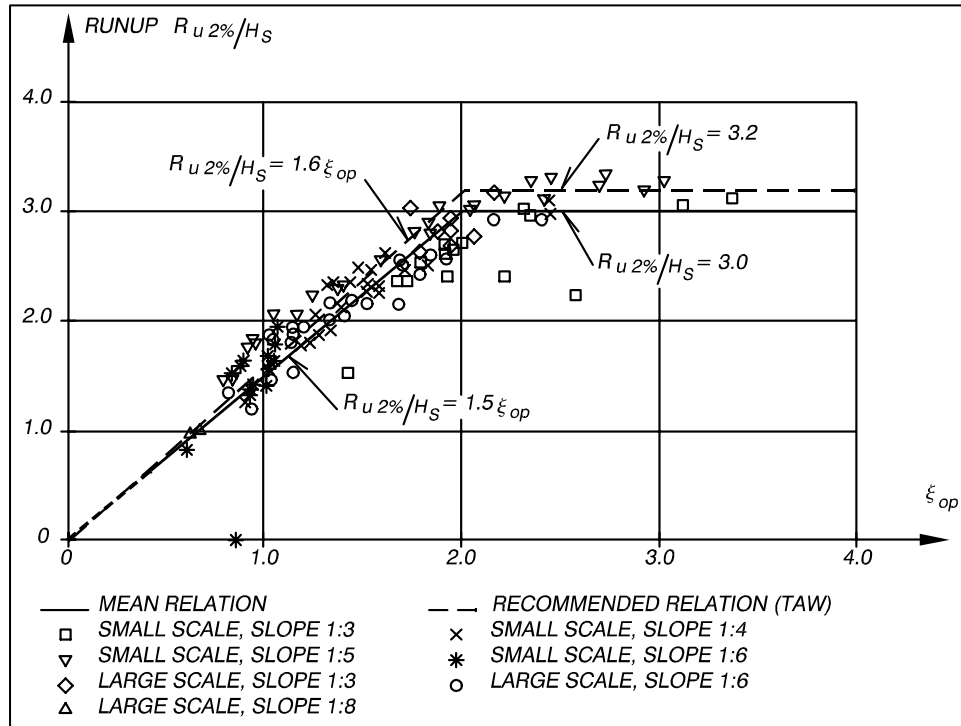


Figure VI-5-5. $R_{u2\%}$ for long-crested head-on waves on smooth slopes. From de Waal and van der Meer (1992)

- The mean relationship, taken as the reference case for Equation VI-5-3, is shown with the solid line and is represented by the expression

$$\frac{R_{u2\%}}{H_s} = \begin{cases} 1.5\xi_{op} & \text{for } 0.5 < \xi_{op} \leq 2 \\ 3.0 & \text{for } 2 < \xi_{op} < 3-4 \end{cases} \quad (\text{VI-5-6})$$

- The dotted line includes a small safety factor, and this relationship is recommended for design by the Technical Advisory Committee on Water Defence in Holland.
- Based on a somewhat reduced data set compared to Figure VI-5-5, the uncertainty on Equation VI-5-6 is described by de Waal and van der Meer (1992) by assuming the factor 1.5 as a stochastic variable with a normal distribution and a coefficient of variation of 0.085.

- Influence of surface roughness on runup. The original values for γ_r given in Dutch publications and in the old *Shore Protection Manual* have been updated based on experiments including large-scale tests with random waves. These factors are given in Table VI-5-3. The new γ_r values taken from de Waal and van der Meer (1992) are valid for $1 < \zeta_{op} < 3-4$. For larger ζ_{op} -values the γ_r factors will slowly increase to 1.

Table VI-5-3
Surface Roughness Reduction Factor γ_r in Equation VI-5-3, Valid for $1 < \zeta_{op} < 3-4$

Type of Slope Surface			γ_r
Smooth, concrete, asphalt			1.0
Smooth block revetment			1.0
Grass (3 cm length)			0.90 - 1.0
1 layer of rock, diameter D , ($H_s/D = 1.5 - 3.0$)			0.55 - 0.6
2 or more layers of rock, ($H_s/D = 1.5 - 6.0$)			0.50 - 0.55
Roughness elements on smooth surface (length parallel to waterline = ℓ , width = b , height = h)			
Quadratic blocks, $\ell = b$			
h/b	b/H_s	area coverage	
0.88	0.12 - 0.19	1/9	0.70 - 0.75
0.88	0.12 - 0.24	1/25	0.75 - 0.85
0.44	0.12 - 0.24	1/25	0.85 - 0.95
0.88	0.12 - 0.18	1/25 (above SWL)	0.85 - 0.95
0.18	0.55 - 1.10	1/4	0.75 - 0.85
Ribs			
1.00	0.12 - 0.19	1/7.5	0.60 - 0.70

- Influence of a berm on runup. A test program at Delft Hydraulics was designed to clarify the influence of a horizontal or almost horizontal berm on wave runup. Figure VI-5-6 shows the range of tested profiles and sea states.

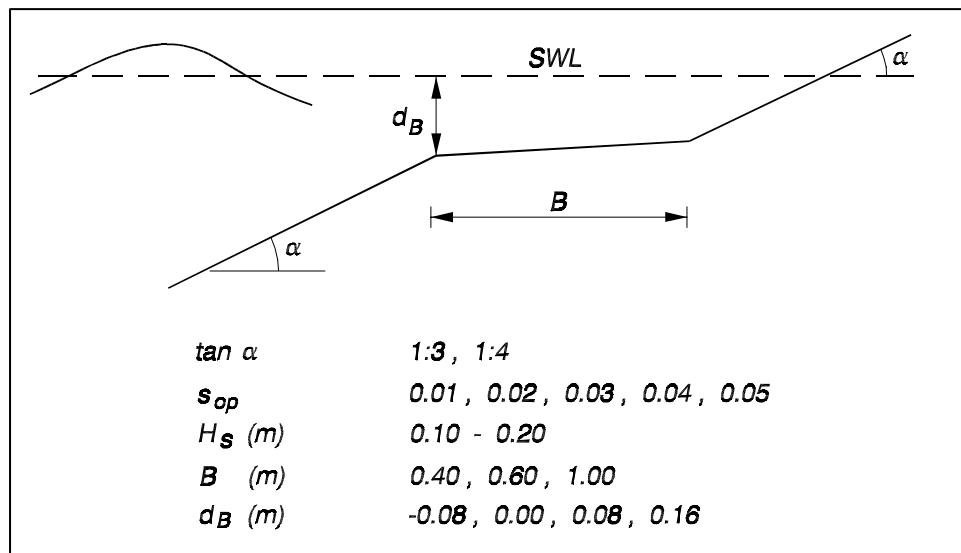


Figure VI-5-6. Parameters in berm test program at Delft Hydraulics

- According to de Waal and van der Meer (1992) the effect of a berm can be taken into account by the following formulation of the reference Equation VI-5-6

$$\frac{R_{u2\%}}{H_s} = \begin{cases} 1.5 \xi_{op} \gamma_r \gamma_b \gamma_h \gamma_\beta = 1.5 \xi_{eq} \gamma_r \gamma_h \gamma_\beta & \text{for } 0.5 < \xi_{eq} \leq 2 \\ 3.0 \gamma_r \gamma_h \gamma_\beta & \text{for } \xi_{eq} > 2 \end{cases} \quad (\text{VI-5-7})$$

where ξ_{eq} is the breaking wave surf similarity parameter based on an equivalent slope (see Figure VI-5-7). The berm influence factor γ_b is defined as

$$\gamma_b = \frac{\xi_{eq}}{\xi_{op}} = 1 - r_B (1 - r_{dB}), \quad 0.6 \leq \gamma_b \leq 1.0 \quad (\text{VI-5-8})$$

where

$$r_B = 1 - \frac{\tan \alpha_{eq}}{\tan \alpha} \quad (\text{VI-5-9})$$

$$r_{dB} = 0.5 \left(\frac{d_B}{H_s} \right)^2, \quad 0 \leq r_{dB} \leq 1$$

and the *equivalent* slope angle α_{eq} and the *average* slope angle α are defined in Figure VI-5-7.

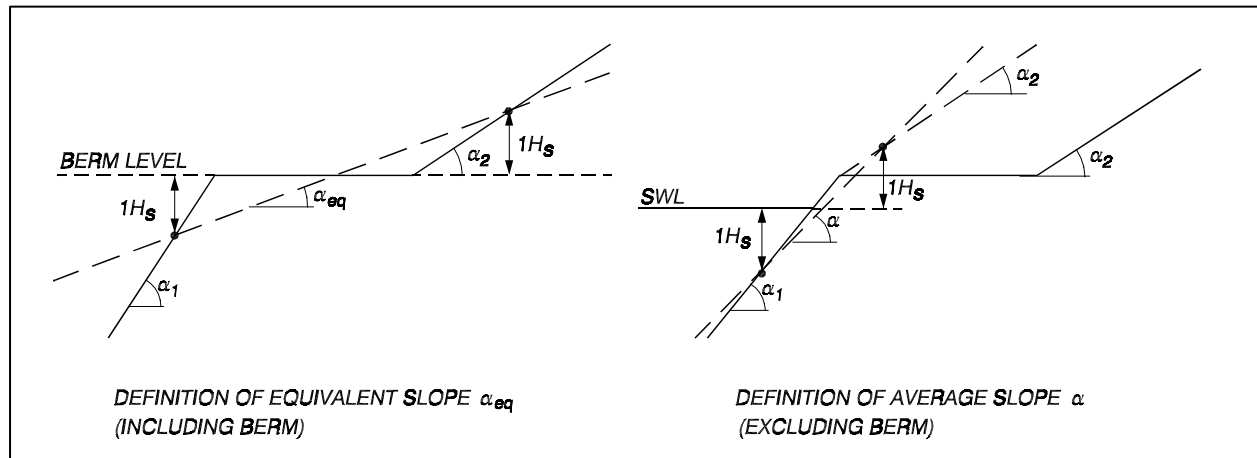


Figure VI-5-7. Definition of α_{eq} and α in Equation VI-5-9

- The influence of the berm can be neglected when the berm horizontal surface is positioned more than $H_s \sqrt{2}$ below SWL. If the berm horizontal surface lies higher than $d_B = H_s \sqrt{2}$ above SWL, then the runup can be set to $R_{u2\%} = d_B$ if $B/H_s \geq 2$. The berm is most effective when lying at SWL, i.e., $d_B = 0$. An optimum berm width B , which corresponds to $\gamma_b = 0.6$, can be determined from the formulae given by Equations VI-5-8 and VI-5-9.
- The use of ξ_{eq} in Equation VI-5-7 is evaluated in Figure VI-5-8 on the basis of the test program given in Figure VI-5-6, which implies $\gamma_r = \gamma_h = \gamma_\beta = 1$.

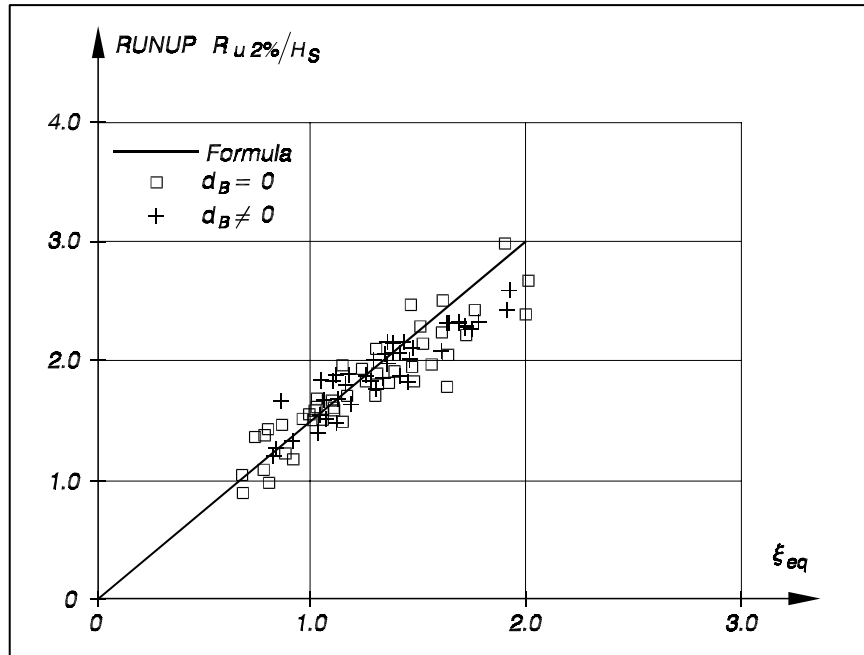


Figure VI-5-8. Evaluation of the use of ξ_{eq} to account for the influence of a berm

- Influence of shallow water on runup. Wave heights in Equation VI-5-7 are characterized by H_s which provides a unique definition for deep water conditions where wave heights are Rayleigh distributed. In shallow water where some waves break before they reach the structure, the wave heights will no longer be Rayleigh distributed. According to de Waal and van der Meer (1992), the influence factor can be estimated as

$$\gamma_h = \frac{H_{2\%}}{1.4H_s} \quad (\text{VI-5-10})$$

where the representative wave heights are specified for the water depth at the toe of the structure ($H_{2\%}/H_s = 1.4$ for Rayleigh distributed wave heights).

- Influence of angle of wave attack on runup. Both the angle of incidence and the directional spreading of the waves influence the runup. A test program for runup on smooth slopes at Delft Hydraulics, as specified in Figure VI-5-9, revealed the variations in the influence factor γ_β as given by Equation VI-5-11 and depicted in Figure VI-5-10.
- Note that γ_β -values larger than 1 were obtained for long-crested waves in the range $10^\circ \leq \beta \leq 30^\circ$, and that values very close to 1 were obtained for short-crested waves for β up to 50° .
- Based on the results, the following formulas for mean values of γ_β were given

Long-crested waves (mainly swell)	$= 1.0$	for $0^\circ \leq \beta \leq 10^\circ$	(VI-5-11)
	$\gamma_\beta = \cos(\beta - 10^\circ)$	for $10^\circ < \beta \leq 63^\circ$	
	$= 0.6$	for $\beta > 63^\circ$	
Short-crested waves	$\gamma_\beta = 1 - 0.0022 \beta$		

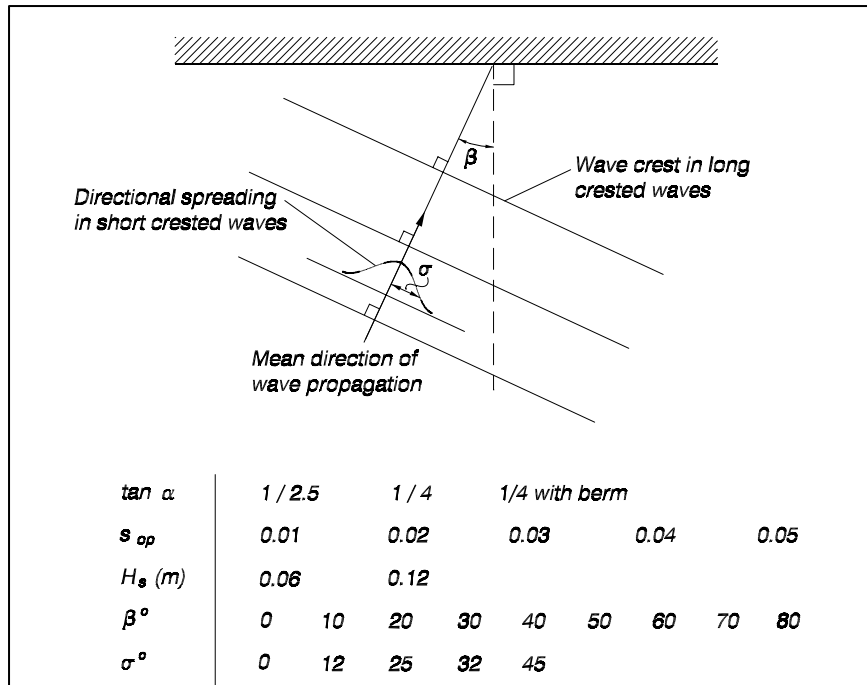


Figure VI-5-9. Test program for wave runup on smooth slopes conducted at Delft Hydraulics, de Waal and van der Meer (1992)

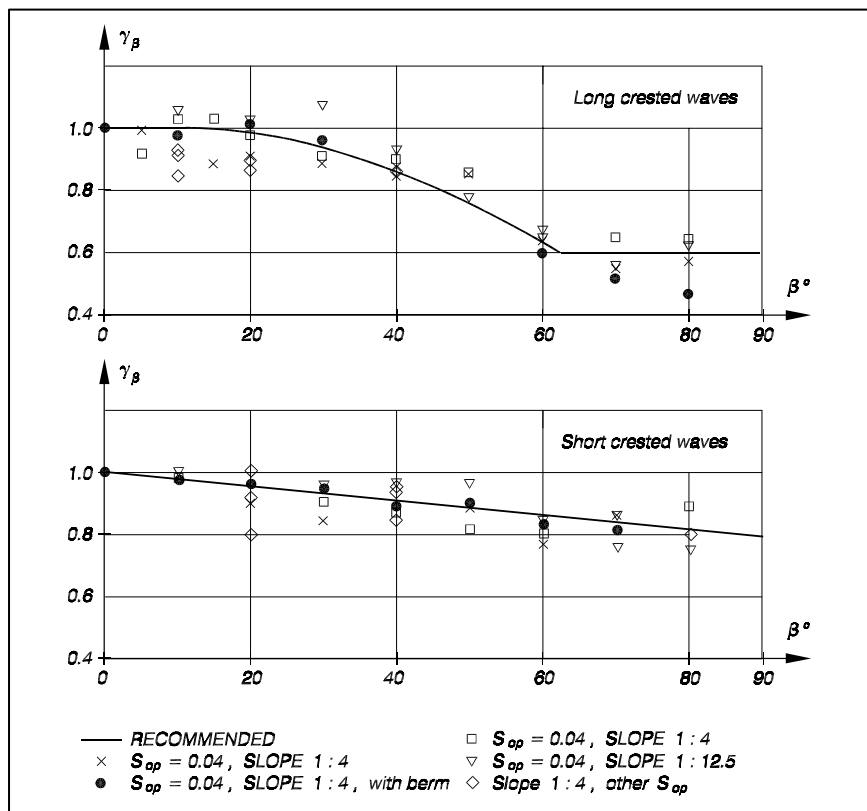


Figure VI-5-10. Influence of angle of incidence β and directional spreading on runup on smooth slopes conducted at Delft Hydraulics; de Waal and van der Meer (1992)

(b) Rock armored slopes, irregular long-crested head-on waves. Runup on rock armored impermeable and permeable slopes was studied by Delft Hydraulics in the test program given in Table VI-5-4.

Table VI-5-4
Test Program(van der Meer 1988)

Slope Angle cot α	Grading D_{85} / D_{15}	Spectral Shape	Core Permeability	Relative Mass Density	Number of Tests	Range $H_s / \Delta D_{n50}$	Range S_{om}
2	2.25	PM	none	1.63	1.9e+31	0.8-1.6	0.005-0.016
3	2.25	PM	none	1.63		1.2-2.3	0.006-0.024
4	2.25	PM	none	1.63		1.2-3.3	0.005-0.059
6	2.25	PM	none	1.63		1.2-4.4	0.004-0.063
3 ¹	1.25	PM	none	1.62		1.4-2.9	0.006-0.038
4	1.25	PM	none	1.62		1.2-3.4	0.005-0-059
3	2.25	narrow	none	1.63		1.0-2.8	0.004-0.054
3	2.25	wide	none	1.63		1.0-2.4	0.004-0.043
3 ¹	1.25	PM	permeable	1.62		1.6-3.2	0.008-0.060
2	1.25	PM	permeable	1.62		1.5-2.8	0.007-0.056
1.5	1.25	PM	permeable	1.62		1.5-2.6	0.008-0.050
2	1.25	PM	homogeneous	1.62		1.8-3.2	0.008-0.059
2	1.25	PM	permeable	0.95		1.7-2.7	0.016-0.037
2	1.25	PM	permeable	2.05		1.6-2.5	0.014-0.032
2 ²	1.25	PM	permeable	1.62		1.6-2.5	0.014-0.031
2 ³	1.25	PM	permeable	1.62		1.4-5.9	0.010-0.046

PM Pierson Moskowitz spectrum
¹ Some tests repeated in Delta Flume
² Foreshore 1:30
³ Low-crested structure with foreshore 1:30

- The core permeability in Table VI-5-4 refers to the structures shown in details *a*, *c* and *d* of Figure VI-5-11, taken from van der Meer (1988). The figure provides definition of a notational permeability parameter *P* which is used in various formulae by van der Meer to take into account the effect of permeability on response to wave action. The value *P* = 0.4 in Figure VI-5-11, detail *b*, is not identified by tests, but instead is an estimated value.
- The runup results from the test program described in Table VI-5-4 are presented in Figure VI-5-12.
- Note that $\xi_{om} = \tan \alpha / (2\pi H_s / g T_{om}^2)^{1/2}$, where T_{om} is the mean wave period, is used instead of ξ_{op} . By using T_{om} instead of T_{op} variations in the width of the wave spectrum are taken into account. The ratio $T_{om} / T_{op} = \xi_{om} / \xi_{op} = 0.79 - 0.87$ for Joint North Sea Wave Program (JONSWAP) spectra and 0.71 - 0.82 for Pierson-Moskowitz spectra.
- The central fit to the data for impermeable rock slopes was given by Delft Hydraulics (1989) as

$$\frac{R_{ui\%}}{H_s} = \begin{cases} A \xi_{om} & \text{for } 1.0 < \xi_{om} \leq 1.5 \\ B (\xi_{om})^C & \text{for } \xi_{om} > 1.5 \end{cases} \quad \text{(VI-5-12)}$$

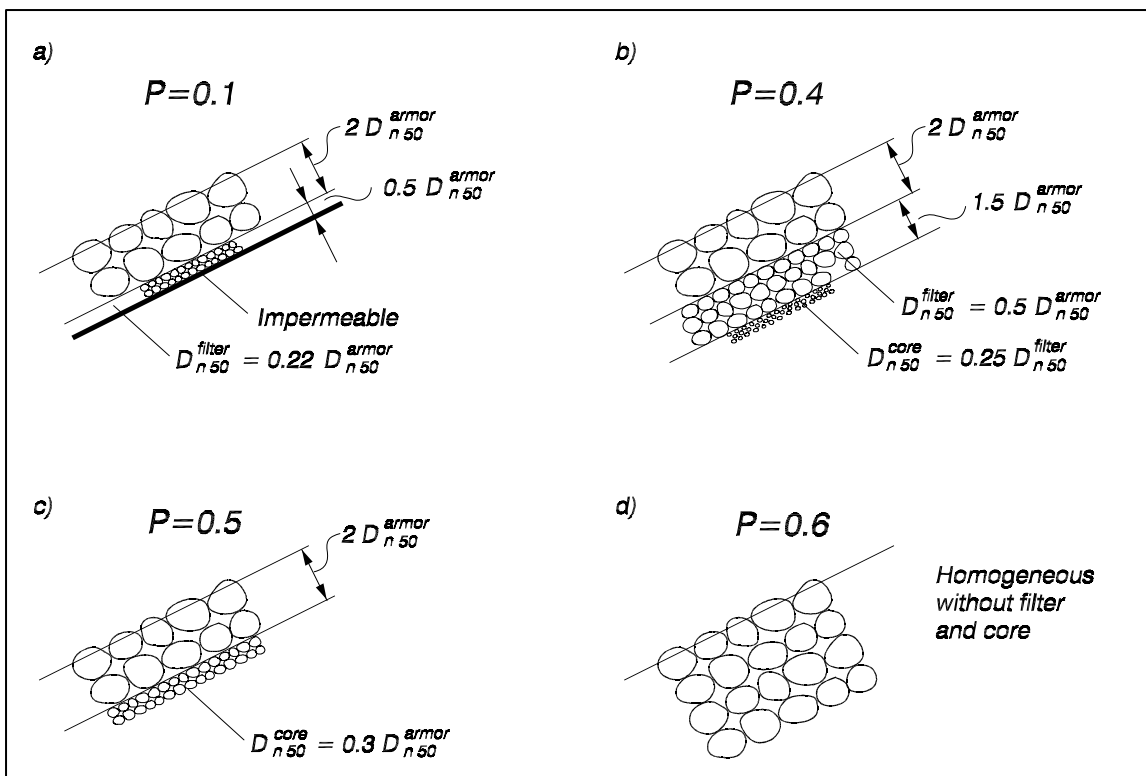


Figure VI-5-11. Notational permeability coefficients (van der Meer 1988)

- The coefficients A , B and C are given in Table VI-5-5. For impermeable slopes the coefficient of variation for A , B and C is 7 percent. Data presented by Ahrens and Heinbaugh (1988a) for maximum runup on impermeable riprap slopes are in agreement with the data represented by Equation VI-5-12.
- Equation VI-5-12 is valid for relatively deep water in front of a structure where the wave height distribution is close to the Rayleigh distribution. Wave breaking on a foreshore results in a truncation in the runup distribution which mainly results in lower runup heights for small exceedence probability levels. However, sometimes higher runup may occur according to observations in the Delft Hydraulics tests and recent tests conducted at Texas A&M University.

(4) Wave runup and rundown on permeable slopes. With respect to runup, permeable structures are defined as structures with core material of such permeability that wave induced porous flow and fluctuations of the internal phreatic line do vary with the frequencies of the waves. The storage capacity of the structure pores results in maximum runup that is smaller than for an equivalent structure with an impermeable core.

(a) Rock armored slopes, irregular long-crested head-on waves. Rock armored permeable slopes with notational permeability $P = 0.5$, as shown in detail *c* of Figure VI-5-11, were tested in irregular head-on waves by Delft Hydraulics in the program specified in Table VI-5-4. The results are shown in Figure VI-5-12, and the corresponding equation for the central fit to the data is given by

$$\begin{aligned}
 R_{ui} \% / H_s &= A \zeta_{om} && \text{for } 1.0 < \zeta_{om} \leq 1.5 \\
 &= B (\zeta_{om})^C && \text{for } 1.5 < \zeta_{om} \leq (D/B)^{1/C} \\
 &= D && \text{for } (D/B)^{1/C} \leq \zeta_{om} < 7.5
 \end{aligned}
 \tag{VI-5-13}$$

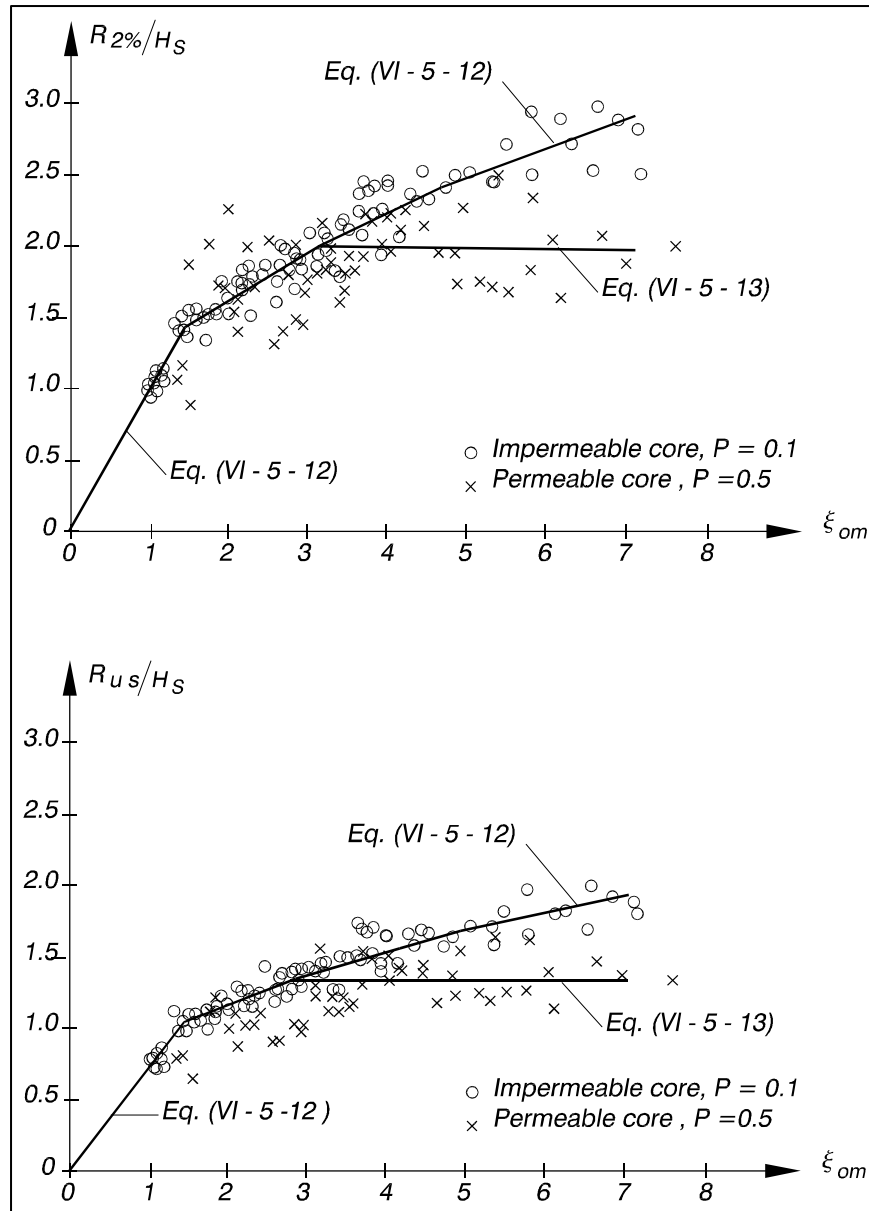


Figure VI-5-12. 2 percent and significant runup of irregular head-on waves on impermeable and permeable rock slopes. Delft Hydraulics (1989)

Table VI-5-5
Coefficients in Equations VI-5-12 and VI-5-13 for Runup of Irregular Head-On Waves on Impermeable and Permeable Rock Armored Slopes

Percent ¹	A	B	C	D ²
0.1	1.12	1.34	0.55	2.58
2.0	0.96	1.17	0.46	1.97
5	0.86	1.05	0.44	1.68
10	0.77	0.94	0.42	1.45
(significant)	0.72	0.88	0.41	1.35
50 (mean)	0.47	0.60	0.34	0.82

¹ Exceedence level related to number of waves

² Only relevant for permeable slopes

- The coefficients A , B , C and D are listed in Table VI-5-5. For permeable structures the coefficient of variation for A , B , C and D is 12 percent. Tests with homogeneous rock structures with notational permeability $P = 0.6$, as shown in detail d of Figure VI-5-11, showed results almost similar to the test results corresponding to $P = 0.5$ as shown in Figure VI-5-12.
- Equation VI-5-13 is valid for relatively deepwater conditions with wave height distributions close to a Rayleigh distribution. Wave breaking due to depth limitations in front of the structure cause truncation of the runup distribution and thereby lower runup heights for small exceedence probability levels. However, higher runup might also occur according to observations in the Delft Hydraulics tests, van der Meer and Stam (1992). The influence on runup for the shallow-water conditions included in the test program given in Table VI-5-4 were investigated for the rock armored permeable slope. However, no systematic deviations from Equation VI-5-13 were observed.

(b) Statistical distribution of runup. The runup of waves with approximately Rayleigh distributed wave heights on rock armored permeable slopes with $\tan \alpha \geq 2$ were characterized by van der Meer and Stam (1992) with a best-fit two-parameter Weibull distribution as follows:

$$Prob(R_u > R_{up\%}) = \exp \left[- \left(\frac{R_{up\%}}{B} \right)^C \right] \text{ or} \quad (VI-5-14)$$

$$R_{up\%} = B(-\ln p)^{1/C} \quad (VI-5-15)$$

where

$R_{up\%}$ = Runup level exceeded by p % of the runup

$$B = H_s \left[0.4 (s_{om})^{-1/4} (\cot \alpha)^{-0.2} \right] \quad (VI-5-16)$$

$$C = \begin{cases} 3.0 (\xi_{om})^{-3/4} & \text{for } \xi_{om} \leq \xi_{omc} \text{ (plunging waves)} \\ 0.52 P^{-0.3} (\xi_{om})^P \sqrt{\cot \alpha} & \text{for } \xi_{om} > \xi_{omc} \text{ (surging waves)} \end{cases} \quad (VI-5-17)$$

$$\xi_{omc} = \left(5.77 P^{0.3} \sqrt{\tan \alpha} \right)^{[1/(P+0.75)]} \quad (VI-5-18)$$

$$s_{om} = \frac{2\pi H_s}{g T_{om}^2}$$

P = notational permeability, see Figure VI-5-11.

- It follows from Equation VI-5-15 that the scale parameter B is equal to $Ru_{37\%}$ ($\ln p = -1$ for $p = 0.37$). If the shape parameter C is equal to 2, then Equation VI-5-14 becomes a Rayleigh distribution. The uncertainty on B corresponds to a coefficient of variation of 6 percent for $P < 0.4$ and 9 percent for $P \geq 0.4$.

- Rundown on rock slopes in the Delft Hydraulics test program listed in Table VI-5-4 gave the following relationship which includes the effect of structure permeability P (see Figure VI-5-11).

$$\frac{R_{d2\%}}{H_s} = 2.1\sqrt{\tan \alpha} - 1.2P^{0.15} + 1.5e^{-(60s_{om})} \quad (\text{VI-5-19})$$

b. *Wave overtopping of structures.*

Wave overtopping occurs when the highest runup levels exceed the crest freeboard, R_c as defined in Figure VI-5-13. The amount of allowable overtopping depends on the function of the particular structure. Certain functions put restrictions on the allowable overtopping discharge. For example access roads and installations placed on the crest of breakwaters and seawalls, berths for vessels as well as reclaimed areas containing roadways, storage areas, and buildings located just behind the breakwater are overtopping design considerations. Design criteria for overtopping should include two levels: Overtopping during normal service conditions and overtopping during extreme design conditions where some damage to permanent installations and structures might be allowed. Very heavy overtopping might be allowed where a breakwater has no other function than protection of harbor entrances and outer basins from waves. However, significant overtopping can create wave disturbances which could lead to damage of moored vessels. Fortunately, waves generated by overtopping usually have much shorter periods than the incident wave train.

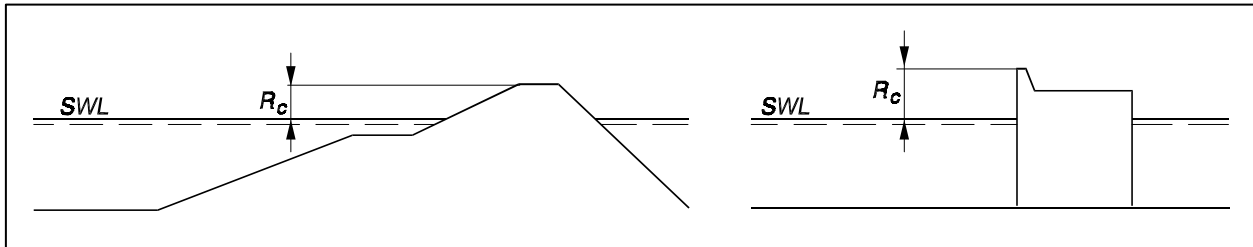


Figure VI-5-13. Definition of crest freeboard, R_c

(1) Admissible average overtopping discharge.

(a) The overtopping discharge from wind-generated waves is very unevenly distributed in time and space because the amount varies considerably from wave to wave. The major part of the overtopping discharge during a storm is due to a small fraction of the waves. In fact the local overtopping discharge (in m^3/s per meter structure) from a single wave can be more than 100 times the average overtopping discharge during the storm peak. Nevertheless, most information on overtopping is given as the time averaged overtopping discharge, q , expressed in m^3/s per meter of structure length. However, some limited information exists on the probability distribution of the volume of overtopping water per wave.

(b) Field studies of tolerable overtopping limits of dikes and revetments have been performed by Tsuruta and Goda (1968), Goda (1970), and Fukuda, Uno, and Irie (1974). Some critical values for overtopping of a breakwater were discussed by Jensen (1984), and Dutch Guidelines on river dikes indicated allowable overtopping rates for inner slopes. Delft Hydraulics tested admissible overtopping rates for grass dikes (Smith, Seijffert, and van der Meer 1994). De Gerloni et al. (1991), and Franco, de Gerloni, and van der Meer (1994) studied the effect of falling water jets on a person, simulating the conditions on breakwater crests. Endoh and Takahashi (1994) performed full-scale tests as well as numerical modeling of overtopping rates which endanger people.

(c) The information from these various studies is condensed in Table VI-5-6, which presents critical values of the average overtopping discharge, q . The values given in this table must be regarded only as rough guidelines because, even for the same value of q , the intensity of water hitting a specific location is very much dependent on the geometry of the structure and the distance from the front of the structure. The maximum intensities might locally be up to two orders of magnitude larger than the value of q . Moreover, what is regarded as acceptable conditions is to a large extent a matter of local traditions and individual opinions.

Table VI-5-6
Critical Values of Average Overtopping Discharges

q m^3/s per m		q $litres/s$ per m			
SAFETY OF TRAFFIC		STRUCTURAL SAFETY			
VEHICLES	PEDESTRIANS	BUILDINGS	EMBANKMENT SEAWALLS	GRASS SEA-DIKES	REVETMENTS
10^0					1000
			Damage even if fully protected	Damage	Damage even for paved promenade
	Very dangerous	Structural damage	Damage if back slope not protected		Damage if promenade not paved
10^{-1}			Damage if crest not protected	Start of damage	
		Dangerous on grass sea dikes, and horizontal composite breakwaters			
10^{-2}					
	Unsafe parking on horizontal composite breakwaters				
	Unsafe parking on vertical wall breakwaters				
10^{-3}					
	Dangerous on vertical wall breakwaters				
10^{-4}					No damage
	Unsafe driving at high speed	Minor damage to fittings, sign posts, etc.	No damage	No damage	
10^{-5}					
	Uncomfortable but not dangerous				
10^{-6}					
	Wet, but not uncomfortable	No damage			
10^{-7}					0.0001
	Safe driving at all speeds				

(d) The wind can carry spray long distances whereas solid (green) water is practically unaffected by the wind. It is important to consider spray because it can cause damage to goods placed on storage areas and can cause icing of vessel superstructures in cold regions.

(e) Overtopping occurs only if the runup level exceeds the freeboard, R_c , of the structure. Figure VI-5-14 shows the notation used to describe profile geometry for several structure types.

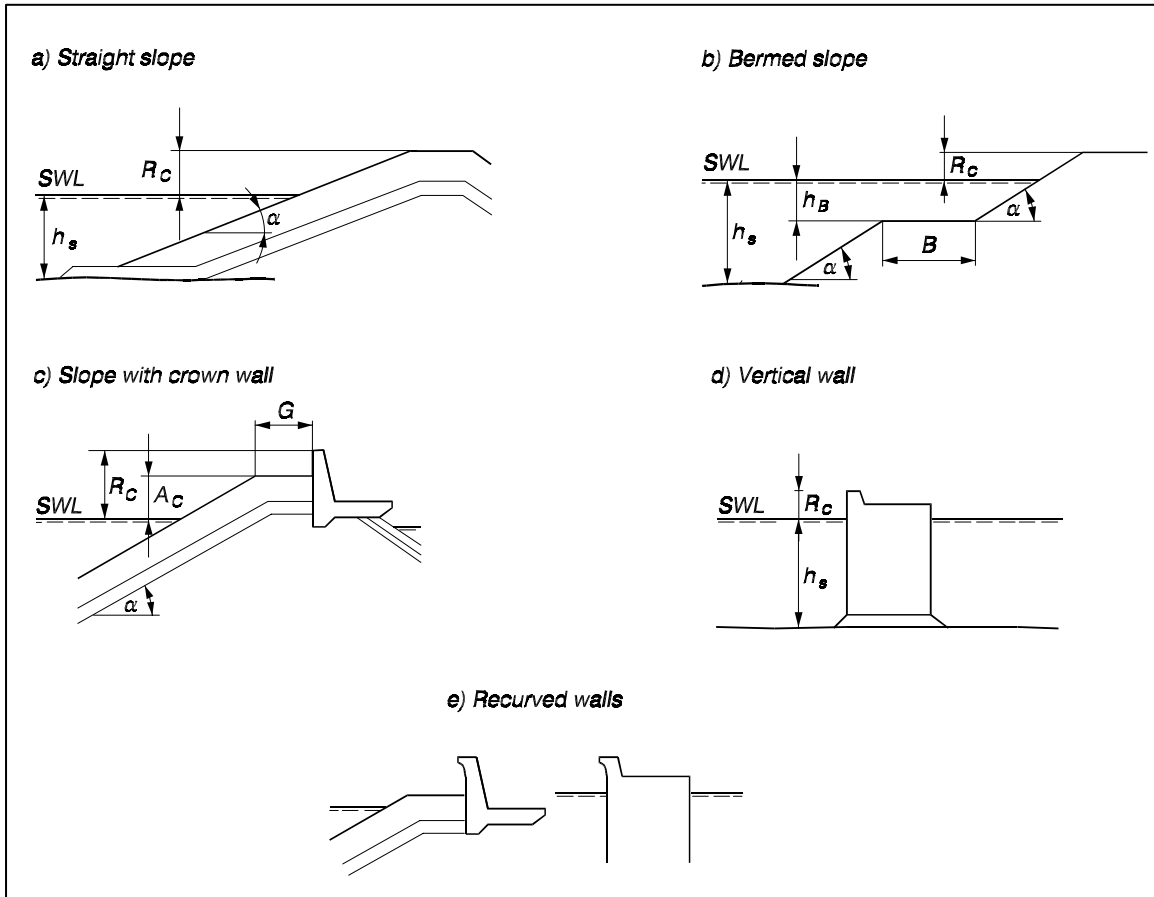


Figure VI-5-14. Structure profile geometrical parameters related to overtopping

(f) The relative freeboard, R_c / H_s , is a simple, but very important, dimensionless parameter for the prediction of overtopping. However, the wave period or wave steepness is also a significant parameter as are geometric parameters related to structure permeability, porosity and surface roughness. Under certain conditions a recurved wave wall as shown in Figure VI-5-14 e is effective in reducing overtopping. For small values of R_c / H_s (< 0.3) when the overtopping is excessive, the detailed geometry of the crest part of the structure becomes less important because the waves just travel over the structure.

(2) Average overtopping discharge formulas.

(a) Sloping structures. Formulae for overtopping are empirical because they are fitted to hydraulic model test results for specific breakwater geometries. In general the average overtopping discharge per unit length of structure, q , is a function of the standard parameters:

$$q = \text{function} (H_s, T_{op}, \sigma, \beta, R_c, h_s, g, \text{structure geometry})$$

where

H_s = significant wave height

T_{op} = wave period associated with the spectral peak in deep water (alternately T_{om})

σ = spreading of short-crested waves

β = angle of incidence for the waves

R_c = freeboard

h_s = water depth in front of structure

g = gravitational acceleration

Two types of mathematical formulations (models) for dimensionless overtopping dominate the literature, i.e.,

$$Q = a_e^{-bR} \quad (\text{VI-5-20})$$

and

$$Q = aR^{-b} \quad (\text{VI-5-21})$$

where Q is a dimensionless average discharge per meter and R is a dimensionless freeboard. Table VI-5-7 gives an overview of the models used in recent overtopping formulae along with the associated definitions for dimensionless discharge and freeboard.

(b) The fitted coefficients a and b in Equations VI-5-20 and VI-5-21 are specific to the front geometry of the structure and must be given in tables. So far no general model for the influence of front geometry exists except for rubble-mound slopes with a seawall (Pedersen 1996), in which case the front geometry (described by the front berm width B , berm crest height A_c , and slope angle α), as well as R_c , enters into R .

(c) Some formulae take into account the reduction in overtopping due to slope surface roughness, berm, shallow water, angle of wave incidence and shortcrestedness, and specific front geometries by dividing R by the respective reduction coefficients: γ_r (Table VI-5-3), γ_b (Equation VI-5-8), γ_h (Equation VI-5-10), γ_β (Equations VI-5-11, VI-5-26, VI-5-29), and γ_s (Table VI-5-13).

(d) Goda (1985) presented diagrams for wave overtopping of vertical revetments and block-mound seawalls on bottom slopes of 1:10 and 1:30. The diagrams are based on model tests with irregular long-crested head-on waves and express average discharge per meter width as a function of wave height, wave steepness, freeboard, and water depth.

- Sloping structures. Tables VI-5-8 to VI-5-12 pertain to sloping-front structures.
- Figure VI-5-15 shows the data basis for Equations VI-5-24 and VI-5-25 which includes the data of Owen (1980, 1982) for straight slopes, data of Führböter, Sparboom, and Witte (1989) and various data sets of Delft Hydraulics. It is seen that Equation VI-5-24 contains some bias for small values of q .
- Vertical front structures.

- Figure VI-5-16 shows the data used to establish Equation VI-5-28. Appropriate values of γ_β from Table VI-5-13 were used in plotting Figure VI-5-16; however γ_s was taken as unity (plain impermeable wall).

Table VI-5-7
Models for Average Overtopping Discharge Formulae

Authors	Structures	Overtopping model	Dimensionless discharge Q	Dimensionless freeboard R
Owen (1980,1982)	Impermeable smooth, rough, straight and bermed slopes	$Q = a \exp(-bR)$	$\frac{q}{g H_s T_{om}}$	$\frac{R_c}{H_s} \left(\frac{s_{om}}{2\pi} \right)^{0.5} \frac{1}{\gamma}$
Bradbury and Allsop (1988)	Rock armored impermeable slopes with crown walls	$Q = a R^{-b}$	$\frac{q}{g H_s T_{om}}$	$\left(\frac{R_c}{H_s} \right)^2 \left(\frac{s_{om}}{2\pi} \right)^{0.5}$
Aminti and Franco (1988)	Rock, cube, and Tetrapod double layer armor on rather impermeable slopes with crown walls, (single sea state)	$Q = a R^{-b}$	$\frac{q}{g H_s T_{om}}$	$\left(\frac{R_c}{H_s} \right)^2 \left(\frac{s_{om}}{2\pi} \right)^{0.5}$
Ahrens and Heimbaugh (1988b)	7 different seawall/revetment designs	$Q = a \exp(-bR)$	$\frac{q}{\sqrt{g H_s^3}}$	$\frac{R_c}{(H_s^2 L_{op})^{1/3}}$
Pedersen and Burcharth (1992)	Rock armored rather impermeable slopes with crown walls	$Q = a R$	$\frac{q T_{om}}{L_{om}^2}$	$\frac{H_s}{R_c}$
van der Meer and Janssen (1995)	Impermeable smooth, rough straight and bermed slopes	$Q = a \exp(-bR)$	$\frac{q}{\sqrt{g H_s^3}} \sqrt{\frac{s_{op}}{\tan \alpha}}$ for $\xi_{op} < 2$	$\frac{R_c}{H_s} \frac{\sqrt{s_{op}}}{\tan \alpha} \frac{1}{\gamma}$ for $\xi_{op} < 2$
			$\frac{q}{\sqrt{g H_s^3}}$ for $\xi_{op} > 2$	$\frac{R_c}{H_s} \frac{1}{\gamma}$ for $\xi_{op} > 2$
Franco et al. (1994)	Vertical wall breakwater with and without perforated front	$Q = a \exp(-bR)$	$\frac{q}{\sqrt{g H_s^3}}$	$\frac{R_c}{H_s} \frac{1}{\gamma}$
Pedersen (1996)	Rock armored permeable slopes with crown walls	$Q = R$	$\frac{q T_{om}}{L_{om}^2}$	$3.2 \cdot 10^{-5} \frac{H_s^5 \tan \alpha}{R_c^3 A_c \cdot B}$

Table VI-5-8
Overtopping Formula by Owen (1980, 1982)

Straight and bermed impermeable slopes, Figures VI-5-14 *a* and *b*.
Irregular, head-on waves.

$$\frac{q}{g H_s T_{om}} = \mathbf{a} \exp \left(-\mathbf{b} \frac{R_c}{H_s} \sqrt{\frac{s_{om}}{2 \pi}} \frac{1}{\gamma_r} \right) \quad (\text{VI-5-22})$$

Coefficients in Eq VI-5-22
Straight smooth slopes.
Non-depth limited waves.

Slope	a	b
1 : 1	0.008	20
1 : 1.5	0.010	20
1 : 2	0.013	22
1 : 3	0.016	32
1 : 4	0.019	47

Surface roughness reduction
factor γ_r .
Updated γ_r -values are given
in Table VI-5-3.

Smooth impermeable (including smooth concrete and asphalt)	1.0
One layer of stone rubble on imperme- able base	0.8
Gravel, gabion mattresses	0.7
Rock riprap with thickness greater than $2 D_{n50}$	0.5 - 0.6

Coefficients in Eq VI-5-22
Bermed smooth slopes.
Non-depth limited waves.

Slope	h_B (m)	B (m)	$\mathbf{a} \cdot 10^4$	\mathbf{b}
1 : 1	-4.0	10	64	20
1 : 2			91	22
1 : 4			145	41
1 : 1	-2.0	5	34	17
1 : 2			98	24
1 : 4			159	47
1 : 1	-2.0	10	48	19
1 : 2			68	24
1 : 4			86	46
1 : 1	-2.0	20	8.8	15
1 : 2			20	25
1 : 4			85	50
1 : 1	-2.0	40	3.8	23
1 : 2			5.0	26
1 : 4			47	51
1 : 1	-1.0	5	155	33
1 : 2			190	37
1 : 4			500	70
1 : 1	-1.0	10	93	39
1 : 2			340	53
1 : 4			300	80
1 : 1	-1.0	20	75	46
1 : 2			34	50
1 : 4			39	62
1 : 1	-1.0	40	12	49
1 : 2			24	56
1 : 4			1.5	63
1 : 1	0	10	97	42
1 : 2			290	57
1 : 4			300	80

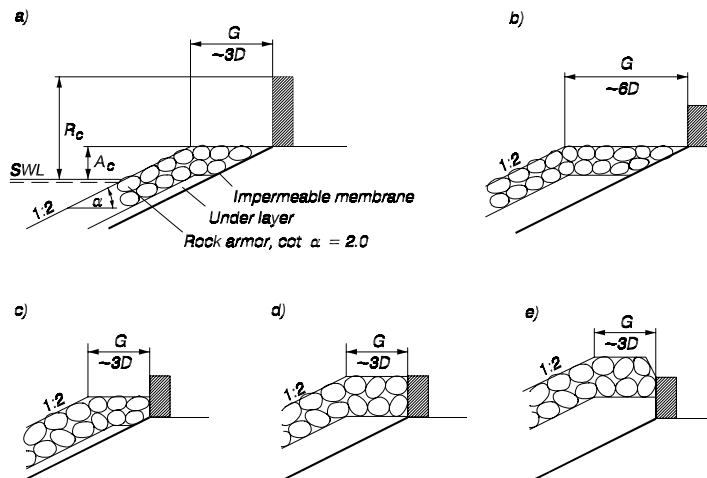
Table VI-5-9
Overtopping Formula by Bradbury and Allsop (1988)

Straight rock armored slope with berm in front of crown wall, Figure VI-5-14c. Slope 1:2. Impermeable membrane at various depths as shown in the following figure. Berm width G is three or six stone diameters. Irregular, head-on waves.

$$\frac{q}{g H_s T_{om}} = a \left[\left(\frac{R_c}{H_s} \right)^2 \sqrt{\frac{s_{om}}{2 \pi}} \right]^{-b} \quad (\text{VI-5-23})$$

Coefficients in Eq VI-5-23. Non-depth limited waves.

Note: "a" coefficients are shown multiplied by 10^9 . For example, a value of 6.7 in the table represents $6.7(10)^{-9}$.

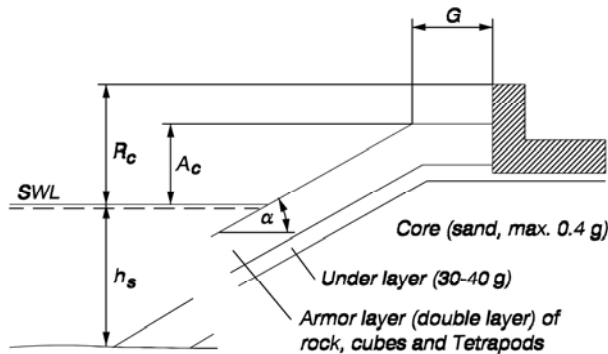


Section	G/H_s	G/R_c	A/R_c	$a \cdot 10^9$	b
a	0.79 - 1.7	0.75	0.28	6.7	3.5
		0.58	0.21	3.6	4.4
		1.07	0.39	5.3	3.5
		0.88	0.32	1.8	3.6
b	1.6 - 3.3	2.14	0.39	1.0	2.8
c	0.79 - 1.7	1.07	0.71	1.6	3.2
d	0.79 - 1.7	1.07	1.00	0.37	2.9
e	0.79 - 1.7	0.83	1.00	1.30	3.8

Table VI-5-10
Coefficients by Aminti and Franco (1988) for Overtopping Formula by Bradbury and Allsop in Table VI-5-9

Straight slope with berm in front of crown wall, Figure VI-5-14c. Rock, cube, and tetrapod armor on rather impermeable core. Only one sea state tested (JONSWAP spectrum). Non-depth limited waves. Irregular, head-on waves.

Note: "a" coefficients are shown multiplied by 10^8 . For example, a value of 17 in the table represents $17(10)^{-8}$.



Tested ranges:

- $H_s = 0.136 \text{ m}$
- $T_{om} = 1.33 \text{ s}$
- $S_{om} = 0.05$
- $h_s/H_s = 2.9$
- $\cot \alpha = 1.33, 2.0$
- $R_c/H_s = 0.6 - 2.0$
- $A_c/H_s = 0.6, 0.75, 1.05$
- $G/H_s = 1.1, 1.85, 2.6$ corresponding to width of 3, 5 and 7 stone diameters.

ARMOR	\cot	G/H_s	$a \cdot 10^8$	b
ROCK	2.00	1.10	17	2.41
		1.85	19	2.30
		2.60	2.3	2.68
	1.33	1.10	5.0	3.10
		1.85	6.8	2.65
		2.60	3.1	2.69
CUBES	2.00	1.10	8.3	2.64
		1.85	15	2.43
		2.60	84	2.38
	1.33	1.10	62	2.20
		1.85	17	2.42
		2.60	1.9	2.82
TETRAPODS	2.00	1.10	1.9	3.08
		1.85	1.3	3.80
		2.60	1.1	2.86
	1.33	1.10	5.6	2.81
		1.85	1.7	3.02
		2.60	0.92	2.98

Table VI-5-11
Overtopping Formula by van der Meer and Janssen (1995)

Straight and bermed impermeable slopes including influence of surface roughness, shallow foreshore, oblique, and short-crested waves, Figures VI-5-14a and VI-5-14b.

$\xi_{op} < 2$

$$\frac{q}{\sqrt{g} H_s^3} \sqrt{\frac{s_{op}}{\tan \alpha}} = 0.06 \exp \left(-5.2 \frac{R_c}{H_s} \frac{\sqrt{s_{op}}}{\tan \alpha} \frac{1}{\gamma_r \gamma_b \gamma_h \gamma_\beta} \right) \quad (\text{VI-5-24})$$

application range: $0.3 < \frac{R_c}{H_s} \frac{\sqrt{s_{op}}}{\tan \alpha} \frac{1}{\gamma_r \gamma_b \gamma_h \gamma_\beta} < 2$

Uncertainty: Standard deviation of factor 5.2 is $\sigma = 0.55$ (See Figure VI-5-15).

$\xi_{op} > 2$

$$\frac{q}{\sqrt{g} H_s^3} = 0.2 \exp \left(-2.6 \frac{R_c}{H_s} \frac{1}{\gamma_r \gamma_b \gamma_h \gamma_\beta} \right) \quad (\text{VI-5-25})$$

Uncertainty: Standard deviation of factor 2.6 is $\sigma = 0.35$ (See Figure VI-5-15).

The reduction factors references are

γ_r Table VI-5-3

γ_b Eq VI-5-8

γ_h Eq VI-5-10

Short-crested waves

$$\gamma_\beta = 1 - 0.0033 \beta$$

Long-crested waves (swell)

$$\gamma_\beta = \left\{ \begin{array}{ll} 1.0 & \text{for } 0^\circ \leq \beta \leq 10^\circ \\ \cos^2(\beta - 10^\circ) & \text{for } 10^\circ < \beta \leq 50^\circ \\ 0.6 & \text{for } \beta > 50^\circ \end{array} \right.$$

(VI-5-26)

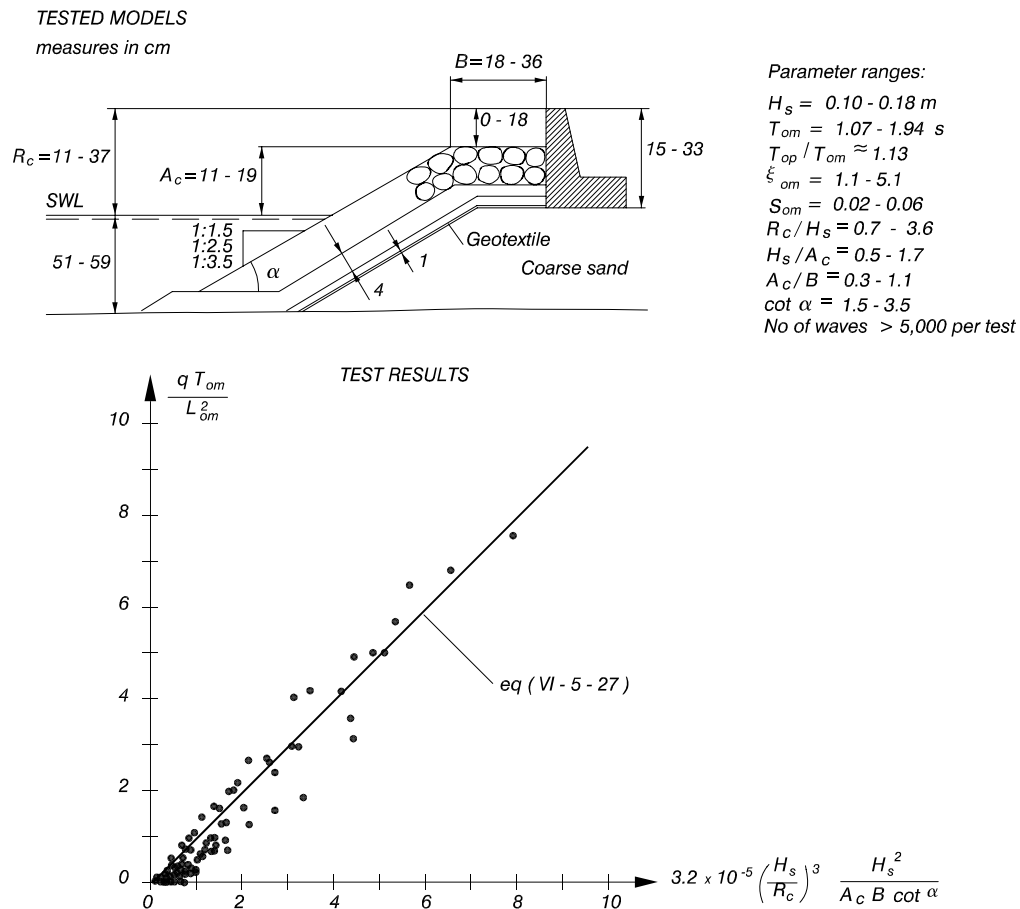
The minimum value of any combination of the γ -factors is 0.5.

Table VI-5-12
Overtopping Formula by Pedersen and Burcharth (1992), Pedersen (1996)

Rock armored permeable slopes with a berm in front of a crown wall, Figure VI-5-14c. Irregular, head-on waves.

$$\frac{q T_{om}}{L_{om}^2} = 3.2 \cdot 10^{-5} \left(\frac{H_s}{R_c} \right)^3 \frac{H_s^2}{A_c B \cot \alpha} \quad (\text{VI-5-27})$$

Notational permeability $P = 0.4$.



Some conservative bias of Eq VI-5-27 for small values of q is observed.

Table VI-5-13
Overtopping Formula by Franco and Franco (1999)

Impermeable and permeable vertical walls. Non-breaking, oblique, long- and short-crested waves.

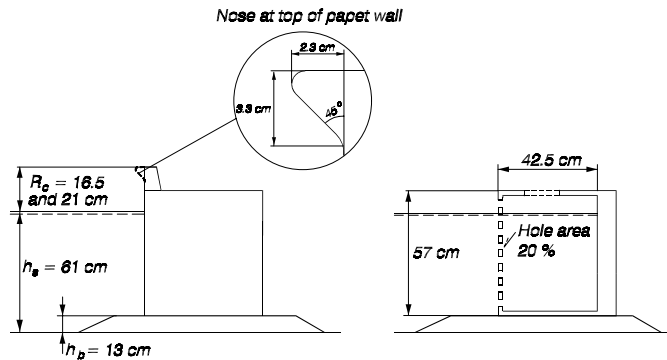
$$\frac{q}{\sqrt{gH_s^3}} = 0.082 \exp\left(-3.0 \frac{R_c}{H_s} \frac{1}{\gamma_\beta \gamma_s}\right) \quad (\text{VI-5-28})$$

Uncertainty: Standard deviation of factor 3.0 = 0.26 (see Figure VI-5-16).

Tested range:

- $H_s = 12.5 - 14.0$ cm
- $s_{op} = 0.04$ (wave steepness)
- $\beta = 0^\circ - 60^\circ$ (angle of incidence)
- $\sigma = \text{app. } 22^\circ \text{ and app. } 28^\circ$ (directional spreading)
- $R_c/H_s = 1.2 \text{ and } 1.6$
- $h_s/H_s = \text{app. } 4.4$
- $h_b/h_s = 0.21$

Tested cross sections:



$$\gamma_\beta = \begin{cases} \left. \begin{array}{l} \cos \beta \text{ for } 0^\circ \leq \beta \leq 37^\circ \\ 0.79 \text{ for } \beta > 37^\circ \end{array} \right\} \text{ Long-crested waves} \\ \left. \begin{array}{l} 0.83 \text{ for } 0^\circ \leq \beta \leq 20^\circ \\ 0.83 \cos(20^\circ - \beta) \text{ for } \beta > 20^\circ \end{array} \right\} \begin{array}{l} \text{Short-crested waves} \\ \sigma = 22^\circ \text{ and } 28^\circ \end{array} \end{cases} \quad (\text{VI-5-29})$$

Front geometry	γ_s
Plain impermeable wall	1.00
Plain impermeable wall with recurved nose	0.78
Perforated front (20% hole area) and deck	0.72 - 0.79
Perforated front (20% hole area) and open deck	0.58

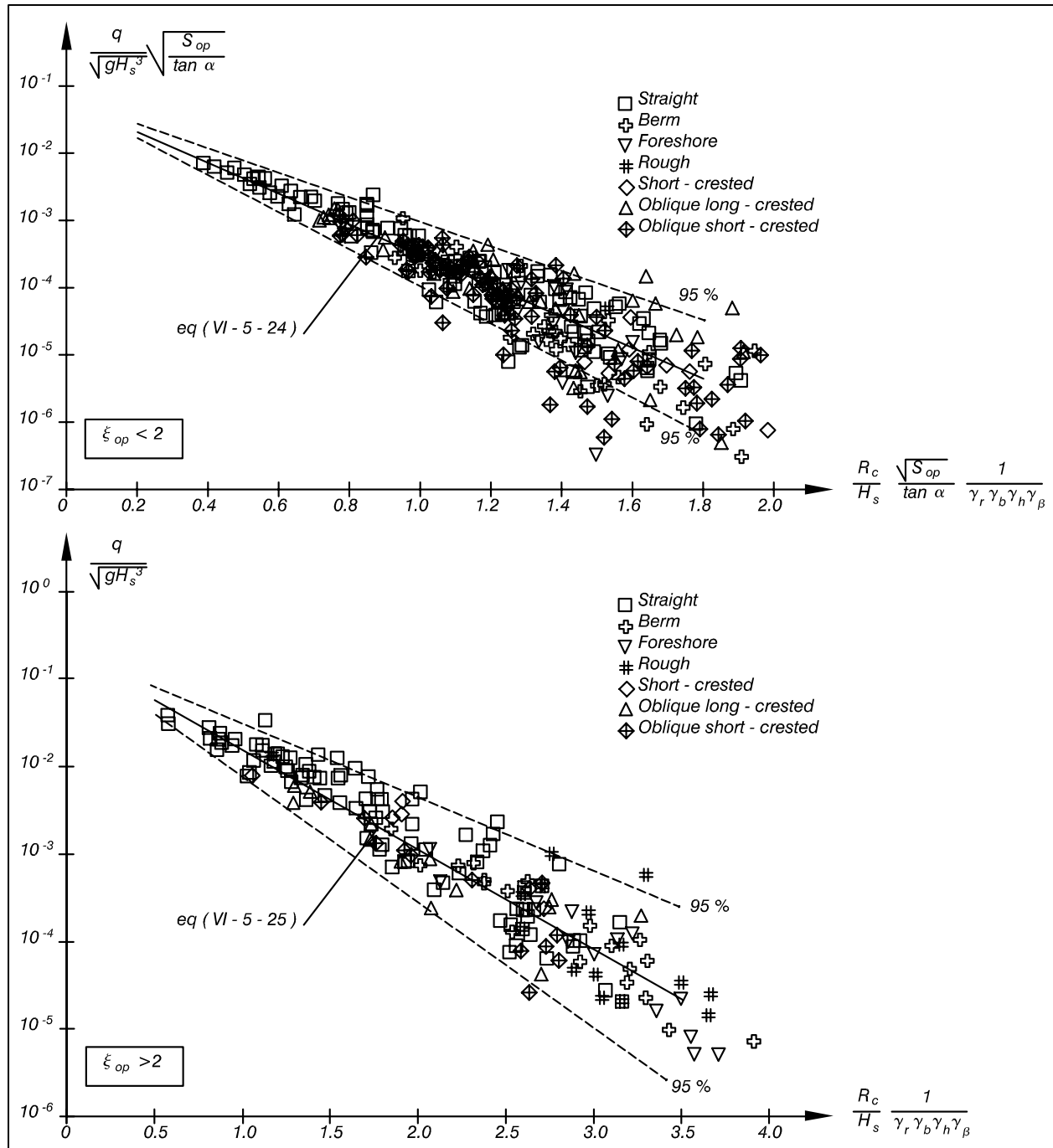


Figure VI-5-15. Wave overtopping data as basis for Equations VI-5-24 and VI-5-25. Fitted mean and 95 percent confidence bands (van der Meer and Janssen 1995)

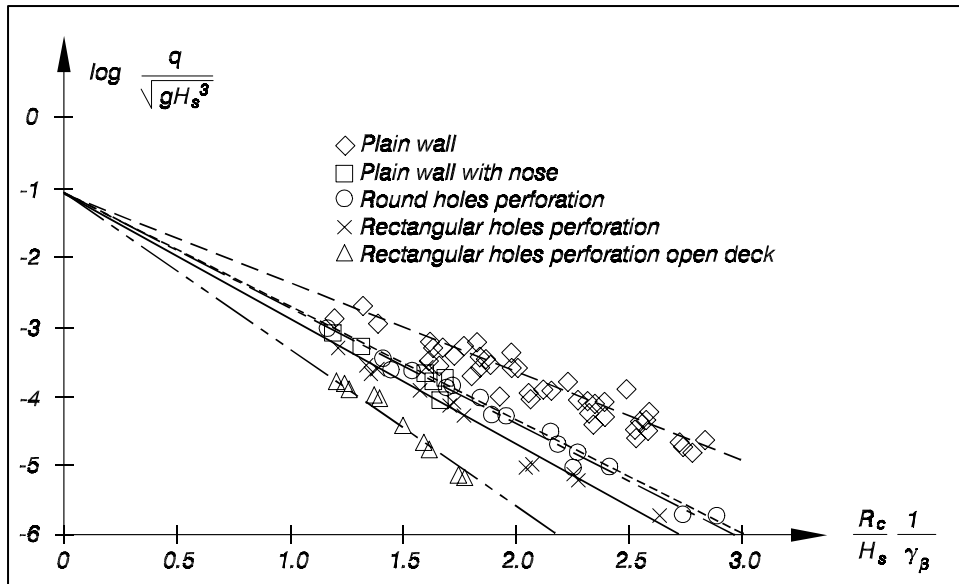


Figure VI-5-16. Vertical wall wave overtopping data plotted with $\gamma_s = 1.0$ (Franco and Franco 1999)

- Figure VI-5-17 shows the same vertical wall overtopping data plotted with appropriate values of γ_β and γ_s from Table VI-5-13. The solid line is Equation VI-5-28.

(3) Overtopping volumes of individual waves. The average overtopping discharge q provides no information about the discharge intensity of the individual overtopping waves. However, such information is important because most damaging impacts on persons, vehicles, and structures are caused by overtopping of large single waves. The overtopping volume per wave has been recorded in model tests and it was found that the probability distribution function for overtopping volume per wave per unit width ($V \text{ m}^3/\text{m}$) follows a Weibull distribution as given in Equation VI-5-30 (Franco, de Gerloni, and van der Meer 1994; van der Meer and Jansson 1995).

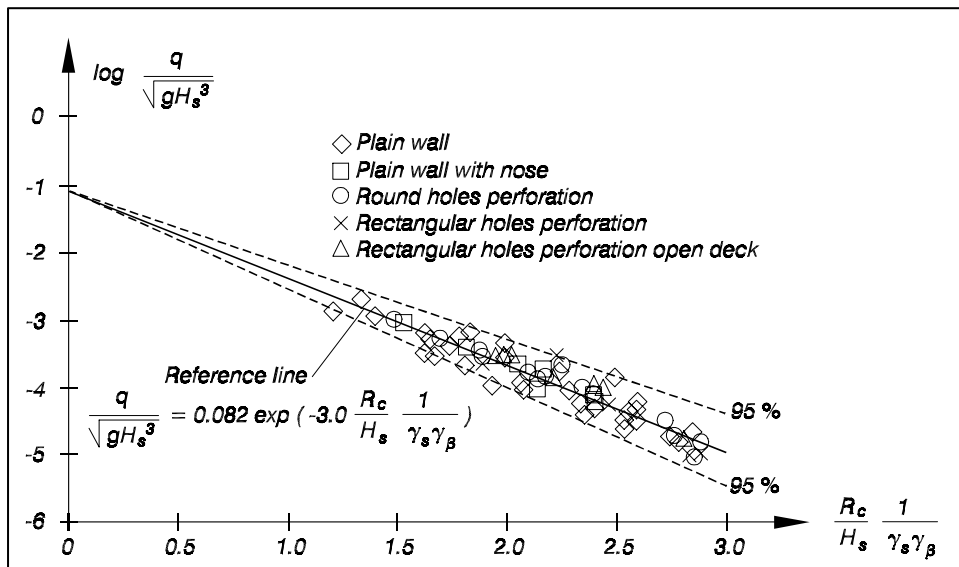


Figure VI-5-17. Vertical wall wave overtopping data with fitted mean and 95 percent confidence bands (Franco and Franco 1999)

$$prob(v > V) = \exp \left[- \left(\frac{V}{B} \right)^{3/4} \right] \text{ or} \quad (VI-5-30)$$

$$V = B \left(-\ln[prob(v > V)] \right)^{4/3} \quad (VI-5-31)$$

with

$$B = 0.84 \frac{T_m q}{P_{ow}} \quad (VI-5-32)$$

where

$prob(v > V)$ = probability of individual wave overtopping volume per unit width, v , being larger than the specified overtopping volume per unit width, V

T_m = average wave period (in units of seconds)

q = average overtopping discharge per unit width (in units of m^3/s per m)

P_{ow} = probability of overtopping per incoming wave (= N_{ow} / N_w)

N_{ow} = number of overtopping waves

N_w = number of incoming waves

If the runup levels follow a Rayleigh distribution, the probability of overtopping per incoming wave can be estimated as

$$P_{ow} = \exp \left[- \left(\frac{R_c}{cH_s} \right)^2 \right] \quad (VI-5-33)$$

where

For sloping structure, irregular waves:

$c = 0.81 \xi_{eq} \gamma_r \gamma_h \gamma_\beta$ with a maximum of $c = 1.62 \gamma_r \gamma_h \gamma_\beta$

For vertical wall structure, irregular, impermeable,
long-crested, nonbreaking, head-on waves:

$c = 0.91$

(VI-5-34)

and

R_c = structure crest height relative to swl

H_s = significant wave height

A first estimate of the maximum overtopping volume per unit width produced by one wave out of the total number of overtopping waves can be calculated using the expression

$$V_{\max} = B(\ln N_{ow})^{4/3} \quad (\text{VI-5-35})$$

c. *Wave reflection.*

(1) Introduction.

(a) Coastal structures reflect some proportion of the incident wave energy. If reflection is significant, the interaction of incident and reflected waves can create an extremely confused sea with very steep waves that often are breaking. This is a difficult problem for many harbor entrance areas where steep waves can cause considerable maneuvering problems for smaller vessels. Strong reflection also increases the sea bed erosion potential in front of protective structures. Waves reflected from some coastal structures may contribute to erosion of adjacent beaches.

(b) Non-overtopped impermeable smooth vertical walls reflect almost all the incident wave energy, whereas permeable, mild slope, rubble-mound structures absorb a significant portion of the energy. Structures that absorb wave energy are well suited for use in harbor basins.

(c) In general incident wave energy can be partly dissipated by wave breaking, surface roughness and porous flow; partly transmitted into harbor basins due to wave overtopping and penetration; and partly reflected back to the sea, i.e.

$$E_i = E_d + E_t + E_r \quad (\text{VI-5-36})$$

where E_i , E_d , E_t , and E_r are incident, dissipated, transmitted, and reflected energy, respectively.

(d) Reflection can be quantified by the bulk reflection coefficient

$$C_r = \frac{H_{sr}}{H_s} = \left(\frac{E_r}{E_i} \right)^{1/2} \quad (\text{VI-5-37})$$

where H_s and H_{sr} are the significant wave heights of incident and reflected waves, respectively, at that position; and E_i and E_r are the related wave energies.

(2) Reflection from non-overtopped sloping structures.

(a) Very long waves such as infragravity and tidal waves are almost fully reflected by any type of impervious structure. Wind-generated waves generally break on slopes (see Table VI-5-1) with the type of wave breaking given as a function of the surf-similarity parameter ζ , defined by Equation VI-5-2. Wave energy dissipation by wave breaking is much greater than dissipation due to surface roughness and porous flow for conventional coastal structures. Therefore, it is relevant to relate the bulk reflection coefficient, C_r , to ζ , (Battjes 1974b; Seelig 1983).

(b) The bulk reflection coefficient for straight non-overtopped impermeable smooth slopes and conventional rubble-mound breakwaters can be estimated from Equation VI-5-38 (Seelig 1983) given in Table VI-5-14. Figure VI-5-18 shows the fitting of the model test results by Allsop and Hettiarachichi (1988). Some scatter in the fitting can be seen.

Table VI-5-14
Wave Reflection coefficients for Non-Overtopped Sloping Structures Based on Seelig (1983) Equation

Head-on waves

$$C_r = \frac{a \xi^2}{(b + \xi^2)} \quad \xi = \frac{\tan \alpha}{\sqrt{\frac{2\pi H}{gT^2}}} \quad (\text{VI-5-38})$$

For irregular wave H is replaced by H_s , T is replaced either by T_p (ξ_{op}) or T_m (ξ_{om}).

Fitted coefficients in Eq VI-5-38

Author	Structure	a	b
Seelig (1983) $2.5 \leq \xi \leq 6$	Impermeable, smooth, straight slopes, regular waves	1.0	5.5
Allsop and Hettiarachchi (1988) range of ξ or ξ_{op} shown in Figure VI-5-18	Dolosse, regular waves (ξ) Slope 1:1.5, 1:2, 1:3	0.56	10.0
	Cobs, regular waves (ξ) Slope 1:1.5, 1:2, 1:3	0.50	6.54
	Tetrapods and Stabit, irregular waves (ξ_{om}) Slope 1:1.33, 1:1.5, 1:2	0.48	9.62
	Shed and Diode, irregular waves (ξ_{om}) Slope 1:1.33, 1:1.5, 1:2	0.49	7.94
Allsop (1990) $3 \leq \xi_{om} \leq 6$	Smooth and impermeable	0.96	4.8
	1 layer rock and stone underlayer on impermeable slope (P=1)	0.64	7.22
	2 layer rock and stone underlayer on impermeable slope (P=1)	0.64	8.85
Benoit and Teisson (1994) $2.7 \leq \xi_{op} \leq 7$	2 layer rock armor $H_s : 0.03 - 0.09m$, $T_p = 1.3s$, $d = 0.4m$ Slope 1:1.33, 1:1.5, 1:2	0.6	6.6
Davidson, et al (1994) $8 \leq \xi_{op} \leq 50$	Field measurement on rock slope 1:1.1 Water depth h in meters		
	$h > 3.25$	0.65	25
	$2.5 \leq h \leq 3.25$	0.60	35
	$h < 2.5$	0.64	80

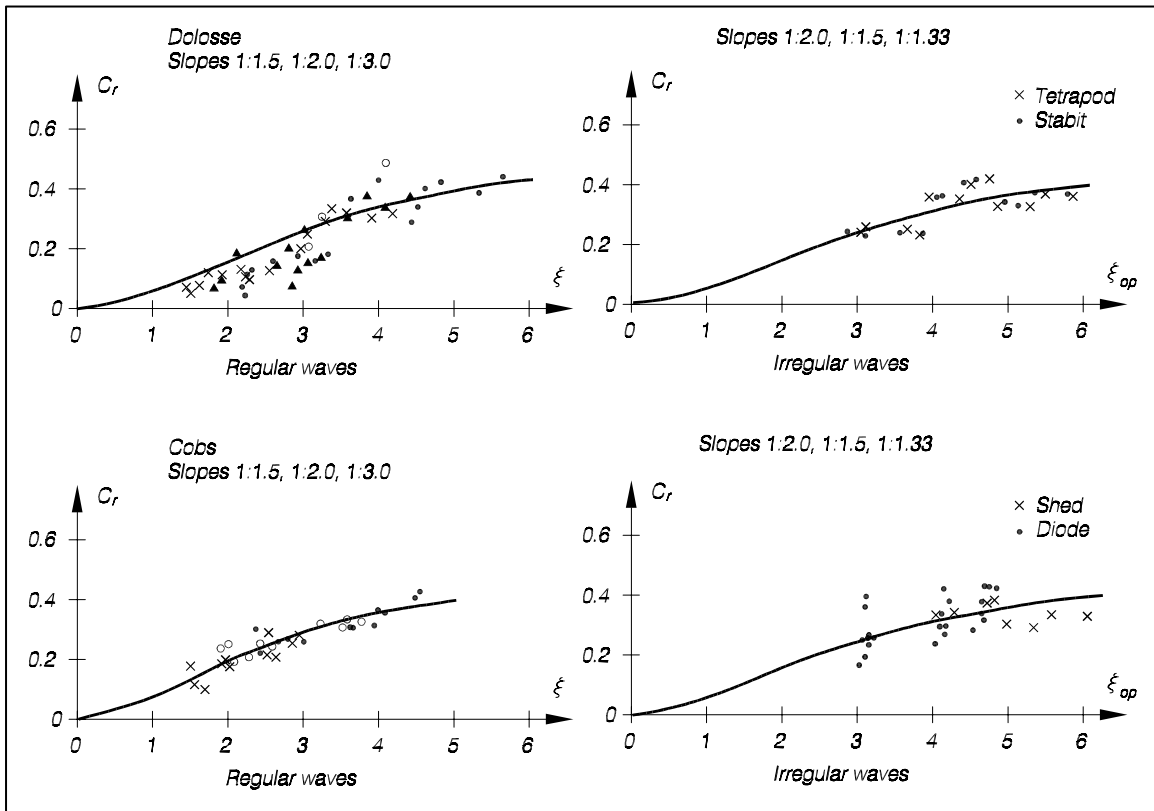


Figure VI-5-18. Reflection coefficients for concrete armor unit slopes. Head-on waves (Allsop and Hettiarachchi 1988)

(c) An alternative formula to Equation VI-5-38 was given by Postma (1989), who analyzed van der Meer's (1988) reflection data (see Table VI-5-4) for non-overtopped rock slopes. Postma introduced the notational permeability P (shown on Figure VI-5-11), the slope angle α and the wave steepness s_{op} in the formula

$$C_r = 0.071(P)^{-0.082} (\cot \alpha)^{-0.62} (s_{op})^{-0.46} \quad (\text{VI-5-39})$$

(d) The uncertainty of Equation VI-5-39 corresponds to a variational coefficient of 0.036.

(e) The effect of a berm in a slope is generally a reduction in C_r . Figure VI-5-19 shows C_r values for a rubble-mound structure with berms of varying width at SWL (Allsop 1990).

(3) Reflection from vertical walls.

(a) Bulk reflection coefficients for plain vertical breakwaters on seabed, for plain vertical breakwaters on rubble foundation, for horizontal composite breakwaters, for sloping top caissons, for single perforated screens, and for perforated caissons are given in Figures VI-5-20, VI-5-21, VI-5-22, VI-5-23, VI-5-24, and VI-5-25, respectively. They were obtained from scaled model tests with irregular, head-on waves. The effect of oblique waves and wave shortcrestedness on plain and perforated vertical wall caissons is shown in Figure VI-5-26.

(b) The influence of wave shortcrestedness and oblique wave approach on reflection from plain impermeable and perforated vertical caissons is illustrated by Figure VI-5-26.

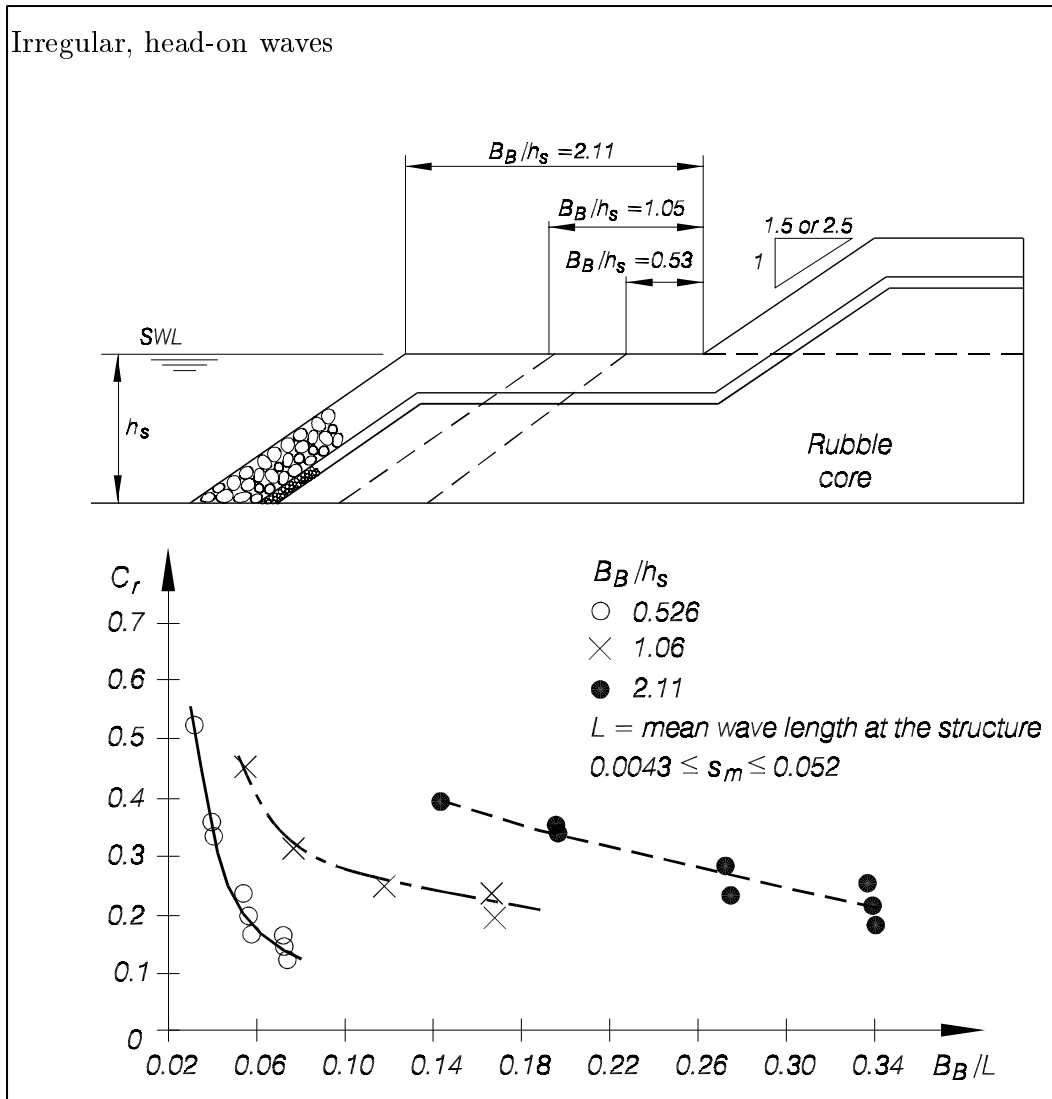


Figure VI-5-19. Wave reflection coefficients for rock armored slope with berm at SWL (Allsop 1990)

(4) Kinematics of reflected irregular waves.

(a) Close to highly reflective coastal structures incident and reflected waves interact with some degree of “phase locking.” This result is a partially standing wave field characterized by nodes and antinodes. For the extreme case of perfectly reflected regular waves, a standing wave field occurs with stationary nodes and antinodes. Reflecting irregular waves create a less noticeable spatial variation of partially standing nodes and antinodes that decrease in magnitude with distance from the structure.

(b) Assuming that the sea surface is comprised of a large number of linear wave trains that can be superimposed, the sea surface elevation adjacent to a reflective structure can be written as

$$\eta = \sum_{i=1}^{\infty} a_i \sqrt{1 + C_{ri}^2 + 2C_{ri} \cos(2k_i x + \theta_i)} \cos(\sigma_i t - \varepsilon_i) \quad (\text{VI-5-42})$$

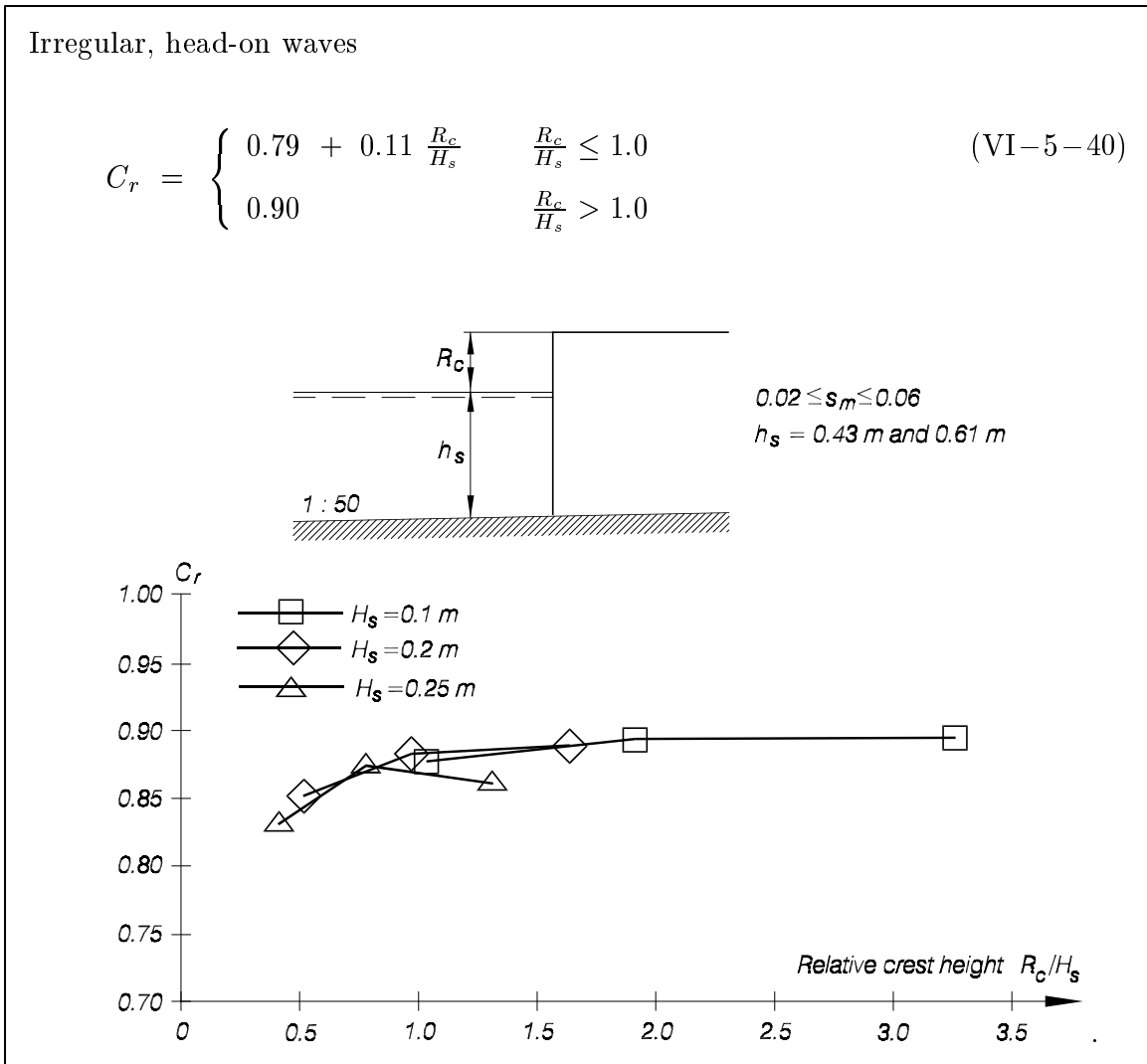


Figure VI-5-20. Wave reflection coefficients for plain vertical breakwater on 1:50 seabed (Allsop, McBride, and Columbo 1994)

and the horizontal component of the wave orbital velocity is given as

$$u = \sum_{i=1}^{\infty} a_i \left(\frac{gk_i}{\sigma_i} \right) \frac{\cosh[k_i(h+z)]}{\cosh(k_i h)} \sqrt{1 + C_{ri}^2 - 2C_{ri} \cos(2k_i x + \theta_i)} \cos(\sigma_i t - \varepsilon_i) \quad (\text{VI-5-43})$$

where

a_i = amplitude of i th incident wave component

k_i = wave number of i th incident wave component

σ_i = angular wave frequency of the i th incident wave component

g = gravitational acceleration

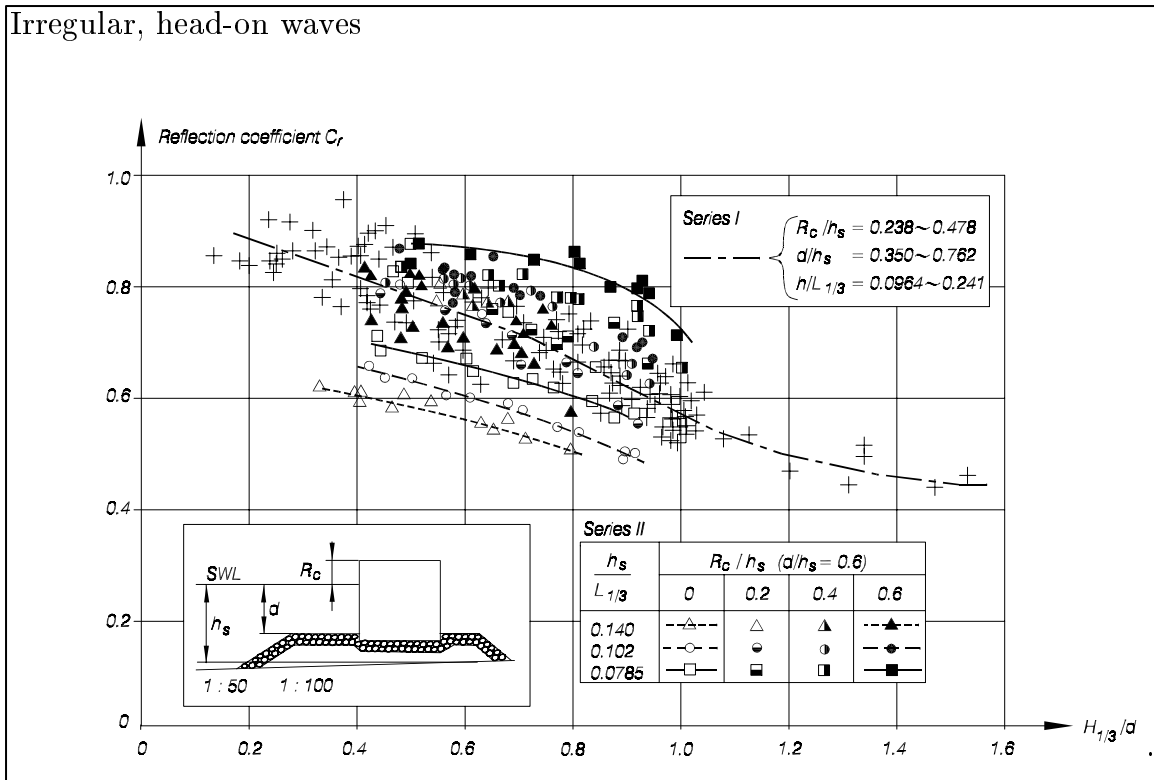


Figure VI-5-21. Wave reflection coefficients for plain vertical breakwater on rubble-mound foundation (Tanimoto, Takahashi, and Kimura 1987)

h = water depth

x = horizontal coordinate with positive toward the structure and $x=0$ located at the structure toe

z = vertical coordinate with $z=0$ at swl and $z=-h$ at bottom

C_{ri} = reflection coefficient of i th incident wave component

θ_i = reflection phase angle of i th incident wave component

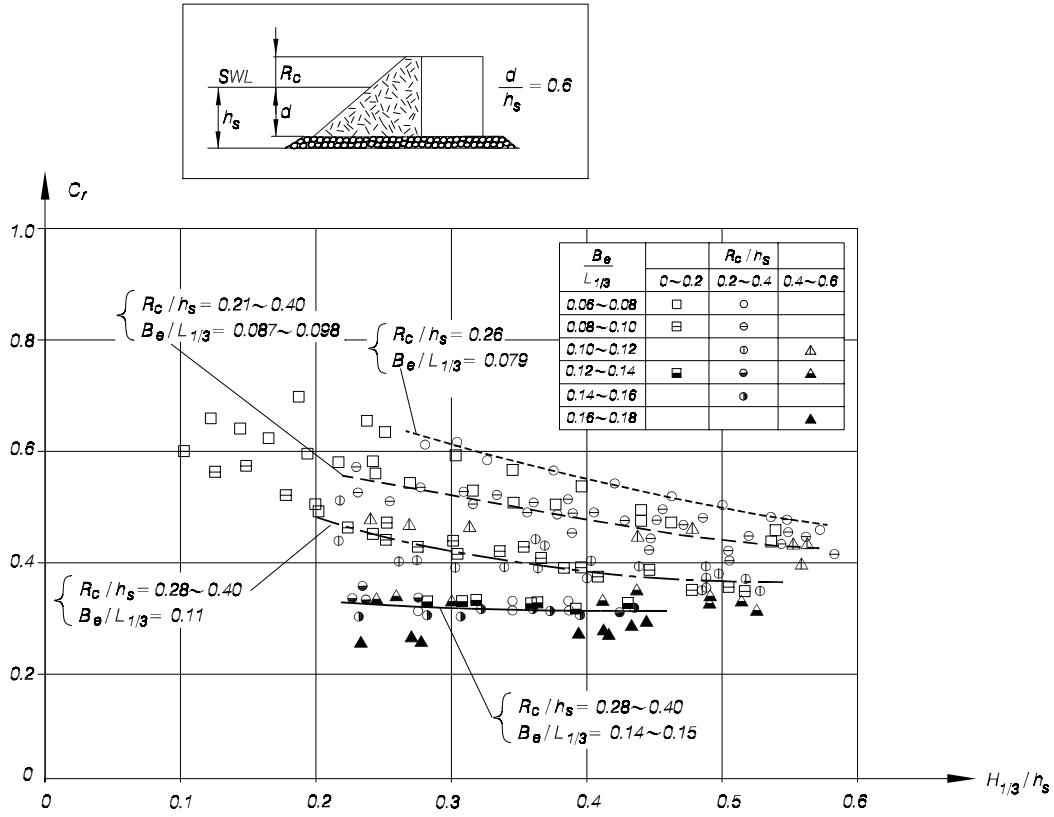
ε_i = random wave phase angle of i th incident wave component

(c) These two equations strictly apply to the case of two-dimensional, nonbreaking, irregular waves propagating over a flat bottom and approaching normal to reflective structures. Similar expressions can be written for the case of oblique reflection of irregular, long-crested waves.

(d) The corresponding equation for estimating the root-mean-squared sea surface elevations is (Goda and Suzuki 1976)

$$\eta_{rms}^2 = \sum_{i=1}^{\infty} \left[1 + C_{ri}^2 + 2C_{ri} \cos(2k_i x + \theta_i) \right] \frac{a_i^2}{2} \quad (\text{VI-5-44})$$

Irregular, head-on waves



$$B_e = b_0 - \left(\frac{\cot \alpha}{h_s + R_c} \right) \left(\int_{-d}^{R_c} \frac{\cosh^2 2\pi(h_s + z)/L}{\cosh^2 2\pi h_s/L} z dz + 0.5R_c^2 \right) \quad (\text{VI-5-41})$$

where b_0 covering width at the still water level
 α slope angle of the structure measured from horizontal
 z upward distance away from the still water level

Figure VI-5-22. Wave reflection coefficients for horizontal composite breakwaters with tetrapod slope 1:1.5 (Tanimoto, Takahashi, and Kimura 1987)

and the root-mean-squared horizontal wave velocity is (Hughes 1992)

$$u_{rms}^2 = \sum_{i=1}^{\infty} \left(\frac{gk_i}{\sigma_i} \right) \frac{\cosh^2 [k_i(h+z)]}{\cosh^2(k_i h)} \left[1 + C_{ri}^2 - 2C_{ri} \cos(2k_i x + \theta_i) \right] \frac{a_i^2}{2} \quad (\text{VI-5-45})$$

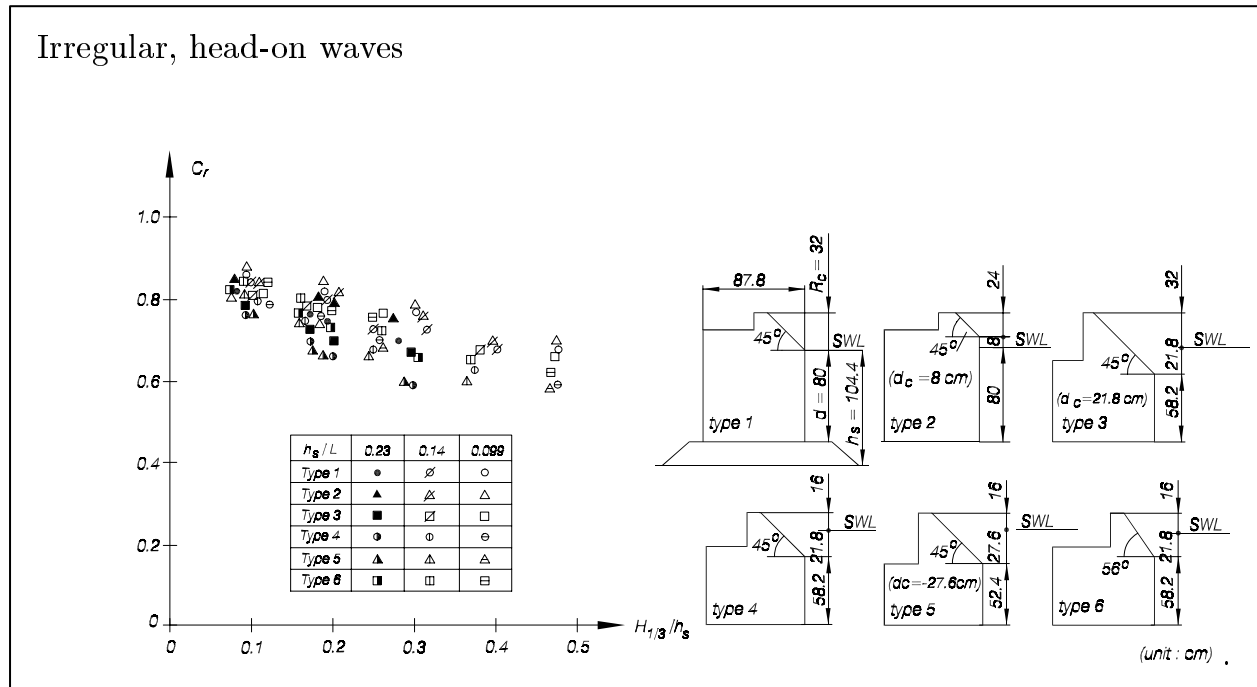


Figure VI-5-23. Wave reflection coefficients for sloping top breakwaters (Takahashi 1996)

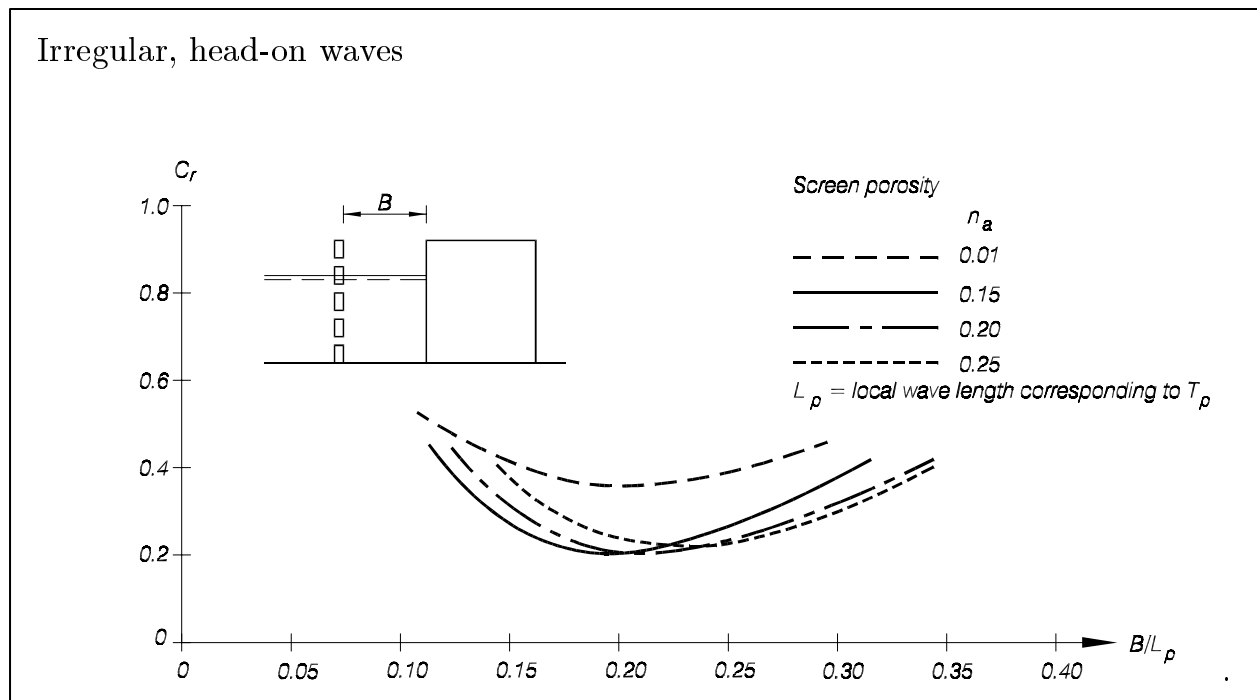


Figure VI-5-24. Wave reflection coefficients for perforated caissons (Allsop and Hettiarachchi 1988)

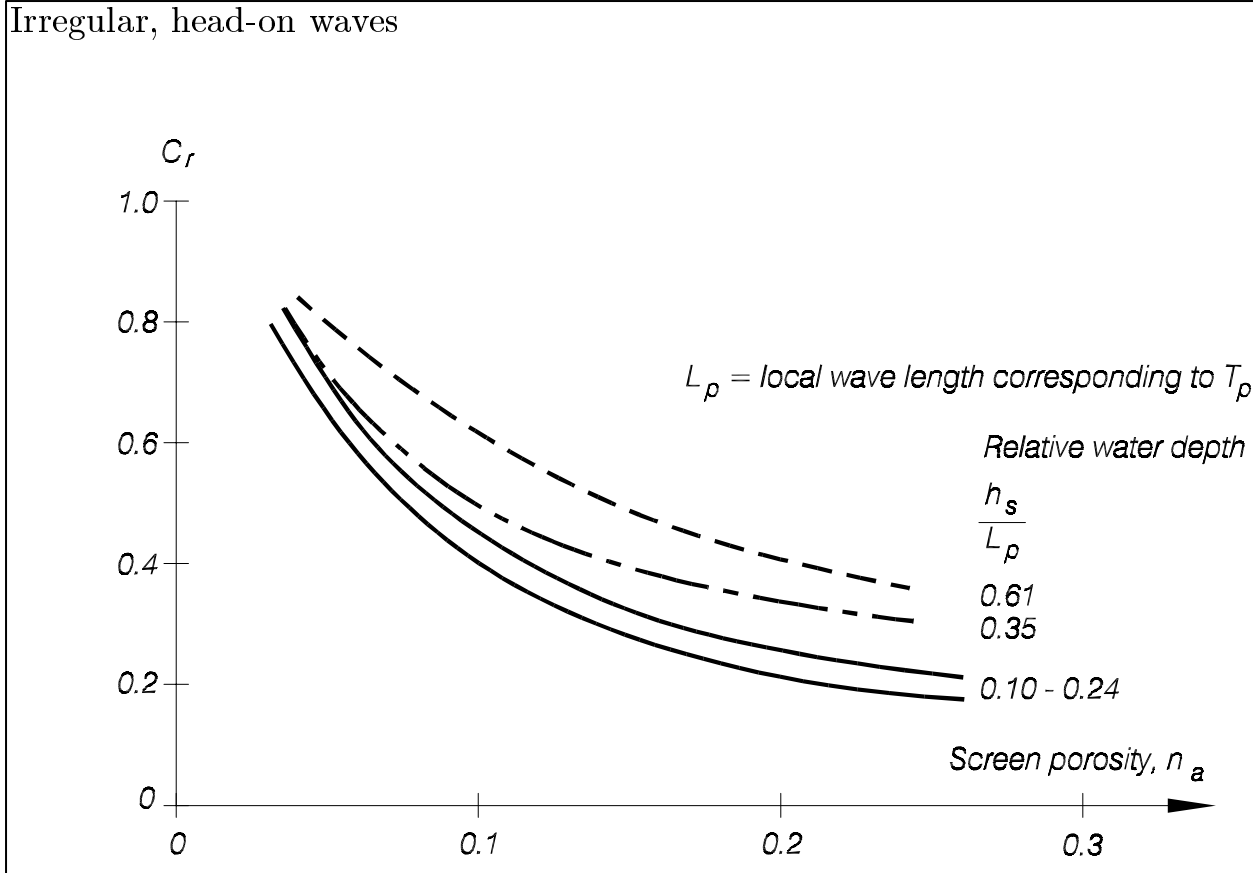


Figure VI-5-25. Wave reflection coefficients for single perforated screen (Allsop and Hettiarachchi 1988)

(e) The root-mean-squared sea surface elevations and horizontal velocities are functions of the incident wave spectrum (a_i, k_i, σ_i), water depth (h), location in the water column relative to the structure toe (x, z), and the reflection coefficient (C_{ri}) and reflection phase angle (θ_i) associated with each wave component in the incident spectrum.

(f) For impermeable vertical walls the reflection coefficient C_{ri} is equal to unity for all wave components and the reflection phase shift is $\theta_i = 0, 2\pi, 4\pi, \dots$. However, for sloping structures reflection is less than perfect, and it is necessary to estimate the reflection coefficient and phase angle as functions of wave component frequency.

(g) Empirical expressions for θ_i and C_{ri} for sloping impermeable and rubble-mound structures have been developed based on laboratory experiments (Hughes and Fowler 1995; Sutherland and O'Donoghue 1998a; Sutherland and O'Donoghue 1998b). The reflection phase for each incident wave component can be estimated from the following expression presented by Sutherland and O'Donoghue (1998a)

$$\theta_i = -8.84\pi\chi^{5/4} \quad (\text{VI-5-46})$$

where

$$\chi = \frac{\sigma_i}{2\pi \tan \alpha} \sqrt{\frac{d_t}{g}} \quad (\text{VI-5-47})$$

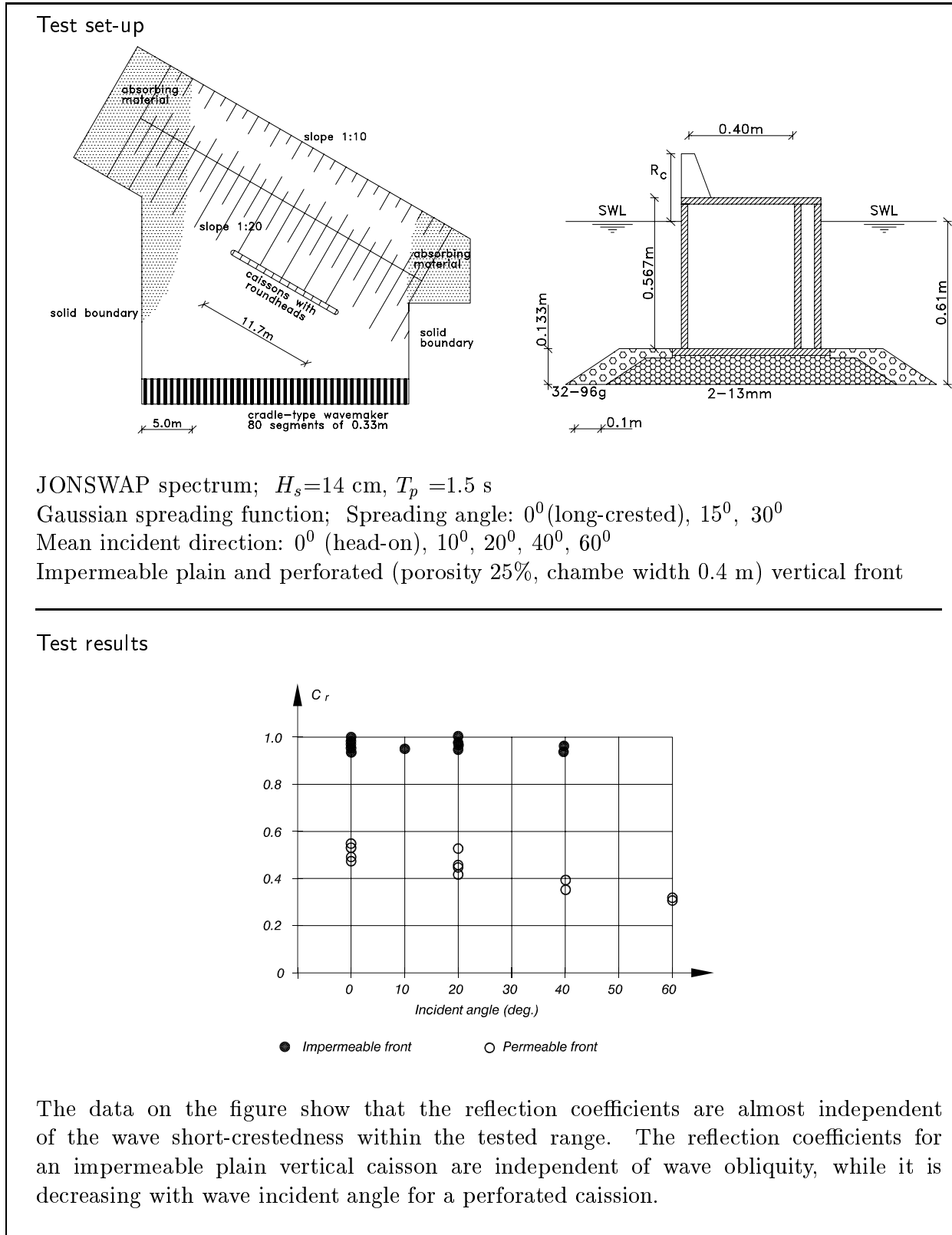


Figure VI-5-26. Wave reflection coefficients for impermeable and permeable vertical breakwaters exposed to oblique, nonbreaking, short-crested waves (Helm-Petersen 1998)

and

d_t = depth at the toe of the sloping structure

α = structure slope

The reflection coefficient for each incident wave component is estimated from recent results of Sutherland and O'Donoghue (1998b) by the empirical expressions

$$C_{ri} = \frac{\xi_{\sigma}^{2.58}}{7.64 + \xi_{\sigma}^{2.58}} \text{ for smooth impermeable slopes} \quad (\text{VI-5-48})$$

$$C_{ri} = \frac{0.82\xi_{\sigma}^2}{22.85 + \xi_{\sigma}^2} \text{ for rubble-mound slopes} \quad (\text{VI-5-49})$$

where

$$\xi_{\sigma} = \frac{\tan \alpha}{\sigma_i} \sqrt{\frac{2\pi g}{H_s}} \quad (\text{VI-5-50})$$

and H_s is the significant wave height of the incident spectrum.

Figure VI-5-27 compares measured data to estimates of u_{rms} at middepth adjacent to a smooth, impermeable laboratory structure on a 1:2 slope. The estimates were made using the measured incident wave spectrum.

Sutherland and O'Donoghue (1997) showed that the two-dimensional expression for root-mean-square velocity can be extended to include the case of obliquely incident, long-crested waves.

d. Wave transmission.

(1) Introduction.

(a) Wave action behind a structure can be caused by wave overtopping and also by wave penetration if the structure is permeable. Waves generated by the falling water from overtopping tend to have shorter periods than the incident waves. Generally the transmitted wave periods are about half that of the incident waves.

(b) Wave transmission can be characterized by a transmission coefficient, C_t , defined either as the ratio of transmitted to incident characteristic wave heights (e.g., H_{st} and H_s) or as the square root of the ratio of transmitted to incident time-averaged wave energy (e.g., E_t and E_i) as given in Equation VI-5-51.

$$C_t = \frac{H_{st}}{H_s} = \left(\frac{E_t}{E_i} \right)^{1/2} \quad (\text{VI-5-51})$$

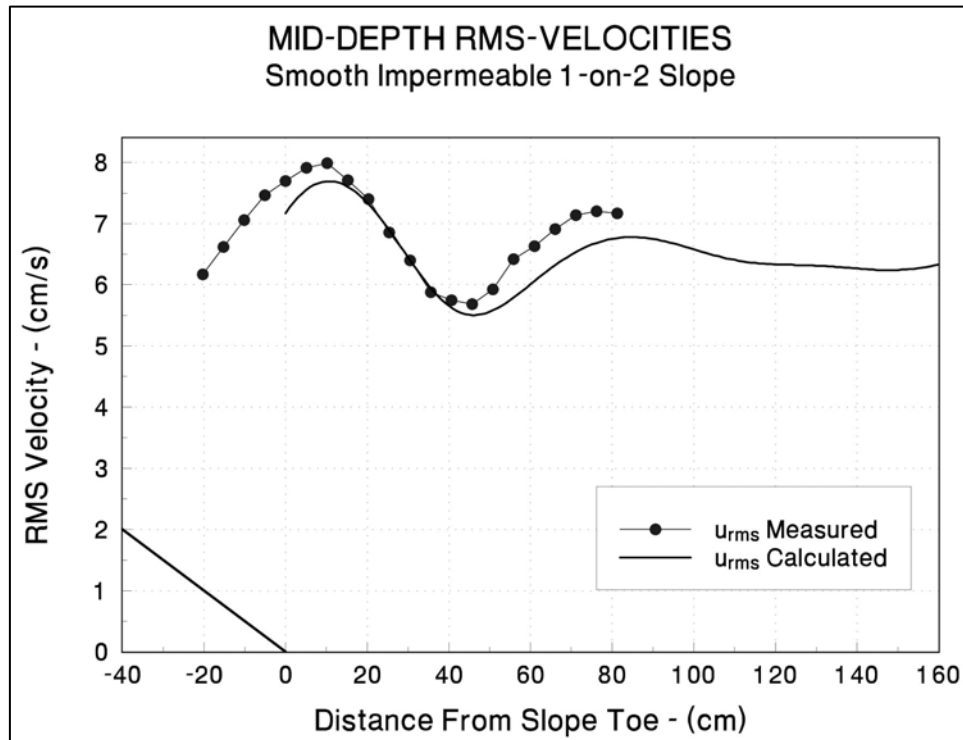


Figure VI-5-27. Measured versus estimated u_{rms} near smooth, impermeable 1:2 slope (Hughes and Fowler 1995)

(c) Specific transmission coefficients for wave overtopping (C_{to}) and wave penetration (C_{tp}) could be defined as follows

$$C_{to} = \frac{H_{st}^{overtop}}{H_s} \quad (VI-5-52)$$

$$C_{tp} = \frac{H_{st}^{penetr.}}{H_s} \quad (VI-5-53)$$

(d) However, in practice it is difficult to distinguish between $H_{st}^{overtop}$ and $H_{st}^{penetr.}$, and consequently, usual practice is to calculate C_t as defined by Equation VI-5-51.

(e) Values of C_t given in the literature are almost all from laboratory experiments, many of which were conducted at rather small scales. Some scale effects might have influenced the results, especially for the proportion of C_t related to wave penetration.

(2) Wave transmission through and over sloping structures.

(a) The total coefficient of wave transmission, C_t , for rock armored low-crested and submerged breakwaters, and reef breakwaters under irregular head-on waves are given in Figure VI-5-28 and Table VI-5-15.

(b) Figure VI-5-29 shows an example of the use of Equation VI-5-54.

Irregular, head-on waves

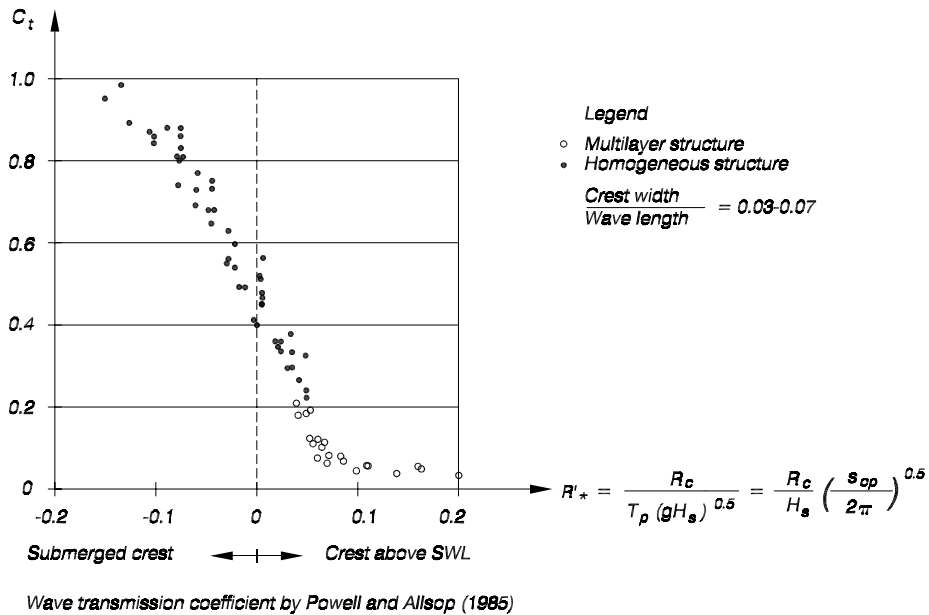
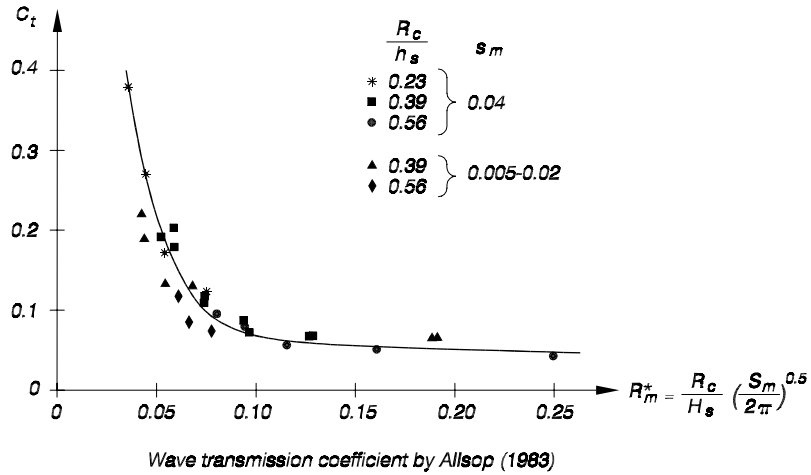
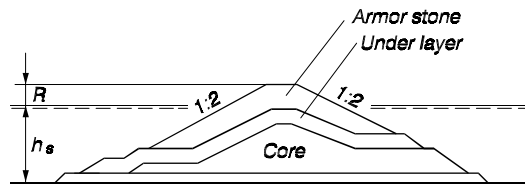


Figure VI-5-28. Wave transmission diagram by Allsop (1983) and Powell and Allsop (1985)

Table VI-5-15
Wave Transmission Formula by van der Meer and d'Angremond (1991) for Rock Armored Low-crested, Submerged, and Reef Breakwaters

Conventional rock armored low-crested breakwaters with their crests above and below still water level, and reef breakwaters, i.e., a homogenous rock structure without filter layers and core. Irregular, head-on waves.

$$C_t = \left(0.031 \frac{H_s}{D_{n50}} - 0.24 \right) \frac{R_c}{D_{n50}} + b \quad (\text{VI-5-54})$$

maximum $C_t = 0.75$, minimum $C_t = 0.075$ conventional structure
maximum $C_t = 0.60$, minimum $C_t = 0.15$ reef type structure

where

$$b = \begin{cases} -5.42 s_{op} + 0.0323 \frac{H_s}{D_{n50}} - 0.0017 \left(\frac{B}{D_{n50}} \right)^{1.84} + 0.51 & \text{conventional structure} \\ -2.6 s_{op} - 0.05 \frac{H_s}{D_{n50}} + 0.85 & \text{reef type structure} \end{cases}$$

H_s – significant wave height of incident waves

D_{n50} – median of nominal diameter of rocks for design conditions

R_c – freeboard, negative for submerged breakwater

B – width of the crest

s_{op} – deepwater wave steepness corresponding to peak period.

The maximum and minimum limits of C_t must be interpreted as the valid ranges of Equation VI-5-54 and not as general limits since it is obvious that C_t can exceed these limits when the crest is deeply submerged. For example when the crest is deeply submerged ($R_c/D_{n50} < -6$) then C_t becomes close to unity.

The formula is based on model test results of Seelig (1980), Powell and Allsop (1985), Daemrich and Kahle (1985), Ahrens (1987), van der Meer (1988) and Daemen (1991).

Tested ranges : $1 < \frac{H_s}{D_{n50}} < 6$ $0.01 < s_{op} < 0.05$ $-2 < R_c/D_{n50} < 6$

Comparison between model test results and results calculated by Eq VI-5-54 gives a standard deviation of $\sigma(C_t) = 0.05$ corresponding to the 90% confidence limits given by $C_t \pm 0.08$.

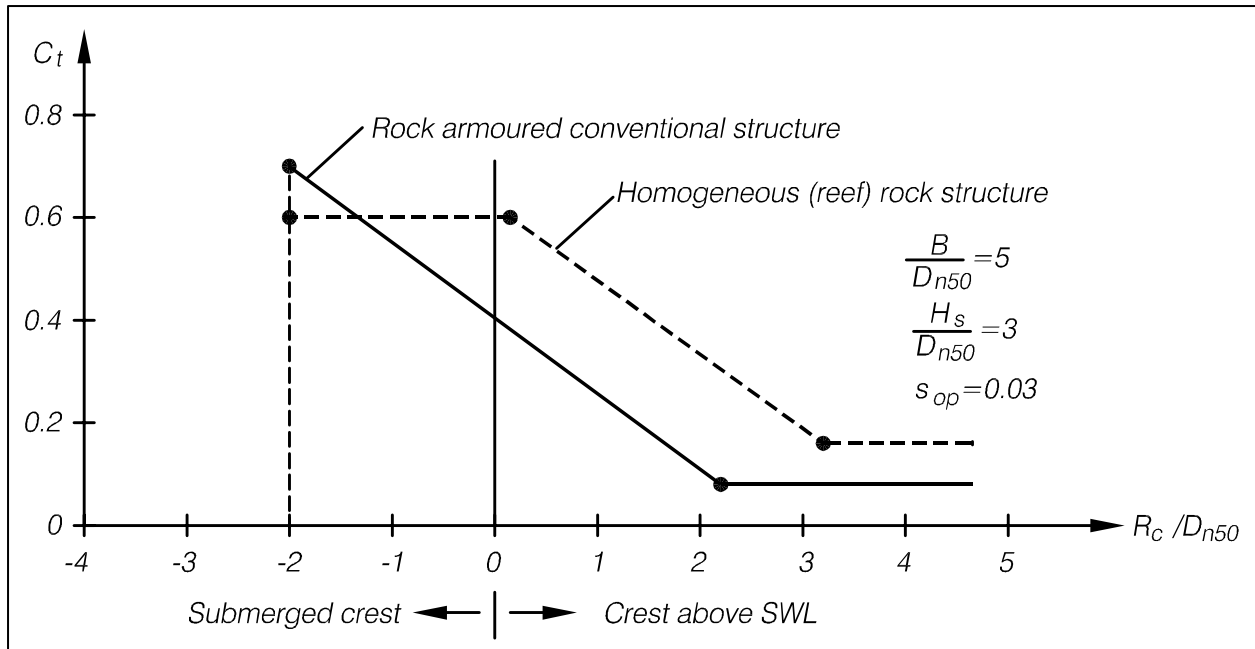


Figure VI-5-29. Example of total wave transmission coefficients, C_t , for conventional and reef type low-crested and submerged breakwaters, calculated from the van der Meer and d'Angremond (1991) formula given by Equation VI-5-54

(c) Breakwaters with complex types of concrete armor units, such as tetrapods or CORE-LOCS® hereafter referred to as Core-Locs, generally have a more permeable crest than rock armored breakwaters, and this results in larger transmission coefficients.

(d) Detached breakwaters for coastal protection are placed in very shallow water and are often built entirely of armor blocks without underlayer and core. Such breakwaters are very permeable and C_{tp} can reach 0.8 in the case of complex armor units and small wave steepnesses.

(3) Wave transmission for vertical structures. Wave transmission for vertical breakwaters is mainly the result of wave overtopping. Therefore the ratio of the breakwater crest height (R_c) to the incident wave height (H_s) is the most important parameter. Wave transmission coefficients for plain vertical breakwaters, horizontal composite breakwaters, sloping top breakwaters and perforated walls are given in Table VI-5-16, Table VI-5-17, Figure VI-5-30, Figure VI-5-31, and Figure VI-5-32, respectively.

VI-5-3. Rubble-Mound Structure Loading and Response

a. Armor layer stability.

(1) Introduction.

(a) Wave forces acting on a rubble-mound slope can cause armor unit movement. This is called hydraulic instability. Breakage of armor units is another type of instability which is discussed in Part VI-5-3c, "Structural integrity of concrete armor units."

(b) Armor unit movements can be rocking, displacement of units out of the armor layer, sliding of a blanket of armor units, and settlement due to compaction of the armor layer. Figure VI-5-33 shows the most typical armor layer failure modes.

Table VI-5-16
Wave Transmission Formula by Goda (1969)

Regular, head-on waves

$$C_t = \begin{cases} \left(0.25 \left(1 - \sin \left(\frac{\pi}{2\alpha} \right) \left(\frac{R_c}{H} + \beta \right) \right)^2 + 0.01 \left(1 - \frac{h_c}{h_s} \right)^2 \right)^{0.5} & \beta - \alpha < \frac{R_c}{H} < \alpha - \beta \\ 0.1 \left(1 - \frac{h_c}{h_s} \right) & \frac{R_c}{H} \geq \alpha - \beta \end{cases} \quad (\text{VI-5-55})$$

$$\alpha = 2.2$$

β is given by the figure

h_c is the vertical distance from water level to the bottom of caissons.

Formula is based on regular wave tests, but can be applied to irregular waves by using H_s for H

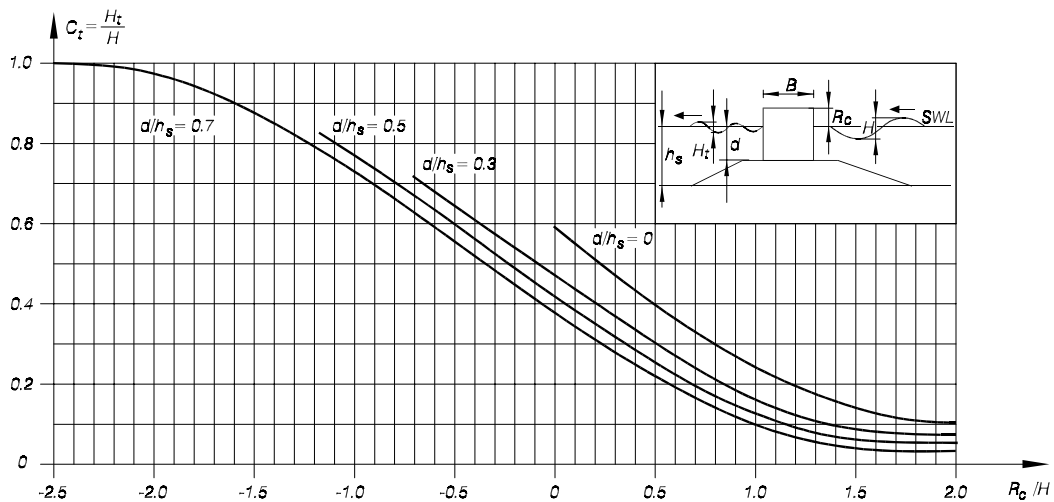
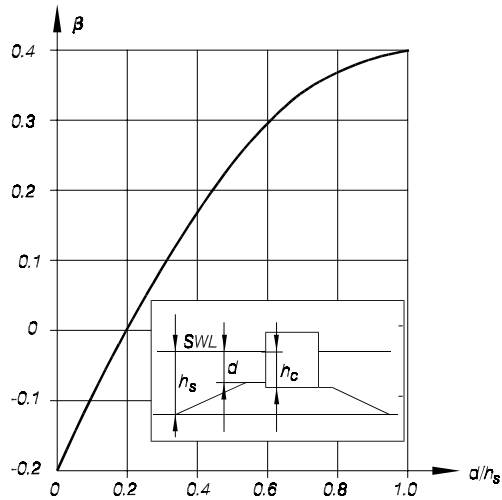


Table VI-5-17
Wave Transmission Formula by Takahashi (1996)

Irregular, head-on and oblique long-crested waves

$$C_t = \left[0.25 \left[\left(1 - \sin \frac{\pi}{4.4} \right) \left(\frac{R_c}{H_{1/3}} + \beta + \beta_s \right) \right]^2 + 0.01 \left(1 - \frac{h_c}{h_s} \right)^2 \right]^{0.5}$$

valid for $\beta + \beta_s - 2.2 < \frac{R_c}{H_{1/3}} < 2.2 - \beta - \beta_s$

(VI-5-56)

$$C_t = 0.1 \left(1 - \frac{h_c}{h_s} \right) \quad \text{valid for } \frac{R_c}{H_{1/3}} \geq 2.2 - \beta - \beta_s$$

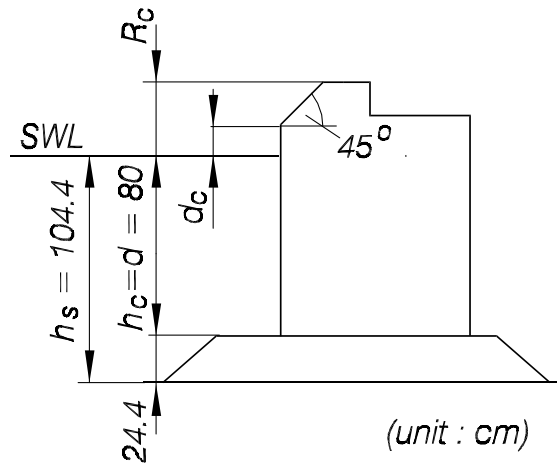
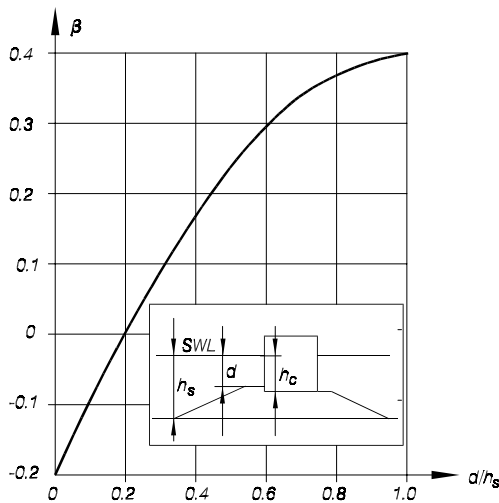
where

$$\beta_s = -0.3 \left[(R_c - 2d_c) / (H_{1/3} \tan \theta) \right]^{0.5}$$

β is given by the figure

d_c is the elevation of the lower edge of the sloping face relative to still-water level, i.e., positive if over SWL and negative if under SWL.

θ is angle of wave incidence with 0° being normal incidence



Irregular, head-on waves

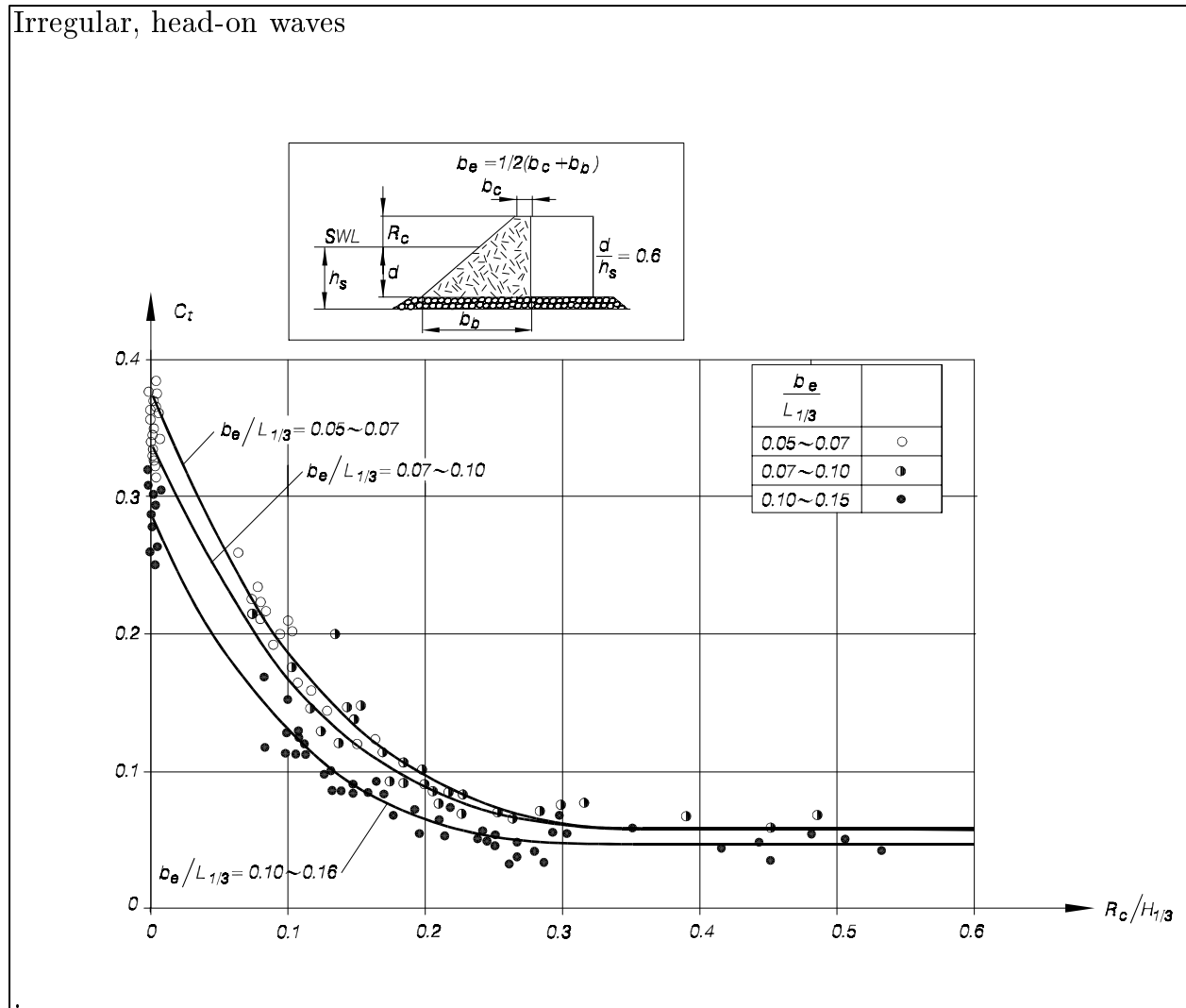


Figure VI-5-30. Wave transmission by overtopping of horizontal composite breakwaters armored with tetrapods (Tanimoto, Takanashi, and Kimura 1987)

(c) The complicated flow of waves impacting armor layers makes it impossible to calculate the flow forces acting on armor units. Moreover, the complex shape of units together with their random placement makes calculation of the reaction forces between adjacent armor units impossible. Consequently, deterministic calculations of the instantaneous armor unit stability conditions cannot be performed, which is why stability formulae are based on hydraulic model tests. The response of the armor units in terms of movements are related directly to parameters of the incident waves, while treating the actual forces as a “black box” transfer function. However, some qualitative considerations of the involved forces can be used to explore the structure of stability formulae.

(2) Stability parameters and structure of stability formulae.

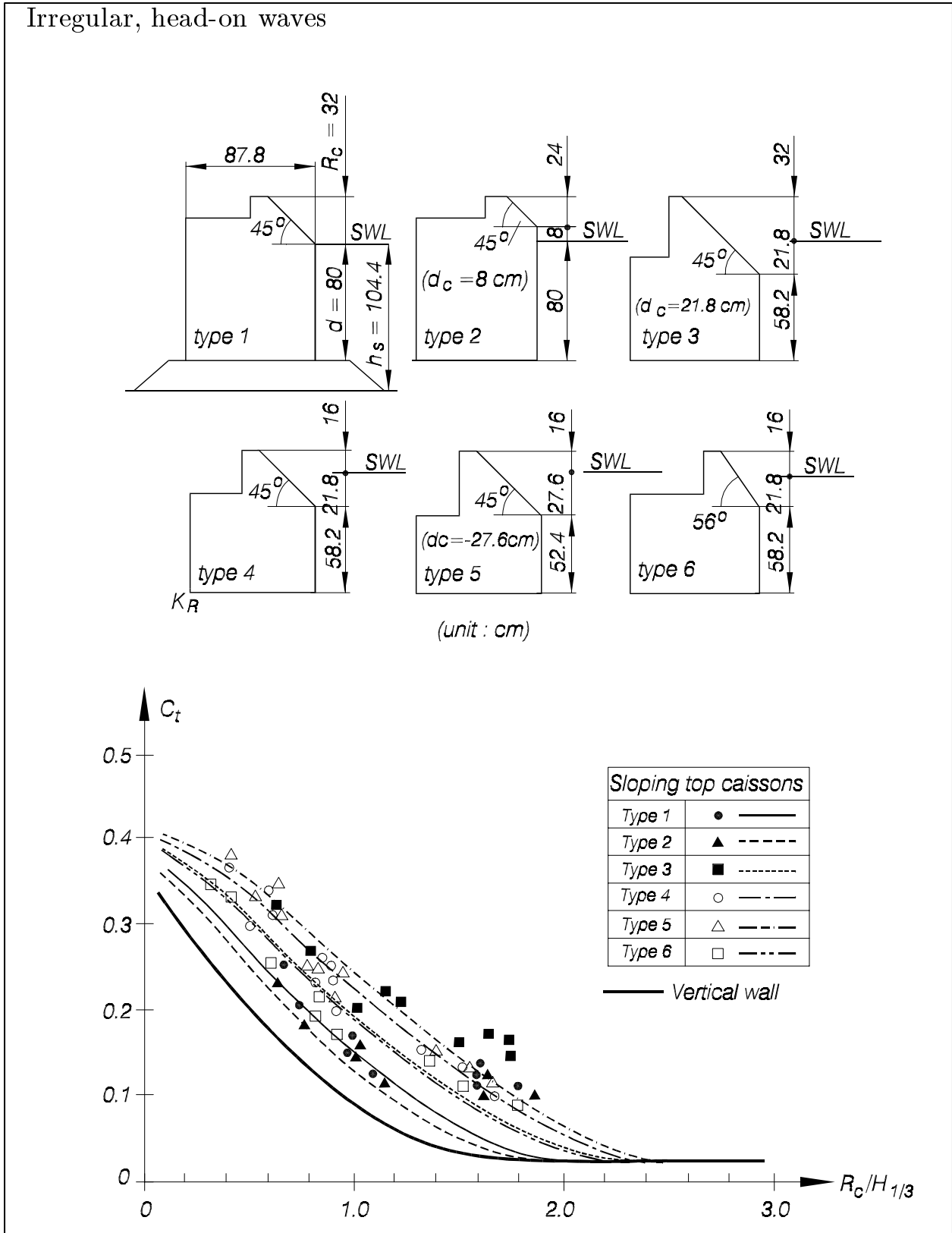


Figure VI-5-31. Wave transmission by overtopping of sloping top structures (Takahashi and Hosoyamada 1994)

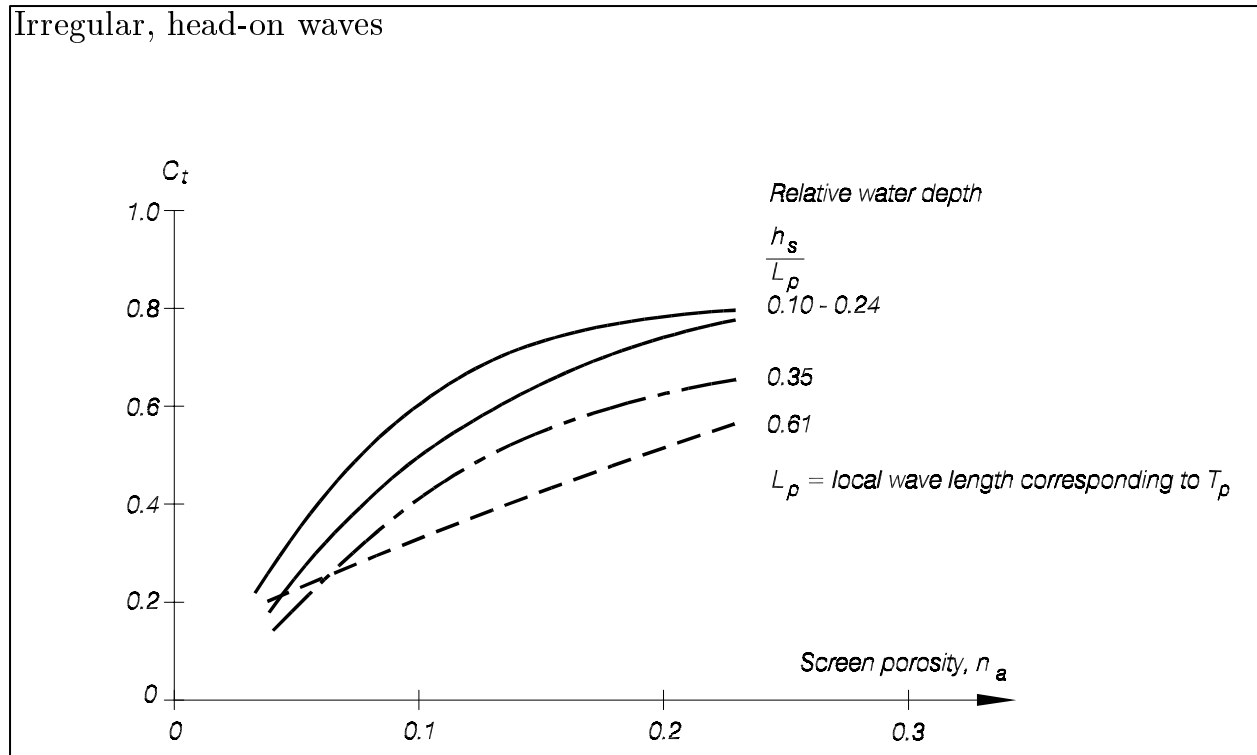


Figure VI-5-32. Wave transmission through perforated single wall (Allsop and Hettiarachchi 1988)

(a) The wave-generated flow forces on armor units might be expressed by a Morison equation containing a drag force F_D , a lift force F_L and an inertia force F_I . The stabilizing force is the gravitational force F_G . Assuming that at the stage of instability drag and lift force dominates the inertia force, a qualitative stability ratio can be formulated as the drag force plus the lift force divided by the gravity force

$$\frac{F_D + F_L}{F_G} \approx \frac{\rho_w D_n^2 v^2}{g(\rho_s - \rho_w) D_n^3} = \frac{v^2}{g \Delta D_n} \quad (\text{VI-5-57})$$

where $D_n = (\text{armor unit volume})^{1/3}$ is the equivalent cube length, ρ_s and ρ_w are the mass densities of armor units and water, respectively, and v is a characteristic flow velocity. By inserting $v \approx (gH)^{1/2}$ for a breaking wave height of H in Equation VI-5-57 the following stability parameter, N_s , is obtained.

$$N_s = \frac{H}{\Delta D_n} \quad (\text{VI-5-58})$$

where $\Delta = (\rho_s/\rho_w - 1)$. Non-exceedence of instability, or a certain degree of damage, can then be expressed in the general form

$$N_s = \frac{H}{\Delta D_n} \leq K_1^a K_2^b K_c^3 \dots \quad (\text{VI-5-59})$$

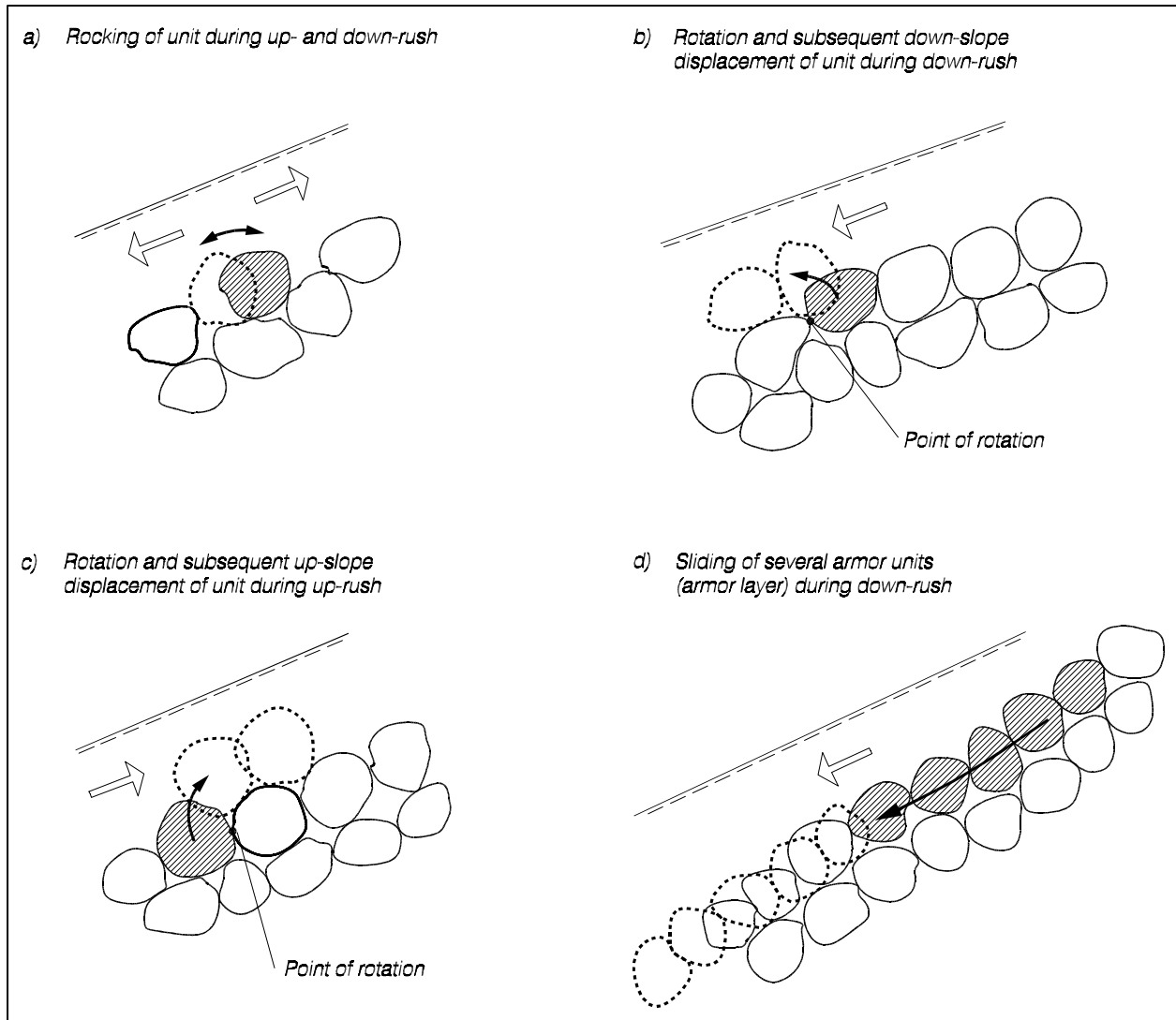


Figure VI-5-33. Typical armor layer failure modes (Burcharth 1993)

where the factors depend on all the other parameters, except H , Δ and D_n , influencing the stability. Table VI-5-18 gives an overview of the sea state and structural parameters influencing armor layer stability. Also given are the combined parameters including wave height-period parameters commonly used in stability formulae. Stability formulae do not contain explicitly all the parameters shown in Table VI-5-18. This together with the stochastic nature of wave load and armor response introduces uncertainty in any stability formula. This uncertainty is in most cases included in Equation VI-5-59 in the form of a Gaussian distributed stochastic variable with a specified mean value and standard deviation.

(b) Simple geometrical considerations of the balance of the forces acting on an armor stone have been used to explore the right-hand side of Equation VI-5-59. Examples are:

Table VI-5-18
Parameters Influencing Hydraulic Stability of Armor Layers

Sea state parameters

- Characteristic wave heights: $H_s, H_{1/3}, H_{mo}, H_{1/10}$, etc.
- Characteristic wave length: L_m, L_{om}, L_p , etc.
- Characteristic wave steepness: s_m, s_{om}, s_p , etc.
- Wave assymetricity
- Shape of wave spectrum: JONSWAP, P-M, TMA etc. and double peak spectra.
- Wave grouping
- Water depth, h
- Wave incident angle, β
- Number of waves, N_z
- Mass density of water, ρ_w

Structural parameters

- Seaward profile of the structure, including armor layer slope angle α , freeboard, etc.
- Mass density of armor units, ρ_s
- Grading of rock armor, $d_{n50}, d_{n15}, d_{n85}$
- Mass M and shape of armor units
- Packing density, placement pattern and layer thickness of main armor
- Porosity and permeability of underlayers, filter layer(s) and core

Combined parameters

$$\Delta = \frac{\rho_s}{\rho_w} - 1$$

$$N_s = \frac{H_s}{\Delta D_n} \quad \text{Shore Protection Manual (1984)}$$

$$N_s^* = N_s s_p^{-1/3} \quad \text{Ahrens (1987)}$$

$$H_0 T_0 = N_s T_m \sqrt{\frac{g}{D_n}} \quad \text{van der Meer (1988)}$$

$$\xi_m = \frac{\tan \alpha}{\sqrt{s_{om}}} \quad \text{Battjes (1974b)}$$

where s_p the local wave steepness

T_m mean wave period

$$s_{om} = \frac{2\pi H_s}{g T_m^2}$$

$$\frac{H}{\Delta D_n} = K \cos \alpha \quad \text{Svee (1962)}$$

$$\frac{H}{\Delta D_n} = (K \cot \alpha)^{1/3} \quad \text{Hudson (1958, 1959)}$$

$$\frac{H}{\Delta D_n} = K (\tan \varphi \cos \alpha - \sin \alpha) \quad \text{Iribarren (1938), Iribarren and Nogales (1954)}$$

where φ is the angle of repose of the armor. The coefficient K includes some level of damage as well as all other influencing parameters not explicitly included in the formulae.

(c) For armor units of complex shape and interlocking capability it is more difficult to make simple realistic force balance models. Qualitatively the difference between interlocking and noninterlocking armor is illustrated in the graphs of Figure VI-5-34, which show the influence of slope angle on the stabilizing effects of gravitational force, interlocking and surface friction. The interlocking effect is significant only for steeper slopes. Price (1979) performed dolos armor pullout tests in the dry that indicated maximum resistance occurs at slope of $\cot \alpha = 2$. As a further demonstration Burcharth and Thompson (1983) showed that dolos armor placed on a horizontal bed and exposed to oscillatory flow is not more stable than rock armor of similar weight.

(3) Definition of armor layer damage.

(a) Damage to armor layers is characterized either by counting the number of displaced units or by measurement of the eroded surface profile of the armor slope. In both cases the damage is related to a specific sea state of specified duration.

The counting method is based on some classification of the armor movements, for example:

- No movement.
- Single armor units rocking.
- Single armor units displaced from their original position by a certain minimum distance, for example D_n or h_a , where h_a is the length (height) of the unit

(b) Displacements can be in terms of units being removed out of the layer or units sliding along the slope to fill in a gap. In case of steep slopes, displacements could also be sliding of the armor layer due to compaction or loss of support.

(c) Damage in terms of displaced units is generally given as the relative displacement, D , defined as the proportion of displaced units relative to the total number of units, or preferably, to the number of units within a specific zone around swl. The reason for limiting damage to a specific zone is that otherwise it would be difficult to compare various structures because the damage would be related to different totals for each structure. Because practically all armor unit movements take place within the levels $\pm H_s$ around swl, the number of units within this zone is sometimes used as the reference number. However, because this number changes with H_s it is recommended specifying a H_s -value corresponding to a certain damage level (as proposed by Burcharth and Liu 1992) or to use the number of units within the levels $\text{swl} \pm n D_n$, where n is chosen such that almost all movements take place within these levels. For example for dolosse $n = 6$ is used.

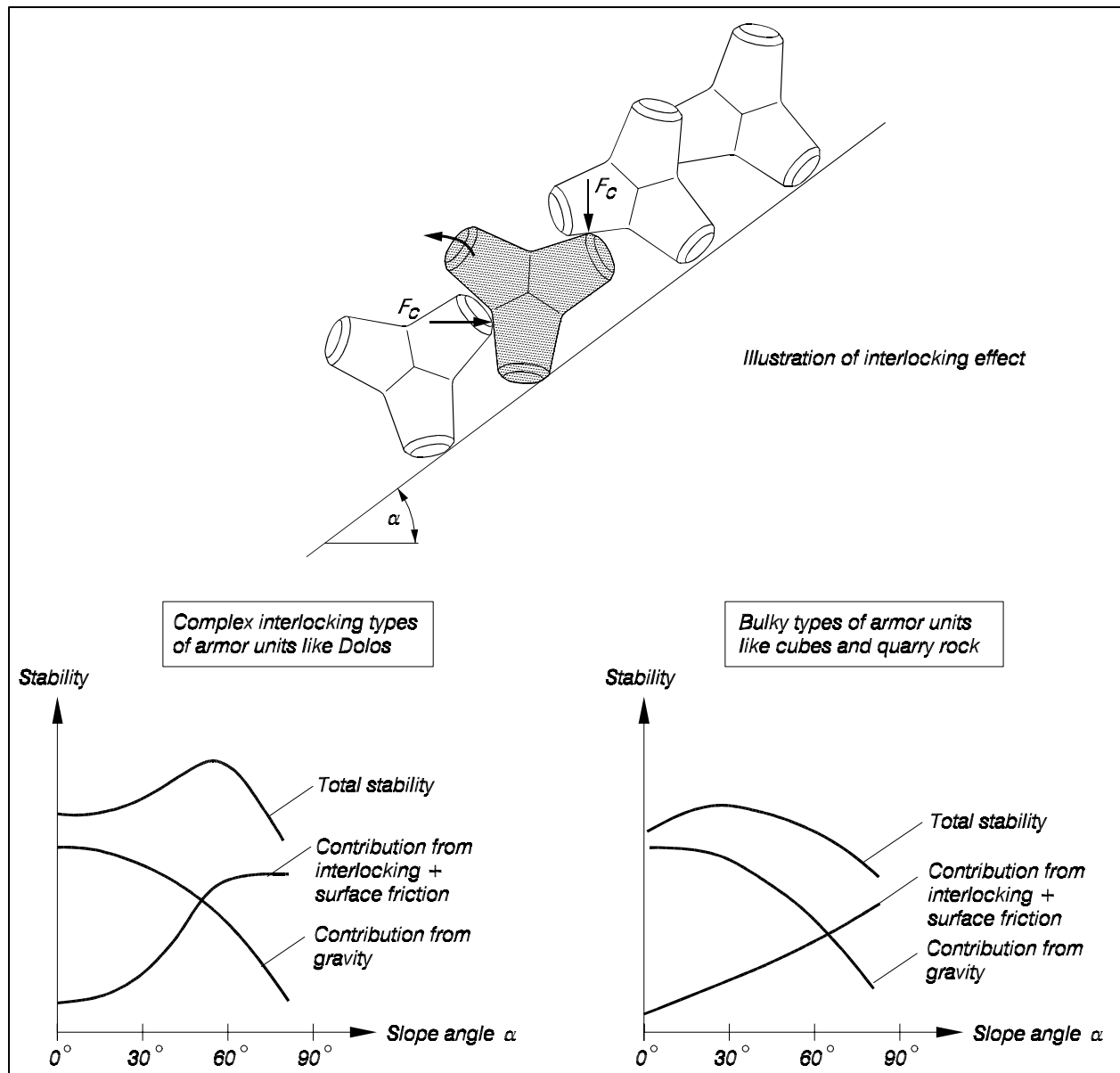


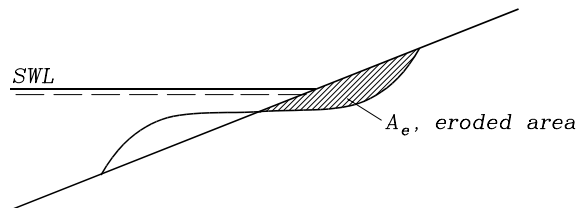
Figure VI-5-34. Illustration of influence of slope angle on the stabilizing effects of gravitational force, interlocking and surface friction (Burcharth 1993)

(d) Damage D can be related to any definition of movements including rocking. The relative number of moving units can also be related to the total number of units within a vertical strip of width D_n stretching from the bottom to the top of the armor layer. For this strip displacement definition, van der Meer (1988) used the term N_{od} for units displaced out of the armor layer and N_{or} for rocking units. The disadvantage of N_{od} and N_{or} is the dependence of the slope (strip) length.

(e) Damage characterization based on the eroded cross-section area A_e around swl was used by Iribarren (1938) and Hudson (1958) (Table VI-5-19). Hudson defined D as the percent erosion of original volume. Iribarren defined the limit of severe damage to occur when erosion depth in the main armor layer reached D_n .

Table VI-5-19
Definition of Damage Parameters D , N_{od} and S

1) Relative displacement within an area	$D = \frac{\text{number of displaced units}}{\text{total number of units within reference area}}$ <p>Displacement has to be defined, e.g., as position shifted more than distance D_n, or displacements out of the armor layer.</p> <p>The reference area has to be defined, e.g., as the complete armor area, or as the area between two levels, e.g., $SWL \pm H_s$, where H_s corresponds to a certain damage, or $SWL \pm nD_n$, where $\pm nD_n$ indicates the boundaries of armor displacements.</p>
2) Number of displaced units within a strip with width D_n (van der Meer 1988)	$N_{od} = \frac{\text{number of units displaced out of armor layer}}{\text{width of tested section} / D_n}$
3) Relative number of displaced units within total height of armor layer (van der Meer 1988)	<p>$\frac{N_{od}}{N_a}$, where N_a is the total number of units within a strip of horizontal width D_n</p> <p>$\frac{N_{od}}{N_a} = D$ if in D the total height of the armor layer is considered, and no sliding $> D_n$ of units parallel to the slope surface takes place</p>
4) Percent erosion of original volume (Hudson 1958)	$D = \frac{\text{average eroded area from profile}}{\text{area of average original profile}} \times 100\%$
5) Relative eroded area (Broderick 1983)	$S = A_e / D_{n50}^2$



(f) Broderick (1983) defined a dimensionless damage parameter for riprap and rock armor given as

$$S = \frac{A_e}{D_{n50}^2} \quad (\text{VI-5-60})$$

which is independent of the length of the slope and takes into account vertical settlements but not settlements and sliding parallel to the slope. S can be interpreted as the number of squares with side length D_{n50} which fit into the eroded area, or as the number of cubes with side length D_{n50} eroded within a strip width D_{n50} of the armor layer. The damage parameter S is less suitable in the case of complex types of armor like dolosse and tetrapods due to the difficulty in defining surface profile. An overview of the damage parameters is given in Table VI-5-19.

If settlements are disregarded the following relationship between N_{od} and S is valid:

$$N_{od} = G(1 - p)S \quad (\text{VI-5-61})$$

where p is the porosity of the armor layer and G is a factor dependent on the armor layer gradation. The range of p is approximately 0.4 - 0.6 with the lowest values corresponding to rock and the highest to dolosse. $G = 1$ for uni-size concrete armor and 1.2 - 1.6 for stone armor. It is seen that N_{od} is roughly equal to $S/2$. Unfortunately Equation VI-5-61 is not generally applicable because experience shows that the relationship depends on the armor slope angle. Table VI-5-20 shows examples of relationships between N_{od} and S as determined from model tests.

(g) A conventional damage level classification and the related values of the damage parameters D , N_{od} and S are given in Table VI-5-21.

(4) Armor layer damage progression.

(a) During the projected service life of a rubble-mound structure, damage to the armor layer may occur if design wave conditions are exceeded or the structure is exposed to repeated storms near the design conditions. Often it is not possible to mobilize and repair armor layer damage before the structure is impacted by additional severe storm waves that could worsen damage and possibly result in structure failure. A method for assessing armor layer damage progression due to multiple storms of differing wave conditions was developed by Melby and Kobayashi (1998a, 1998b) and Melby (1999). The method is based on seven long-duration physical model tests simulating various combinations of successive storms. The 1:2 sloping structure was protected with uniform armor stone (five tests) or wide-graded riprap (two tests). Irregular breaking wave conditions generally exceeding the design wave condition were used with the highest wave conditions causing moderate overtopping of the structure. Two water depths were used in the testing. The average damage as a function of time was given by Melby (1999) in terms of time domain wave parameters as

$$\bar{S}(t) = \bar{S}(t_n) + 0.025 \frac{(N_s)_n^5}{(T_m)_n^{1/4}} (t^{1/4} - t_n^{1/4}) \quad \text{for } t_n \leq t \leq t_{n+1} \quad (\text{VI-5-62})$$

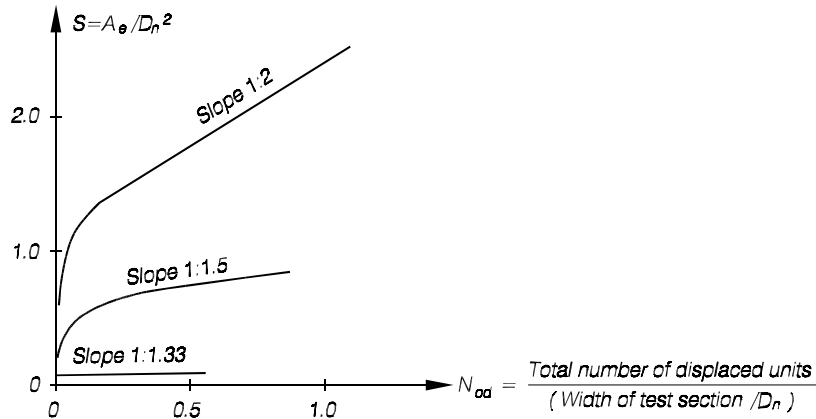
or in terms of frequency domain wave parameters

$$\bar{S}(t) = \bar{S}(t_n) + 0.0202 \frac{(N_{mo})_n^5}{(T_p)_n^{1/4}} (t^{1/4} - t_n^{1/4}) \quad \text{for } t_n \leq t \leq t_{n+1} \quad (\text{VI-5-63})$$

Table VI-5-20
Examples of Experimentally Determined Relationships Between N_{od} and S

van der Meer (1988)	{	Cubes, slope 1:1.5	$N_{od} = (S - 0.4)/1.8$
		Tetrapod, slope 1:1.5	$N_{od} = (S - 1)/2$
		Accropode, slope 1:1.33	$N_{od} = (S - 1)/2$

Holtzhausen and Zwamborn (1991) Accropodes



with

$$\bar{S} = \frac{A_e}{D_{n50}^2} \quad N_s = \frac{H_s}{\Delta D_{n50}} \quad N_{mo} = \frac{H_{mo}}{\Delta D_{n50}} \quad \Delta = \frac{\rho_a}{\rho_w} - 1 \quad (\text{VI-5-64})$$

where t_n is the time at start of storm n , and t is time at end of storm n . (Time has the same units as wave period.) The wave parameters are local incident wave conditions not too far seaward of the structure toe, and the subscript n refers to those wave parameters associated with storm n . The standard deviation of average damage was given by the expression

$$\sigma_s = 0.5\bar{S}^{-0.65} \quad (\text{VI-5-65})$$

(b) For a specified sequence of storms of given duration Equation VI-5-62 or VI-5-63 is solved with the damage result from the previous storm being the initial damage for the next storm. Reasonable sequences of wave parameters and storm durations must be estimated using probabilistic methods based on long-term wave measurements or hindcasts.

Table VI-5-21
Damage Classification and Related Values of the Damage Parameters D , N_{od} and S

No damage	No unit displacement. Note that S might not be equal to zero due to settlement
Initial damage	Few units are displaced. This damage level corresponds to the <i>no-damage</i> level used in <i>Shore Protection Manual</i> 1977 and 1984 in relation to the Hudson formula stability coefficient, where the <i>no-damage</i> level is defined as 0-5% displaced units within the zone extending from the middle of the crest height down the seaward face to a depth below SWL equal to a H_s -value which causes the damage 0-5%.
Intermediate damage ranging from moderate to severe damage	Units are displaced but without causing exposure of the under or filter layer to direct wave attack
Failure	The underlayer or filter layer is exposed to direct wave attack

Damage level by D for two-layer armor

Unit	Slope	Initial damage	Intermediate damage	Failure	Reference
Rock ¹	1:2-1:3	0-5%	5-10%	$\geq 20\%$	Jackson (1968)
Cube ²	1:1.5-1:2		4%		Brorsen et al. (1974)
Dolosse ²	1:1.5	0-2%		$\geq 15\%$	Burcharth and Liu (1992)
Accropode ^{2,3}	1:1.33	0%	1-5%	$\geq 10\%$	Burcharth et al. (1998)

¹ D is defined as percentage of eroded volume.

² D is defined as percentage of units moved more than D_n within the following level restricted areas: For rock see definition under initial damage, for cube $SWL \pm 6D_n$, for Dolosse $SWL \pm 6D_n$, for Accropodes between levels $SWL + 5D_n$ and $-9D_n$.

³ One-layer armor cover layer.

Damage level by N_{od} for two-layer armor (van der Meer 1988)

Unit	Slope	Initial damage	Intermediate damage	Failure
Cube	1:1.5	0		2
Tetrapods	1:1.5	0		1.5
Accropode	1:1.33	0		0.5

Damage level by S for two-layer armor (van der Meer 1988)

Unit	Slope	Initial damage	Intermediate damage	Failure
Rock	1 : 1.5	2	3-5	8
Rock	1 : 2	2	4-6	8
Rock	1 : 3	2	6-9	12
Rock	1 : 4 - 1 : 6	3	8-12	17

Melby and Kobayashi also noted that average damage was related to the armor layer eroded depth, d_e , cover depth, d_c , and the upslope eroded length, l_e as defined in Figure VI-5-35.

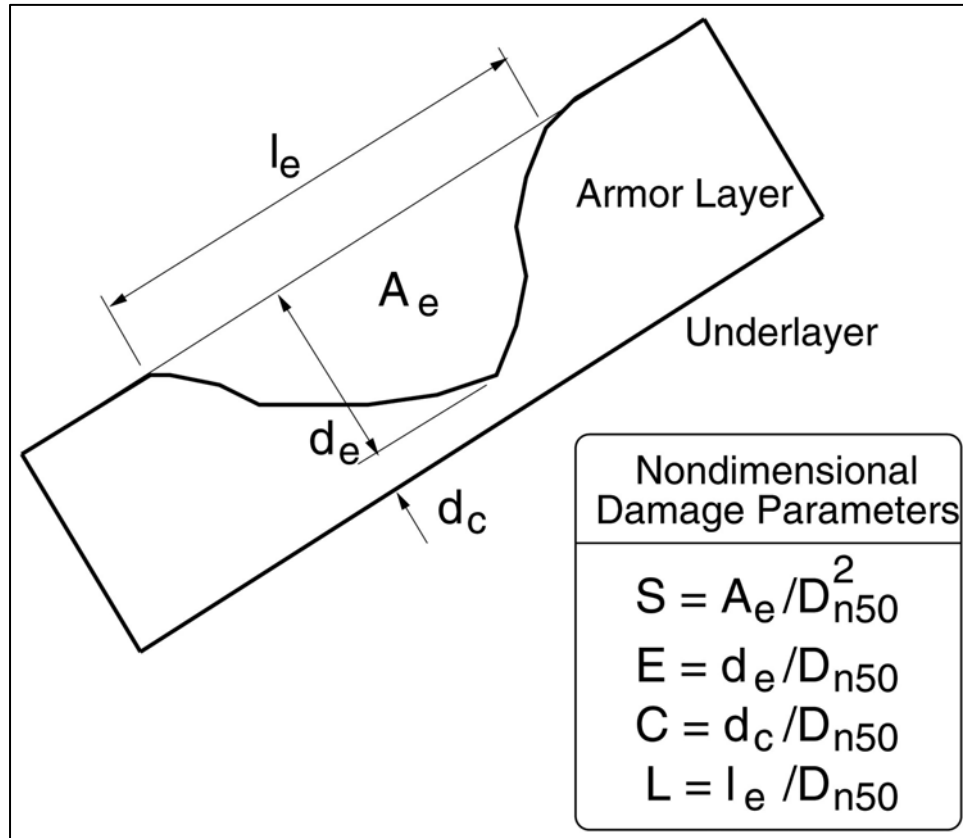


Figure VI-5-35. Damage parameters for structure armor layer (after Melby and Kobayashi 1998b)

In terms of the nondimensional parameters presented in Figure VI-5-35, these relationships were given as

$$\begin{aligned} \bar{E} &= 0.46\bar{S}^{-0.5} & \sigma_E &= 0.26 - 0.00007(\bar{S} - 7.8)^4 \\ \bar{C} &= C_o - 0.1\bar{S} & \sigma_C &= \sigma_{C_o} + 0.098 - 0.002(\bar{S} - 7)^2 \\ \bar{L} &= 4.4\bar{S}^{-0.5} \end{aligned} \tag{VI-5-66}$$

where σ_e and σ_c are the standard deviations of the average nondimensional eroded depth and cover depth, respectively; and C_o is the zero-damage cover layer thickness.

(c) The nondimensional eroded depth in Equation VI-5-66 could be used to estimate average damage in rock armor from an observed eroded depth after a severe storm. This estimate could then be used in Equation VI-5-62 or VI-5-63 to predict damage progression from subsequent storms.

(d) Although the previous damage progression relationships are based on a small number of laboratory experiments, they were formulated to be conservative in the estimates. The more difficult problem is to develop good realizations of storm sequences.

(5) Practical formulae for hydraulic stability of armor layers.

(a) Formulae for hydraulic stability of armor layers are almost exclusively based on small scale model tests. Large scale model tests for verification of small scale model test results have been performed in few cases. Adjustment of formulae due to prototype experience seems not to be reported in the literature.

(b) Generally small scale hydraulic tests of armor layer stability are assumed to be conservative if any bias is present. Nevertheless, armor stability formulae should be applied only for conceptual design, and the uncertainty of the formulae should be considered. When the formulae do not cover the actual range of structure geometries and sea states, preliminary designs should be model tested before actual construction. Major structures should always be tested in a physical model.

(c) Some of the factors by which armor stability formulae can be classified are as follows:

- Type of armor unit.
- Deep or shallow-water wave conditions.
- Armor layers crest level relative to wave runup and swl.
- Structures with and without superstructure.

(d) Type of armor unit distinguishes between rock armor, for which shape and grading must be defined, and uni-size concrete armor units.

(e) Deepwater conditions correspond to Rayleigh distributed wave height at the structure, i.e., depth-limited wave breaking does not take place. Shallow-water conditions correspond to non-Rayleigh distributed wave heights at the structure, i.e., depth limitations cause wave breaking in front of, or in the worst case, directly upon the structure.

(f) Overtopping affects the armor stability. When the crest is lower than the runup level, wave energy can pass over the structure. Thus, the size of the front slope armor can be reduced while the size of the crest and rear slope armor must be increased compared to non-overtopped structures. With respect to armor stability it is common to distinguish between

- Non-overtopped or marginally overtopped structures.
- Low-crested structures, i.e., overtopped structures but with crest level above swl.
- Submerged structures, i.e., the crest level is below swl.

(g) The remainder of this section presents armor layer stability formulae for use in designing coastal structures. These stability formulae can be used in the context of reliability based design using the partial safety factors given in the tables of Part VI-6-6, "Partial Safety Factor System for Implementing Reliability in Design." Guidance for designing structure cross sections is given in Part VI-5-3e, "Design of Structure Cross Section," and complete design examples for specific structure types are given in Part VI-7, "Example Problems."

- Structure trunk stability. Stability formulae for front slope armor on structure trunks are presented in the following tables outlined as follows:

Armor Unit	Non-Overtopped	Overtopped	Submerged
Rock	Tables VI-5-22/23	Tables VI-5-24/26	Tables VI-5-25/26
Concrete cubes	Table VI-5-29		
Tetrapods	Table VI-5-30		
Dolosse	Table VI-5-31		
ACCROPODES [®]	Tables VI-5-32/33		
CORE-LOC [®]	Table VI-5-34		
Tribars	Table VI-5-36		

- Information on rear side armor stability is given in Table VI-5-28. A formula for stability of reef breakwater is presented in Table VI-5-27. A formula for stability of armor in front of a vertical wall is presented in Table VI-5-35. Rubble-mound structure head stability is given in Tables VI-5-37/38. Parapet walls are placed on top of rubble-mound structures to reduce overtopping by deflecting the uprushing waves back into the sea. This generally reduces the front slope armor stability. A low wall behind a wide front armor berm will hardly affect the armor stability (see Figure VI-5-36a). On the other hand a high wall with a relatively deep foundation situated behind a narrow front armor berm will significantly reduce the armor stability (see Figure VI-5-36b).

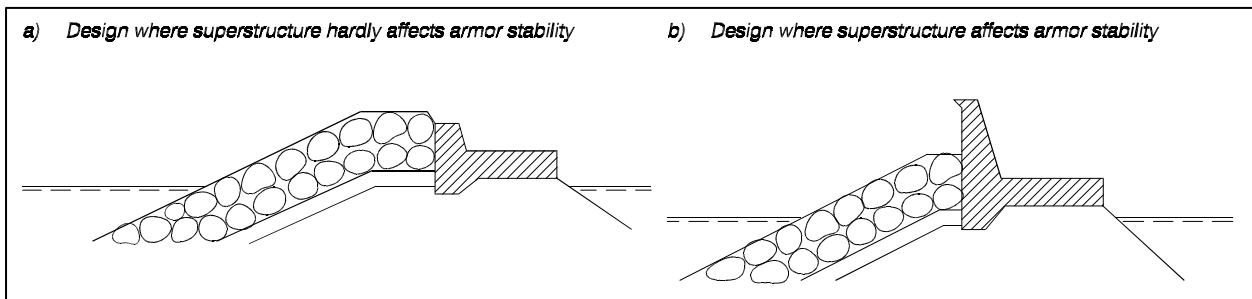


Figure VI-5-36. Illustration of superstructure designs causing insignificant and significant reduction in front slope armor stability

- No generally applicable formulae are available for reduction in front slope armor stability caused by parapet walls.
- Laboratory test limitations. All of the various armor stability criteria represented by the equations and empirical coefficients in Tables VI-5-22 to VI-5-36 were developed in laboratory physical models, most often at reduced scale. Although field experience has added validation to some of these stability formulae, designers should be aware of the following limitations when applying laboratory stability results to prototype conditions.

Table VI-5-22
Rock, Two-Layer Armored Non-Overtopped Slopes (Hudson 1974)

Irregular, head-on waves

$$\frac{H}{\Delta D_{n50}} = (K_D \cot \alpha)^{1/3} \quad \text{or} \quad M_{50} = \frac{\rho_s H^3}{K_D \left(\frac{\rho_s}{\rho_w} - 1\right)^3 \cot \alpha} \quad (\text{VI-5-67})$$

where H Characteristic wave height (H_s or $H_{1/10}$)
 D_{n50} Equivalent cube length of median rock
 M_{50} Medium mass of rocks, $M_{50} = \rho_s D_{n50}^3$
 ρ_s Mass density of rocks
 ρ_w Mass density of water
 Δ $(\rho_s / \rho_w) - 1$
 α Slope angle
 K_D Stability coefficient

K_D -values by SPM 1977, $H = H_s$, for slope angles $1.5 \leq \cot \alpha \leq 3.0$. (Based entirely on regular wave tests.)

Stone shape	Placement	Damage, D^4			
		0-5%		5-10%	10-15%
		Breaking waves ¹	Nonbreaking waves ²	Nonbreaking waves	Nonbreaking waves
Smooth, rounded	Random	2.1	2.4	3.0	3.6
Rough angular	Random	3.5	4.0	4.9	6.6
Rough angular	Special ³	4.8	5.5		

K_D -values by SPM 1984, $H = H_{1/10}$.

Stone shape	Placement	Damage, $D^4 = 0\text{-}5\%$	
		Breaking waves ¹	Nonbreaking waves ²
Smooth rounded	Random	1.2	2.4
Rough angular	Random	2.0	4.0
Rough angular	Special ³	5.8	7.0

- ¹ Breaking waves means depth-limited waves, i.e., wave breaking takes place in front of the armor slope. (Critical case for shallow-water structures.)
- ² No depth-limited wave breaking takes place in front of the armor slope.
- ³ Special placement with long axis of stone placed perpendicular to the slope face.
- ⁴ D is defined according to SPM 1984 as follows: The percent damage is based on the volume of armor units displaced from the breakwater zone of active armor unit removal for a specific wave height. This zone extends from the middle of the breakwater crest down the seaward face to a depth equivalent to the wave height causing zero damage below still-water level.

Shore Protection Manual (1977) versus *Shore Protection Manual* (1984): When considering that $H_{1/10} = 1.27H_s$ for Rayleigh distributed wave heights (non-depth-limited waves) it is seen that the recommendations of *Shore Protection Manual* (1984) introduce a considerable safety factor compared to the practice based on *Shore Protection Manual* (1977).

Uncertainty of the formula: The coefficient of variation of Eq VI-5-67 is estimated to be 18% by van der Meer (1988). Melby and Mlaker (1997) reported a coefficient of variation for K_D of 25% for stone and 20% for Dolosse.

Table VI-5-23
Rock, Two-Layer Armored Non-Overtopped Slopes (van der Meer 1988)

Irregular, head-on waves

$$\frac{H_s}{\Delta D_{n50}} = 6.2 \cdot S^{0.2} P^{0.18} N_z^{-0.1} \xi_m^{-0.5} \quad \text{Plunging waves : } \xi_m < \xi_{mc} \quad (\text{VI-5-68})$$

$$\frac{H_s}{\Delta D_{n50}} = 1.0 \cdot S^{0.2} P^{-0.13} N_z^{-0.1} (\cot \alpha)^{0.5} \xi_m^P \quad \text{Surging waves : } \xi_m > \xi_{mc} \quad (\text{VI-5-69})$$

$$\xi_m = s_m^{-0.5} \tan \alpha \quad \xi_{mc} = \left(6.2 P^{0.31} (\tan \alpha)^{0.5} \right)^{1/(P+0.5)}$$

where	H_s	Significant wave height in front of breakwater
	D_{n50}	Equivalent cube length of median rock
	ρ_s	Mass density of rocks
	ρ_w	Mass density of water
	Δ	$(\rho_s/\rho_w) - 1$
	S	Relative eroded area (see Table VI-5-21 for nominal values)
	P	Notional permeability (see Figure VI-5-11)
	N_z	Number of waves
	α	Slope angle
	s_m	Wave steepness, $s_m = H_s/L_{om}$
	L_{om}	Deepwater wavelength corresponding to mean wave period

Validity:

- 1) Equations VI-5-68 and VI-5-69 are valid for non-depth-limited waves. For depth-limited waves H_s is replaced by $H_{2\%}/1.4$.
- 2) For $\cot \alpha \geq 4.0$ only Eq VI-5-68 should be used.
- 3) $N_z \leq 7, 500$ after which number equilibrium damage is more or less reached.
- 4) $0.1 \leq P \leq 0.6$, $0.005 \leq s_m \leq 0.06$, $2.0 \text{ tonne}/m^3 \leq \rho \leq 3.1 \text{ tonne}/m^3$
- 5) For the 8 tests run with depth-limited waves, breaking conditions were limited to spilling breakers which are not as damaging as plunging breakers. Therefore, Eqs VI-5-68 and VI-5-69 may not be conservative in some breaking wave conditions.

Uncertainty of the formula: The coefficient of variation on the factor 6.2 in Eq VI-5-68 and on the factor 1.0 in Eq VI-5-69 are estimated to be 6.5% and 8%, respectively.

Test program: See Table VI-5-4.

Table VI-5-24
Rock, Two-Layer Armored Overtopped, but Not Submerged, Low-crested Slopes

Powell and Allsop (1985) analyzed data by Allsop (1983) and proposed the stability formula

$$\frac{N_{od}}{N_a} = a \exp \left[b s_p^{-1/3} H_s / (\Delta D_{n50}) \right] \quad \text{or} \quad \frac{H_s}{\Delta D_{n50}} = \frac{s_p^{1/3}}{b} \ln \left(\frac{1}{a} \frac{N_{od}}{N_a} \right) \quad (\text{VI-5-70})$$

where values of the empirical coefficients a and b are given in the table as functions of freeboard R_c and water depth h . N_{od} and N_a are the number of units displaced out of the armor layer and the total number of armor layer units, respectively.

Values of coefficients a and b in Eq VI-5-70.

R_c/h	$a \cdot 10^4$	b	wave steepness H_s/L_p
0.29	0.07	1.66	<0.03
0.39	0.18	1.58	<0.03
0.57	0.09	1.92	<0.03
0.38	0.59	1.07	>0.03

van der Meer (1991) suggested that the van der Meer stability formulae for non-overtopped rock slope, Eqs VI-5-68 and VI-5-69, be used with $f_i D_{n50}$ substituted for D_{n50} . The reduction factor f_i is given as

$$f_i = \left(1.25 - 4.8 \frac{R_c}{H_s} \sqrt{\frac{s_{op}}{2\pi}} \right)^{-1} \quad (\text{VI-5-71})$$

where R_c is the freeboard, $s_{op} = H_s/L_{op}$, and L_{op} is deepwater wavelength corresponding to the peak wave period. Limits of Eq VI-5-71 are given by

$$0 < \frac{R_c}{H_s} \sqrt{\frac{s_{op}}{2\pi}} < 0.052$$

- Some of the earlier results were obtained using monochromatic waves, whereas most of the more recent model tests used irregular waves. Numerous studies have suggested that the monochromatic wave height leading to armor instability roughly corresponds to the significant wave height of irregular waves; however, not all studies have found this correspondence. For preliminary design for nonbreaking wave conditions always use a stability formula based on irregular wave testing if possible. For breaking wave conditions monochromatic wave stability results will be conservative.
- It is generally thought that the higher waves associated with wave groups are responsible for armor layer damage. Typically irregular wave stability model tests use wave trains with assumed random phasing of the spectral components. Over the course of the testing wave groups of differing characteristics impact the structure, and the assumption is that these wave groups are representative of nature. However, it is possible that nonrandom phasing occurs in nature, particularly in shallow water (Andrews and Borgman 1981). Therefore, use of regular wave stability results will be appropriate in some cases.

Table VI-5-25
Rock, Submerged Breakwaters with Two-Layer Armor on Front, Crest and Rear Slope (van der Meer 1991)

Irregular, head-on waves

$$\frac{h'_c}{h} = (2.1 + 0.1 S) \exp(-0.14 N_s^*) \quad (\text{VI-5-72})$$

where h Water depth

h'_c Height of structure over seabed level ($h - h'_c$ is the water depth over the structure crest).

S Relative eroded area

N_s^* Spectral stability number, $N_s^* = \frac{H_s}{\Delta D_{n50}} s_p^{-1/3}$

Uncertainty of the formula: The uncertainty of Eq VI-5-72 can be expressed by considering the factor 2.1 as a Gaussian distributed stochastic variable with mean of 2.1 and standard deviation of 0.35, i.e., a coefficient of variation of 17%.

Data source: Givler and Sorensen (1986): regular head-on waves, slope 1:1.5

van der Meer (1991): irregular head-on waves, slope 1:2

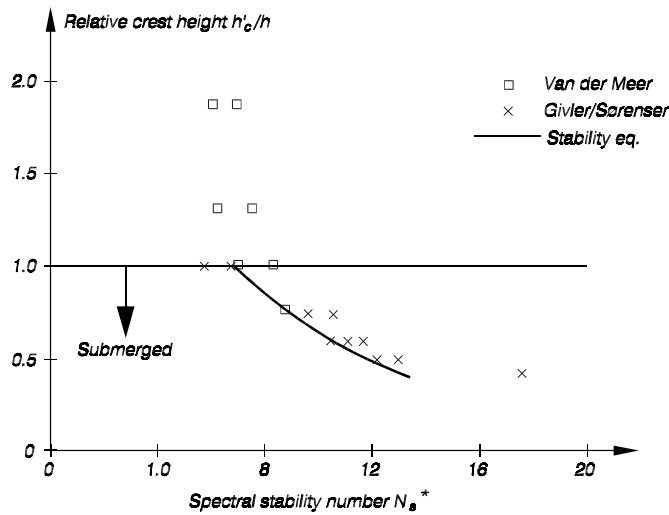
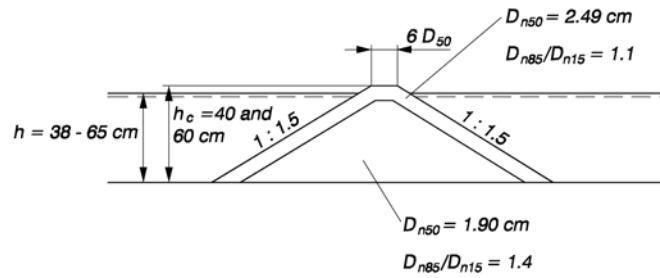


Table VI-5-26
Rock, Two-Layer Armored Low-Crested and Submerged Breakwaters (Vidal et al. 1992)

Tested trunk cross section



Tested ranges

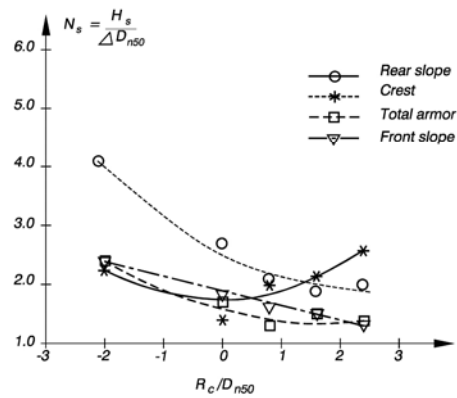
Irregular, head-on waves

Spectral $H_s = 5-19$ cm, $T_p = 1.4$ and 1.8 sec.

Free board : $-5\text{cm} \leq R_c = h_c - h \leq 6\text{cm}$

Dimensionless freeboard: $-2 \leq R_c/D_{n50} \leq 2.4$

Stability corresponding to initiation of damage, $S = 0.5-1.5$



Stability corresponding to extraction of some rocks from lower layer, $S = 2.0-2.5$.

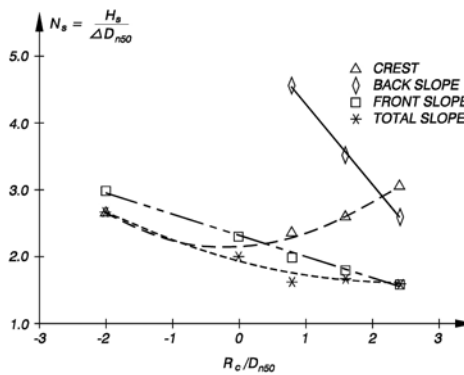
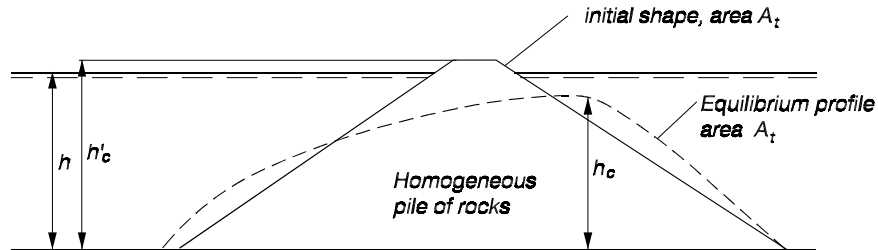


Table VI-5-27
Rock, Low-Crested Reef Breakwaters Built Using Only One Class of Stone

Irregular, head-on waves

van der Meer (1990)

Trunk cross section of reef breakwater



The equilibrium height of the structure

$$h_c = \sqrt{\frac{A_t}{\exp(aN_s^*)}} \quad \text{with a maximum of } h'_c \quad (\text{VI-5-73})$$

where A_t area of initial cross section of structure

h water depth at toe of structure

h'_c initial height of structure

$$N_s^* = \frac{H_s}{\Delta D_{n50}} s_p^{-1/3}$$

$$a = -0.028 + 0.045 \frac{A_t}{(h'_c)^2} + 0.034 \frac{h'_c}{h} - 6 \times 10^{-9} \frac{A_t^2}{D_{n50}^4}$$

Data source: Ahrens (1987), van der Meer (1990)

Powell and Allsop (1985) analyzed data by Ahrens, Viggosson, and Zirkle (1982) and Ahrens (1984) and proposed the stability formula

$$\frac{N_{od}}{N_a} = a \exp[b H_s / (\Delta D_{n50})] \quad \text{or} \quad \frac{H_s}{\Delta D_{n50}} = \frac{1}{b} \ln \left(\frac{1}{a} \frac{N_{od}}{N_a} \right) \quad (\text{VI-5-74})$$

where values of the empirical coefficients a and b are given in the table as functions of freeboard R_c and water depth h . N_{od} and N_a are the number of displaced rocks and the total number of rocks in the mound, respectively.

Values of coefficients a and b in Eq (VI-5-74).

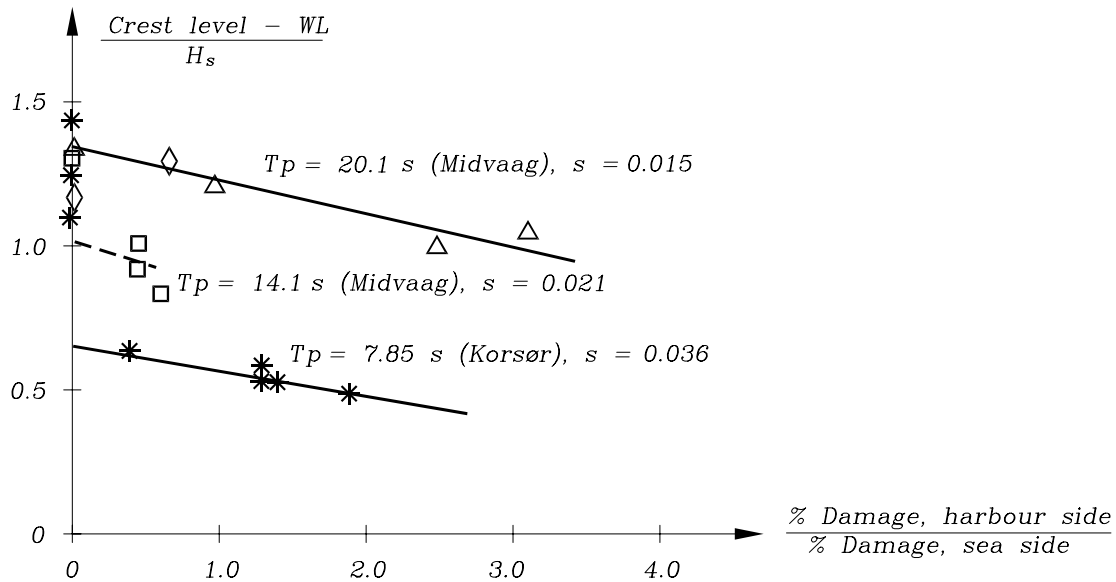
R_c/h	$a \cdot 10^4$	b
0.0	15	0.31
0.2	17	0.33
0.4	4.8	0.53

Valid for $0.0012 < H_s/L_p < 0.036$

Table VI-5-28
Rock, Rear Slope Stability of Two-Layer Armored Breakwaters Without Superstructures (Jensen 1984)

Irregular, head-on waves

Jensen (1984) reported results from two case studies of conventional rock armored rubble-mound breakwaters with the main armor carried over the crests and the upper part of the rear slope. Crest width was approximately 3–4 stone diameters. Although Jensen points out that the results are very project dependent, these results could be useful for preliminary estimates. Wave steepness significantly influences the rear side damage.



- Hand-built armor layers on laboratory structures could be tighter than are armor layers typically constructed in the prototype. This leads to unconservative stability results. In particular special placement of armor in the laboratory is unlikely to be reproduced as well on the job site, especially below the water surface where placement will be much more random. For this reason it may be advisable to use stability criteria for random placement as a basis for design.
- Armor stability formulae are intended for use in preliminary design phases and for estimating material quantities. When feasible, preliminary designs should be confirmed and optimized with hydraulic model tests.

Table VI-5-29
Concrete Cubes, Two-Layer Armored Non-Overtopped Slopes

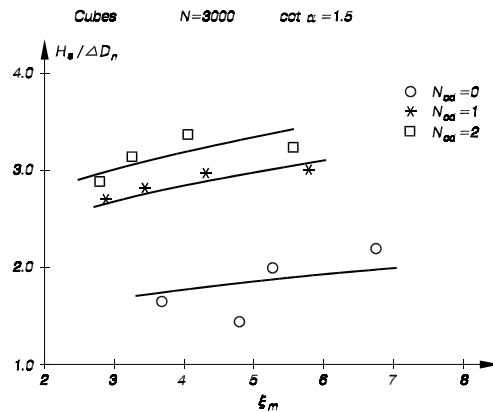
van der Meer (1988b)

$$N_s = \frac{H_s}{\Delta D_n} = \left(6.7 N_{od}^{0.4} / N_z^{0.3} + 1.0 \right) s_m^{-0.1} \quad (\text{VI-5-75})$$

- where
- H_s Significant wave height in front of breakwater
 - ρ_s Mass density of concrete
 - ρ_w Mass density of water
 - Δ $(\rho_s / \rho_w) - 1$
 - D_n Cube length
 - N_{od} Number of units displaced out of the armor layer within a strip width of one cube length D_n
 - N_z Number of waves
 - s_{om} Wave steepness, $s_{om} = H_s / L_{om}$

Valid for: Non-depth-limited wave conditions. Irregular head-on waves
Two layer cubes randomly placed on 1:1.5 slope
Surf similarity parameter range $3 < \xi_m < 6$

Uncertainty of the formula: corresponds to a coefficient of variation of approximately 0.10



Brorsen, Burcharth, and Larsen (1974)

Brorsen, Burcharth, and Larsen gave the following average N_s and corresponding K_D -values for a two layer concrete cube armor, random placement, slope angles $1.5 \leq \cot \alpha \leq 2.0$ and non-depth-limited irregular waves

Damage level	$N_s = \frac{H_s}{\Delta D_n}$	K_D	
		slope 1 : 1.5	slope 1 : 2
Onset, $D = 0\%$	1.8 - 2.0	3.9 - 5.3	2.9 - 4.0
Moderate, $D = 4\%$	2.3 - 2.6	8.1 - 12	6.1 - 8.8

Table VI-5-30
Tetrapods, Two-Layer Armored Non-Overtopped Slopes

van der Meer (1988b) for non-depth-limited waves

$$N_s = \frac{H_s}{\Delta D_n} = \left(3.75 N_{od}^{0.5} / N_z^{0.25} + 0.85 \right) s_{om}^{-0.2} \quad (\text{VI-5-76})$$

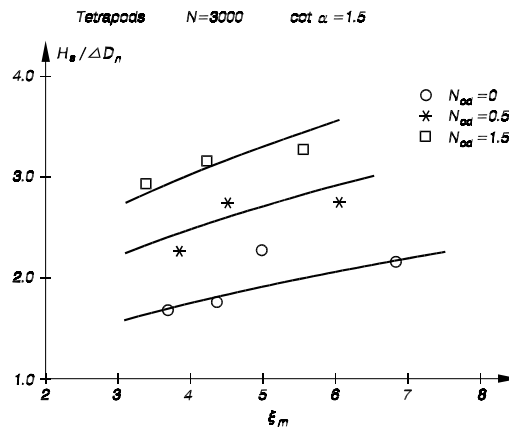
where	H_s	Significant wave height in front of breakwater
	ρ_s	Mass density of concrete
	ρ_w	Mass density of water
	Δ	$(\rho_s / \rho_w) - 1$
	D_n	Equivalent cube length, i.e., length of cube with the same volume as Tetrapods
	N_{od}	Number of units displaced out of the armor layer within a strip width of one cube length D_n
	N_z	Number of waves
	s_{om}	Wave steepness, $s_{om} = H_s / L_{om}$

Valid for: Non-depth limited wave conditions, Irregular head-on waves

Two layer tetrapods on 1:1.5 slope

Surf similarity parameter range $3.5 < \xi_m < 6$

Uncertainty of the formula: corresponds to a coefficient of variation of approximately 0.10



d'Angremond, van der Meer, and van Nes (1994) for depth-limited waves

$$N_s = \frac{H_{2\%}}{\Delta D_n} = 1.4 \left(3.75 N_{od}^{0.5} / N_z^{0.25} + 0.85 \right) s_{om}^{-0.2} \quad (\text{VI-5-77})$$

In deep water the ratio $H_{2\%} / H_s = 1.4$ for Rayleigh distributed waves. In shallow water this ratio decreases with decreasing relative water depth due to wave breaking.

Table VI-5-31
Dolos, Non-Overtopped Slopes (Burcharth and Liu 1992)

$$N_s = \frac{H_s}{\Delta D_n} = (47 - 72 r) \varphi_{n=2} D^{1/3} N_z^{-0.1}$$

$$= (17 - 26 r) \varphi_{n=2}^{2/3} N_{od}^{1/3} N_z^{-0.1} \quad (\text{VI-5-78})$$

where	H_s	Significant wave height in front of breakwater
	ρ_s	Mass density of concrete
	ρ_w	Mass density of water
	Δ	$(\rho_s/\rho_w) - 1$
	D_n	Equivalent cube length, i.e., length of cube with the same volume as dolosse
	r	Dolos waist ratio
	φ	Packing density
	D	Relative number of units within levels SWL $\pm 6.5 D_n$ displaced one dolos height h , or more (e.g., for 2% displacement insert $D = 0.02$)
	N_{od}	Number of displaced units within a strip width of one equivalent cube length D_n
	N_z	Number of waves. For $N_z \geq 3000$ use $N_z = 3000$

Valid for: Breaking and nonbreaking wave conditions
Irregular head-on waves, two layer randomly placed dolosse with a 1:1.5 slope

$$0.32 < r < 0.42$$

$$0.61 < \varphi < 1$$

$$1\% < D < 15\%$$

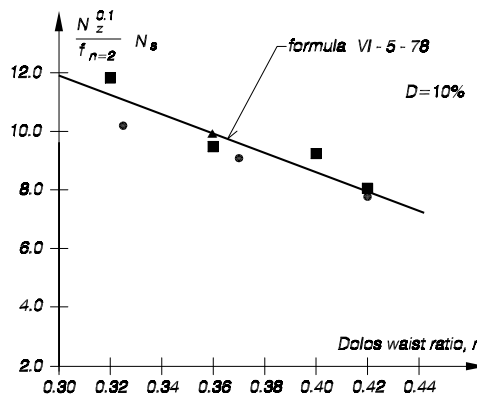
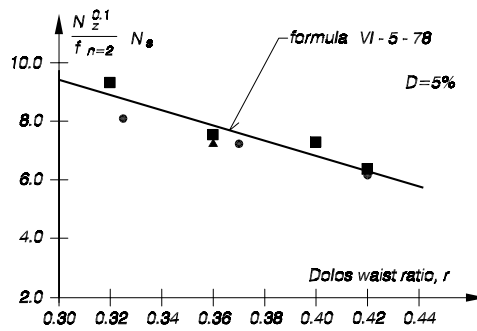
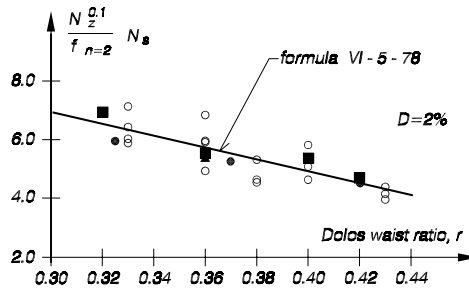
$$2.49 < \xi_0 < 11.7$$

Slope angle: The effect of the slope angle on the hydraulic stability is not included in Eq VI-5-78. Brorsen, Burcharth, and Larsen (1974) found only a marginal influence for slopes in the range 1:1 to 1:3.

Uncertainty of the formula: corresponds to a coefficient of variation of approximately 0.22.

(continued)

Table VI-5-31 (Concluded)



Legend:

Reference	ϕ_{n-2}	Repeated No	Duration (min.)	ξ_{mo}
▲ Brorsen et al. (1974)	1 (App.)	2	60	2.49-5.37
■ Burcharth et al. (1986)	0.61-0.7	5 or 15	20	3.04-4.49
○ Holtzhausen et al. (1990)	1	3 or 8	60	2.91-7.6
● Burcharth et al. (1992)	0.74	20	5	3.23-11.7

Fit of hydraulic stability formula for a two-layer randomly placed dolos armor on a slope of 1:1.5. Damage levels, $D = 2\%$, 5% and 10% displaced units within levels $SWL \pm 6.5D_n$.

Table VI-5-32
ACCROPODE® (van der Meer 1988b)

$$N_s = \frac{H_s}{\Delta D_n} = \begin{cases} 3.7 & \text{no damage} \\ 4.1 & \text{failure} \end{cases} \quad (\text{VI-5-79})$$

- where H_s Significant wave height in front of breakwater
 ρ_s Mass density of concrete
 ρ_w Mass density of water
 Δ $(\rho_s/\rho_w) - 1$
 D_n Equivalent cube length, i.e., length of cube with the same volume as Accropode

Valid for: Irregular, head-on waves
 Nonbreaking wave conditions
 One layer of Accropodes on slope 1:1.33 placed in accordance with SOGREAH recommendations
 No influence of number of waves were found except after start of failure.

Uncertainty of the formula: The standard deviation of the factors 3.7 and 4.1 is approximately 0.2.

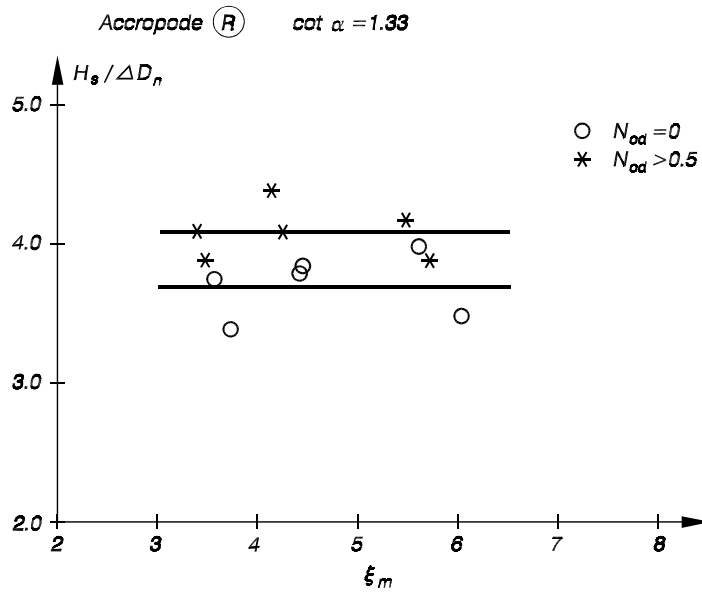


Table VI-5-33
ACCROPODE®, Non-Overtopped or Marginally Overtopped Slopes (Burcharth et al. 1998)

$$N_s = \frac{H_s}{\Delta D_n} = A \left(D^{0.2} + 7.70 \right) \quad \text{or} \quad D = 50 \left(\frac{H_s}{\Delta D_n} - 3.54 \right)^5 \quad (\text{VI-5-80})$$

- where
- H_s Significant wave height in front of breakwater
 - ρ_s Mass density of concrete
 - ρ_w Mass density of water
 - Δ $(\rho_s/\rho_w) - 1$
 - D_n Equivalent cube length, i.e., length of cube with the same volume as Accropode
 - D Relative number of units displaced more than distance D_n
 - A Coefficient with mean value $\mu = 0.46$ and coefficient of variation $\sigma/\mu = 0.02 + 0.05(1 - D)^6$, where σ is the standard deviation

Valid for: Irregular, head-on waves

Breaking and nonbreaking wave conditions

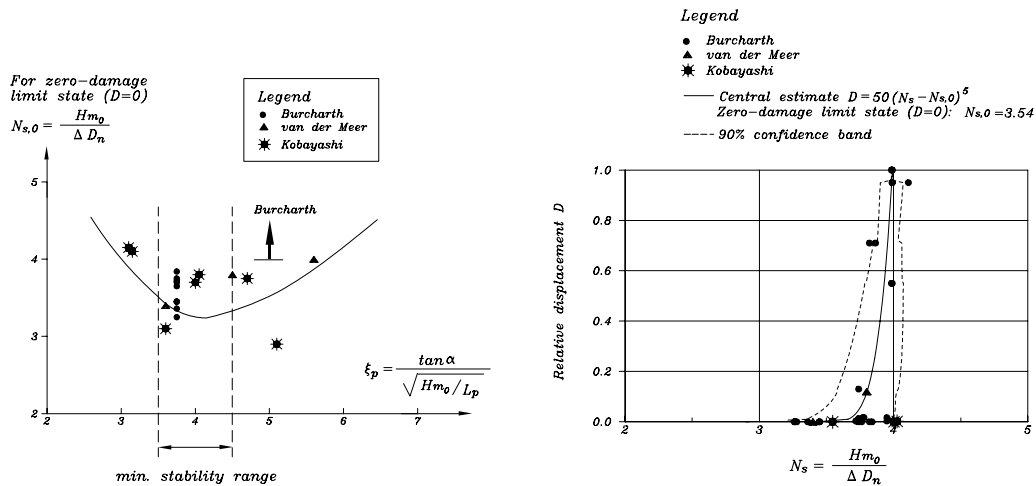
One layer of Accropodes on 1:1.33 slope placed in accordance with SOGREAH recommendations

Accropodes placed on filter layer and conventional quarry rock run

$3.5 < \xi_m < 4.5$ (minimum stability range, see figure)

No influence of number of waves were found except after start of failure.

Uncertainty of the formula: see figure and explanation of A .



SOGREAH recommends for preliminary design the following K_D -values to be used in Eq VI-5-67.

$$K_D = \begin{cases} 15 & \text{Nonbreaking waves} \\ 12 & \text{Breaking waves} \end{cases}$$

Table VI-5-34
CORE-LOC ®, Non or Marginally Overtopped Slopes (Melby and Turk 1994; Turk and Melby 1997)

Irregular, head-on waves

$$\frac{H}{\Delta D_{n50}} = (K_D \cot \alpha)^{1/3} \quad \text{or} \quad M_{50} = \frac{\rho_c H^3}{K_D \left(\frac{\rho_c}{\rho_w} - 1\right)^3 \cot \alpha} \quad (\text{VI-5-81})$$

- where H Characteristic wave height (H_s)
 D_{n50} Equivalent length of cube having same mass as Core-Loc, $D_{50} = (M_{50}/\rho_c)^{1/3}$
 M_{50} Mass of Core-Loc armor unit, $M_{50} = \rho_c (D_{n50})^3$
 ρ_c Mass density of concrete
 ρ_w Mass density of water
 Δ $(\rho_c/\rho_w) - 1$
 α Slope angle
 K_D Stability coefficient

Trunk section stability. Melby and Turk (1994) found no reasonable ($K_D < 50$) irregular breaking or nonbreaking wave conditions that would destabilize the layer. For an armor layer exposed to regular depth-limited plunging to collapsing waves, $K_D = 16$ in Equation VI-5-81 is recommended for preliminary design of all trunk sections. The recommended value of K_D is conservative, and it represents a zero-damage condition with little to no armor unit rocking. Site specific physical model tests will usually yield higher values.

Head section stability. $K_D = 13$ is recommended for preliminary design of head sections exposed to both breaking and nonbreaking oblique and head-on waves.

Stability test parameters

Model parameters	$M_{50} = 219$ g; Depths: 36 and 61 cm; Height: 90 cm
Wave parameters	$4.6 \leq H_{mo} \leq 36$ cm; $1.5 \leq T_p \leq 4.7$ sec
Structure slope, α	1V:1.33H and 1V:1.5H
Surf similarity parameter	$2.13 \leq \zeta_o \leq 15.9$
Relative depth	$0.012 \leq d/L_o \leq 0.175$
Wave steepness	$0.001 \leq H_{mo}/L_o \leq$ breaking

Placement. Core-Locs are intended to be randomly placed in a single-unit thick layer on steep or shallow slopes. They are well suited for use in repairing existing dolos structures because they interlock well with dolosse when properly sized (length of Core-Loc central flume is 92 percent of the dolosse fluke length).

Table VI-5-35
Tetrapods, Horizontally Composite Breakwaters (Hanzawa et al. 1996)

$$N_s = \frac{H_s}{\Delta D_n} = 2.32 \left(N_{od} / N_z^{0.5} \right)^{0.2} + 1.33 \quad (\text{VI-5-82})$$

- where H_s Significant wave height in front of breakwater
 ρ_s Mass density of concrete
 ρ_w Mass density of water
 Δ $(\rho_s / \rho_w) - 1$
 D_n Equivalent cube length, i.e., length of cube with the same volume as Tetrapods
 N_{od} Number of units displaced out of the armor layer within a strip width of one cube length D_n
 N_z Number of waves

Test range: The formula was obtained by fitting of earlier model test results and five real project model tests

- Irregular head-on waves
- Water depth: 0.25 - 0.50 m
- Slope: 1:1.5
- Foreshore : 1:15 - 1:100
- Mass of Tetrapods: 90 - 700 g
- H_s : 8 - 25.9 cm; T_s : 1.74 - 2.5 s; s_{om} : 0.013 - 0.04

Uncertainty of the formula: Not given. Tanimoto, Haranaka, and Yamazaki (1985) gave the standard deviation of N_{od} equal to $0.36N_{od}^{0.5}$

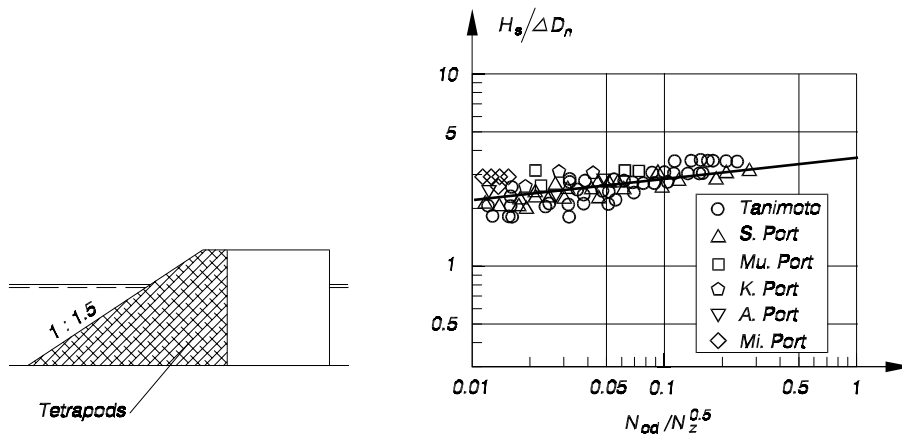


Table VI-5-36
Tribars, Non-Overtopped or Minor Overtopped Slopes, Random and Uniform Placement

Regular, head-on waves

$$\frac{H}{\Delta D_{n50}} = (K_D \cot \alpha)^{1/3} \quad \text{or} \quad M_{50} = \frac{\rho_s H^3}{K_D \left(\frac{\rho_s}{\rho_w} - 1 \right)^3 \cot \alpha} \quad \text{(VI-5-83)}$$

- where
- H Characteristic wave height (H_s)
 - D_{n50} Equivalent cube length of median rock
 - M_{50} Median mass of stone armor unit, $M_{50} = \rho_s (D_{n50})^3$
 - ρ_s Mass density of stone
 - ρ_w Mass density of water
 - Δ $(\rho_s/\rho_w) - 1$
 - α Slope angle
 - K_D Stability coefficient

Trunk section stability

K_D -values by *Shore Protection Manual* (1984), $H - H_{1/10}$, 0% to 5% damage

Placement	Layers	Breaking waves ¹	Nonbreaking waves ²	Slope angle $\cot \alpha$
Random	2	9.0	10.0	1.5 – 3.0
Pattern-placed	1	12.0	15.0	(not given)

¹ Depth-limited breaking with waves breaking in front of and on the armor slope.

- Design wave height considerations. In shallow water the most severe wave condition for design of any part of a rubble-mound structure is usually the combination of predicted water depth and extreme incident wave height and period that produces waves which would break directly on the structure. In some cases, particularly for steep foreshore slopes, waves breaking offshore will strike directly on the structure. Goda (1985) recommended computing the design wave height a distance $5H_s$ from the structure toe to account for the travel distance of large breakers. A shallow-water coastal structure exposed to a variety of water depths, especially a shore-perpendicular structure such as a groin, should have wave conditions investigated for each range of water depths to determine the highest breaking wave that might impact any part of the structure. For example, a groin that normally experiences wave forces on its armor layer near the seaward end might become submerged during storm surges, and the worst breaking wave condition could occur on a more landward portion of the groin. The effect of oblique wave approach on armor layer stability has not yet been sufficiently quantified. Tests in the European Marine Science and Technology (MAST) program seemed to indicate relatively little reduction in damage for rock armored slopes subjected to oblique wave approach angles up to 60 deg compared to waves of normal incidence (Allsop 1995). The stability of any rubble-mound structure exposed to oblique wave attack should be confirmed with physical model tests.

(6) Structure head section stability.

(a) Under similar wave conditions the round head of a rubble-mound structure normally sustains more extensive and more frequent damage than the structure trunk. One reason is very high cone-overflow velocities, sometimes enhanced in certain areas by wave refraction. Another reason is the reduced support from neighboring units in the direction of wave overflow on the lee side of the cone as shown in Figure VI-5-37. This figure also illustrates the position of the most critical area for armor layer instability. The toe within the same area is also vulnerable to damage in shallow-water situations, and a toe failure will often trigger failure of the armor layer see Part VI-5-6b(2), "Scour at sloping structures."

(b) Table VI-5-37 presents stability criteria for stone and dolos rubble-mound structure heads subjected to breaking and nonbreaking waves without overtopping, and Table VI-5-38 gives stability criteria for tetrapod and tribar concrete armor units.

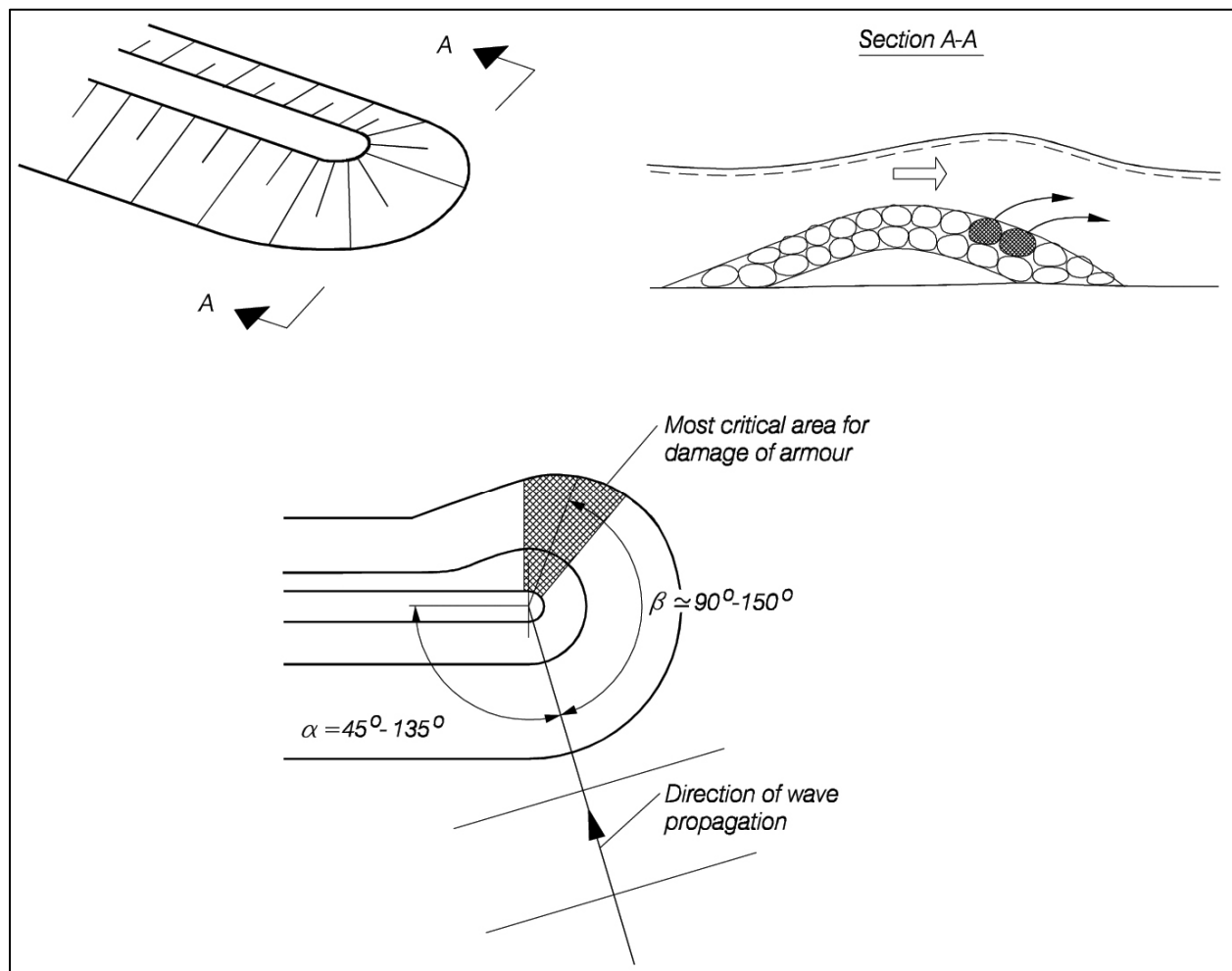


Figure VI-5-37. Illustration of critical areas for damage to armor layers in the round head (Burcharth 1993)

Table VI-5-37
Rock and Dolos Breakwater Head Stability, No Overtopping (Carver and Heimbaugh 1989)

Rock and dolos armor, monochromatic waves

Mostly monochromatic waves with a few irregular wave cases
 Breaking and nonbreaking waves
 Incident wave angles: 0°, 45°, 90°, 135° (note: 0° is wave crests perpendicular to trunk)

$$\frac{H}{\Delta D_{n50}} = A\xi^2 + B\xi + C_c \quad (\text{VI-5-84})$$

where

$$\xi = \frac{\tan \alpha}{(H/L)^{1/2}}$$

- and
- H Characteristic wave height
 - D_{n50} Equivalent cube length of median rock
 - ρ_s Mass density of stone
 - ρ_w Mass density of water
 - Δ $(\rho_s / \rho_w) - 1$
 - L Local wavelength at structure toe
 - α Structure armor slope
 - A, B, C_c Empirical coefficients

Table of coefficients for use in Equation VI-5-84

Armor Type	A	B	C _c	Slope	Range of ξ
Stone	0.272	-1.749	4.179	1V to 1.5H	2.1 – 4.1
Stone	0.198	-1.234	3.289	1V to 2.0H	1.8 – 3.4
Dolos	0.406	-2.800	6.881	1V to 1.5H	2.2 – 4.4
Dolos	0.840	-4.466	8.244	1V to 2.0H	1.7 – 3.2

Notes: The curves giving the best fit to the data were lowered by two standard deviations to provide a conservative lower envelope to the stability results.

A limited number of tests using irregular waves produced corresponding results with T_p equivalent to the monochromatic period and H_{mo} equal to the monochromatic wave height.

Table VI-5-38
Tetrapod and Tribar Breakwater Head Section Stability, No Overtopping

Regular, head-on waves

$$\frac{H}{\Delta D_{n50}} = (K_D \cot \alpha)^{1/3} \quad \text{or} \quad M_{50} = \frac{\rho_s H^3}{K_D \left(\frac{\rho_s}{\rho_w} - 1 \right)^3 \cot \alpha} \quad (\text{VI-5-85})$$

- where H Characteristic wave height (H_s)
 D_{n50} Equivalent cube length of median rock
 M_{50} Median mass of stone armor unit, $M_{50} = \rho_s (D_{n50})^3$
 ρ_s Mass density of stone
 ρ_w Mass density of water
 Δ $(\rho_s / \rho_w) - 1$
 α Slope angle
 K_D Stability coefficient

Head Section Stability.

K_D -values by *Shore Protection Manual* (1984), $H = H_{1/10}$, 0 percent to 5 percent damage

Armor Unit	Placement	Layers	Breaking Waves ¹	Nonbreaking Waves ²	Slope Angle cot α
Tetrapod	Random	2	5.0 ³	6.0	1.5
			4.5	5.5	2.0
			3.5	4.0	3.0
Tribar	Random	2	8.3	9.0	1.5
			7.8	8.5	2.0
			6.0	6.5	3.0
Tribar	Pattern	1	7.5	9.5	(not given)

¹ Depth-limited breaking with waves breaking in front of and on the armor slope.

² No depth-limited breaking occurs in front of the armor slope.

³ K_D values shown in italics are unsupported by tests results and are provided only for preliminary design purposes.

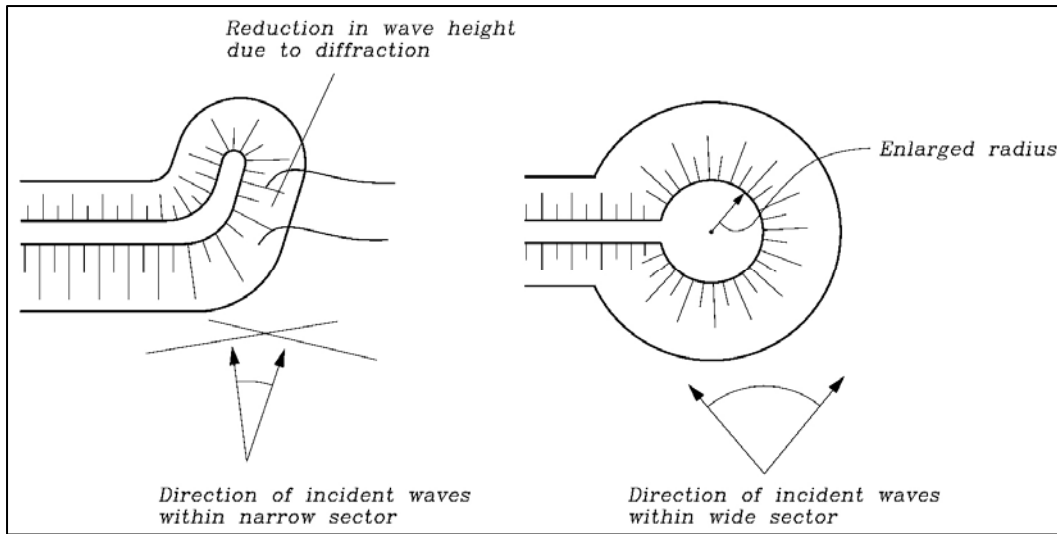


Figure VI-5-38. Illustration of improvement of round head stability by change of geometry (Burcharth 1993)

(c) The stability in the critical area of the roundhead might be improved by increasing the head diameter or adding a tail as shown in Figure VI-5-38. Besides obtaining better support from neighboring units, a reduction in wave heights by diffraction is also achieved before the waves reach the vulnerable rear side. Optimization of the slope angle and the layout geometry of cone roundheads can only be achieved by physical model tests because quantitative information on roundhead stability is limited.

(d) The armor layer at bends and corners is generally more exposed than in straight trunk sections. A convex bend or corner will often follow the seabed contours because construction in deeper water increases costs dramatically. Refraction might then cause an increase of the wave height as illustrated in Figure VI-5-39, which in turn increases wave runup and overtopping. Moreover, in sharper convex corners and bends the lateral support by neighbor blocks is reduced as in the case of roundheads. A concave bend or corner will often be exposed to larger waves than the neighboring trunk sections due to the concentration of wave energy by oblique reflection on the slope (Figure VI-5-39). Consequently, runup and overtopping will also be increased.

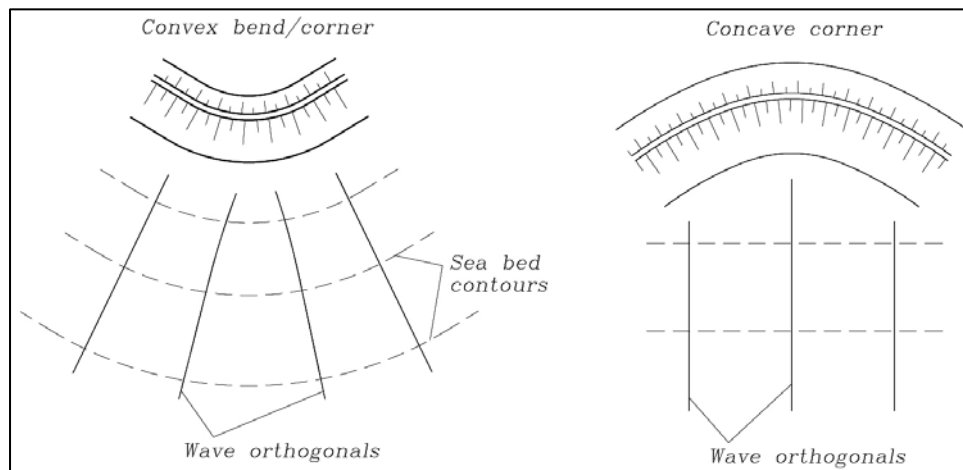


Figure VI-5-39. Convex and concave bends and corners

(7) Riprap armor stability.

(a) The previous armor stability formulations are intended for fairly uniform distributions of armor stone or for uniform size concrete armor units. Riprap armor is characterized by fairly wide gradations in rock size with a large size difference between the largest and smallest stones in the distribution. Use of graded riprap cover layers is generally more applicable to revetments than to breakwaters or jetties. A limitation on the use of graded riprap is that the design wave height should be less than about 1.5 m. At higher design wave heights uniform-size armor units are usually more economical.

Generally, the maximum and minimum stone weights in riprap gradations should be limited to

$$W_{\max} = 4.0W_{50} \quad W_{\min} = 0.125W_{50}$$

where W_{50} is the median stone weight. The median stone mass for a stable riprap distribution can be determined using the Hudson equation

$$M_{50} = \frac{\rho_r H_{10\%}^3}{K_{RR} \left(\frac{\rho_r}{\rho_w} - 1 \right)^3 \cot \alpha} \quad (\text{VI-5-86})$$

where ρ_r is the mass density of the riprap, K_{RR} is the riprap stability coefficient, and the other variables are as defined for Equation VI-5-67 in Table VI-5-22. Recommended conservative stability coefficients (0 percent to 5 percent damage) are $K_{RR} = 2.2$ for breaking waves and $K_{RR} = 2.5$ for nonbreaking waves (Ahrens 1981b). Melby and Kobayashi (1998b) showed that deterioration of riprap and uniform armor with equivalent median stone weights were similar. Therefore, Equation VI-5-62 through VI-5-66 could be used to estimate damage progression for both narrow gradations and riprap. The van der Meer (1988) equation (see Table VI-5-23) can also be used to design riprap armor.

(b) An examination of riprap field performance at 14 different dams across the La Grande Hydroelectric complex in Quebec, Canada, generally confirmed the validity of Equation VI-5-86 (Belfadhel, Lefebvre, and Rohan 1996; also see discussion of this paper by van der Meer 1997). Design of riprap armor layer cross sections is covered in Part VI-5-3e, "Design of structure cross section." A complete design example for a riprap armored slope is included in Part VI-7, "Example Problems."

b. Granulated filters and geotextile filter stability. In coastal engineering, filter layers are defined as layers that protect the underlying base material or soil from erosion by waves and currents without excessive buildup of pore pressure in the underlying material. Filter functions can be achieved using either one or more layers of granulated material such as gravel or small stone of various grain sizes, geotextile fabric, or a combination of geotextile overlaid with granulated material. This section covers the function and design of granulated filters. Design criteria for geotextile filter cloth used in filter application are given in Part VI-4-7, "Geotextiles and Plastics." Design of rubble-mound structure underlayers is covered in Part VI-5-3e, "Design of structure cross section."

(1) Filter layer functions. Filter layers are designed to achieve one or more of the following objectives in coastal structures:

- Prevent migration of underlying sand or soil particles through the filter layer voids into the overlying rubble-mound structure layers. Leeching of base material could be caused by turbulent flow within the structure or by excessive pore pressures that can wash out fine particles. Without a filter layer,

foundation or underlayer material would be lost and the stones in the structure layer over the filter would sink into the void resulting in differential settlement and decreased structure crest elevation.

- Distribution of structure weight. A bedding filter layer helps to distribute the structure's weight over the underlying base material to provide more uniform settlement. A levelled bedding layer also ensures a more uniform baseplate load on caisson structures.
- Reduction of hydrodynamic loads on the structure's outer stone layers. A granular filter layer can help dissipate flow energy whereas a geotextile filter will not be as effective in this regard.

(a) Granulated filters are commonly used as a bedding layer on which a coastal structure rests, or in construction of revetments where the filter layer protects the underlying embankment. Filter layers are also needed in rubble-mound structures having cores composed of fine materials like sand or gravel. Stone blankets (used to prevent erosion due to waves and currents) also reduce leeching of the underlying sand or soil, but in this situation stability of the stone blanket material in waves and currents is an important design concern. Design of stone blankets is covered in Part VI-5-3f, "Blanket stability in current fields."

(b) It is advisable to place coastal structures on a bedding layer (along with adequate toe protection) to prevent or reduce undermining and settlement. When rubble structures are founded on cohesionless soil, especially sand, a filter blanket should be provided to prevent differential wave pressures, currents, and groundwater flow from creating an unstable foundation condition through removal of particles. Even when a filter blanket is not needed, bedding layers may be used to prevent erosion during construction, to distribute structure weight, or to retain and protect a geotextile filter cloth. Bedding layers are not necessary where depths are greater than about three times the maximum wave height, where the anticipated bottom current velocities are below the incipient motion level for the average-size bed material, or where the foundation is a hard, durable material such as bedrock.

(c) In some situations granular filters have several advantages over geotextile filters in coastal construction (Permanent International Association of Navigation Congresses (PIANC) 1992).

- The filter elements (stone, gravel, sand, etc.) are usually very durable.
- Granular filters provide a good contact interface between the filter and base material below and between the filter and overlying layers. This is important for sloping structures.
- Granular bedding layers can help smooth bottom irregularities and thus provide a more uniform construction base.
- The porosity of granular filters help damp wave energy.
- Self-weight of the filter layer contributes to its stability when exposed to waves and currents during construction whereas geotextiles may have to be weighted under similar conditions..
- The loose nature of the filter elements allows the filter to better withstand impacts when larger stones are placed on the filter layer during construction or the stones shift during settlement.
- Granular filter layers are relatively easy to repair, and in some instances may be self-healing.
- Filter materials are widely available and inexpensive.

(d) The major disadvantage of granular filters is the difficulty of assuring uniform construction underwater to obtain the required thickness of the filter layer.

(e) Placing larger armor stone or riprap directly on geotextile filter cloth is likely to puncture the fabric either during placement or later during armor settlement. Placing a granular filter layer over the geotextile fabric protects it from damage. In this application there is more flexibility in specifying the filter stone gradation because the geotextile is retaining the underlying soil.

(2) Granulated filter failure modes. Granular filter layers fail their intended function when:

- (a) The base layer is eroded through the filter layer. Erosion can occur either by outgoing flow washing out particles perpendicular to the base/filter interface or by wave- and current-induced external flows parallel to the interface.
- (b) The filter layer becomes internally unstable. Instability occurs in filters having a very wide gradation when the finer fraction of the filter grain-size distribution is flushed out of the layer between the coarser material. This could result in compaction of the filter layer, differential settlement of the overlayers, and gradual increase in layer permeability.
- (c) The interface between adjacent granular layers becomes unstable, and lateral shearing motion occurs between layers constructed on a slope.
- (d) The filter layer fails to protect the underlying geotextile fabric from punctures and loss of soil through the filter cloth.

(3) Granulated filter design criteria.

(a) Design criteria for granular filters were originally based on the geometry of voids between packed, uniform spheres. Allowances for grain-size distributions (and many successful field applications) led to the following established geometric filter design criteria. (Design guidance for exposed filter layers must also consider instability due to flow as discussed in Part VI-5-3f, "Blanket stability in current fields.")

- Retention criterion. To prevent loss of the foundation or core material by leeching through the filter layer, the grain-size diameter exceeded by 85 percent of the filter material should be less than approximately four or five times the grain-size diameter exceeded by the coarsest 15 percent of the foundation or underlying material, i.e.,

$$\frac{d_{15(\text{filter})}}{d_{85(\text{foundation})}} < (4 \text{ to } 5) \quad (\text{VI-5-87})$$

The coarser particles of the foundation or base material are trapped in the voids of the filter layer, thus forming a barrier for the smaller sized fraction of the foundation material. The same criterion can be used to size successive layers in multilayer filters that might be needed when there is a large disparity between void sizes in the overlayer and particle sizes in the material under the filter. Filter layers overlying coarse material like quarry spall and subject to intense dynamic forces should be designed similar to a rubble-mound structure underlayer with

$$\frac{W_{50(\text{filter})}}{W_{50(\text{foundation})}} < (15 \text{ to } 20) \quad (\text{VI-5-88})$$

- Permeability criterion. Adequate permeability of the filter layer is needed to reduce the hydraulic gradient across the layer. The accepted permeability criterion is

$$\frac{d_{15(\text{filter})}}{d_{15(\text{foundation})}} > (4 \text{ to } 5) \quad (\text{VI-5-89})$$

- Internal stability criterion. If the filter material has a wide gradation, there may be loss of finer particles causing internal instability. Internal stability requires

$$\frac{d_{60(\text{filter})}}{d_{10(\text{filter})}} < 10 \quad (\text{VI-5-90})$$

- Layer thickness. Filter layers constructed of coarse gravel or larger material should have a minimum thickness at least two to three times the diameter of the larger stones in the filter distribution to be effective. Smaller gravel filter layer thickness should be at least 20 cm, and sand filter layers should be at least 10 cm thick (Pilarczyk 1990). These thickness guidelines assume controlled above-water construction. In underwater placement, bedding layer thickness should be at least two to three times the size of the larger quarrystones used in the layer, but never less than 30 cm thick to ensure that bottom irregularities are completely covered. Considerations such as shallow depths, exposure during construction, construction method, and strong hydrodynamic forces may dictate thicker filters, but no general rules can be stated. For deeper water the uncertainty related to construction often demands a minimum thickness of 50 cm.
- Bedding layer over geotextile fabric. In designs where a geotextile fabric is used to meet the retention criterion, a covering layer of quarry spalls or crushed rock (10-cm minimum and 20-cm maximum) should be placed to protect against puncturing by the overlying stones. Recommended minimum bedding layer thickness in this case is 60 cm, and filtering criteria should be met between the bedding layer and overlying stone layer.

(b) Examples of typical granular filters and bedding layers are illustrated in Lee (1972), who discussed and illustrated applications of granular and geotextile filters in coastal structures. Design of filters for block-type revetments with large holes in the cover layer can be found in the PIANC (1992) reference.

(c) The previous geometric granular filter criteria are widely accepted in practice, and they are recommended in cases when an appreciable pressure gradient is expected perpendicular to the soil/filter interface. However, these rules may be somewhat conservative in situations without significant pressure gradients and when flow is parallel to the filter layer.

(d) The need for reliable granular filter design guidance under steady flow and cyclic design conditions fostered research by Delft Hydraulics Laboratory in support of the Oosterschelde Storm Surge Barrier in The Netherlands. Stationary and cyclic flow both parallel to and perpendicular to the filter layer were investigated by de Graauw, van der Meulen, and van der Does de Bye (1984). They developed hydraulic filter criteria based on an expression for critical hydraulic gradient parallel to the filter/soil interface. This method assumes that erosion of base material is caused by shear stresses rather than groundwater pressure gradients; and where this is the case, the geometric filter requirements can be relaxed.

(e) The filter design guidance of de Graauw et al. was expressed in terms of the filter d_{15} , base material d_{50} , filter porosity, and critical shear velocity of the base material; and acceptable values for the critical

gradient were given by graphs for each of the flow cases. Design of a hydraulic granular filter requires good understanding of the character of flow within the filter layer, e.g., steady flow in channels. In these cases the method of de Graauw et al. (1984) can be used. More recent research aimed at improving granular filter design criteria was reported by Bakker, Verheij, and deGroot (1994).

(4) Granulated filter construction aspects.

(a) Granular filter construction above water creates no special problems, and accurate placement is straightforward. However, constructing a filter beneath the water surface is somewhat more problematic. If small-size filter material with a wide gradation is dropped into place, there is a risk of particle segregation by size. This risk can be decreased by using more uniform material and minimizing the drop distance. Another problem is maintaining adequate layer thickness during underwater placement. This has led to the recommended layer thickness being greater than required by the geometric filter criteria. Finally, filter or bedding layers placed underwater are exposed to eroding waves and currents until the overlays are placed. Depending on site-specific conditions, this factor may influence the construction sequence or the time of year chosen for construction.

(b) It is common practice to extend the bedding layer beneath rubble-mound structures at least 1.5 m beyond the toe of the cover stone to help reduce toe scour. Some low rubble-mound structures have no core, and instead are composed entirely of armor layer and underlayers. These structures should have a bedding layer that extends across the full width of the structure.

c. *Structural integrity of concrete armor units.*

(1) Introduction.

(a) Figure VI-5-40 shows examples of the wide variety of existing concrete armor units. These might be divided into the following categories related to the structural strength:

Massive or blocky (e.g., cubes including Antifer type, parallelepiped block, grooved cube with hole)

Bulky (e.g., seabee, Core-Loc[®], Accropode[®], Haro[®], dolos with large waist ratios)

Slender (e.g., tetrapod, dolos with smaller waist ratios)

Multi-hole cubes (e.g., shed, cob)

(b) The units are generally made of conventional unreinforced concrete except the multi-hole cubes where fiber reinforcement is sometimes used.

(c) For slender units such as dolos with small waist ratios, various types of high-strength concrete and reinforcement (conventional rebars, prestressing, fibers, scrap iron, steel profiles) have been considered. However, reinforcement has only been used in few cases because it generally seems to be less cost-effective and because of the risk of rapid corrosion of the steel reinforcement.

(d) Hydraulic stability of armor layers is reduced if the armor units disintegrate causing reduction of the stabilizing gravitational force and possible interlocking effects. Moreover, broken armor unit pieces might be thrown around by wave action and thereby trigger additional breakage at an increased rate. In order to prevent this, it is necessary to ensure structural integrity of the armor units.

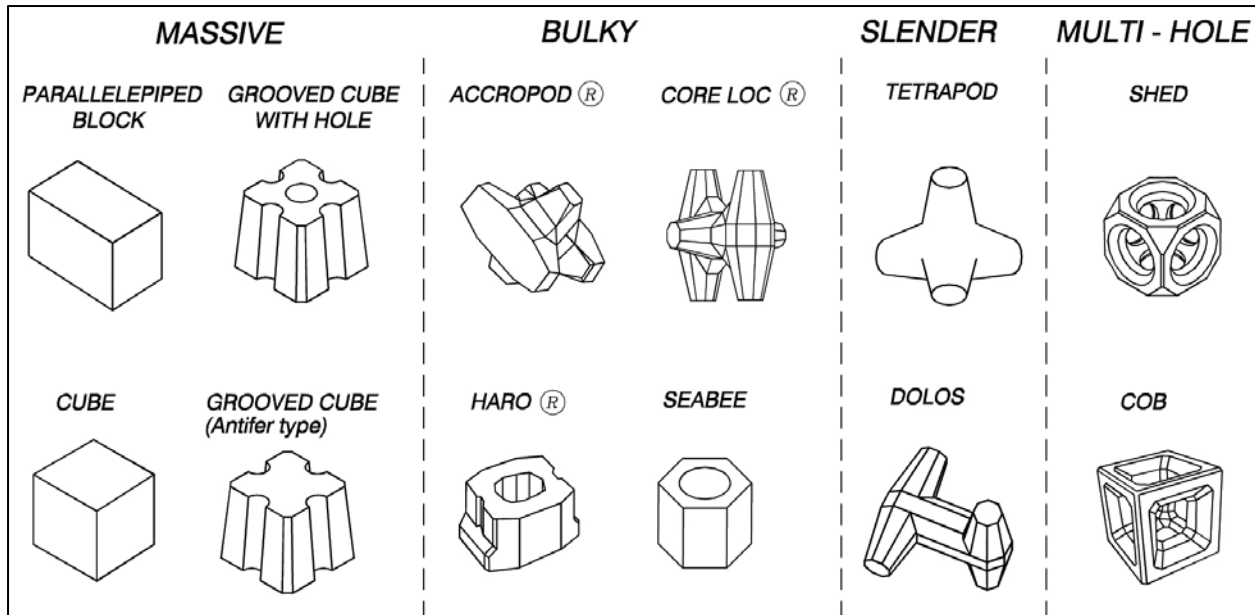


Figure VI-5-40. Examples of concrete armor units

(e) Unreinforced concrete is a brittle material with a low tensile strength, f_T , on the order of 2-6 MPa and a compressive strength, f_C , which is one order of magnitude larger than f_T . Consequently, crack formation and breakage is nearly always caused by load induced tensile stresses, σ_T , that exceed f_T . The magnitude of f_T is therefore more important than f_C in armor unit concrete, and specifications should focus on achieving adequate values of f_T . It is important to note that f_T decreases with repeated load due to fatigue effects.

(f) The different categories of concrete armor units are not equally sensitive to breakage. Slender units are the most vulnerable because the limited cross-sectional areas give rise to relatively large tensile stresses. Some recent failures of breakwaters armored with tetrapods and dolosse were caused by breakage of the units into smaller pieces having less hydraulic stability than the intact armor units.

(g) Massive units will generally have the smallest tensile stresses due to the distribution of loads over large cross-sectional areas. However, breakage can take place if the units experience impacts due to less restrictive hydraulic stability criteria and if the concrete quality is poor with a low f_T . This latter point is related mainly to larger units where temperature differences during the hardening process can create tensile stresses which exceed the strength of the weak young concrete, thus resulting in microcracking of the material (thermal cracking). If massive units are made of good quality concrete and not damaged during handling, and if the armor layer is designed for marginal displacements, there will be no breakage problems. This statement also holds for the bulky units under the same precautions.

(h) The different types of loads on armor units and load origins are listed in Table VI-5-39.

(2) Structural design formulae for dolosse and tetrapods. Based on model tests with instrumented units, Burcharth (1993b), Burcharth and Liu (1995) and Burcharth et al. (1995b) presented a dimensional formula for estimation of the relative breakage of dolosse and tetrapods (fraction of total units) as presented in Table VI-5-40. Figures VI-5-41 and VI-5-42 compare the formulae to breakage data. Design diagrams for dolos were also presented in Burcharth and Liu (1992).

Table VI-5-39
Types and Origins of Loads on Armor Units (Burcharth 1993b)

TYPES OF LOADS	ORIGIN OF LOADS
Static	Weight of units
	Prestressing of units due to wedge effect and arching caused by movement under dynamic loads
Dynamic	Pulsating
	Gradually varying wave forces
	Earthquake loads
	Impact
Abrasion	Collisions between units when rocking or rolling, collision with underlayers or other structural parts
	Missiles of broken units
	Collisions during handling, transport, and placing
Thermal	High-frequency wave slamming
	Impacts of suspended sand, shingle, etc.
Chemical	Temperature differences during the hardening (setting) process after casting
	Freeze – thaw cycles
Chemical	Alkali-silica and sulphate reactions, etc.
	Corrosion of steel reinforcement

(a) Stress determination. Structural design methodologies for dolosse have also been proposed by Anglin et al. (1990) (see Table VI-5-41); Melby (1990, 1993); Zwamborn and Phelp (1990); and Melby and Turk (1992). The methods of Zwamborn and Phelp are based primarily on prototype failure tests, and therefore, are site specific.

- Melby (1990, 1993) provided a method to determine the design tensile stress for a dolos layer and discussed a computer program to compute this design stress. Figure VI-5-43 shows wave height in meters versus maximum flexural tensile stress in MPa for several dolos waist ratios and several Hudson stability coefficients. In this case, the wave height was used to determine a dolos weight using the Hudson stability equation. Figure VI-5-44 shows dolos weight in metric tons versus maximum flexural tensile stress in MPa for several dolos waist ratios. Both figures were generated using a tensile stress exceedance value of $E=2$ percent for the condition where the given stress level is exceeded in approximately 2 percent of the units on the slope. In addition, a structure slope of 1V:2H and a specific gravity of $\rho_a/\rho_w = 2.40$ were used to compute the stress level, although the effect of these parameters on the stress was negligible over typical ranges of these parameters. Further, Figure VI-5-44 was not affected by the choice of stability coefficient.

(b) Reinforced dolos design. Melby and Turk (1992) extended the method of Melby (1993) to include a level I reliability analysis and conventional reinforced concrete design methodology (American Concrete Institute (ACI) 1989). The following technique utilizes a probabilistic principal stress computed using any of the previous methods. These methods allow the designer to consider unreinforced concrete, conventional steel rebar reinforcement, or prestressing in a unified format. The basic design equation, following structural concrete design conventions, equates a factored strength with a factored load as

Table VI-5-40
Breakage Formula for Dolosse and Tetrapods (Burcharth 1993b, Burcharth and Liu 1995, Burcharth et al. 1995b, Burcharth et al. 2000)

$$B = C_0 M^{C_1} f_T^{C_2} H_s^{C_3} \quad (\text{VI-5-91})$$

where B Relative breakage
 M Armor unit mass in ton, $2.5 \leq M \leq 50$
 f_T Concrete static tensile strength in MPa, $2 \leq f_T \leq 4$
 H_s Significant wave height in meters
 C_0, C_1, C_2, C_3 Fitted parameters

The effects of static, pulsating, and impact stresses are included in the formula.

Fitted parameters for the breakage formula

	Waist ratio	Variational Coef. of C_0	C_0	C_1	C_2	C_3
Trunk of dolosse	0.325	0.188	0.00973	-0.749	-2.58	4.143
	0.37	0.200	0.00546	-0.782	-1.22	3.147
	0.42	0.176	0.01306	-0.507	-1.74	2.871
Round-head of dolosse	0.37	0.075	0.025	-0.65	-0.66	2.42
Trunk of tetrapods		0.25	0.00393	-0.79	-2.73	3.84

Summary of the hydraulic model tests

	Dolos trunk	Dolos round-head	Tetrapod trunk
Breakwater slope α	1.5	1.5	1.5
Foreshore	1:20	horizontal	1:50
Water depth at toe (cm)	23	50	30 and 50
Height of breakwater (cm)	60	70	55 and 75
Mass of units (kg)	0.187	0.187	0.290
Concrete density (tons/m ²)	2.3	2.3	2.3
Spectral peak period T_p (s)	1.5-3	1.5-2.5	1.3-2.8
Significant wave height H_s (cm)	5.7-17.7	5-13	8.8-27.3
Surf similarity parameter $\xi = (H_s/L_p)^{-0.5} \tan \alpha$	3-7.5	3.8-7.5	2.7-4.1

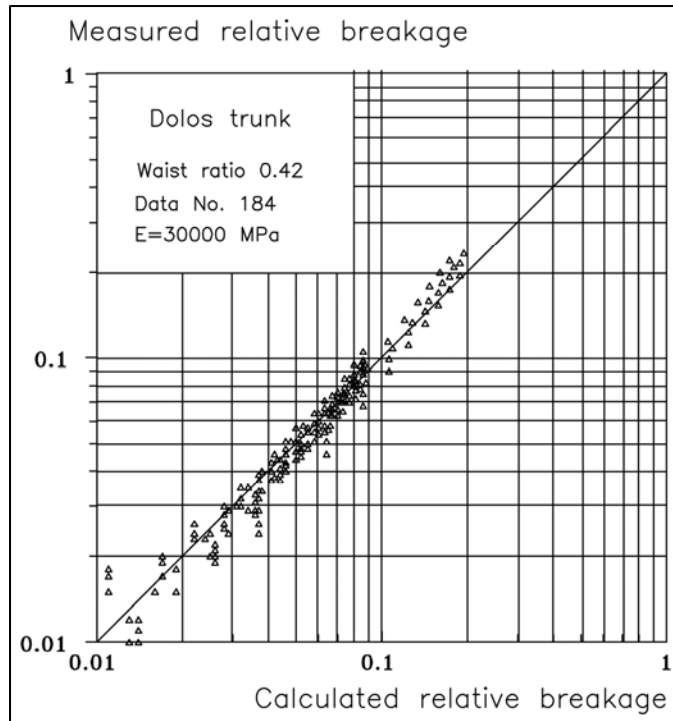


Figure VI-5-41. Breakage formula for dolosse (Burcharth 1993b; Burcharth and Liu 1995; Burcharth et al. 1995b)

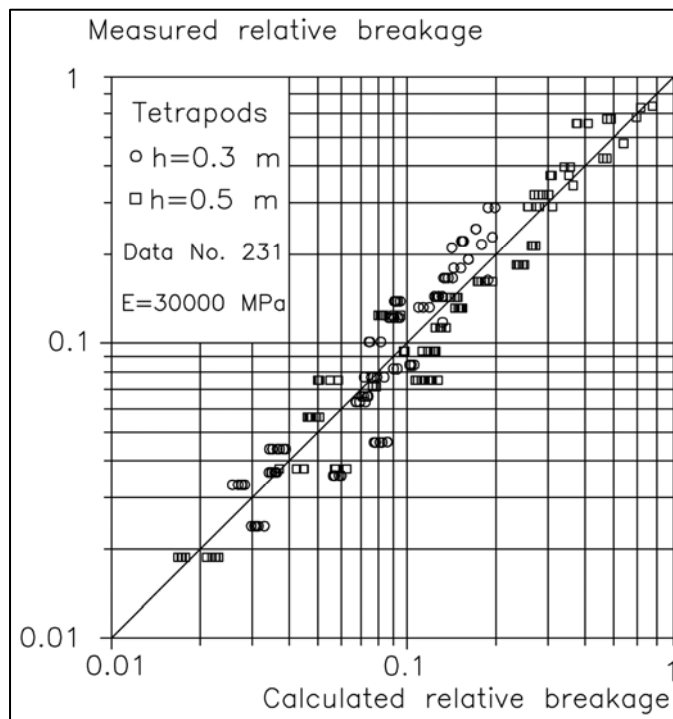


Figure VI-5-42. Breakage formula for tetrapods (Burcharth 1993b, Burcharth and Liu 1995, Burcharth et al. 1995b)

Table VI-5-41
Stress Prediction Formulae for Dolosse (Anglin et al. 1990)

Anglin et al. (1990) developed a dolos structural design methodology based on small scale measurements of strain in laboratory hydraulic models. Only the static stresses were considered. The criterion for allowable static tensile stress in a dolos at a vertical distance D_v down from the crest on a dry structure was proposed as

$$n(\sigma_s)_p < f_T \quad (\text{VI-5-92})$$

where

- f_T = Prototype concrete static tensile strength (MPa)
- $(\sigma_s)_p$ = Static principal stress in model dolos with probability of exceedance, p
- n = Model scale factor

The static principal stress is estimated as

$$(\sigma_s)_p = 10^{(\log(\sigma_s)_{est} + 0.31[\Phi^{-1}(p)])} \quad (\text{VI-5-93})$$

with

$$\log(\sigma_s)_{est} = -2.28 + 0.91\alpha + 0.30\left(\frac{D_v}{n} - 0.45\right) + 0.34l \quad (\text{VI-5-94})$$

and the model scale factor was given as

$$n = 9.43\left(\frac{W}{0.1549w_a}\right)^{1/3} \quad (\text{VI-5-95})$$

and

- α = Tangent of seaward armor slope
- l = Layer (0 for top; 1 for bottom)
- D_v = Vertical distance from crest to stressed dolos location
- $\Phi^{-1}(p)$ = Tabulated inverse normal variate (see next page)
- W = Prototype armor unit weight
- w_a = Armor concrete specific weight

(Continued)

Table VI-5-41 (Concluded)

Values for the inverse normal variate in Eq VI-5-93 are given in the box to the right.

Probability of exceedance	$\Phi^{-1}(p)$
0.1	1.28
0.05	1.65
0.02	2.05
0.01	2.33

Equations VI-5-92 through VI-5-95 are limited to the range of values:

$$0.4 \leq \alpha \leq 0.67 ; 0.3 \text{ m} \leq D_v/n \leq 0.6 \text{ m} ;$$

$$r = 0.32 \text{ where } r \text{ is the dolos waist ratio}$$

Another model study examined the combined effects of static and quasistatic (wave-induced pulsating loads) under nonbreaking regular wave conditions, but did not include impact stresses. The criterion for allowable tensile stress in a dolos located a vertical distance, D_{swl} , from the swl was given as

$$n(\sigma_t)_p < f_T \quad \text{(VI-5-96)}$$

where

$$(\sigma_t)_p = (\sigma_t)_{est} + 0.001[\Phi^{-1}(p)] \quad \text{(VI-5-97)}$$

$$(\sigma_t)_{est} = 0.905(\sigma_s)_{est} + 0.639(\sigma_q)_{est} \quad \text{(VI-5-98)}$$

$$\log(\sigma_q)_{est} = -2.36 + 0.15\alpha + 0.01\left(\frac{T}{\sqrt{n}}\right) + 0.29\left(\frac{D_{swl}}{n}\right) + 2.20\left(\frac{H}{n}\right) \quad \text{(VI-5-99)}$$

and

$(\sigma_t)_p$ = Total static and pulsating principal stress in model armor unit with probability of occurrence,

$(\sigma_q)_p$ = Pulsating principal stress in model armor unit with probability of occurrence, p

$(\sigma_s)_p$ = Static principal stress with probability of occurrence, p , from Eq VI-5-94

H = Regular wave height

T = Regular wave period

D_{swl} = Vertical distance from swl to location of stressed dolos. (Positive above swl, negative below swl.)

n = Model scale factor from Eq VI-5-95

α = Tangent of seaward armor slope

$\Phi^{-1}(p)$ = Tabulated inverse normal variate from the preceding box

Equations VI-5-96 through VI-5-99 are limited in application to the range of values:

$$0.05 \text{ m} \leq H/n \leq 0.25 \text{ m} ; 0.4 \leq \alpha \leq 0.67 ; 0.3 \text{ m} \leq D_v/n \leq 0.6 \text{ m} ;$$

$$1.25 \text{ s} \leq T/(n)^{1/2} \leq 2.5 \text{ s} ; -0.1 \text{ m} \leq D_{swl}/n \leq +0.1 \text{ m}$$

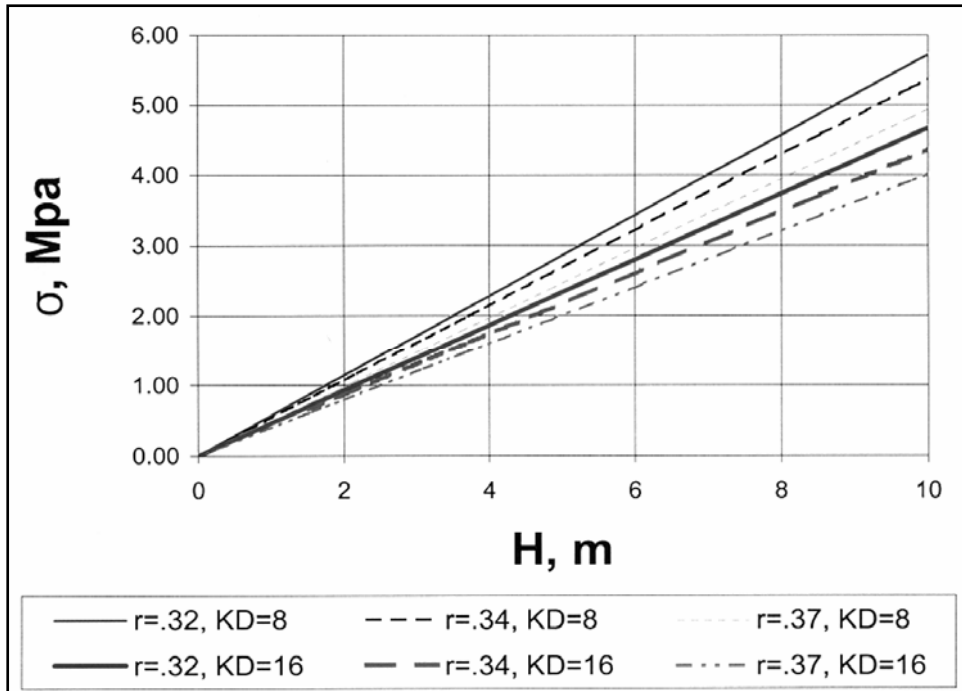


Figure VI-5-43. Wave height versus maximum flexural tensile stress for several dolos waist ratios

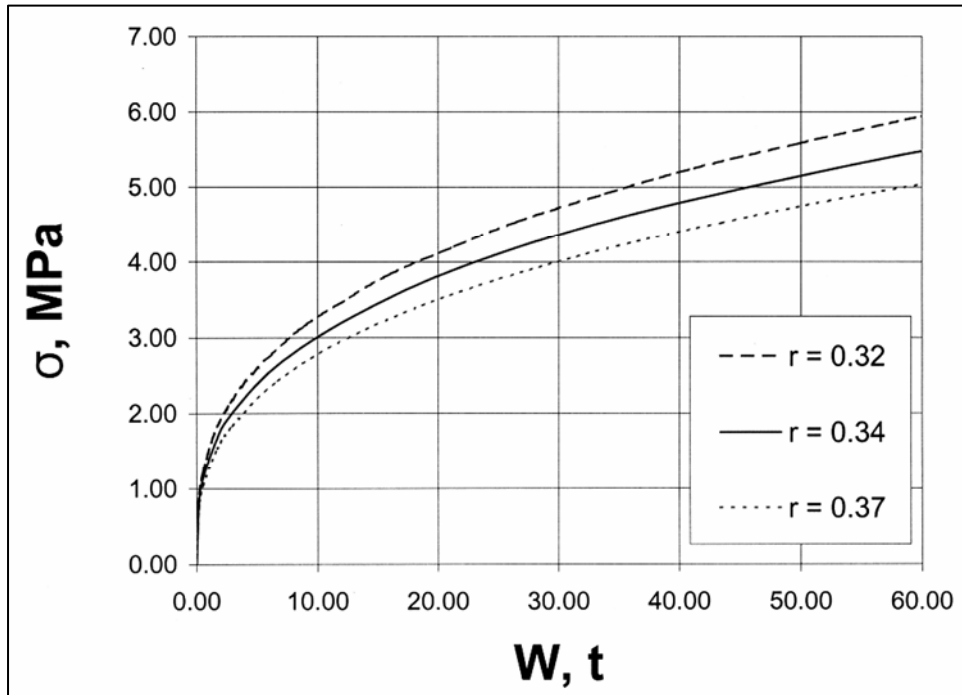


Figure VI-5-44. Dolos mass versus maximum flexural tensile stress for several dolos waist ratios

$$\gamma Q_n = \phi R_n \quad (\text{VI-5-100})$$

where γ and ϕ are the load and strength factors, respectively, to account for uncertainty in nominal load Q_n and nominal strength R_n . Melby and Turk noted that the load factor ranges from 1.0 to 1.2 for typical values of exceedance probability for stress. American Concrete Institute (ACI) (1989) recommends $\phi = 0.85$ for torsion. To facilitate reinforcement design, Melby and Turk assumed a circular cross section and decomposed Equation VI-5-100 into a flexure equation

$$\gamma S_M k_M \sigma_1 < \phi (0.7 M_{cr}) \quad (\text{VI-5-101})$$

and a torsional equation

$$\gamma S_T k_T \sigma_1 < \phi (0.7 T_{cr} + T_s) \quad (\text{VI-5-102})$$

where σ_1 is the principal stress, $S_M = 0.1053(rC)^3$ and $S_T = 0.2105(rC)^3$ are the section moduli for flexure and torsion, r is the dolos waist ratio, C is the dolos fluke length, and $k_M = k_T = 0.6$ are the moment and torque contribution factors, $M_{cr} = T_{cr} = 0.7 f_{ct}$ are the critical strengths of the concrete in moment and torque, f_{ct} is the concrete splitting tensile strength, and T_s is the strength contribution from the torsional steel reinforcement. The inequality in Equations VI-5-101 and VI-5-102 assures that the factored tensile strength will be greater than the factored tensile load.

- The technique for steel reinforcement design utilizes conventional structural design techniques. Torsional steel is specified first, and it is only required in the shank because the flukes are not likely to be twisted. Details are given in ACI 318-89 (ACI 1989). Assuming a circular section for the dolos shank, the amount of torsional steel is given as $T_s = R_h A_s f_y$, where R_h is the distance to the center of the section, A_s is the total area of steel intersecting the crack, and f_y is the yield strength of the steel. Substituting T_s into Equation VI-5-102 yields the equation for required torsional steel, i.e.,

$$A_s > \frac{\gamma (S_T k_T \sigma_1) - \phi (0.7 T_{cr})}{\phi f_y R_h} \quad (\text{VI-5-103})$$

- The number of bars required is then given by $n = A_s / A_b$, where A_b is the cross-sectional area of hoop reinforcing bars, and the spacing is $s = 1.5\pi R_h / n$, assuming the crack extends three-fourths of the distance around the circumference.
- For flexural reinforcement design, it is assumed that the concrete offers no resistance in tension. Nominal strength is reached when the crushing strain in the outer fiber of the concrete is balanced by the yield strain in the steel rebar. The balanced failure condition using the Whitney rectangular stress block is prescribed in ACI 318-89, Part 10 (ACI 1989). The solution requires an iterative approach because the neutral axis is a priori unknown. Assuming a rebar size, the neutral axis is located by solving the quadratic equation that results from balancing the compressive force moment from the Whitney stress block with the tensile force moment from the steel. Once the neutral axis is determined, the nominal moment from the steel can be determined and substituted into Equation VI-5-101 to determine if the quantity of steel is adequate to balance the flexural design load. After determining the amount of flexural steel required, typical checks of compressive stress, shear, bond, minimum reinforcement, and temperature steel should be made as per ACI 318-89.

(c) Prestressed dolos design. Prestressing acts reduce principal stress. The principal stress reduction factor is given by

$$\xi = 0.5 \left((k_M - \lambda) + \sqrt{(k_M - \lambda)^2 + 4k_T^2} \right) \quad (\text{VI-5-104})$$

where λ is the ratio of applied precompressive stress to design principal stress. This equation was substituted into the moment-torque interaction relations to get design equations for torsion and flexure as follows:

$$\gamma_\xi^x k_T \sigma_1 = 0.5 \phi \sqrt{\frac{f_c}{1 + 4 \left(\frac{k_M S_M}{k_T S_T} \right)^2}} \quad (\text{VI-5-105})$$

$$\gamma_\xi^x k_M \sigma_1 = 0.5 \phi \sqrt{\frac{f_c}{1 + 0.25 \left(\frac{k_T S_T}{k_M S_M} \right)^2}} \quad (\text{VI-5-106})$$

where f_c is the concrete compressive strength. These equations are similar to Equations VI-5-101 and VI-5-102, but they are for prestressed concrete design. Details for determining prestressing steel requirements are given in ACI 318-89 (ACI 1989).

(3) Ultimate impact velocities end equivalent drop height.

(a) For evaluation of the placing technique during construction it is important to consider the ultimate impact velocities. The lowering speed of the crane at the moment of positioning of the units must be much slower than the values given in Table VI-5-42. The values of ultimate impact velocities given in Table VI-5-42 are rough estimates corresponding to solid body impact against a heavy rigid concrete base which causes breakage resulting in a mass loss of 20 percent or more. If the armor units are not dropped on a hard rigid surface but instead on soil or a rock underlayer, the ultimate impact velocities can be significantly higher than those given in Table VI-5-42.

Table VI-5-42
Approximate Values of Ultimate Rigid Body Impact Velocities for Concrete Armor Units (Burcharth 1993b)

Armor Unit	Impact Velocity of the Unit's Center (m/s)	Equivalent Drop Height of the Unit's Center (m)
Cube < 5 tonne	5 - 6	1.2 - 1.8
20 tonne	4 - 5	0.8 - 1.2
50 tonne	3 - 4	0.4 - 0.8
Tetrapod	2	0.2
Dolos, waist ratio 0.42	2	0.2
Dolos, waist ratio 0.32	1 - 1.5	0.05 - 0.12

(b) When placing units underwater, a heavy swell might impose rather large horizontal velocities on a unit suspended from a crane. It is obvious from the values in Table VI-5-42 that free-fall dropping of concrete armor units by quick release from a crane should be avoided because even small drop heights can cause breakage. This is also true for underwater placement because the terminal free-fall velocity underwater exceeds the limiting values given in Table VI-5-42 except for very small massive types of units.

(4) Thermal stresses.

(a) As concrete cures, the heat of hydration increases the temperature. Because of the fairly low thermal conductivity of concrete and because of the poor insulation of conventional formwork (e.g., steel shutter), a higher temperature will be reached in the center part of the armor unit than on the concrete surface. The temperature difference will create differential thermal expansion, and internal thermal stresses will develop in the concrete. The temperature differences and resulting thermal stresses increase with the distance between the armor unit center and the surface of the unit. Tensile stresses can easily exceed the limited strength of the fresh young concrete thus causing formation of microcracks. Unfortunately, it is not possible to see thermal cracks because they will close at the surface due to the thermal contraction of the concrete as it cools.

(b) The curing process is very complicated and theoretically it can only be dealt with in an approximate manner, mainly because the description of creep and relaxation processes of the hardening concrete are not precise enough to avoid large uncertainties in the calculations. Calculations are performed by the use of special finite element computer programs for three-dimensional bodies. Necessary input is data on the concrete mix including the composition (type) of the cement, the concrete temperature when poured, the geometry of the units, the type of formwork (conductivity/insulation), the environmental climate (air temperature and wind velocities as function of time), and the cycling time for removal of the formwork. The output of the calculations is the development of stresses and related crack formation as function of time. Figure VI-5-45 shows an example of such a calculation for a 70-tonne cube.

(c) The cube will have no visible sign of weakness, but it will be fragile and brittle because the cracked regions at the surfaces and in the center will have almost zero tensile strength and the noncracked regions will be in tension. This means that not only the strength, but also the fatigue life and the resistance to deterioration, will be reduced.

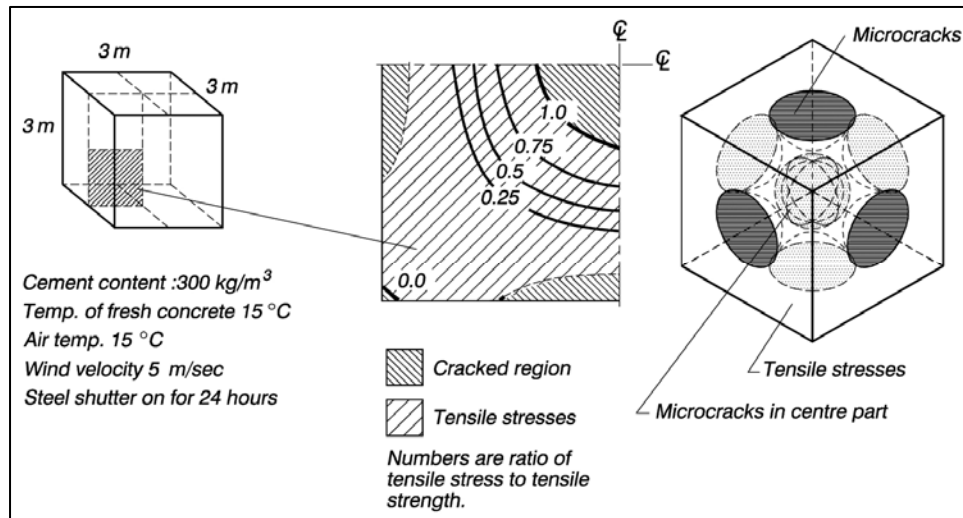


Figure VI-5-45. Example of calculation of thermal stresses and cracked regions in a 70-tonne cube 100 hr after casting (Burcharth 1993b)

(d) Thermal stress calculations are complicated and must be performed using numerical models described in the concrete literature. However, a very important rule of thumb for avoiding thermal cracks is that the temperature difference during curing should not exceed 20° C between any two points within the concrete element. The temperature difference is easy to monitor by placing/casting copper-constantan thermo-wire (e.g., 2 x 0.7 mm²) in the concrete. The wire insulation must be removed at the tips which are placed at positions in the center and near the surface of the units where the temperatures are maximum and minimum,

respectively. Temperature readings can then be monitored by connecting a pocket instrument to the free wire ends.

(e) There are several measures related to concrete technology for the prevention of damaging thermal stresses, but they all involve some drawbacks as described by Table VI-5-43.

Measure to Reduce Thermal Stresses	Drawback
Use of less cement	Reduced long-term durability due to higher porosity. Slower development of strength, longer cycle time for forms
Use of low-heat cement or retarder	Higher production costs due to slower development of strength, longer cycle time for forms, larger casing and stockpiling area needed
Cooling of water and aggregates	Higher production costs
Use of insulation during part of the curing period	Higher production costs

(f) Another way of dealing with the thermal stress problem is to keep the effective dimensions of the armor units as small as possible. For cubes it can be done by making a hole as was done in the hot-climate Bosaso Harbor project in Somalia. Figure VI-5-46 shows examples of the temperature development in 30-tonne blocks with and without a hole. The reduced temperature difference introduced by the hole is clearly seen by comparison of the two blocks casted during winter time. In fact it was easier to keep the 20° C temperature difference limit in a 30-tonne unit with a hole than in a 7-tonne unit without a hole.

(5) Fatigue in concrete armor units.

(a) The strength of concrete decreases with the number of stress cycles. Each stress cycle larger than a certain stress range will cause partial fracture in some parts of the material matrix resulting in a decreased yield strength. Repeated loads cause an accumulative effect which might result in macro cracks, and ultimately, breakage of the structural element.

(b) The number of stress cycles caused by wave action will be in the order of 200 million during 50 years structural life in the North Atlantic area. About 10 million cycles will be caused by larger storm waves. In subtropical and tropical areas the number of storm wave cycles is generally one or two orders of magnitude less.

(c) Fatigue for conventional unreinforced concrete exposed to uniaxial and flexural stress conditions with zero mean stress is given in Table VI-5-44.

d. Toe stability and protection.

(1) Introduction.

(a) The function of a toe berm is to support the main armor layer and to prevent damage resulting from scour. Armor units displaced from the armor layer may come to rest on the toe berm, thus increasing toe berm stability. Toe berms are normally constructed of quarry-run, but concrete blocks can be used if quarry-run material is too small or unavailable.

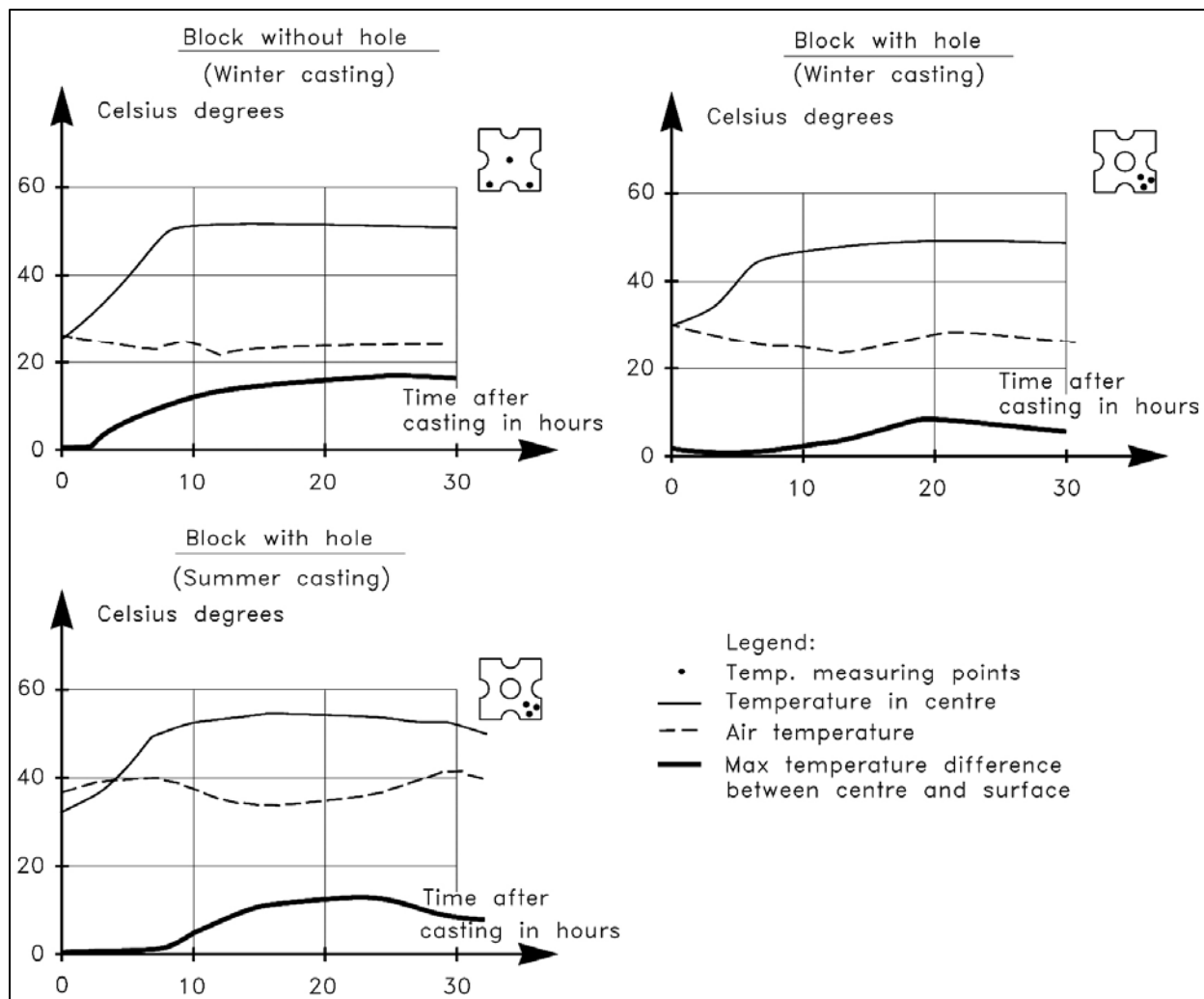


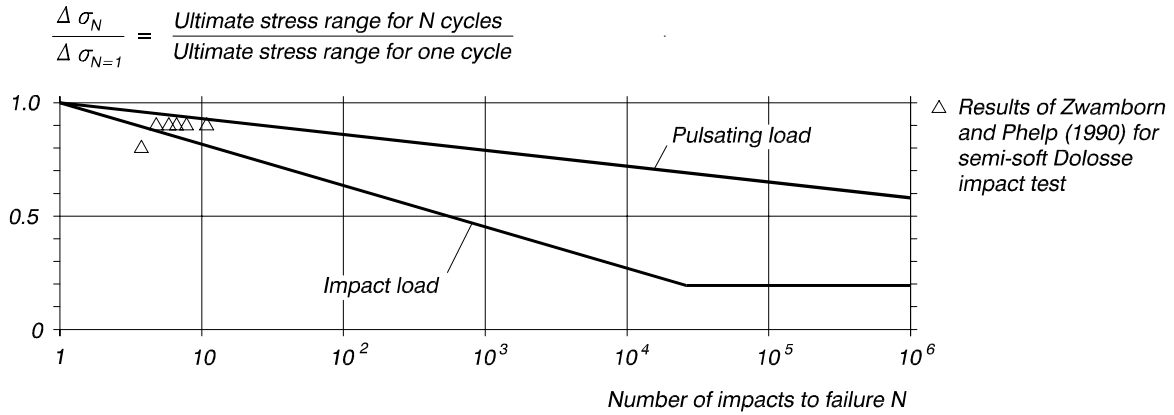
Figure VI-5-46. Examples of temperature development during curing in 30-tonne modified cubes with and without a hole (Burcharth et al. 1991)

(b) In very shallow water with depth-limited design wave heights, support of the armor layer at the toe is ensured by placing one or two extra rows of main armor units at the toe of the slope as illustrated in Figure VI-5-47a. This is a stable solution provided that scour does not undermine the toe causing the armor layer to slide as illustrated by Figure VI-5-48. In shallow water it is usually possible to use stones or blocks in the toe that are smaller than the main armor, as shown in Figure VI-5-47 b. In deep water, there is no need for the main armor to cover the slope at greater depths, and the toe berm can be constructed at a level above the seabed as illustrated by Figure VI-5-47c.

(c) Toe berm stability is affected by wave height, water depth at the top of the toe berm, width of the toe berm, and block density. However, wave steepness does not appear to be a critical toe berm stability parameter.

(d) Model tests with irregular waves indicate that the most unstable location is at the shoulder between the slope and the horizontal section of the berm. The instability of a toe berm will trigger or accelerate the instability of the main armor. Lamberti (1995) showed that moderate toe berm damage has almost no influence on armor layer stability, whereas high damage of the toe berm severely reduces the armor layer stability. Therefore, in practice it is economical to design toe berms that allow for moderate damage.

Table VI-5-44
Fatigue for Conventional Unreinforced Concrete Exposed to Uniaxial and Flexural Stress Conditions With Zero Mean Stress (Burcharth 1984)



It should be noted that the ultimate impact load strength for one stress cycle is on the order of 1.4 to 1.5 times the ultimate pulsating load strength in the case of uniaxial tension and compression, respectively. For flexural stresses a factor of approximately 1.4 should be applied. The ultimate pulsating load strength properties for one cycle can be taken to be equal to those found for static load conditions.

Data basis for fatigue curve

Author(s)	Loading condition	Specimens
Tepfers and Kutti (1979)	pulsating tension and compression	cubes of 150 mm length
Tait and Mills (1980)	pulsating tension	Dolosse of 300 mm height
Fagerlund and Larsson (1979)	impact compression	cylinders of 100 mm diameter
Zielinski, Reinhardt, and Körmeling (1981)	impact tension	cylinders of 74 mm diameter
Burcharth (1984)	impact flexural stress	Dolosse of 790 mm height

Zwamborn and Phelps (1990) performed drop tests with 9-ton Dolosse on a horizontal underlayer of quarry rock. This relatively soft base created a milder dynamic response than the solid rigid concrete base used by other authors. As seen from the figure Zwamborn and Phelps's data are in between the two curves which might be regarded as upper and lower limits for the fatigue effect.

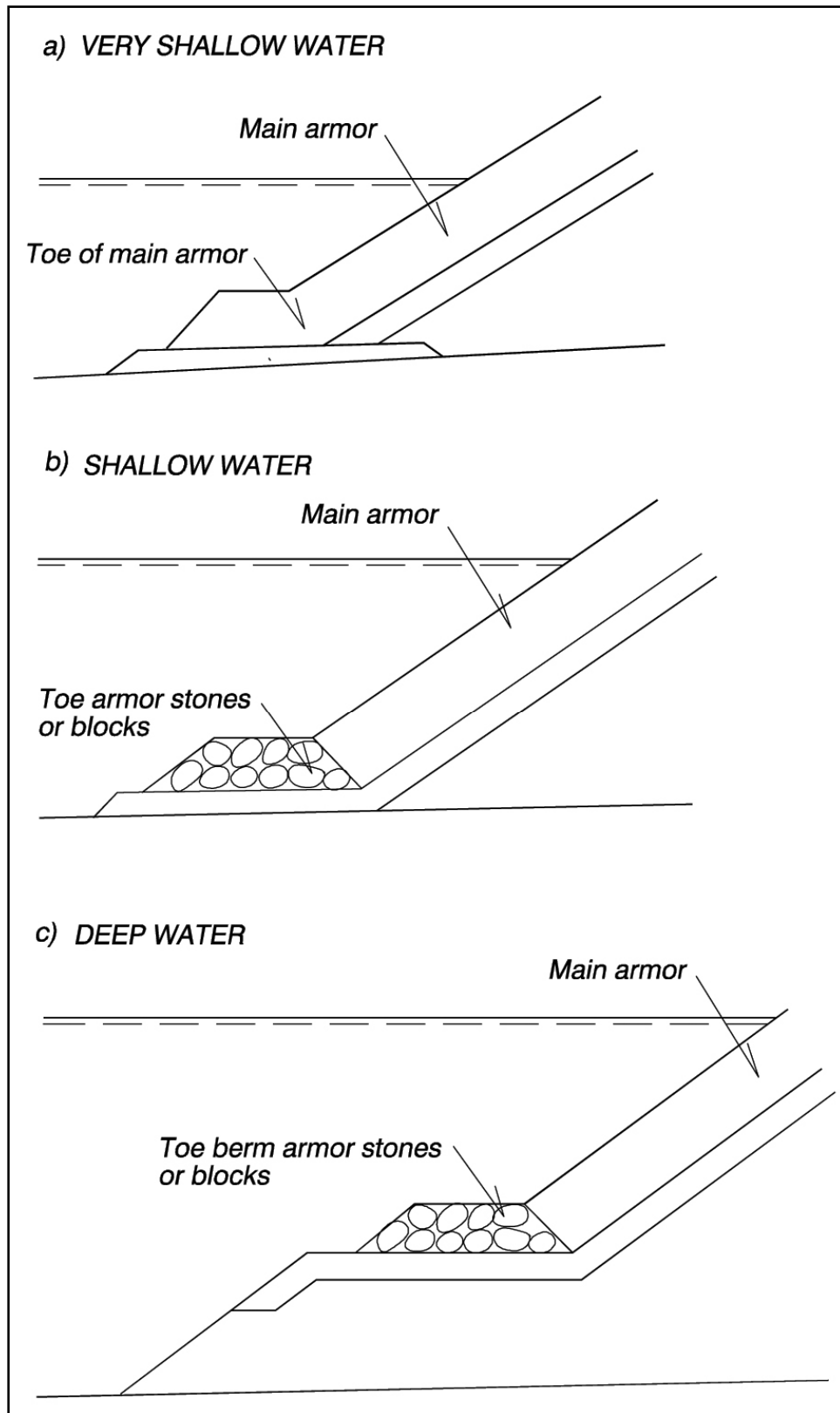


Figure VI-5-47. Typical toe and toe berm solutions in rubble-mound breakwater design

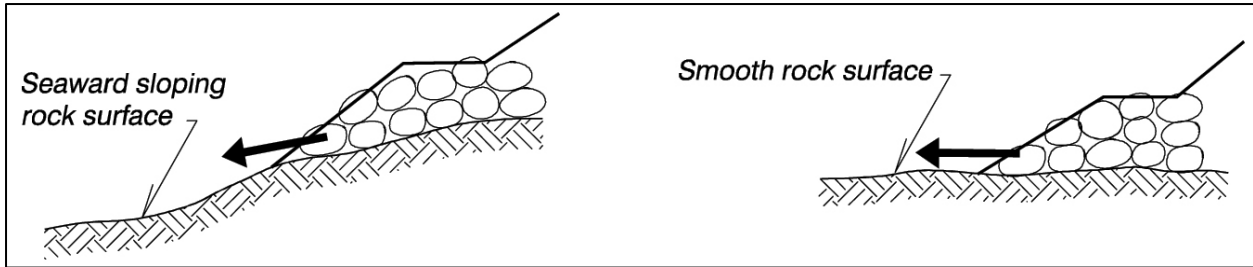


Figure VI-5-48. Example of potential instability of the stones placed on rock seabed

(e) Rock seabeds often provide a poor foundation for the toe berm because of seaward sloping and/or rather smooth surfaces. Toe stability will be difficult to obtain, especially in shallow water with wave breaking at the structure (see Figure VI-5-48). Toe stones placed on hard bottoms can be supported by a trench or anchor bolts as sketched in Figure VI-5-49.

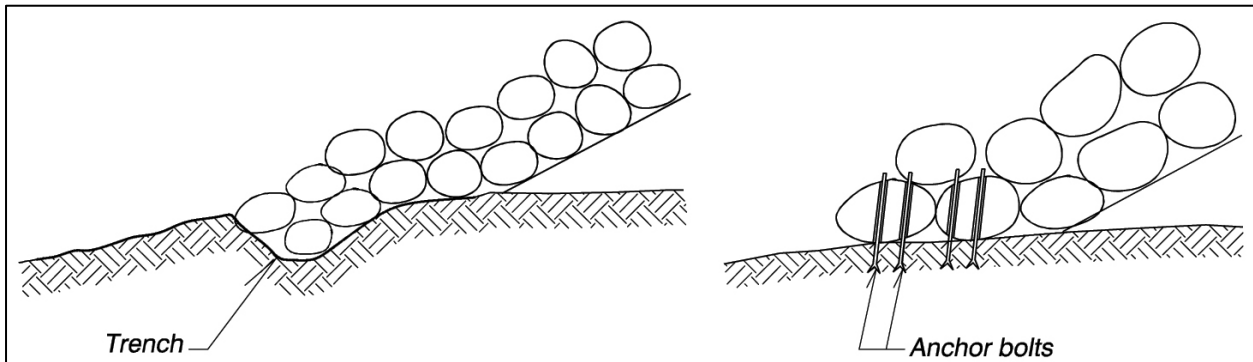


Figure VI-5-49. Support of the stones by a trench or anchor bolts

(f) Scour in front of the toe berm can also trigger a failure. The depth of toe protection required to prevent scour can be estimated from the scour depth prediction methods discussed in Part VI-5-6, "Scour and Scour Protection." Typical forms of scour toe protection are illustrated in Figure VI-5-50.

(2) Practical toe stability formulas for waves. Toe berm stability formulas are based exclusively on small scale physical model tests. These formulas are presented in the following tables.

Waves	Structure	Table
Regular, head-on and oblique	Sloping and vertical, trunk and head section	VI-5-45
Irregular, head-on	Trunk of sloping structure	VI-5-46 & VI-5-47
Irregular, head-on	Trunk of vertical structure	VI-5-48

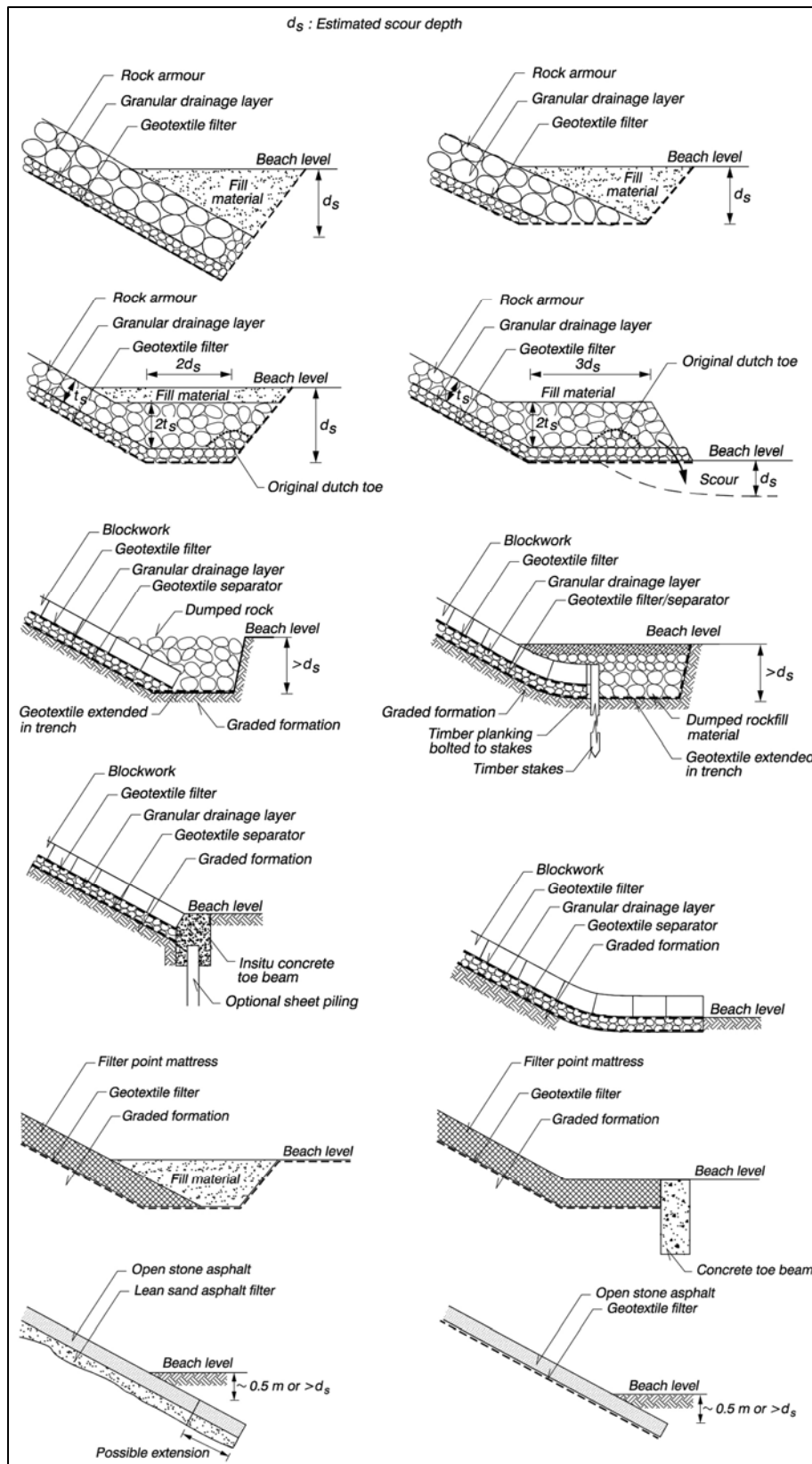
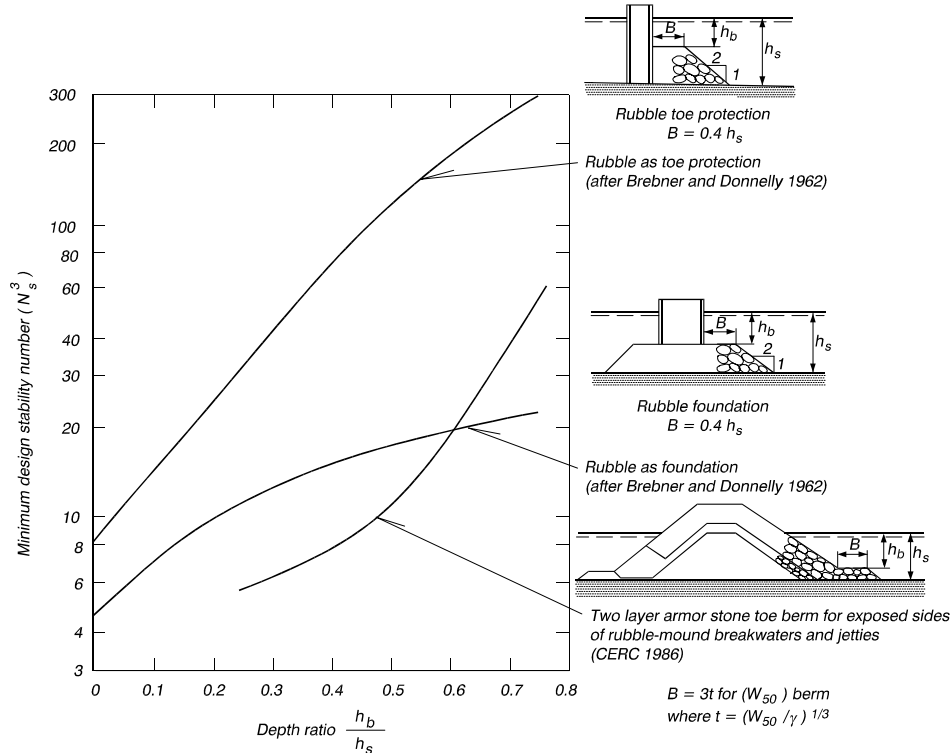


Figure VI-5-50. Typical seawall toe designs where scour is foreseen (McConnell 1998)

Table VI-5-45
Stability of Toe Berm Tested in Regular Waves (Markle 1989)

Regular waves, head-on and oblique



where $N_s = H / (\Delta D_{n50})$
 H Wave height in front of breakwater
 Δ $(\rho_s / \rho_w) - 1$
 ρ_s Mass density of stones
 ρ_w Mass density of water
 D_{n50} Equivalent cube length of median stone

Remarks: The curves in the figure are the lower boundary of N_s -values associated with acceptable toe berm stability (i.e., some stone movement occurs; but the amount of movement is minor and acceptable, which shows that the toe is not overdesigned)

(3) Foot protection blocks.

(a) Foot protection blocks have been applied to prevent foundation erosion at the toe of vertical structures as shown in Figure VI-5-51.

(b) According to Japanese practice the blocks are rectangular concrete blocks with holes (approximately 10 percent opening ratio) to reduce the antistabilizing pressure difference between the top and bottom of the blocks. Figure VI-5-52 shows a typical 25-tonne block.

Table VI-5-46
Stability of Toe Berm Formed by 2 Layers of Stone Having Density 2.68 tonnes/m³. Variable Berm Width, and Sloping Structures (van der Meer, d'Angremond, and Gerding 1995)

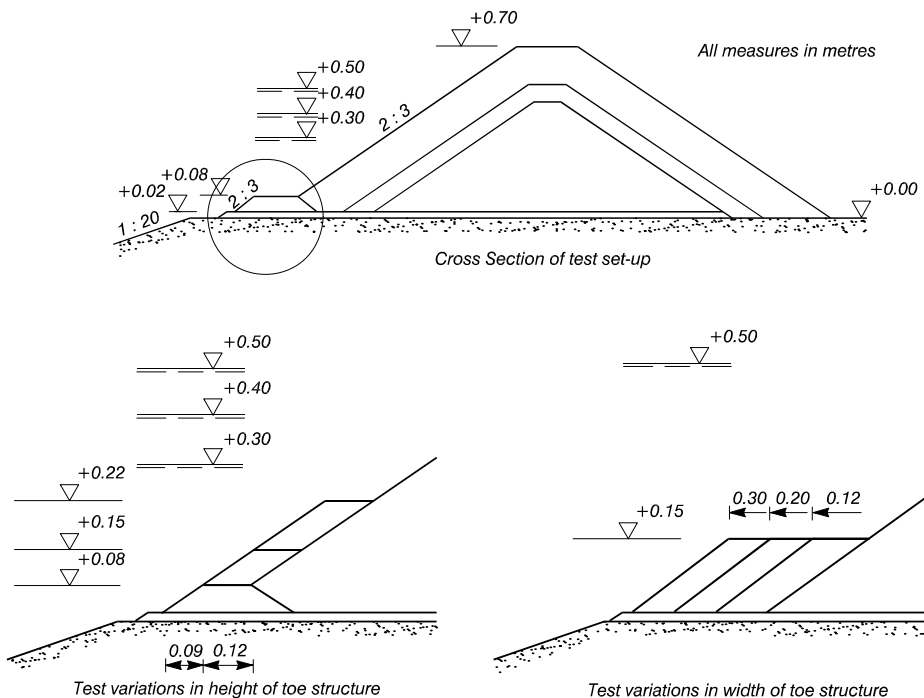
$$N_s = \frac{H_s}{\Delta D_{n50}} = \left(0.24 \frac{h_b}{D_{n50}} + 1.6 \right) N_{od}^{0.15} \quad (\text{VI-5-107})$$

where H_s Significant wave height in front of breakwater
 Δ $(\rho_s/\rho_w) - 1$
 ρ_s Mass density of stones
 ρ_w Mass density of water
 D_{n50} Equivalent cube length of median stone
 h_b Water depth at top of toe berm
 N_{od} Number of units displaced out of the armor layer within a strip width of D_{n50} . For a standard toe size of about 3-5 stones wide and 2-3 stones high:

$$N_{od} = \begin{cases} 0.5 & \text{no damage} \\ 2 & \text{acceptable damage} \\ 4 & \text{severe damage} \end{cases}$$

For a wider toe berm, higher N_{od} values can be applied.

Tested cross sections



(Continued on next page)

(Continued)

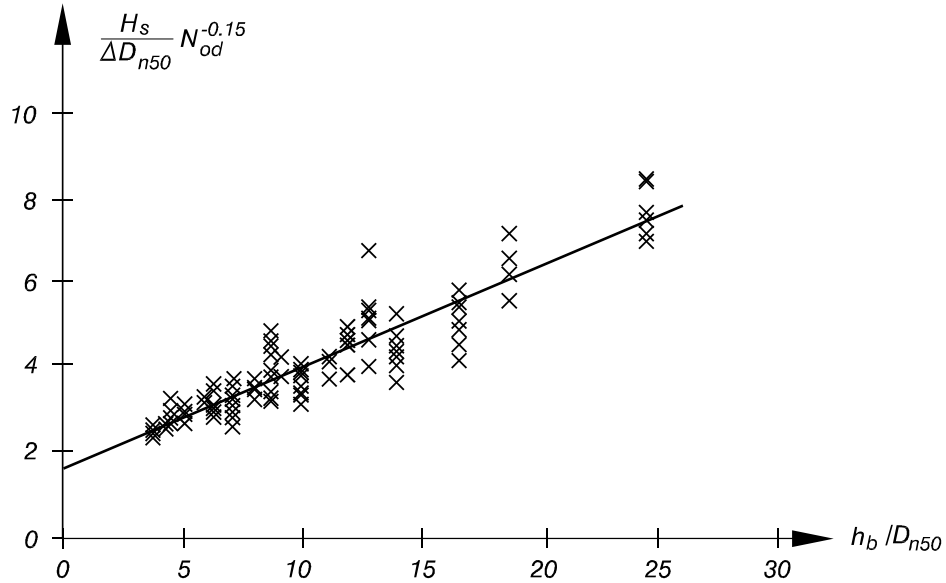
Table VI-5-46 (Concluded)

Valid for: Irregular head-on waves; nonbreaking, breaking and broken

Toe berm formed of two layers of stones with $\rho_s = 2.68 \text{ tonnes}/m^3$
($168 \text{ lb}/ft^3$)

$$0.4 < h_b/h_s < 0.9, \quad 0.28 < H_s/h_s < 0.8, \quad 3 < h_b/D_{n50} < 25$$

where h_s is the water depth in front of the toe berm



Uncertainty of the formula: corresponding to a coefficient of variation of approximately 0.10.

Table VI-5-48
Stability of Toe Berm Formed by Two Layers of Stones in Front of Vertical Impermeable Wall Structure

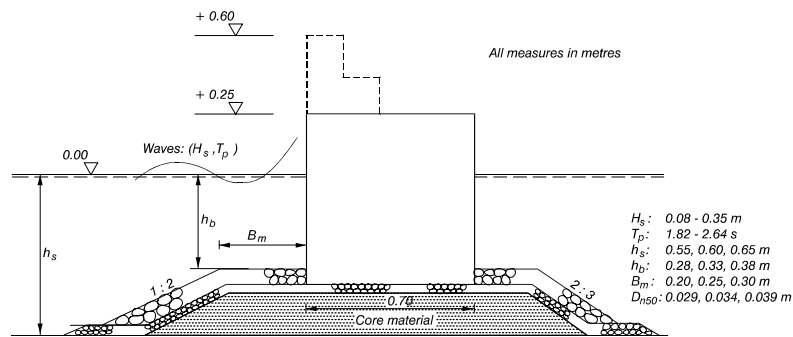
Madrigal and Valdés (1995) for two layers of quarrrstones

$$N_s = \frac{H_s}{\Delta D_{n50}} = \left(5.8 \frac{h_b}{h_s} - 0.6 \right) N_{od}^{0.19} \quad (\text{VI-5-109})$$

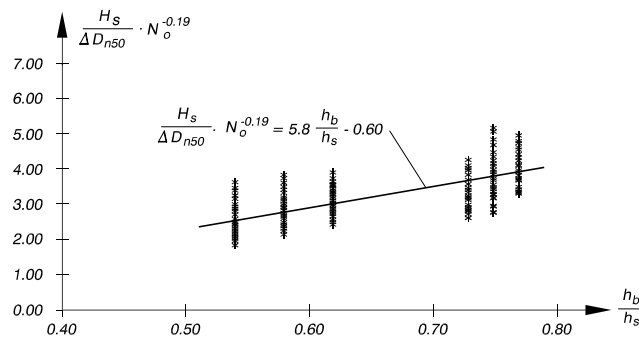
where H_s Significant wave height in front of breakwater
 Δ $(\rho_s / \rho_w) - 1$
 ρ_s Mass density of stones
 ρ_w Mass density of water
 D_{n50} Equivalent cube length of median stone
 h_b Water depth at top of toe berm
 h_s Water depth in front of toe berm
 N_{od} Number of units displaced out of the armor layer within a strip width of D_{n50}

$$N_{od} = \begin{cases} 0.5 & \text{start of damage (1-3\% of units displaced)} \\ 2 & \text{acceptable damage (5-10\% of units displaced)} \\ 5 & \text{severe damage (20-30\% of units displaced)} \end{cases}$$

Tested cross sections



Valid for: Irregular head-on waves. Toe berm formed of two layers of stones with $\Delta = 1.65$
 $0.5 < h_b/h_s < 0.8$; $7.5 < h_b/D_{n50} < 17.5$; $0.3 < B_m/h_s < 0.55$



Uncertainty of the formula: Not given

(Continued)

Table VI-5-48 (Concluded)

Tanimoto, Yagyu, and Goda (1982), Takahashi, Tanimoto, and Shimosako (1990) for two layers of quarrrystones

$$N_s = \frac{H_s}{\Delta D_{n50}} = \max \left\{ 1.8, 1.3 \frac{1 - \kappa}{\kappa^{1/3}} \frac{h'}{H_s} + 1.8 \exp \left(-1.5 \frac{(1 - \kappa)^2}{\kappa^{1/3}} \frac{h'}{H_s} \right) \right\} \quad (\text{VI-5-110})$$

$$\kappa = \kappa_1 \kappa_2$$

$$\kappa_1 = 2kh' / \sinh(2kh')$$

$$\kappa_2 = \max \left\{ 0.45 \sin^2 \theta \cos^2(kB \cos \theta), \cos^2 \theta \sin^2(kB \cos \theta) \right\}$$

where H_s Significant wave height in front of breakwater
 Δ $(\rho_s / \rho_w) - 1$
 ρ_s Mass density of stones
 ρ_w Mass density of water
 D_{n50} Equivalent cube length of median stone
 h' Water depth on top of toe berm (excluding armor layer)
 B Width of toe berm
 k Wave number $k = 2\pi / L_p$
 θ Wave incident angle ($\theta = 0^\circ$ for head-on)

Valid for: Irregular head-on and oblique waves
 Toe berm formed by two layers of quarrrystones
 $\Delta = 1.65$

Uncertainty of the formula: Not given

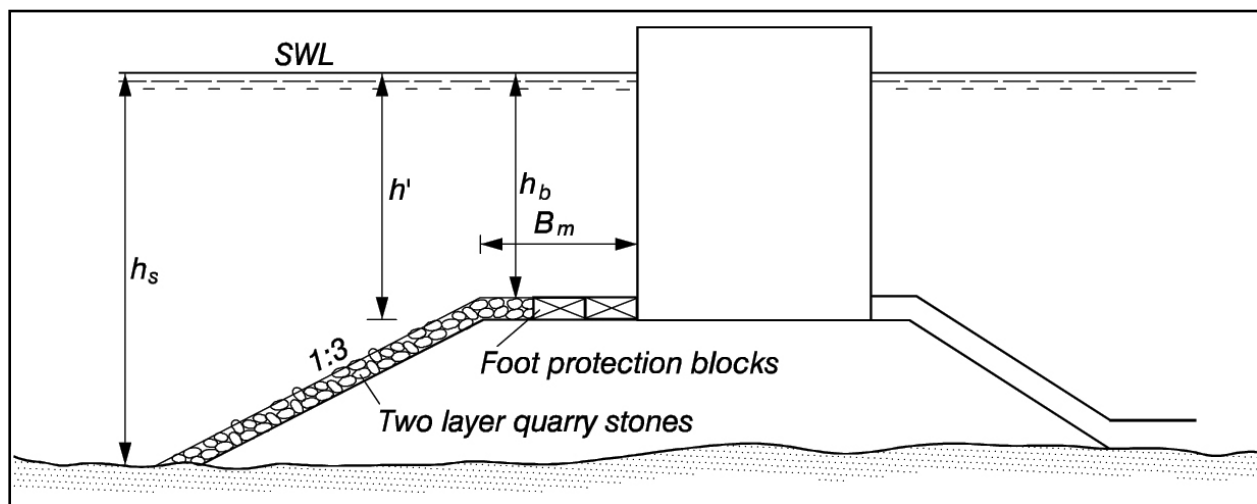


Figure VI-5-51. Illustration of foot protection blocks for vertical structures

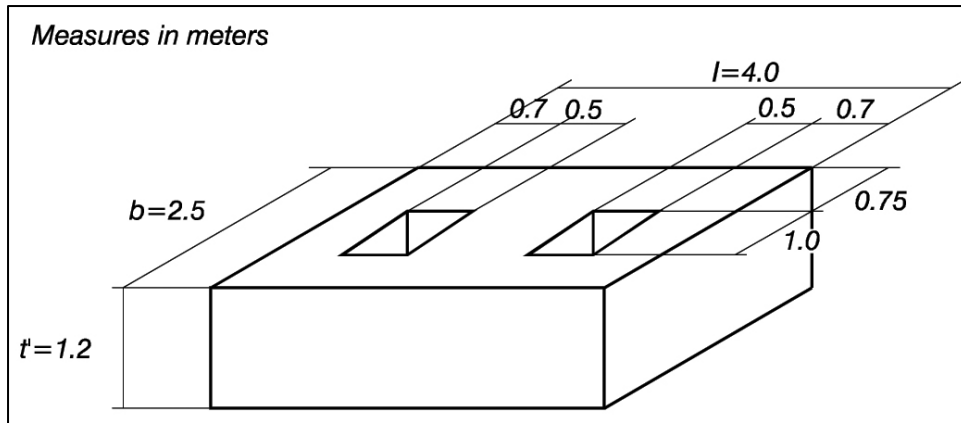


Figure VI-5-52. Example of Japanese foot protection block

Figure VI-5-53 shows a diagram taken from Takahashi (1996) for the determination of the necessary block thickness t' as functions of wave height H and the ratio of water depths h_b/h_s at the berm and in front of the structure as shown back on Figure VI-5-51.

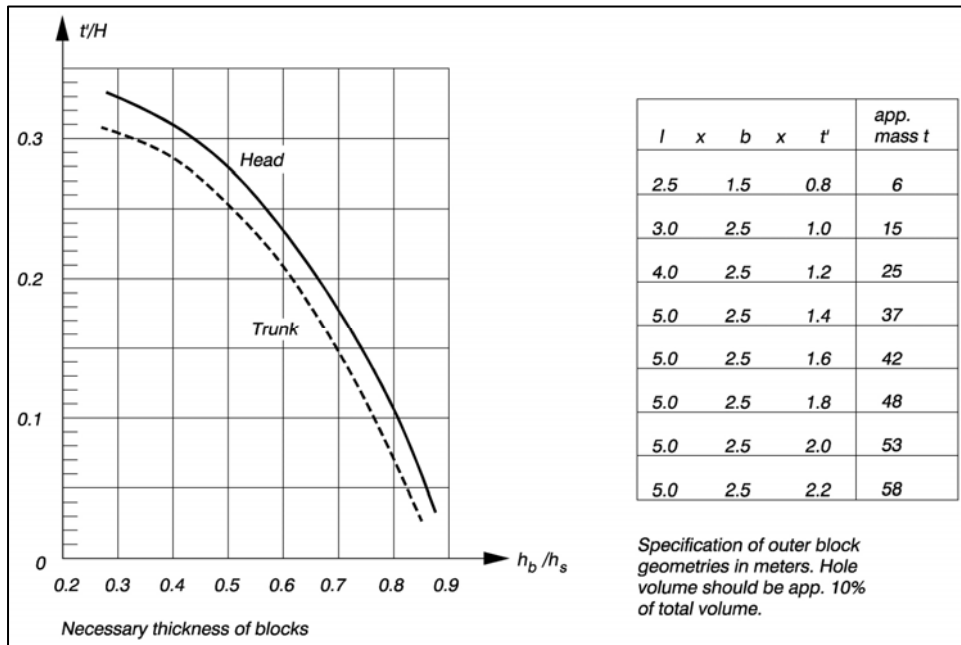


Figure VI-5-53. Design of foot protection blocks according to Japanese practice

(c) Stable foot protection blocks do reduce the pressure induced current in the mound, even when there are 10 percent openings in the blocks. Thus the risk of erosion of a sandy seabed underneath a thin rubble mound bedding layer is reduced too.

(4) Toe stability in combined waves and currents.

(a) Coastal structures, such as entrance jetties, are exposed to waves combined with currents running parallel to the structure trunk. In certain circumstances toe stability may be decreased due to the vectorial combination of current and maximum wave orbital velocity. For normal wave incidence the combined wave and current vector magnitude is not greatly increased. However, in the case of jetties where waves approach

the jetty trunk at large oblique angles (relative to the normal), the combined velocity magnitude becomes large, and toe stability is jeopardized.

(b) Smith (1999) conducted 1:25-scale laboratory experiments to develop design guidance for jetty structures where oblique waves combine with opposing (ebb) currents. Smith found that small current magnitudes did not destabilize toes designed in accordance with guidance given by Markle (1989) and presented in Table VI-5-45. But damage did occur as currents were increased, and a pulsating effect was observed in the wave downrush as the wave orbital velocity combined with the ebb current.

(c) The test configuration had waves approaching at an angle of 70 deg from the normal to the structure trunk, and wave heights were adjusted until breaking occurred on the structure. This is fairly typical scenario for jettied entrance channels. Both regular and irregular wave conditions were used in the tests. Generally, less damage was recorded for equivalent irregular waves, but this was attributed to the relatively short duration of the wave runs during the experiments. The range of model parameters tested, and the prototype equivalents for the 1:25-scale model, are shown in the following tabulation. Generally, currents less than 15 cm/s in the model (0.75 m/s prototype) did not affect toe stability.

Parameter	Model Value	Prototype Equivalent
Depth	24 cm and 30 cm	6.1 m and 7.6 m
Wave Period	1.7 - 3.0 s	8.5 - 15.0 s
Ebb Current	0.0 - 46 cm/s	0.0 - 2.3 m/s
Wave Height	Breaking	Breaking

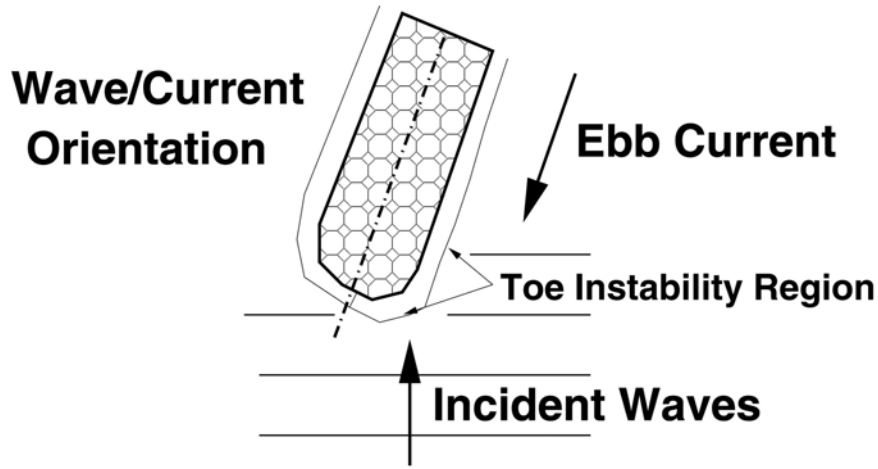
(d) Smith developed a procedure to modify Markle's toe stability criterion to account for currents flowing parallel to the structure. Strictly, the method is intended for situations where waves approach at a large angle from the normal (55-80 deg). Application to situations with wave approach more normal to the structure will yield conservative design guidance. The iterative procedure is outlined in Table VI-5-49.

e. Design of structure cross-section.

(1) Introduction.

(a) A rubble-mound structure is normally composed of a bedding layer and a core of quarry-run stone covered by one or more layers of larger stone and an exterior layer or layers of large quarystone or concrete armor units. Typical rubble-mound cross sections are shown in Figures VI-5-54 and VI-5-55. Figure VI-5-54 illustrates cross-section features typical of designs for breakwaters exposed to waves on one side (seaward) and intended to allow minimal wave transmission to the other (leeward) side. Breakwaters of this type are usually designed with crests elevated to allow overtopping only in very severe storms with long return periods. Figure VI-5-55 shows features common to designs where the breakwater may be exposed to substantial wave action from both sides, such as the outer portions of jetties, and where overtopping is allowed to be more frequent. Both figures show a more complex idealized cross section and a recommended cross section. The idealized cross section provides more complete use of the range of materials typically available from a quarry, but it is more difficult to construct. The recommended cross section takes into account some of the practical problems involved in constructing submerged portions of the structure.

Table VI-5-49
Stability Under Combined Waves and Currents (Smith 1999)



The current-modified stability number is calculated by the formula

$$(N_s)_c = a \left(\frac{U + u}{\sqrt{gh_s}} \right) \quad (\text{VI-5-111})$$

where

$$u = \frac{g H T}{2 L} \quad (\text{VI-5-112})$$

$$a = 51.0 \left(\frac{h_b}{h_s} \right) - 26.4 \quad (\text{VI-5-113})$$

and

- u = maximum wave orbital velocity in shallow water
- U = current magnitude
- g = gravity
- h_s = total water depth
- h_b = water depth over toe berm
- H = breaking wave height
- T = wave period
- L = local wavelength

Procedure: For a given wave condition, first calculate the stability number, N_s , using Markle's method from Table VI-5-45 for sloping rubble-mound structures. Then calculate a current-modified stability number from Equation VI-5-111. If $(N_s)_c > N_s$, the toe stone is unstable, and the procedure is repeated using a larger toe stone to calculate new values of N_s and h_b .

Uncertainty of the Formula: Unknown

EM 1110-2-1100 (Part VI)
1 Jun 06

(b) Figures VI-5-54 and VI-5-55 include tables giving average layer rock size in terms of the stable primary armor unit weight, W , along with the gradation of stone used in each layer (right-hand column). To prevent smaller rocks in the underlayer from being pulled through an overlayer by wave action, the following criterion for filter design may be used to check the rock-size gradations given in Figures VI-5-54 and VI-5-55.

$$D_{15}(\text{cover}) \leq 5D_{85}(\text{under}) \quad (\text{VI-5-114})$$

where $D_{85}(\text{under})$ is the diameter exceeded by the coarsest 15 percent of the underlayer and $D_{15}(\text{cover})$ is the diameter exceeded by the coarsest 85 percent of the layer immediately above the underlayer.

(c) Stone sizes are given by weight in Figures VI-5-54 and VI-5-55 because the armor in the cover layers is selected by weight at the quarry, but the smaller stone sizes are selected by dimension using a sieve or a grizzly. Thomsen, Wohlt, and Harrison (1972) found that the sieve size of stone corresponds approximately to

$$D_{\text{sieve}} \approx 1.15 \left(\frac{W}{w_a} \right)^{1/3} \quad (\text{VI-5-115})$$

where W is the stone weight and w_a is the stone unit weight. Table VI-5-50 lists weights and approximate dimensions for a wide range of stone sizes having stone specific weight of 25.9 kN/m^3 (165 lb/ft^3). The dimensions listed for stone weighing several tons corresponds to the approximate size of the stone determined from visual inspection. Layer thickness should not be estimated as multiples of the dimensions given in Table VI-5-50 because that does not allow for stone intermeshing. Layer thickness is correctly estimated using Equation VI-5-117.

(d) Structure design is part of the overall project planning and design process as illustrated by the generic design diagrams given in Figures V-1-1 through V-1-3 in Part V-1-1-h. Figure VI-5-56 presents a logic diagram for preliminary design of rubble-mound structures. Included in the diagram are three phases: structure geometry, evaluation of construction technique, and evaluation of design materials.

(e) As part of the design analysis indicated in the logic diagram of Figure VI-5-56, the following structure geometric features should be investigated:

- Crest elevation and width.
- Concrete cap for rubble-mound structures.
- Thickness of armor layer and underlayers.
- Bottom elevation of primary cover layer.
- Toe berm for cover layer stability.
- Structure head and leeside cover layer.
- Secondary cover layer.

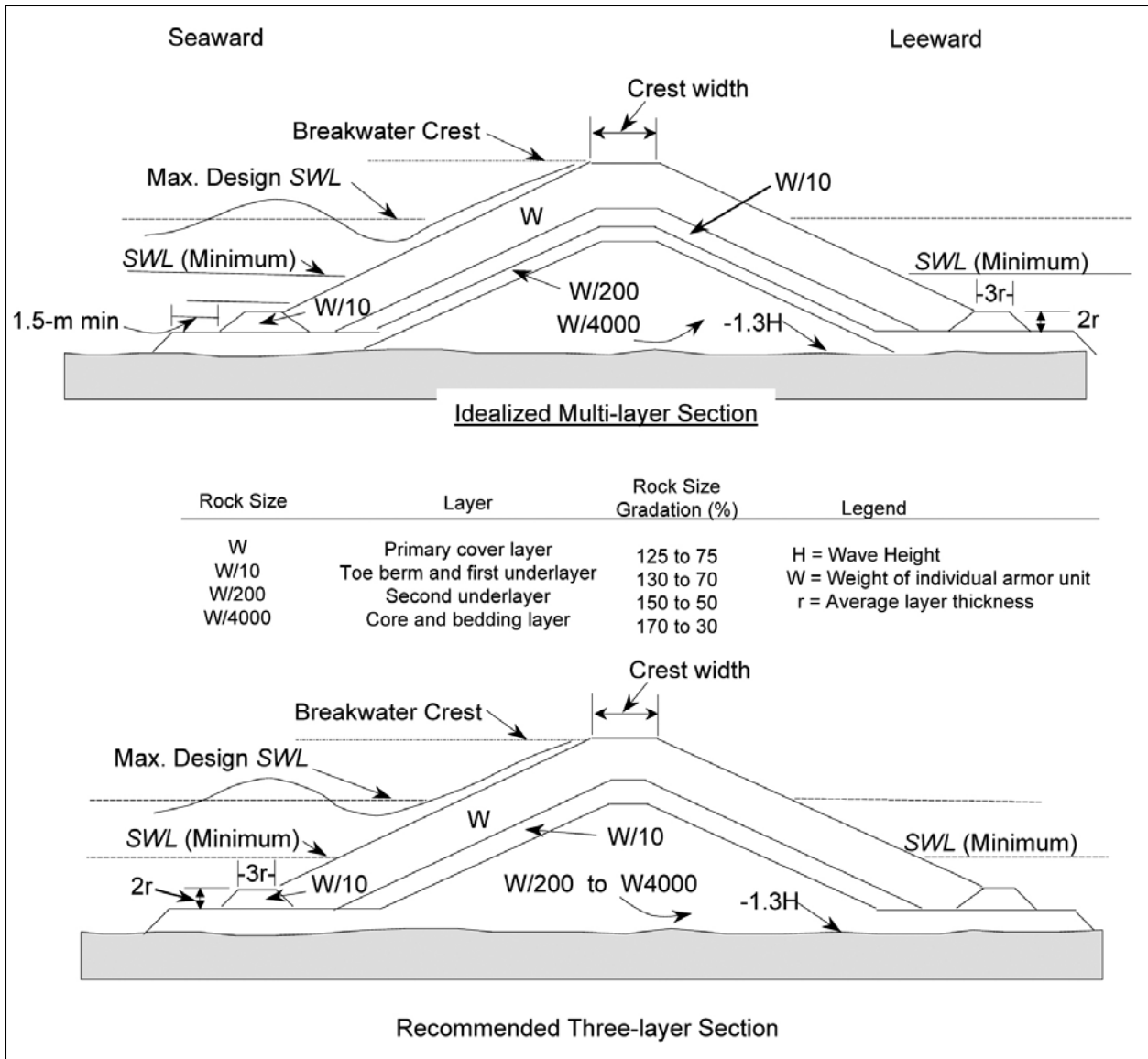


Figure VI-5-54. Rubble-mound section for seaward wave exposure with zero-to-moderate overtopping conditions

- Underlayers.
- Bedding layers and filter blanket layer (see Part VI-5-3b, “Granulated and geotextile filter stability.”)
- Scour protection at toe see Part VI-5-6, “Scour and Scour Protection.”
- Toe berm for foundation stability see Part VI-5-3d, “Toe stability and protection,” and Part VI-5-5, “Foundation Loads.”

(f) The following sections describe design aspects for the previously listed geometric features.

(2) Crest elevation and width.

EM 1110-2-1100 (Part VI)
1 Jun 06

Table VI-5-50
Weight and Size Selection Dimensions of Quarystone¹

Weight mt	Dimension		Weight		Dimension		Weight		Dimension		Weight		Dimension		
	m	ft	kg	(lb)	m	(ft)	kg	(lb)	m	cm	(in.)	kg	(lb)	cm	(in.)
0.907	0.81	(2.64)	45.36	(100)	0.30	(0.97)	2.27	(5)	10.92	(4.30)					
1.814	1.02	(3.33)	90.72	(200)	0.38	(1.23)	4.54	(10)	13.77	(5.42)	5.08	0.23	(0.5)	5.08	(2.00)
2.722	1.16	(3.81)	136.08	(300)	0.43	(1.40)	6.81	(15)	15.77	(6.21)					
3.629	1.28	(4.19)	181.44	(400)	0.50	(1.54)	9.07	(20)	17.35	(6.83)	6.40	0.45	(1.0)	6.40	(2.52)
4.536	1.38	(4.52)	226.80	(500)	0.51	(1.66)	11.34	(25)	18.70	(7.36)					
5.443	1.46	(4.80)	272.16	(600)	0.54	(1.77)	13.61	(30)	19.86	(7.82)	7.32	0.68	(1.5)	7.32	(2.88)
6.350	1.54	(5.05)	317.52	(700)	0.57	(1.86)	15.88	(35)	20.90	(8.23)					
7.258	1.61	(5.28)	362.88	(800)	0.60	(1.95)	18.14	(40)	21.84	(8.60)	8.05	0.91	(2.0)	8.05	(3.17)
8.165	1.67	(5.49)	408.24	(900)	0.62	(2.02)	20.41	(45)	22.73	(8.95)					
9.072	1.73	(5.69)	453.60	(1000)	0.64	(2.10)	22.68	(50)	23.55	(9.27)	8.66	1.13	(2.5)	8.66	(3.41)
9.979	1.79	(5.88)	498.96	(1100)	0.66	(2.16)	24.95	(55)	24.31	(9.57)					
10.866	1.84	(6.05)	544.32	(1200)	0.68	(2.23)	27.22	(60)	25.02	(9.85)	9.22	1.36	(3.0)	9.22	(3.63)
11.793	1.89	(6.21)	589.68	(1300)	0.70	(2.27)	29.48	(65)	25.70	(10.12)					
12.700	1.94	(6.37)	635.04	(1400)	0.72	(2.35)	31.75	(70)	26.34	(10.37)	9.70	1.59	(3.5)	9.70	(3.82)
13.608	1.98	(6.51)	680.40	(1500)	0.73	(2.40)	34.02	(75)	26.95	(10.61)					
14.515	2.03	(6.66)	725.76	(1600)	0.75	(2.45)	36.29	(80)	27.53	(10.84)	10.13	1.81	(4.0)	10.13	(3.99)
15.422	2.07	(6.79)	771.12	(1700)	0.76	(2.50)	38.56	(85)	28.09	(11.06)					
16.330	2.11	(6.92)	816.48	(1800)	0.78	(2.55)	40.82	(90)	28.65	(11.28)	10.54	2.04	(4.5)	10.54	(4.15)
17.237	2.15	(7.05)	861.84	(1900)	0.80	(2.60)	43.09	(95)	29.16	(11.48)					
18.144	2.19	(7.17)	907.20	(2000)	0.81	(2.64)	45.36	(100)	29.54	(11.63)	10.92	2.27	(5.0)	10.92	(4.30)

¹ Dimensions correspond to size measured by sieve, grizzly, or visual inspection for stone of 25.9 kilonewtons per cubic meter unit weight. Do not use for determining structure crest width or layer thickness.

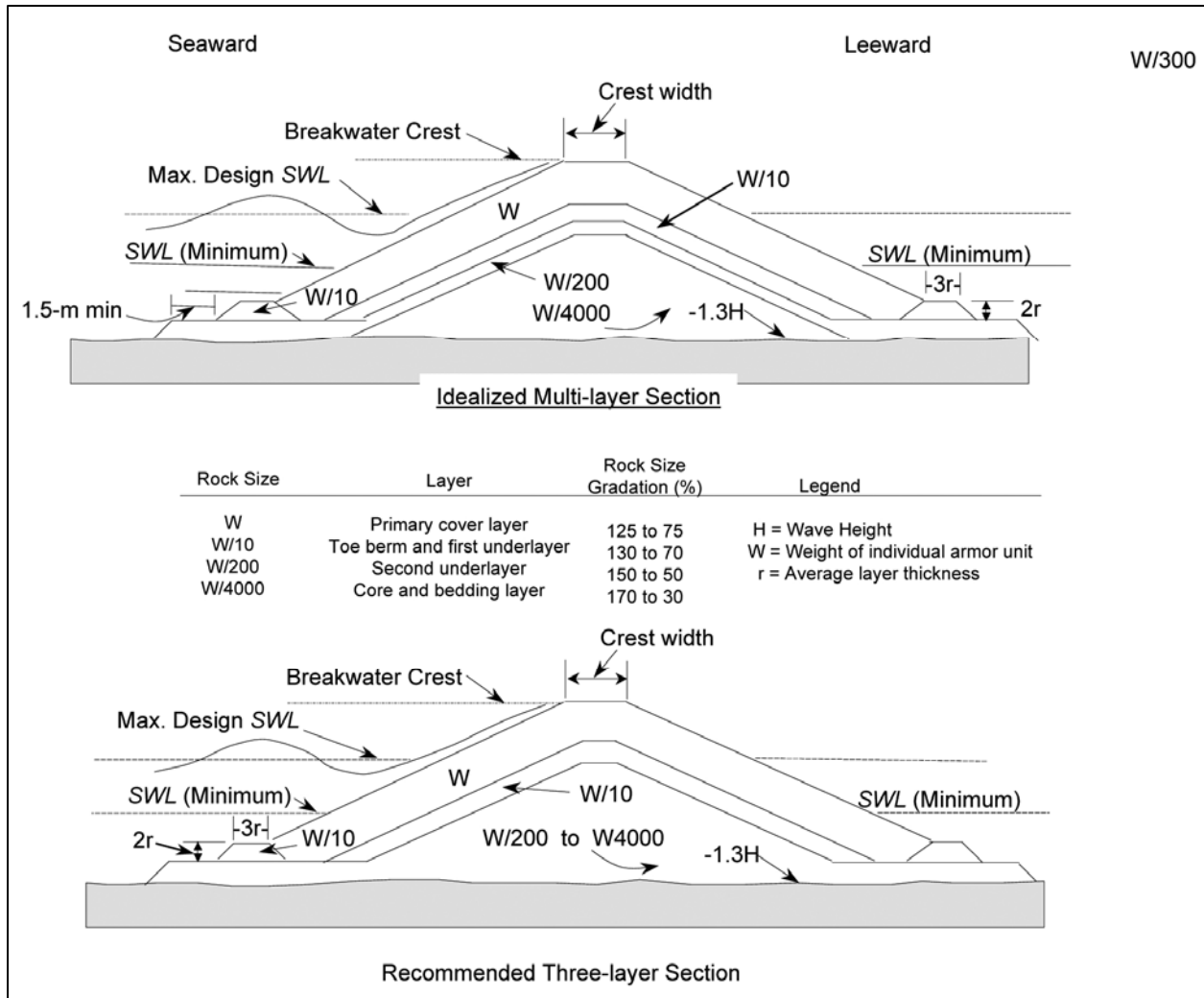


Figure VI-5-55. Rubble-mound section for wave exposure on both sides with moderate overtopping conditions

(a) Overtopping of a rubble-mound structure such as a breakwater or jetty usually can be tolerated if the waves generated by the overtopping do not cause damage behind the structure. Overtopping will occur if the crest elevation is lower than the wave runup, as estimated using the procedures in Part VI-5-2a, "Wave runup and rundown on structures." If the armor layer is chinked, or in other ways made smoother or less permeable, maximum runup will be increased.

(b) The selected crest elevation should be the lowest that provides the protection required. Excessive overtopping of a breakwater or jetty can cause choppiness of the water surface behind the structure and can be detrimental to harbor operations such as small craft mooring and most types of commercial cargo transfer. Overtopping of a rubble seawall or revetment can cause serious erosion behind the structure and flooding of the backshore area. Jetty overtopping is tolerable if it doesn't affect navigation in the channel. Signs warning pedestrians of overtopping dangers should be prominently posted on any publicly accessible structure designed for occasional wave overtopping.

(c) Crest width depends greatly on the degree of allowable overtopping; however, this dependency has not been quantified into general design guidance. The general rule of thumb for overtopping conditions is that minimum crest width should equal the combined widths of three armor units ($n = 3$) as determined by the formula

$$B = nk_{\Delta} \left(\frac{W}{w_a} \right)^{1/3} \quad (\text{VI-5-116})$$

where

B = crest width

n = number of stones ($n = 3$ is recommended minimum)

k_{Δ} = layer coefficient from Table VI-5-51

W = primary armor unit weight

w_a = specific weight of armor unit material

Where there is no overtopping, crest width is not critical; but in either case the crest must be wide enough to accommodate any construction and maintenance equipment that might operate directly on the structure.

(d) The sketches in Figures VI-5-54 and VI-5-55 show the primary armor cover layer extending over the crest. Armor units designed according to the non-overtopping stability formulas in Part VI-5-3a, "Armor layer stability," are probably stable on the crest for minor overtopping. For low-crested structures where frequent, heavy overtopping is expected, use the appropriate stability formula given in the Part VI-5-3a tables for preliminary design. Physical model tests are strongly recommended to confirm the stability of the crest and backside armor under heavy overtopping conditions. Model testing is almost imperative to check the overtopping stability of concrete armor units placed on the crest which may be less stable than equivalent stone armor.

(3) Concrete cap for rubble-mound structures.

(a) Placed concrete may be added to the cover layer of rubble-mound jetties and breakwaters for purposes such as filling the interstices of stones in the cover layer crest and side slopes as far down as wave action permits, or as large monolithic blocks cast in place. Placed concrete may serve any of four purposes: to strengthen the crest, to deflect overtopping waves away from impacting directly on the leeside slope, to increase the crest height, and to provide roadway access along the crest for construction or maintenance purposes.

(b) Massive concrete caps have been used with cover layers of precast concrete armor units to replace armor units of questionable stability on an overtopped crest and to provide a rigid backup to the top rows of armor units on the slopes. To accomplish this dual purpose, the cap can be a slab with a solid or permeable parapet (Czerniak and Collins 1977; Jensen 1983) a slab over stone grouted to the bottom elevation of the armor layer, or a solid or permeable block (Lillevang 1977; Markle 1982). Massive concrete caps must be placed after a structure has settled or must be sufficiently flexible to undergo settlement without breaking up (Magoon et al. 1974).

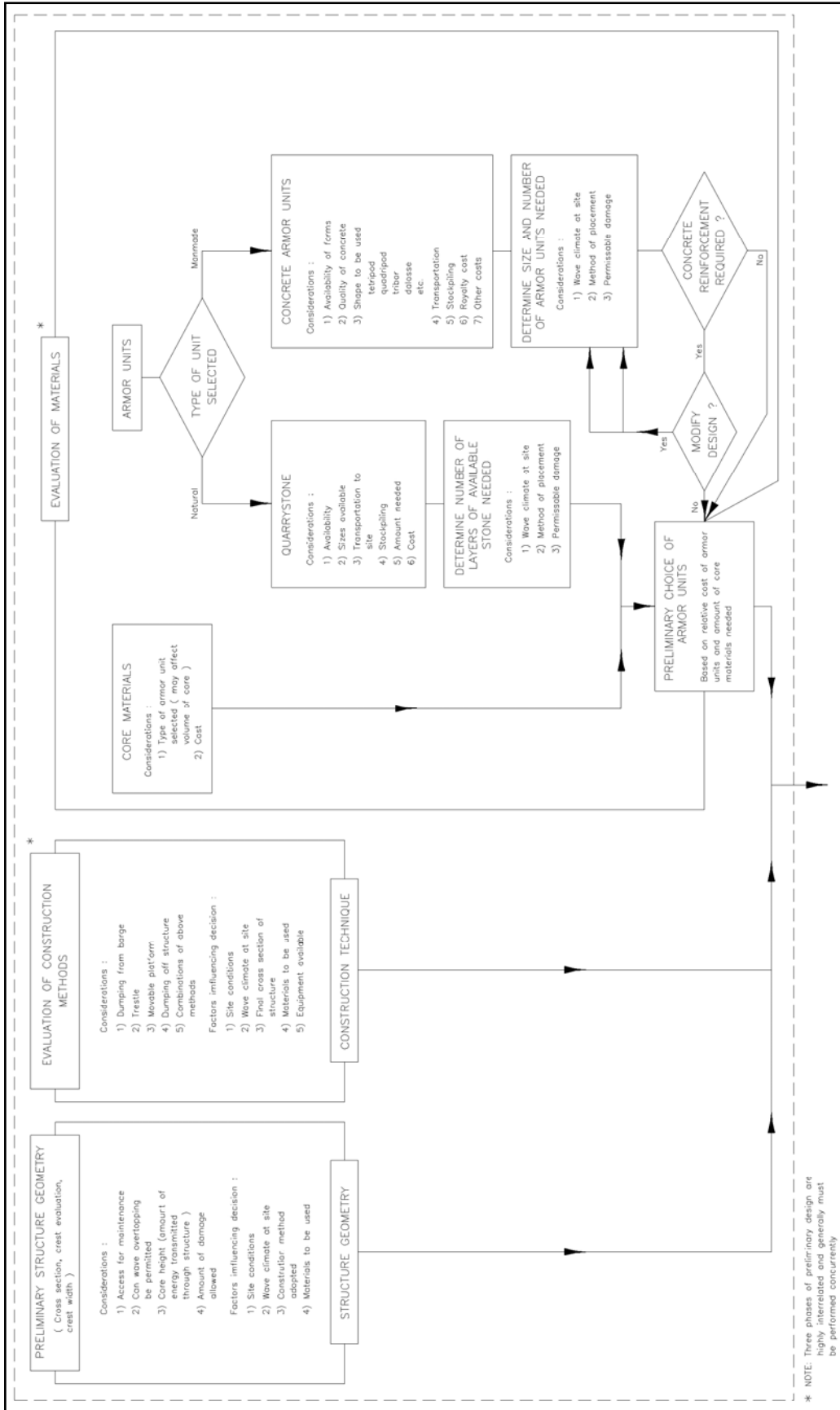


Figure VI-5-56. Logic diagram for preliminary design of rubble-mound structures

(c) Concrete caps with solid vertical or sloped walls reflect waves out through the upper rows of armor units, perhaps causing loss of those units. Solid slabs and blocks can trap air beneath them, creating uplift forces during heavy wave action that may crack or tip the cap (Magoon et al. 1974). A permeable cap decreases both of these problems. A parapet can be made permeable, and vertical vents can be placed through the slab or block itself (Mettam 1976). Lillevang (1977) designed a breakwater crest composed of a vented block cap placed on an unchinked, ungrouted extension of the seaward slope's underlayer, a permeable base reaching across the crest.

(d) Ribbed caps are a compromise between the solid block and a covering of concrete armor units. The ribs are large, long, rectangular members of reinforced concrete placed perpendicular to the axis of a structure in a manner resembling railroad ties. The ribs are connected by reinforced concrete braces, giving the cap the appearance of a railroad track running along the structure crest. This cap serves to brace the upper units on the slopes, yet is permeable in both the horizontal and vertical directions.

(e) Ribbed caps have been used on U.S. Army Corps of Engineers breakwaters at Maalea Harbor (Carver and Markle 1981), at Kahului (Markle 1982), on Maui, and Pohoiki Bay, all in the State of Hawaii.

(f) Waves overtopping a concrete cap can damage the leeside armor layer. The width of the cap and the shape of its lee side can be designed to deflect overtopping waves away from the structure's lee side (Czerniak and Collins 1977; Lillevang 1977; and Jensen 1983). Ribbed caps help dissipate waves.

(g) High parapet walls have been added to caps to deflect overtopping seaward and allow the lowering of the crest of the rubble mound itself. These walls present the same reflection problems described above and complicate the design of a stable cap (Mettam 1976; Jensen 1983). Hydraulic model tests by Carver and Davidson (1976, 1983) have investigated the stability of caps with high parapet walls proposed for Corps structures. Part VI-5-4d, "Stability of concrete caps and caissons against sliding and overturning," provides design guidance.

(h) To evaluate the need for a massive concrete cap to increase structural stability against overtopping, consideration should be given to the cost of including a cap versus the cost of increasing dimensions to prevent overtopping and for construction and maintenance purposes. A massive concrete cap is not necessary for the structural stability of a structure composed of concrete armor units when the difference in elevation between the crest and the limit of wave runup on the projected slope above the structure is less than 15 percent of the total wave runup. For this purpose, an all-rubble structure is preferable, and a concrete cap should be used only if substantial savings would result. Maintenance costs for an adequately designed rubble structure are likely to be lower than for any alternative composite-type structure. The cost of a concrete cap should also be compared to the cost of covering the crest with flexible, permeable concrete armor units, perhaps larger than those used on the slopes, or large quarrystone armor. Hydraulic model tests are recommended to determine the most stable and economical crest designs for major structures.

(i) Experience indicates that concrete placed in the voids on the structure slopes has little structural value. By reducing slope roughness and surface porosity, the concrete increases wave runup. The effective life of the concrete is short, because the bond between concrete and stone is quickly broken by structure settlement. Such filling increases maintenance costs. For a roadway, a concrete cap can usually be justified if frequent maintenance of armor slopes is anticipated. A smooth surface is required for wheeled vehicles; tracked equipment can be used on ribbed caps.

(4) Thickness of armor layer and underlayers.

(a) The thickness of the cover layer and underlayers is calculated using the formula

$$r = nk_{\Delta} \left(\frac{W}{w_a} \right)^{1/3} \quad (\text{VI-5-117})$$

and the placing density (number of armor units per unit area) is estimated using the equation

$$\frac{N_a}{A} = nk_{\Delta} \left(1 - \frac{P}{100} \right) \left(\frac{w_a}{W} \right)^{2/3} \quad (\text{VI-5-118})$$

where r is the average layer thickness, n is the number of quarrystone or concrete armor units in the thickness (typically $n = 2$), W is the weight of individual armor units, w_a is the specific weight of the armor unit material, and N_a is the required number of individual armor units for a given surface area, A . The layer coefficient (k_{Δ}) and cover layer average porosity (P) in percent were experimentally determined, and values are given in Table VI-5-51. Equations VI-5-117 and VI-5-118 can be used with either metric or English units.

(b) The specified placing or packing density must be strictly maintained during construction to assure proper interlocking, and therefore hydraulic stability, of the armor layer. During placement, packing density can be maintained by specifying a mean and allowable deviation for the centroidal distance (in three dimensions) between units, or it can be maintained by counting units in a specified area. For grid placement, each subsequent row of armor units is typically offset laterally from the previous lower row to avoid failure planes. To specify the placement grid, D_H is the distance between the centroids of two adjacent units on the same horizontal row and D_U is the distance between the centroids of units upslope in the plane of the structure slope. Values of D_H and D_U for specific armor sizes and packing density coefficients appropriate for Core-Loc and Accropod units can be obtained from the vendor or license holder. Within any matrix of armor units, every effort should be made to achieve maximum interlocking. The maximum centroidal distance D_{max} should not exceed 110 percent of the values specified. Greater spacing may jeopardize interlocking and the integrity of the armor layer.

(c) The thickness r of a layer of riprap is the greater of either 0.3 m, or one of the following, whichever of the three is greatest:

$$r = 2.0 \left(\frac{W_{50}}{w_a} \right)^{1/3} \quad (\text{VI-5-119})$$

where W_{50} is the weight of the 50-percent size in the riprap gradation, or

$$r = 1.25 \left(\frac{W_{max}}{w_a} \right)^{1/3} \quad (\text{VI-5-120})$$

Table VI-5-51
Layer Coefficient and Porosity for Various Armor Units

Armor Unit	n	Placement	Layer Coefficient k_A	Porosity P (percent)
Quarystone (smooth) ¹	2	Random	1.02	38
Quarystone (rough) ²	2	Random	1.00	37
Quarystone (rough) ²	≥3	Random	1.00	40
Quarystone (parallepiped) ³	2	Special	--	27
Quarystone ⁴	Graded	Random	--	37
Cube (modified) ¹	2	Random	1.10	47
Tetrapod ¹	2	Random	1.04	50
Tribar ¹	2	Random	1.02	54
Tribar ¹	1	Uniform	1.13	47
dolos ⁵	2	Random	0.94	56
Core-Loc ⁶	Vol. < 5 m ³	Random	1.51	60
	5 < Vol. < 12 m ³			63
	12 < Vol. < 22m ³			64
Accropod ⁷	Vol. < 5 m ³	Random	1.51	57
	5 < Vol. < 12 m ³			59
	12 < Vol. < 22m ³			62

¹ Hudson (1974)
² Carver and Davidson (1983)
³ Layer thickness is twice the average long dimension of the parallelepiped stones. Porosity is estimated from tests on one layer of uniformly placed modified cubes (Hudson 1974).
⁴ The minimum layer thickness should be twice the cubic dimension of the W_{50} riprap. Check to determine that the graded layer thickness is ≥1.25 the cubic dimension of the W_{max} riprap (see Equations VI-5-119 and VI-5-120).
⁵ Carver and Davidson (1977)
⁶ Turk and Melby (1997)
⁷ Accropod informational brochure

where W_{max} is the heaviest stone in the gradation. The specified layer thickness should be increased by 50 percent for riprap placed underwater if conditions make placement to design dimensions difficult. The placing density of riprap is defined as the total weight of riprap placed (W_T) per unit area (A) of structure slope. Riprap placing density can be estimated as

$$\frac{W_T}{A} = r w_a \left(1 - \frac{P}{100} \right) \quad \text{(VI-5-121)}$$

(5) Bottom elevation of primary cover layer.

(a) When water depth is greater than $1.5 H$ (where H is the irregular wave height parameter used to determine a stable primary armor unit weight), the armor units in the cover layer should be extended downslope to an elevation below minimum SWL equal to the design wave height H as shown in Figure VI-5-54. For water depths less than $1.5 H$ extend the cover layer armor units to the toe as shown in Figure VI-5-55. Model tests to determine the bottom elevation of the primary cover layer and the type of armor placement should be conducted when feasible. Revetment cover layers located in shallow water should be extended seaward of the structure toe on sandy bottoms to serve as scour protection.

(b) Increased stability for special-placement parallelepiped stone (see higher K_D values in Table VI-5-22) can only be obtained if a toe mound is carefully placed to support the quarystone with their long axes perpendicular to the structure slope. For dolosse it is recommended that the bottom rows of units in the primary cover layer be “special placed” on top of the secondary cover layer as shown in Figure VI-5-54, on top of the toe berm as shown in Figure VI-5-55, or on the bottom itself. This placement is highly dependent on wave conditions and water clarity. Site-specific model studies have placed the bottom layer of dolosse with vertical flukes away from the slope and the second row placed so that the units overlap the horizontal flukes of the bottom layer. This helps assure interlocking with the random-placed units farther up the slope (Bottin, Chatham, and Carver 1976), and provides better toe stability than random placement. The seaward dolosse in the bottom row should be placed with the bottom of the vertical flukes one-half the length of the units back from the design surface of the primary armor layer to produce the design layer thickness.

(c) Core-Loc units can be placed randomly along the toe, but experiments indicate a pattern placement along the toe is more stable and should be used when the breakwater is built in shallow, depth-limited conditions. For the bottom layer, individual Core-Loc units are set in a three-point stance in cannon fashion with the central fluke pointing seaward, up at a 45-deg angle like the cannon barrel. All toe units are placed side-by-side with minimal space between adjacent units. The second course of units is laid atop of the toe units such that they straddle each toe unit. Once the second row has been placed, all subsequent Core-Loc armor units are placed in a random matrix. While placing these units in a variety of random orientations, care must be taken to assure that all overlying units are interlocked with and constrain underlying units.

(6) Toe berm for cover layer stability.

(a) Structures exposed to breaking waves should have a quarystone toe berm to protect the toe of the primary armor layer (see Figure VI-5-55). Design guidance for toe berm dimensions and stone size is given in Part VI-5-3d, “Toe stability and protection.”

(b) The toe berm may be placed before or after the adjacent cover layer. For special-placement quarystone or uniform-placement tribars, the toe berm serves as a base, and it must be placed first. When placed after the cover layer, the toe berm must be high enough to provide bracing up to at least half the height of the toe armor units. Usually, this requirement is exceeded by the design guidance recommended in Part VI-5-3d.

(7) Structure head and leeside cover layer.

(a) Armoring of the head of a breakwater or jetty should be the same on the leeside slope as on the seaside slope for a distance of about 15 to 45 m from the structure end. This distance depends on such factors as structure length and crest elevation at the seaward end. (See Tables VI-5-37 and VI-5-38 for sizing stable armor units for heads.)

(b) Design of leeside cover layers depends on the extent of wave overtopping, any waves or surges acting directly on the lee slope, structure porosity, and differential hydrostatic head resulting in uplift forces that may dislodge armor units on the back slope. If the crest elevation is established to prevent possible overtopping, the weight of armor units and the bottom elevation of the back slope cover layer should depend on the lesser wave action on the lee side (if any) and the porosity of the structure. Under minor overtopping the armor weight calculated for the seaward side primary cover layer should be used on the lee side down to at least the SWL or $-0.5 H$ for preliminary designs. However, model testing may be needed to determine stable armor weights for overtopping wave impacts.

(c) For heavy overtopping of breaking waves in shallow water, the primary armor layer on the lee side should be extended to the bottom as shown in Figure VI-5-55. Where concrete caps are employed, stability of the leeside armor during overtopping should be verified with model tests. When both sides of a structure are exposed to similar wave action (groins and jetties), both slopes should have similar designs.

(8) Secondary cover layer.

(a) If the armor units in the primary and secondary cover layers are of the same material, the weight of armor units in the secondary cover layer, between $-1.5 H$ and $-2.0 H$, should be greater than about one-half the weight of armor units in the primary cover layer. Below $-2.0 H$, the weight requirements can be reduced to about $W/15$ for the same slope condition (see Figure VI-5-54). If the primary cover layer is quarrystone, the weights for the secondary quarrystone layers should be ratioed from the weight of quarrystone that would be required for the primary cover layer. The use of a single size of concrete armor unit for all cover layers (i.e., upgrading the secondary cover layer to the same size as the primary cover layer) may prove to be economically advantageous when the structure is located in shallow water as shown in Figure VI-5-55 where the primary cover layer is extended down the entire slope.

(b) The secondary cover layer (shown in Figure VI-5-54 from elevation $-1.5 H$ to the bottom) should be as thick as, or thicker than, the primary cover layer. As an example, cover layers of quarrystone of two-stone thickness ($n = 2$) will require a secondary cover layer thickness of $n = 2.5$ for the slope between elevations $-H$ and $-2.0 H$, and a thickness of $n = 5$ for the slope below an elevation of $-2.0 H$. These layer thicknesses are based on the armor unit weight ratios given in Figure VI-5-54.

(c) The interfaces between the secondary cover layers and the primary cover layer are shown at the slope of 1-to-1.5 on Figure VI-5-54. Steeper slopes for the interfaces may contribute to the stability of the cover armor, but material characteristics and site wave conditions during construction may require using a flatter slope than shown in the figure.

(9) Underlayers.

(a) The first underlayer directly beneath the primary armor units (see Figures VI-5-54 and VI-5-55) should have a minimum thickness of two quarrystones ($n = 2$). The first underlayer stones should weigh about one-tenth of the weight of the overlying armor units ($W/10$) if the cover layer and first underlayer are both quarrystone, or the first underlayer is quarrystone and the cover layer is concrete armor units with a stability coefficient of $K_D \leq 12$ (see Tables VI-5-29, VI-5-33, VI-5-34, VI-5-36). When the cover layer armor unit $K_D > 12$ (dolosse, Core-Loc, and uniformly-placed tribars) the first underlayer quarrystone weight should be about one-fifth the weight of the overlying unit ($W/5$). The larger size promotes increased interlocking between the first underlayer and the concrete armor units of the primary cover layer. Hydraulic model tests (Carver and Davidson 1977; Carver 1980) indicate for quarrystone armor units and dolosse on a breakwater trunk exposed to nonbreaking waves that the underlayer stone size could range from $W/5$ to $W/20$ with little effect on armor stability, wave runup or rundown. If the underlayer stone proposed for a given structure is available with a gradation in the range of $W/5$ to $W/20$, the structure should be model tested with that underlayer gradation to determine if this economical material will support a stable primary cover layer of planned armor units when exposed to the site design conditions.

(b) The second underlayer beneath the primary cover layer and upper secondary cover layer (above $-2.0 H$) should have a minimum equivalent thickness of two quarrystones and a weight about $1/20$ the weight of the stones in the first underlayer. In terms of primary armor unit weight this is approximately $1/20 \times W/10 = W/200$ for quarrystone and some concrete armor units.

(c) The first underlayer beneath the lower secondary cover layer (below $-2.0 H$ on Figure VI-5-54) should also have a minimum of two thicknesses of quarystone. Stones in this layer should weigh about $1/20$ of the immediately overlying armor unit weight. In terms of primary armor unit weight this is approximately $1/20 \times W/15 = W/300$ for units of the same material. The second underlayer for the secondary armor below $-2.0 H$ can be as light as $W/6000$, or equal to the core material size.

(d) For the recommended cross section in Figure VI-5-54 when the primary armor is quarystone and/or concrete units with $K_D \leq 12$, the first underlayer and the cover layer below $-2.0 H$ should have quarystone weights between $W/10$ and $W/15$. If the primary armor is concrete armor units with $K_D > 12$, the first underlayer and cover armor below $-2.0 H$ should be quarystone with weights between $W/5$ and $W/10$.

(e) For graded riprap cover layers the minimum requirement for the underlayers (if one or more are required) is

$$D_{15}(\text{cover}) \leq 5D_{85}(\text{under}) \quad (\text{VI-5-122})$$

where $D_{15}(\text{cover})$ is the diameter exceeded by the coarsest 85 percent of the riprap or underlayer on top and $D_{85}(\text{under})$ is the diameter exceeded by the coarsest 15 percent of the underlayer or soil below (Ahrens 1981b). For a revetment where the riprap and the underlying soil satisfy the size criterion, no underlayer is necessary. Otherwise, one or more of the following is required.

(f) The size criterion for riprap is more restrictive than the general filter criterion given in Part VI-5-3b, "Granulated and geotextile filter stability." The riprap criterion requires larger stone in the lower layer to prevent the material from washing through the voids in the upper layer as cover layer stones shift during wave action. A more conservative underlayer than required by the minimum criterion may be constructed of stone with a 50-percent size of about $W_{50}/20$. This larger stone will produce a more permeable underlayer and should reduce runup and increase interlocking between the cover layer and underlayer. However, be sure to check the underlayer gradation against the underlying soil to assure the minimum criterion of Equation VI-5-122 is met.

(g) The underlayers should be at least three thicknesses of the W_{50} stone, but never less than 0.23 m (Ahrens 1981b). The thickness can be calculated using Equation VI-5-119 with a coefficient of 3 rather than 2. Because a revetment is placed directly on the soil or fill material of the bank it protects, a single underlayer also functions as a bedding layer or filter blanket.

f. Blanket stability in current fields. Stone blankets constructed of randomly-placed riprap or uniformly sized stone are commonly used to protect areas susceptible to erosion by fast-flowing currents. Blanket applications include lining the bottom and sloping sides of flow channels and armoring regions of tidal inlets where problematic scour has developed. Design of stable stone or riprap blankets is based on selecting stone sizes such that the shear stress required to dislodge the stones is greater than the expected shear stress at the bottom developed by the current.

(1) Boundary layer shear stress.

(a) Prandl established a universal velocity profile for flow parallel to the bed given by

$$\frac{u}{v_*} = \frac{1}{\kappa} \ln \left(\frac{y}{k_s} \right) + B \quad (\text{VI-5-123})$$

EM 1110-2-1100 (Part VI)
1 Jun 06

where

κ = von Karman constant (= 0.4)

y = elevation above the bed

u = velocity at elevation y

k_s = boundary roughness

B = function of Reynolds number (= 8.5 for fully rough, turbulent flow)

v_* = shear velocity (= $(\tau_o / \rho_w)^{1/2}$)

τ_o = shear stress acting on the bed

ρ_w = density of water

Equation VI-5-123 can be expressed in terms of the mean flow velocity, \bar{u} , by integrating over the depth, i.e.,

$$\frac{\bar{u}}{v_*} = \frac{1}{h} \int_0^h \frac{u}{v_*} dy = \frac{1}{\kappa} \ln \left(\frac{h}{k_s} \right) + B - \frac{1}{\kappa} \quad (\text{VI-5-124})$$

or

$$\frac{\bar{u}}{v_*} = 2.5 \ln \left(\frac{11h}{k_s} \right) \quad (\text{VI-5-125})$$

when fully rough turbulent flow is assumed, which is usually the case for flow over stone blankets. Equation VI-5-125 assumes uniform bed roughness and currents flowing over a distance sufficient to develop the logarithmic velocity profile over the entire water depth.

(b) Bed roughness k_s over a stone blanket is difficult to quantify, but it is usually taken to be proportional to a representative diameter d_a of the blanket material, i.e., $k_s = C_1 d_a$. Substituting for k_s and v_* in Equation VI-5-125 and rearranging yields an equation for shear stress given by

$$\tau_o = \frac{w_w}{g} \left[\frac{\bar{u}}{2.5 \ln \left(\frac{11h}{C_1 d_a} \right)} \right]^2 \quad (\text{VI-5-126})$$

where $w_w = \rho_w g$ is the specific weight of water.

(2) Incipient motion of stone blankets.

(a) Stone blankets are stable as long as the individual armor stones are able to resist the shear stresses developed by the currents. Incipient motion on a horizontal bed can be estimated from Shield's diagram (Figure III-6-7) for uniform flows. Fully rough turbulent flows occur at Reynolds numbers where Shields parameter is essentially constant, i.e.,

$$\Psi = \frac{\tau}{(\rho_a - \rho_w)gd_a} \approx 0.04 \quad (\text{VI-5-127})$$

where

τ = shear stress necessary to cause incipient motion

ρ_a = density of armor stone

Rearranging Equation VI-5-127 and adding a factor K_1 to account for blankets placed on sloping channel side walls gives

$$\tau = 0.04K_1(w_a - w_w)d_a \quad (\text{VI-5-128})$$

where w_a is the specific weight of armor stone ($= \rho_a g$), and

$$K_1 = \sqrt{1 - \frac{\sin^2 \theta}{\sin^2 \varphi}} \quad (\text{VI-5-129})$$

with

θ = channel sidewall slope

φ = angle of repose of blanket armor [$\approx 40^\circ$ for riprap]

(b) Equating Equations VI-5-126 and VI-5-128 gives an implicit equation for the stable blanket diameter d_a . However, by assuming the logarithmic velocity profile can be approximated by a power curve of the form

$$\ln\left(\frac{11h}{C_1 d_a}\right) \approx C_2 \left(\frac{h}{d_a}\right)^\beta$$

an explicit equation is found having the form

$$\frac{d_a}{h} = C_T \left[\left(\frac{w_w}{w_a - w_w} \right)^{\frac{1}{2}} \left(\frac{\bar{u}}{\sqrt{K_1 g h}} \right) \right]^{(1-2\beta)} \quad (\text{VI-5-130})$$

where all the constants of proportionality have been included in C_T . Equation VI-5-130 implies that blanket armor stability is directly proportional to water depth and flow Froude number, and inversely proportional to the immersed specific weight of the armor material. The unknown constants, C_T and β , have been empirically determined from laboratory and field data.

(3) Stone blanket stability design equation.

(a) Stable stone or riprap blankets in current fields should be designed using the following equation from Engineer Manual 1110-2-1601.

$$\frac{d_{30}}{h} = S_f C_s \left[\left(\frac{w_w}{w_a - w_w} \right)^{\frac{1}{2}} \left(\frac{\bar{u}}{\sqrt{K_1 g h}} \right) \right]^{\frac{5}{2}} \quad (\text{VI-5-131})$$

where

d_{30} = stone or riprap size of which 30 percent is finer by weight

S_f = safety factor (minimum = 1.1) to allow for debris impacts or other unknowns

C_s = stability coefficient for incipient motion
 = 0.30 for angular stone
 = 0.38 for rounded stone

(b) EM 1110-2-1601 presents additional coefficients for channel bends and other situations where riprap size must be increased due to flow accelerations. The methodology is also summarized in Maynard (1998). Equation VI-5-131 is based on many large-scale model tests and available field data, and the exponent and coefficients were selected as a conservative envelope to most of the scatter in the stability data. Riprap stone sizes as specified by Equation VI-5-131 are most sensitive the mean flow velocity, so good velocity estimates are needed for economical blanket designs.

(c) Alternately, Equation VI-5-131 can be rearranged for mean flow velocity to give the expression

$$\bar{u} = \left(\frac{1}{S_f C_s} \right)^{\frac{2}{5}} \left(\frac{h}{d_{30}} \right)^{\frac{1}{10}} \left[g K_1 \left(\frac{w_a - w_w}{w_w} \right) d_{30} \right]^{\frac{1}{2}} \quad (\text{VI-5-132})$$

(d) Equation VI-5-132, which is similar to the well-known Isbash equation, can be used to determine the maximum mean velocity that can be resisted by riprap having d_{30} of a given size. The main difference between Equation VI-5-132 and the Isbash equation is that the Isbash equation multiplies the term in square brackets by a constant whereas Equation VI-5-132 multiplies the square-bracketed term by a depth-dependent factor that arises from assuming a shape for the boundary layer. The Isbash equation is more conservative for most applications, but it is still used for fast flows in small water depths and in the vicinity of structures such as bridge abutments.

(e) By assuming the blanket stones are spheres having weight given by

$$W_{30} = \frac{\pi}{6} w_a d_{30}^3 \quad (\text{VI-5-133})$$

where W_{30} is the stone weight for which 30 percent of stones are smaller by weight, Equation VI-5-131 can be expressed in terms of stone weight as

$$\frac{W_{30}}{w_a h^3} = \frac{\pi}{6} (S_f C_s)^3 \left[\left(\frac{w_w}{w_a - w_w} \right)^{\frac{1}{2}} \left(\frac{\bar{u}}{\sqrt{K_{18}gh}} \right) \right]^{\frac{15}{2}} \quad (\text{VI-5-134})$$

(4) Stone blanket gradation.

(a) All graded stone distributions (riprap) used for stone blankets should have distributions conforming to the weight relationships given below in terms of W_{30} or $W_{50 \min}$ (EM 1110-2-1601).

$$W_{50 \min} = 1.7 W_{30} \quad (\text{VI-5-135})$$

$$W_{100 \max} = 5W_{50 \min} = 8.5W_{30} \quad (\text{VI-5-136})$$

$$W_{100 \min} = 2 W_{50 \min} = 3.4 W_{30} \quad (\text{VI-5-137})$$

$$W_{50 \max} = 1.5 W_{50 \min} = 2.6 W_{30} \quad (\text{VI-5-138})$$

$$W_{15 \max} = 0.5 W_{50 \max} = 0.75 W_{50 \min} = 1.3 W_{30} \quad (\text{VI-5-139})$$

$$W_{15 \min} = 0.31 W_{50 \min} = 0.5 W_{30} \quad (\text{VI-5-140})$$

(b) Recommended thickness of the blanket layer, r , depends on whether placement is submerged or in the dry as specified by the following formulas.

(c) For blankets placed above water, the layer thickness should be

$$r = 2.1 \left(\frac{W_{50 \min}}{w_a} \right)^{\frac{1}{3}} = 2.5 \left(\frac{W_{30}}{w_a} \right)^{\frac{1}{3}} \quad (\text{VI-5-141})$$

with a minimum blanket thickness of 0.3 m. Blankets placed below water should have layer thickness given by

$$r = 3.2 \left(\frac{W_{50 \min}}{w_a} \right)^{\frac{1}{3}} = 3.8 \left(\frac{W_{30}}{w_a} \right)^{\frac{1}{3}} \quad (\text{VI-5-142})$$

with a minimum blanket thickness of 0.5 m.

VI-5-4. Vertical-Front Structure Loading and Response

a. *Wave forces on vertical walls.*

(1) Wave-generated pressures on structures are complicated functions of the wave conditions and geometry of the structure. For this reason laboratory model tests should be performed as part of the final design of important structures. For preliminary designs the formulae presented in this section can be used within the stated parameter limitations and with consideration of the uncertainties. Three different types of wave forces on vertical walls can be identified as shown in Figure VI-5-57.

- (a) Nonbreaking waves: Waves do not trap an air pocket against the wall (Figure VI-5-57a). The pressure at the wall has a gentle variation in time and is almost in phase with the wave elevation. Wave loads of this type are called pulsating or quasistatic loads because the period is much larger than the natural period of oscillation of the structures. (For conventional caisson breakwaters the period is approximately one order of magnitude larger.) Consequently, the wave load can be treated like a static load in stability calculations. Special considerations are required if the caisson is placed on fine soils where pore pressure may build up, resulting in significant weakening of the soil.
- (b) Breaking (plunging) waves with almost vertical fronts: Waves that break in a plunging mode develop an almost vertical front before they curl over (see Figure VI-5-57b). If this almost vertical front occurs just prior to the contact with the wall, then very high pressures are generated having extremely short durations. Only a negligible amount of air is entrapped, resulting in a very large single peaked force followed by very small force oscillations. The duration of the pressure peak is on the order of hundredths of a second.
- (c) Breaking (plunging) waves with large air pockets: If a large amount of air is entrapped in a pocket, a double peaked force is produced followed by pronounced force oscillations as shown in Figure VI-5-57c. The first and largest peak is induced by the wave crest hitting the structure at point A, and it is similar to a hammer shock. The second peak is induced by the subsequent maximum compression of the air pocket at point B, and it is referred to as compression shock, (Lundgren 1969). In the literature this wave loading is often called the "Bagnold type." The force oscillations are due to the pulsation of the air pocket. The double peaks have typical spacing in the range of milliseconds to hundredths of a second. The period of the force oscillations is in the range 0.2-1.0 sec.

(2) Due to the extremely stochastic nature of wave impacts there are no reliable formulas for prediction of impulsive pressures caused by breaking waves. Determination of impact pressures in model tests is difficult because of scale effects related to the amount and size of air bubbles and size and shape of air pockets. Also the instrumentation, data sampling, and analyses need special attention to avoid bias by dynamic amplification and misinterpretation when scaling to prototype values. Another problem related to model tests is the sensitivity of the shock loads on the shape and kinematics of the breaking waves. This calls for a very realistic and statistically correct reproduction of natural waves in laboratory models.

(3) Impulsive loads from breaking waves can be very large, and the risk of extreme load values increases with the number of loads. Therefore, conditions resulting in frequent wave breaking at vertical structures should be avoided. Alternatives include placing a mound of armor units in front of the vertical wall structure to break the waves before they can break directly on the wall, or using a rubble-mound structure in place of the vertical wall structure.

(4) Frequent wave breaking at vertical structures will not take place for oblique waves with angle of incidence larger than 20 deg from normal incidence. Nor will it take place if the seabed in front of the structure has a mild slope of about 1:50 or less over a distance of at least several wavelengths, and the vertical wall has no sloping foundation at the toe of the wall.

(5) The use of a sloping-front face from about still-water level (swl) to the crest is very effective in reducing large impact pressures from breaking waves. In addition, the direction of the wave forces on the sloping part (right angle to the surface) helps reduce the horizontal force and the tilting moment. Structures with sloping tops might be difficult to optimize where large water level variations are present. Also, a sloping-front structure allows more overtopping than a vertical wall structure of equivalent crest height.

EXAMPLE PROBLEM VI-5-1

FIND:

Riprap distribution for a stable scour blanket over a nearly horizontal bottom

GIVEN:

The following information is known (English system units shown in parentheses)

Specific weight of riprap, $w_a = 25.9 \text{ kN/m}^3$ (165 lb/ft³)

Specific weight of water, $w_w = 10.05 \text{ kN/m}^3$ (64 lb/ft³)

Bottom slope, $\theta = 0 \text{ deg}$ i.e., $K_1 = 1.0$

Water depth, $h = 6 \text{ m}$ (19.7 ft)

Depth-averaged mean velocity, $\bar{u} = 2.5 \text{ m/s}$ (8.2 ft/s)

Stability coefficient, $C_s = 0.38$ i.e., rounded stone

Factor of safety, $S_f = 1.1$

Gravitational acceleration, $g = 9.81 \text{ m/s}^2$ (32.2 ft/s²)

SOLUTION:

From Equation VI-5-134

$$\frac{W_{30}}{w_a h^3} = \frac{\pi}{6} [(1.1)(0.38)]^3 \left[\left(\frac{10.05 \text{ kN/m}^3}{[25.9 - 10.05] \text{ kN/m}^3} \right)^{\frac{1}{2}} \left(\frac{2.5 \text{ m/s}}{\sqrt{(1.0)(9.81 \text{ m/s}^2)(6 \text{ m})}} \right) \right]^{\frac{15}{2}} = 1.54(10)^{-6}$$

The W_{30} weight is found as

$$W_{30} = 1.54(10)^{-6} w_a h^3 = 1.54(10)^{-6} (25.9 \text{ kN/m}^3)(6 \text{ m})^3 = 0.0086 \text{ kN} = 8.6 \text{ N} (1.9 \text{ lb})$$

The rest of the riprap distribution is found using Equations VI-5-135 - VI-5-140, i.e.,

$$W_{50 \text{ max}} = 2.6 (8.6 \text{ N}) = 22.4 \text{ N} (5.0 \text{ lb})$$

$$W_{50 \text{ min}} = 1.7 (8.6 \text{ N}) = 14.6 \text{ N} (3.3 \text{ lb})$$

$$W_{100 \text{ max}} = 8.5 (8.6 \text{ N}) = 73.1 \text{ N} (16.4 \text{ lb})$$

$$W_{100 \text{ min}} = 3.4 (8.6 \text{ N}) = 29.2 \text{ N} (6.6 \text{ lb})$$

$$W_{15 \text{ max}} = 1.3 (8.6 \text{ N}) = 11.2 \text{ N} (2.5 \text{ lb})$$

$$W_{15 \text{ min}} = 0.5 (8.6 \text{ N}) = 4.3 \text{ N} (1.0 \text{ lb})$$

Blanket layer thickness for underwater placement is found using Equation VI-5-142

$$r = 3.8 \left(\frac{0.0086 \text{ kN}}{25.9 \text{ kN/m}^3} \right)^{\frac{1}{3}} = 0.26 \text{ m} (0.86 \text{ ft})$$

The calculated value for blanket thickness is less than the minimum value, so use $r = 0.5 \text{ m}$ (1.6 ft).

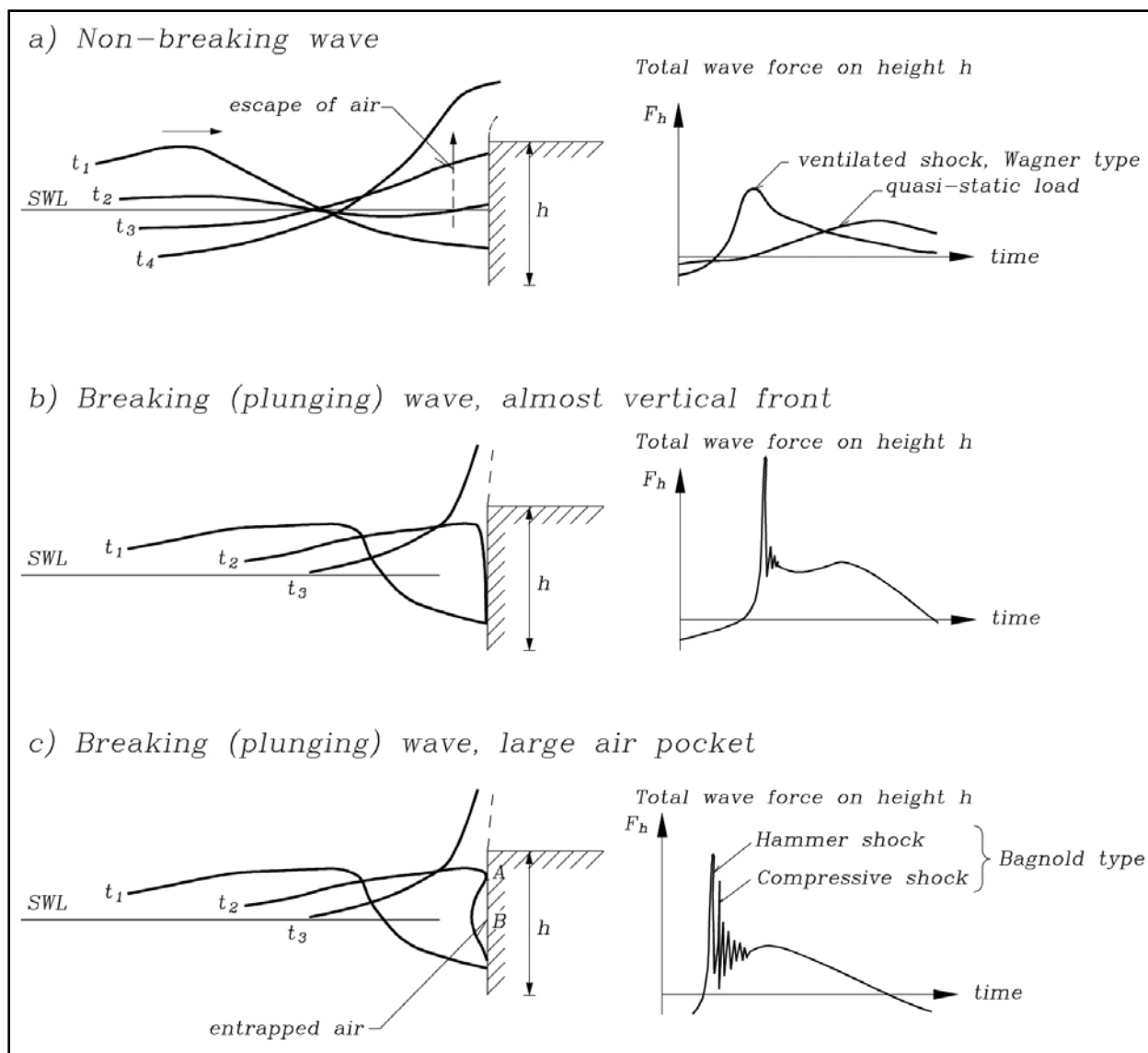


Figure VI-5-57. Illustration of vertical wall wave forces from nonbreaking and breaking waves

(6) It is important to investigate the effect of sloping rubble protection or any rubble foundation that extends in front of a vertical wall to make sure the slope does not trigger wave breaking, causing frequent impact loads on the wall.

(7) Figure VI-5-58 shows a system for identifying types of total horizontal wave loadings on the vertical-front structures as a function of structure geometry and wave characteristics (Kortenhaus and Oumeraci 1998). The system is based on two-dimensional model tests with irregular head-on waves. It should be noted that conditions for three-dimensional waves and oblique waves are different. Also note that the diagram does not cover situations where wave breaking takes place in a wider zone in front of the structure, i.e., typical shallow-water situations with depth-limited waves and seabeds flatter than 1:50.

b. *Wave-generated forces on vertical walls and caissons.*

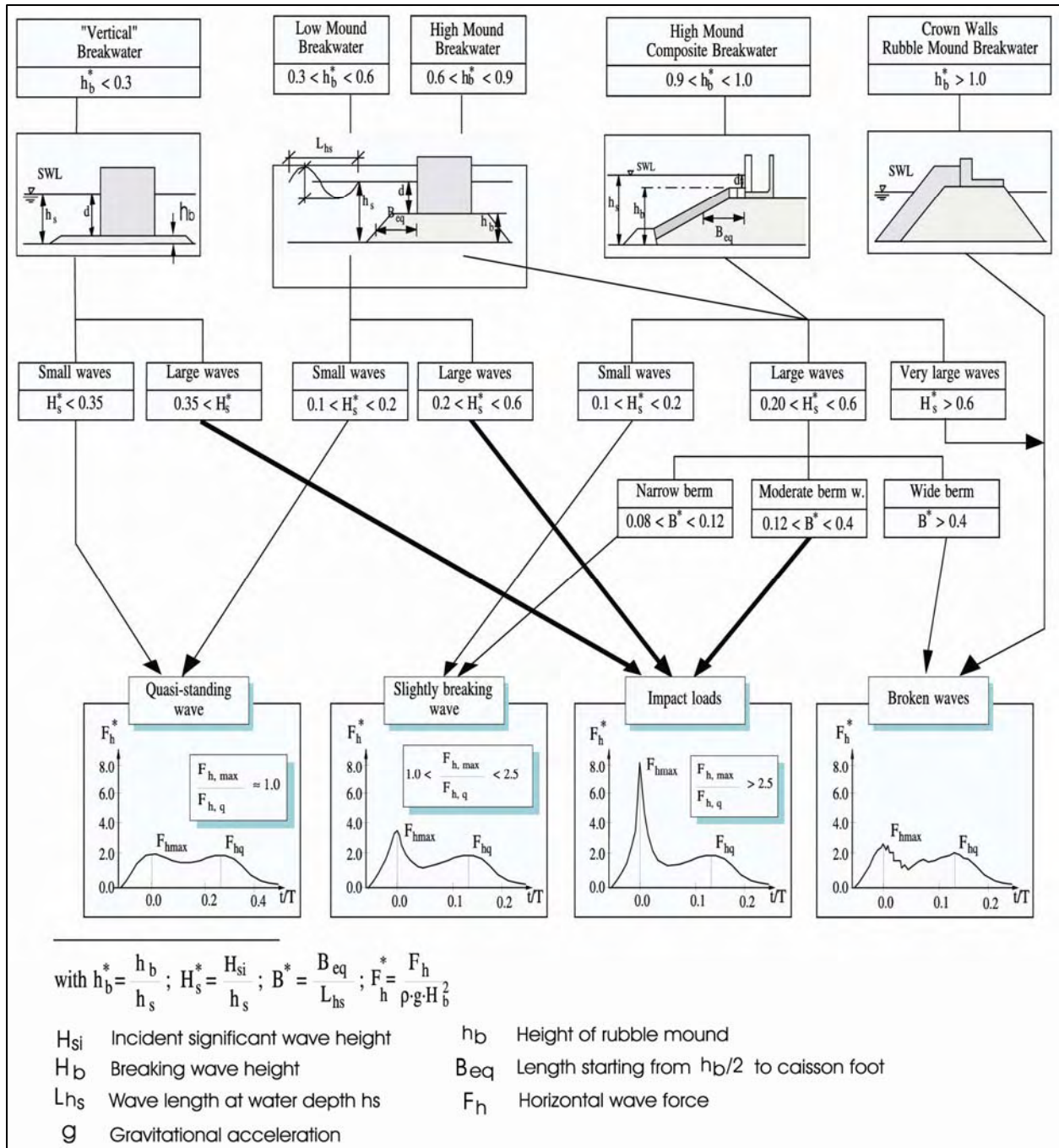


Figure VI-5-58. Identification of types of total horizontal wave loadings on vertical wall structure exposed to head-on long-crested irregular waves (Kortenhaus and Oumeraci 1998). Not valid if breaker zone is present in front of the structure

(1) Two-dimensional wave forces on vertical walls. Nonbreaking waves incident on smooth, impermeable vertical walls are completely reflected by the wall giving a reflection coefficient of 1.0. Where wales, tiebacks, or other structural elements increase the wall surface roughness and retard the vertical water motion at the wall, the reflection coefficient will be slightly reduced. Vertical walls built on rubble bases will also have a reduced reflection coefficient.

(a) The total hydrodynamic pressure distribution on a vertical wall consists of two time-varying components: the hydrostatic pressure component due to the instantaneous water depth at the wall, and the dynamic pressure component due to the accelerations of the water particles. Over a wave cycle, the force found from integrating the pressure distribution on the wall varies between a minimum value when a wave trough is at the wall to a maximum value when a wave crest is at the wall as illustrated by Figure VI-5-59 for the case of nonovertopped walls or caissons.

(b) Notice in the right-hand sketch of Figure VI-5-59 the resulting total hydrodynamic load when the wave trough is at the vertical wall is less than the hydrostatic loading if waves were not present and the water was at rest. For bulkheads and seawalls this may be a critical design loading because saturated backfill soils could cause the wall to fail in the seaward direction (see Figures VI-2-63 and VI-2-71). Therefore, water level is a crucial design parameter for calculating forces and moments on vertical walls.

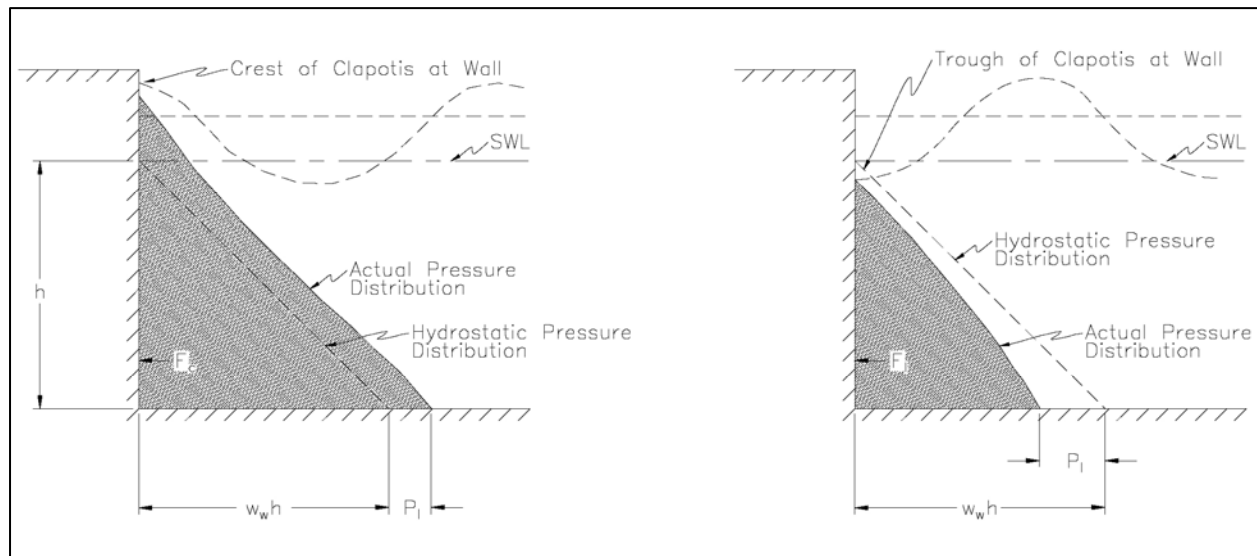


Figure VI-5-59. Pressure distributions for nonbreaking waves

(c) Wave overtopping of vertical walls provides a reduction in the total force and moment because the pressure distribution is truncated as shown schematically in Figure VI-5-60. Engineers should consider the effect overtopping might have on land-based vertical structures by creating seaward pressure on the wall caused by saturated backfill or ponding water.

(d) This section provides formulae for estimating pressure distributions and corresponding forces and overturning moments on vertical walls due to nonbreaking and breaking waves. Most of the methodology is based on the method presented by Goda (1974) and extended by others to cover a variety of conditions. These formulae provide a unified design approach to estimating design loads on vertical walls and caissons.

(e) Important Note: All of the methods in this section calculate the pressure distribution and resulting forces and moments for only the wave portion of the hydrodynamic loading. The hydrostatic pressure distribution from the swl to the bottom is excluded (see Figure VI-5-59). For a caisson structure, the swl hydrostatic forces would exactly cancel; however, it will be necessary to include the effect of the swl hydrostatic pressure for vertical walls tied into the shoreline or an embankment.

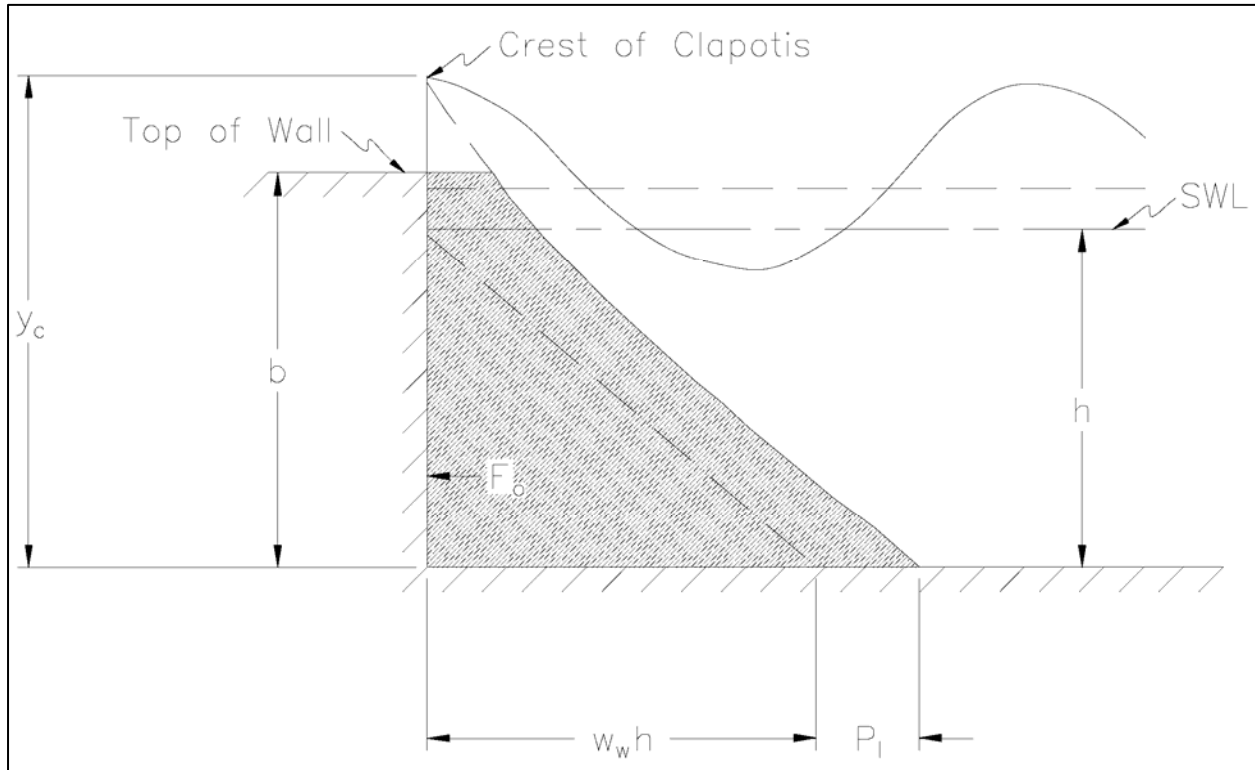
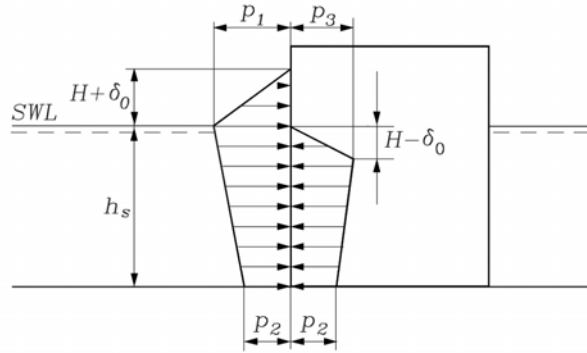


Figure VI-5-60. Pressure distributions on overtopped vertical wall

(f) The formulae given in the following tables are exclusively based on small-scale model tests. They are presented as follows:

Formula	Waves	Structure	Table
Sainflou formula	Standing	Impermeable vertical wall	VI-5-52
Goda formula	2-D oblique	Impermeable vertical wall	VI-5-53
Goda formula, modified by Takahashi, Tanimoto, and Shimosako 1994a	Provoked breaking	Impermeable vertical wall	VI-5-54
Goda formula forces and moments	Provoked breaking	Impermeable vertical wall	VI-5-55
Goda formula modified by Tanimoto and Kimura 1985	2-D head-on	Impermeable inclined wall	VI-5-56
Goda formula modified by Takahashi and Hosoyamada 1994	2-D head-on	Impermeable sloping top	VI-5-57
Goda formula modified by Takahashi, Tanimoto, and Shimosako 1990	2-D head-on	Horizontal composite structure	VI-5-58
Goda formula modified by Takahashi, Tanimoto, and Shimosako 1994b	3-D head-on	Vertical slit wall	VI-5-59

Table VI-5-52
The Sainflou Formula for Head-on, Fully Reflected, Standing Regular Waves (Sainflou 1928)



$$p_1 = (p_2 + \rho_w g h_s) \frac{H + \delta_o}{h_s + H + \delta_o} \quad (\text{VI-5-143})$$

$$p_2 = \frac{\rho_w g H}{\cosh(2\pi h_s / L)} \quad (\text{VI-5-144})$$

$$p_3 = \rho_w g (H - \delta_o) \quad (\text{VI-5-145})$$

$$\delta_o = \frac{\pi H^2}{L} \coth \frac{2\pi h_s}{L} \quad (\text{VI-5-146})$$

where H Wave height. In case of irregular waves, H should be taken as a characteristic wave height. In Japan $H_{1/3}$ is used, while in other countries $H_{1/10}$ might be used.

p_1 Wave pressure at the still water level, corresponding to wave crest

p_2 Wave pressure at the base of the vertical wall

p_3 Wave pressure at the still water level, corresponding to wave trough

δ_o Vertical shift in the wave crest and wave trough at the wall

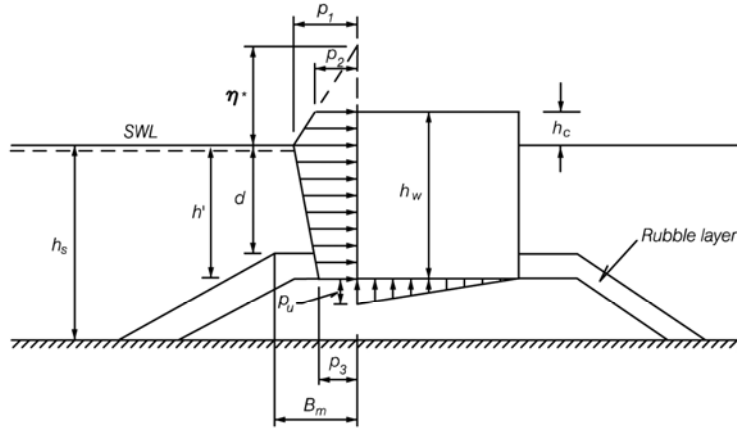
ρ_w Water density

h_s Water depth at the foot of the structure

L Local wave length.

Remarks. The Sainflou formula for conditions under wave crest and wave trough were derived theoretically for the case of regular waves and a vertical wall. The formula cannot be applied in cases where wave breaking and/or overtopping takes place.

Table VI-5-53
Goda Formula for Irregular Waves (Goda 1974; Tanimoto et al. 1976) (Continued)



$$\eta^* = 0.75(1 + \cos\beta) \lambda_1 H_{design} \quad (\text{VI-5-147})$$

$$p_1 = 0.5(1 + \cos\beta)(\lambda_1 \alpha_1 + \lambda_2 \alpha_* \cos^2\beta) \rho_w g H_{design} \quad (\text{VI-5-148})$$

$$p_2 = \begin{cases} \left(1 - \frac{h_c}{\eta^*}\right) p_1 & \text{for } \eta^* > h_c \\ 0 & \text{for } \eta^* \leq h_c \end{cases} \quad (\text{VI-5-149})$$

$$p_3 = \alpha_3 p_1 \quad (\text{VI-5-150})$$

$$p_u = 0.5(1 + \cos\beta) \lambda_3 \alpha_1 \alpha_3 \rho_w g H_{design} \quad (\text{VI-5-151})$$

where

β Angle of incidence of waves (angle between wave crest and front of structure)
 H_{design} Design wave height defined as the highest wave in the design sea state at a location just in front of the breakwater. If seaward of a surf zone Goda (1985) recommends for practical design a value of $1.8 H_s$ to be used corresponding to the 0.15% exceedence value for Rayleigh distributed wave heights. This corresponds to $H_{1/250}$ (mean of the heights of the waves included in 1/250 of the total number of waves, counted in descending order of height from the highest wave). Goda's recommendation includes a safety factor in terms of positive bias as discussed in Table VI-5-55. If within the surf zone, H_{design} is taken as the highest of the random breaking waves at a distance $5H_s$ seaward of the structure.

$$\alpha_* = \alpha_2$$

$$\alpha_1 = 0.6 + 0.5 \left[\frac{4\pi h_s/L}{\sinh(4\pi h_s/L)} \right]^2$$

$$\alpha_2 = \text{the smallest of } \frac{h_b - d}{3h_b} \left(\frac{H_{design}}{d} \right)^2 \text{ and } \frac{2d}{H_{design}}$$

$$\alpha_3 = 1 - \frac{h_w - h_c}{h_s} \left[1 - \frac{1}{\cosh(2\pi h_s/L)} \right]$$

L Wavelength at water depth h_b corresponding to that of the significant wave $T_s \approx 1.1T_m$, where T_m is the average period.

h_b Water depth at a distance of $5H_s$ seaward of the breakwater front wall.

λ_1, λ_2 and λ_3 are modification factors depending on the structure type. For conventional vertical wall structures, $\lambda_1 = \lambda_2 = \lambda_3 = 1$. Values for other structure types are given in related tables.

(Continued)

Table VI-5-53. (Concluded)

Uncertainty and bias of formulae: See Table VI-5-55.

Tested ranges:	water depth (cm)	wave height (cm)	wave period (s)	mound height (cm)
	35	7.1-31.2	2	0 & 15
	45	6.7-41.6	1.7	0 & 25
	45	7.6-32.8	1.3	0 & 25
	45	9.2-22.9	1	0 & 25

The formulae have been calibrated with the cases of 21 slidings and 13 nonslidings of the upright sections of the prototype breakwaters in Japan.

Table VI-5-54

Goda Formula Modified to Include Impulsive Forces from Head-on Breaking Waves (Takahashi, Tanimoto, and Shimosako 1994a)

The modification of Goda's formula concerns the formula for the pressure p_1 at the still water level (SWL). The coefficient α_* is modified as

$$\begin{aligned} \alpha_* &= \text{largest of } \alpha_2 \text{ and } \alpha_I \\ \alpha_2 &= \text{the smallest of } \frac{h_b - d}{3h_b} \left(\frac{H_{design}}{d} \right)^2 \text{ and } \frac{2d}{H_{design}} \\ \alpha_I &= \alpha_{I0} \cdot \alpha_{I1} \\ \alpha_{I0} &= \begin{cases} H_{design}/d & \text{for } H_{design}/d \leq 2 \\ 2.0 & \text{for } H_{design}/d > 2 \end{cases} \\ \alpha_{I1} &= \begin{cases} \frac{\cos \delta_2}{\cosh \delta_1} & \delta_2 \leq 0 \\ \frac{1}{\cosh \delta_1 \cdot (\cosh \delta_2)^{\frac{1}{2}}} & \delta_2 > 0 \end{cases} \\ \delta_1 &= \begin{cases} 20 \cdot \delta_{11} & \text{for } \delta_{11} \leq 0 \\ 15 \cdot \delta_{11} & \text{for } \delta_{11} > 0 \end{cases} \\ \delta_{11} &= 0.93 \left(\frac{B_m}{L} - 0.12 \right) + 0.36 \left(\frac{h_s - d}{h_s} - 0.6 \right) \\ \delta_2 &= \begin{cases} 4.9 \cdot \delta_{22} & \text{for } \delta_2 \leq 0 \\ 3 \cdot \delta_{22} & \text{for } \delta_2 > 0 \end{cases} \\ \delta_{22} &= -0.36 \left(\frac{B_m}{L} - 0.12 \right) + 0.93 \left(\frac{h_s - d}{h_s} - 0.6 \right) \end{aligned}$$

where H_{design} , L , d , h_s , h_b , B_m are given in the figure and text of Table VI-5-53.

Range of tested parameters:	Regular waves
	bottom slope 0.01
	$h_s = 42 \text{ cm and } 54 \text{ cm}$
	$d = 7 - 39 \text{ cm}$
	$B_m = 2.5 - 200 \text{ cm}$
	$H = 17.2 - 37.8 \text{ cm}$
	$T = 1.8 - 3 \text{ sec.}$

Table VI-5-55
Resulting Wave Induced Forces and Moments, and Related Uncertainties and Bias When Calculated From Wave Load Equations by Goda and Takahashi

Per running meter of the breakwater the wave induced horizontal force, F_H , the uplift force, F_U , and the reduced weight of the vertical structure due to buoyancy, F_G , can be calculated from equations by Goda and Takahashi as follows:

$$F_H = U_{F_H} \left[\frac{1}{2}(p_1 + p_2)h_c + \frac{1}{2}(p_1 + p_3)h' \right] \quad (\text{VI-5-152})$$

$$F_U = U_{F_U} \cdot \frac{1}{2}p_u \cdot B \quad (\text{VI-5-153})$$

$$F_G = \rho_c \cdot g B \cdot h_w - \rho_w \cdot g B \cdot h' \quad (\text{VI-5-154})$$

where ρ_c Mass density of the structure
 ρ_w Mass density of the water
 U_{F_H} Stochastic variable signifying the bias and the uncertainty related to the horizontal force
 U_{F_U} Stochastic variable signifying the bias and the uncertainty related to the uplift force
 h' Submerged height of the wall from the toe to the still water level.
 B Vertical structure width

The corresponding moments at the heel of the caisson breakwater are:

$$M_H = U_{M_H} \left[\frac{1}{6}(2p_1 + p_3)h'^2 + \frac{1}{2}(p_1 + p_2)h'h_c + \frac{1}{6}(p_1 + 2p_2)h_c^2 \right] \quad (\text{VI-5-155})$$

$$M_U = U_{M_U} \cdot \frac{1}{3}p_u \cdot B^2 \quad (\text{VI-5-156})$$

$$M_G = \frac{1}{2}B^2g(\rho_ch_w - \rho_wh') \quad (\text{VI-5-157})$$

where U_{M_H} Stochastic variable signifying the bias and the uncertainty of the horizontal moment
 U_{M_U} Stochastic variable signifying the bias and the uncertainty of the uplift moment.

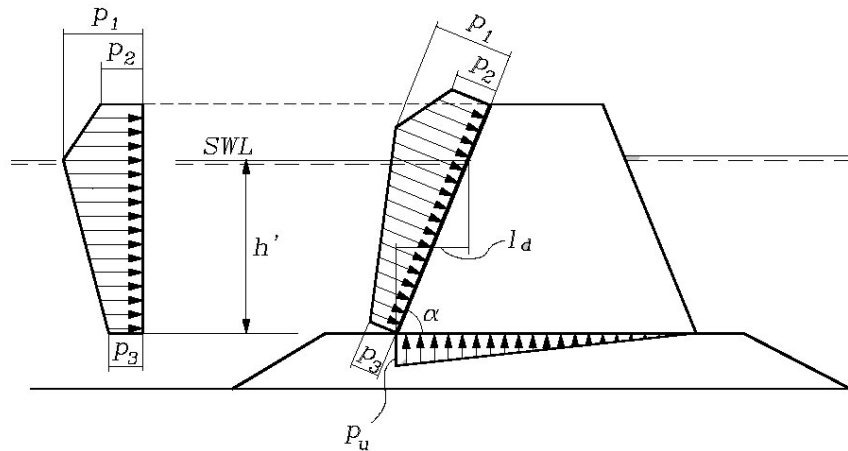
Uncertainty and bias of the Goda formulae in Table VI-5-53. Based on reanalysis by Juhl and van der Meer (1992), Bruining (1994), and van der Meer, Juhl, and van Driel (1994) of various model tests performed at Danish Hydraulic Institute and Delft Hydraulics. The mean values and standard deviations of the stochastic variables U are given as

Uncertainty and bias of horizontal wave induced force, uplift force, horizontal moment and uplift moment (vertical composite type)

Stochastic variable	Mean value	no model tests		model test performed	
		Stand. dev.	$\frac{\sigma_{X_i}}{\mu_{X_i}} \%$	Stand. dev.	$\frac{\sigma_{X_i}}{\mu_{X_i}} \%$
X_i	μ_{X_i}				
U_{F_H}	0.90	0.25	0.22	0.05	0.055
U_{F_U}	0.77	0.25	0.32	0.05	0.065
U_{M_H}	0.81	0.40	0.49	0.10	0.12
U_{M_U}	0.72	0.37	0.51	0.10	0.14

Table VI-5-56
Wave Loads on Impermeable Inclined Walls (Tanimoto and Kimura 1985)

Tanimoto and Kimura (1985) performed model tests and demonstrated that the Goda formula can be applied by projection of the Goda wave pressures calculated for a vertical wall with the same height (crest level) as illustrated in the figure.



The wave induced uplift pressure on the base plate is reduced compared to the vertical face case. Consequently λ_3 for the calculation of p_u in the Goda formula is modified as

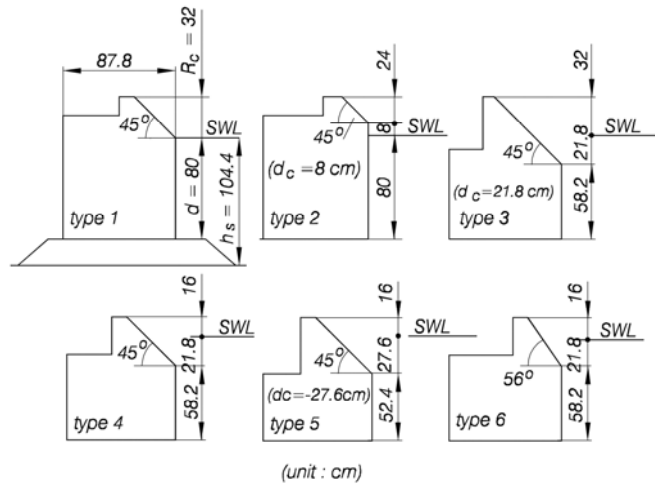
$$\lambda_3 = \exp \left[-2.26(7.2 \ell_d / L)^3 \right] \quad (\text{VI-5-158})$$

where $\ell_d = h' \cot \alpha$ and L is the wavelength.

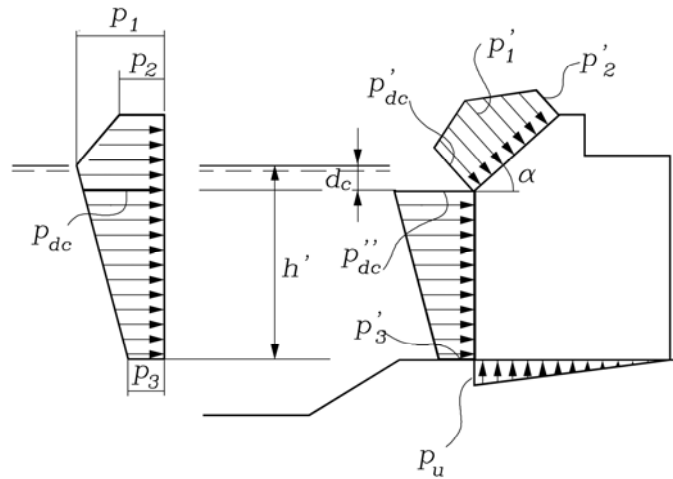
Eq VI-5-158 is valid for $\alpha \geq 70^\circ$ and $\ell_d < 0.1L$.

Table VI-5-57
Wave Loads on Sloping Top Structures (Takahashi and Hosoyamada 1994)

Tested cross sections



Pressure distribution



$$p'_1 = \lambda_{SL} p_1 \sin \alpha, \quad p'_2 = \lambda_{SL} p_2 \sin \alpha, \quad p'_{dc} = \lambda_{SL} p_{dc} \sin \alpha \quad (\text{VI-5-159})$$

$$p''_{dc} = \lambda_V p_{dc}, \quad p'_3 = \lambda_V p_3$$

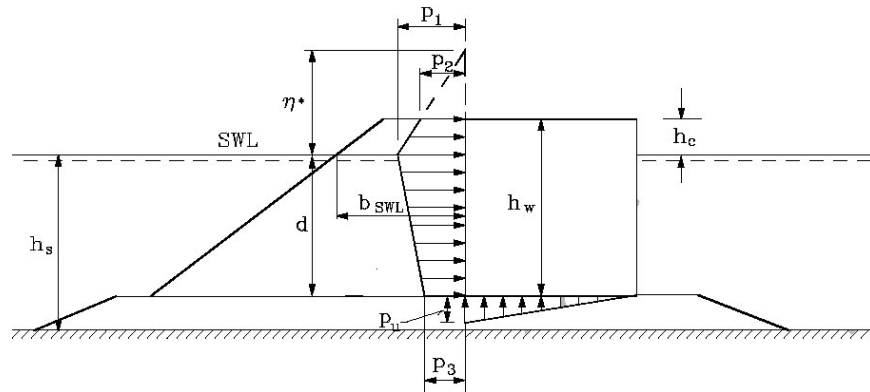
where

$$\lambda_{SL} = \frac{1}{\sin^2 \alpha} \min[1.0, \max(\sin^2 \alpha, 1 + 0.46 \cos^2 \alpha - 23 \cos^2 \alpha H/L)]$$

$$\lambda_V = \min[1.0, \max(1.1, 1.1 + 11d_c/L) - 5.0H/L]$$

p_1, p_2, p_3, p_{dc} & p_u are calculated from the Goda formula (Table VI-5-53)

Table VI-5-58
Wave Loads on Vertical Walls Protected by a Rubble-Mound Structure (Takahashi, Tanimoto, and Shimosako 1990)



λ_1 , λ_2 and λ_3 in the Goda formula are modified as:

$$\lambda_1 = \lambda_3 = \begin{cases} 1.0 & H_{design}/h_s < 0.3 \\ 1.2 - 0.67(H_{design}/h_s) & 0.3 \leq H_{design}/h_s \leq 0.6 \\ 0.8 & H_{design}/h_s > 0.6 \end{cases} \quad (VI-5-160)$$

$$\lambda_2 = 0$$

Validity range: These values presume that the rubble consists of blocks of the complex types like Tetrapods and Dolosse. Also, the width of the block section at the top of the vertical wall should be no less than twice the height of a block. The front slope is approximately 1 : 1.5. The model tests cover the parameter intervals: $h_s/L_{1/3} = 0.07 - 0.11$ and $b_{SWL}/L_{1/3} = 0.046 - 0.068$.

Uncertainty and bias: From the test results the mean value, μ_{λ_1} , and the variational coefficient, $\frac{\sigma_{\lambda_1}}{\mu_{\lambda_1}}$, of λ_1 are estimated to be approximately

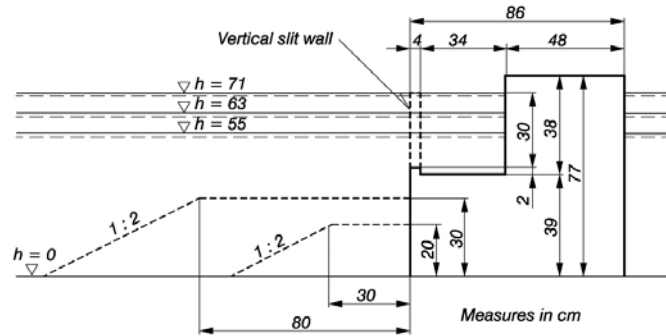
$$\mu_{\lambda_1} = \begin{cases} 0.90 & H_{design}/h_s < 0.4 \\ 0.90 - (H_{design}/h_s - 0.4) & 0.4 \leq H_{design}/h_s \leq 0.7 \\ 0.60 & 0.7 < H_{design}/h_s < 0.8 \end{cases} \quad (VI-5-161)$$

and

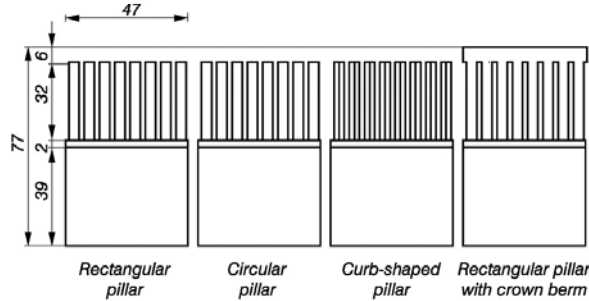
$$\frac{\sigma_{\lambda_1}}{\mu_{\lambda_1}} = 5\% - 10\%$$

Table VI-5-59
Wave Pressures from Regular Head-on Waves on Caissons with Vertical Slit Front Face and Open Wave Chamber
(Tanimoto, Takahashi, and Kitatani 1981; Takahashi, Shimosako, and Sakaki 1991) (Continued)

Cross sections

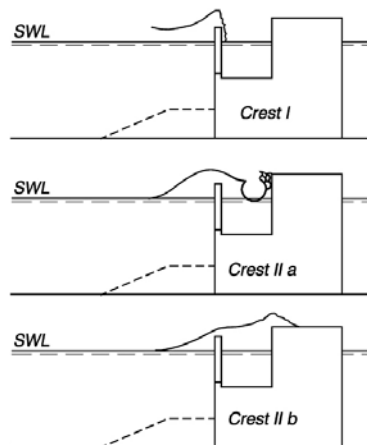


Screen porosity (relative area of openings) = 33 %
 □□□□□□ □□□□□□ □□□□□□ □□□□□□



Tested wave range: Regular head-on waves
 Incident wave height: 10-30 cm
 Wave period: 1.5, 2.0, 2.5 s

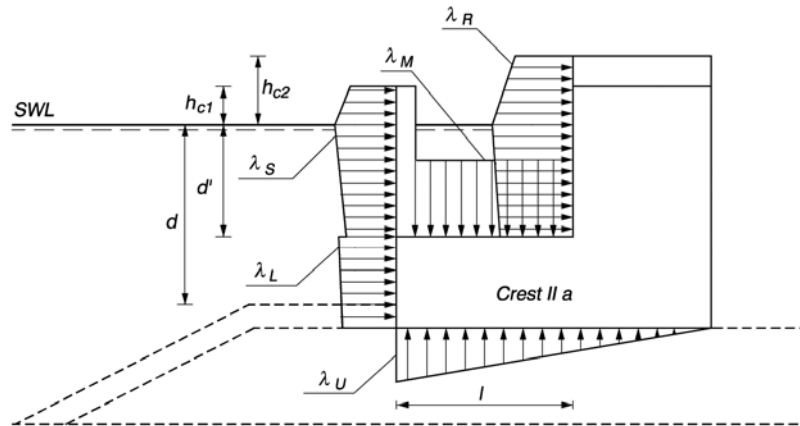
Considered wave crest faces



(Continued)

Table VI-5-59. (Concluded)

Pressure distribution



Pressure calculation: Use the Goda formulae with modified λ_1 , λ_2 and λ_3 as given in the following table. For example, the wave pressure on the slit wall in the case of Crest-I is calculated by the Goda formulae with λ_1 and λ_2 replaced by λ_{S1} and λ_{S2} , respectively.

Modification factors for vertical slit wall caisson (From Takahashi et al. 1994b).

		Crest-I	Crest-IIa	Crest-IIb
Slit wall	λ_{S1}	0.85	0.7	0.3
	λ_{S2}	0.4 ($\alpha^* \leq 0.75$) 0.3/ α^* ($\alpha^* > 0.75$)	0	0
Impermeable part of front wall	λ_{L1}	1	0.75	0.65
	λ_{L2}	0.4 ($\alpha^* \leq 0.5$) 0.2/ α^* ($\alpha^* > 0.5$)	0	0
Wave chamber rear wall	λ_{R1}	0	20l/3L' ($l/L' \leq 0.15$) 1.0 ($l/L' > 0.15$)	1.4 ($H/h \leq 0.1$) 1.6 - 2H/h ($0.1 < H/h < 0.3$) 1.0 ($H/h \geq 0.3$)
	λ_{R2}	0	0.56 ($\alpha^* \leq 25/28$) 0.5/ α^* ($\alpha^* > 25/28$)	0
Wave Chamber bottom slab	λ_{M1}	0	20l/3L' ($l/L' \leq 0.15$) 1.0 ($l/L' > 0.15$)	1.4 ($H/h \leq 0.1$) 1.6 - 2H/h ($0.1 < H/h < 0.3$) 1.0 ($H/h \geq 0.3$)
	λ_{M2}	0	0	0
Uplift force	λ_{U3}	1	0.75	0.65

In the calculation of α^* for the rear wall, α_1 should be replaced by α'_1 which is obtained with the parameters d' , L' and B'_M instead of d , L and B_M respectively, where d' is the depth in the wave chamber, L' is the wavelength at water depth d , $B'_M = l - (d - d')$, and l is the width of the wave chamber including the thickness of the perforated vertical wall.

(g) Wave pressure distributions for breaking waves are estimated using Table VI-5-54, and the corresponding forces and moments are calculated from Table VI-5-55. Not included in this manual is the older breaking wave forces method of Minikin as detailed in the *Shore Protection Manual* (1984). As noted in the *Shore Protection Manual* the Minikin method can result in very high estimates of wave force, "as much as 15 to 18 times those calculated for nonbreaking waves." These estimates are too conservative in most cases and could result in costly structures.

(h) On the other hand, there may be rare circumstances where waves could break in just the right manner to create very high impulsive loads of short duration, and these cases may not be covered by the range of experiment parameters used to develop the guidance given in Table VI-5-54. In addition, scaled laboratory models do not correctly reproduce the force loading where pockets of air are trapped between the wave and wall as shown in Figure VI-5-57. For these reasons, it may be advisable to design vertical-front structures serving critical functions according to Minikin's method given in *Shore Protection Manual* (1984).

(2) Vertical wave barriers.

(a) A vertical wave barrier is a vertical partition that does not extend all the way to the bottom as illustrated by the definition sketch in Figure VI-5-61. Wave barriers reduce the transmitted wave height while allowing circulation to pass beneath the barrier. A useful application for vertical wave barriers is small harbor protection.

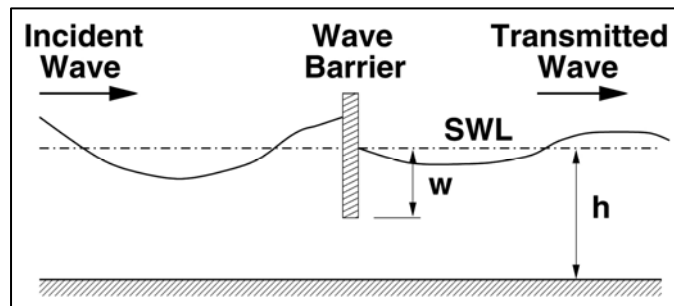


Figure VI-5-61. Wave barrier definition sketch

(b) Kriebel, Sollitt, and Gerken (1998) presented small- and large-scale laboratory measurements of forces on vertical wave barriers and found that existing methods for estimating wave forces on wave barriers overpredicted measured forces by about a factor of 2. They also presented an eigenvalue expansion method for calculating theoretical wave forces, and the predicted forces matched the experiment measurements within 10-20 percent. Both regular and irregular wave experiments were used in the analysis.

(c) Estimation of wave forces using the eigenvalue expansion method involves solving matrix equations for unknown coefficients under the physical constraints of no flow through the barrier and matching dynamic pressure in the gap beneath the barrier. However, this method must be programmed on a computer to obtain force estimates.

(d) An empirical equation for estimating forces on vertical wave barriers was developed for this manual based on the large-scale laboratory irregular wave measurements presented in Kriebel et al. (1998). Their experiments used solid vertical plates having penetration values of $w/h = 0.4, 0.5, 0.6,$ and 0.7 placed in a 3-m water depth. Time series of total force on the plate were recorded, and significant force amplitudes per unit width of barrier were calculated from the zeroth-moment of the force spectra as

$$F_{mo} = \frac{1}{2} \left(4 \sqrt{m_o} \right) \frac{1}{B} \quad (\text{VI-5-162})$$

where m_o is the area beneath the measured force spectrum and B is the horizontal width of the barrier. The 1/2-factor arises because the force spectrum also includes forces directed seaward, which are approximately the same magnitude as the landward directed forces (Kriebel et al. 1998).

(e) The relative force measurements per unit width of barrier are shown in Figure VI-5-62. The significant force per unit width (F_{mo}) is nondimensionalized by the significant force per unit width (F_o) for a vertical wall extending over the entire depth, given by the equation

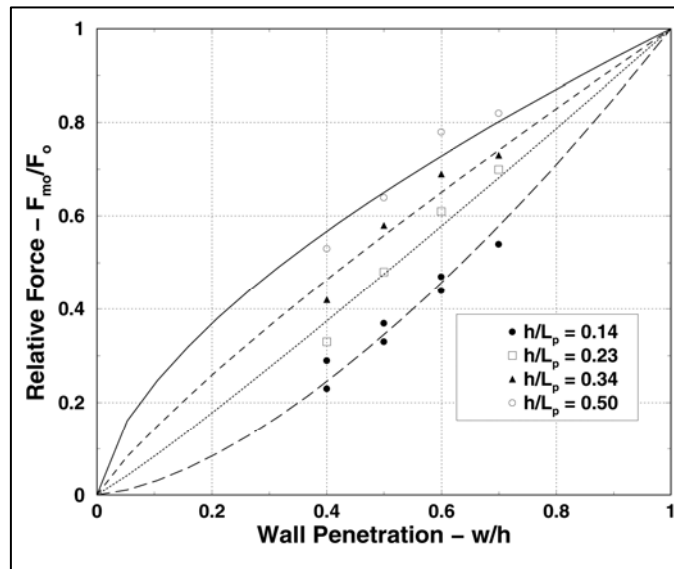


Figure VI-5-62. Best-fit wave barrier force data

$$F_o = \rho g H_{mo} \frac{\sinh k_p h}{k_p \cosh k_p h} \quad (\text{VI-5-163})$$

where

ρ = water density

g = gravity

H_{mo} = incident significant wave height

k_p = wave number associated with the spectral peak period, T_p

h = water depth at the barrier

(f) The lines in Figure VI-5-62 are best-fit curves of the form $F_{mo}/F_o = (w/h)^m$. The exponents (m) are plotted in Figure VI-5-63 as a function of relative depth, h/L_p , along with a best-fit power curve.

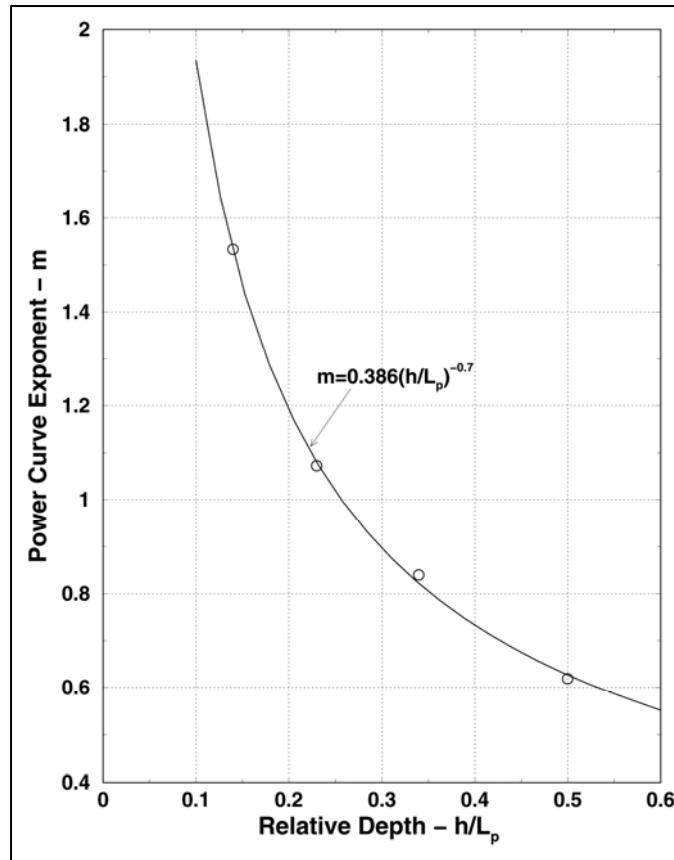


Figure VI-5-63. Power curve exponents

(g) The resulting empirical predictive equation is then given by

$$F_{mo} = F_o \left(w/h \right)^{0.386(h/L_p)^{-0.7}} \quad (\text{VI-5-164})$$

where

F_{mo} = significant force per unit width of barrier

F_o = significant force per unit width of vertical wall (Equation VI-5-163)

w = barrier penetration depth

h = water depth

L_p = local wavelength associated with the peak spectral period, T_p

(h) A comparison of the measured force values versus estimates based on the empirical Equation VI-5-164 is shown in Figure VI-5-64.

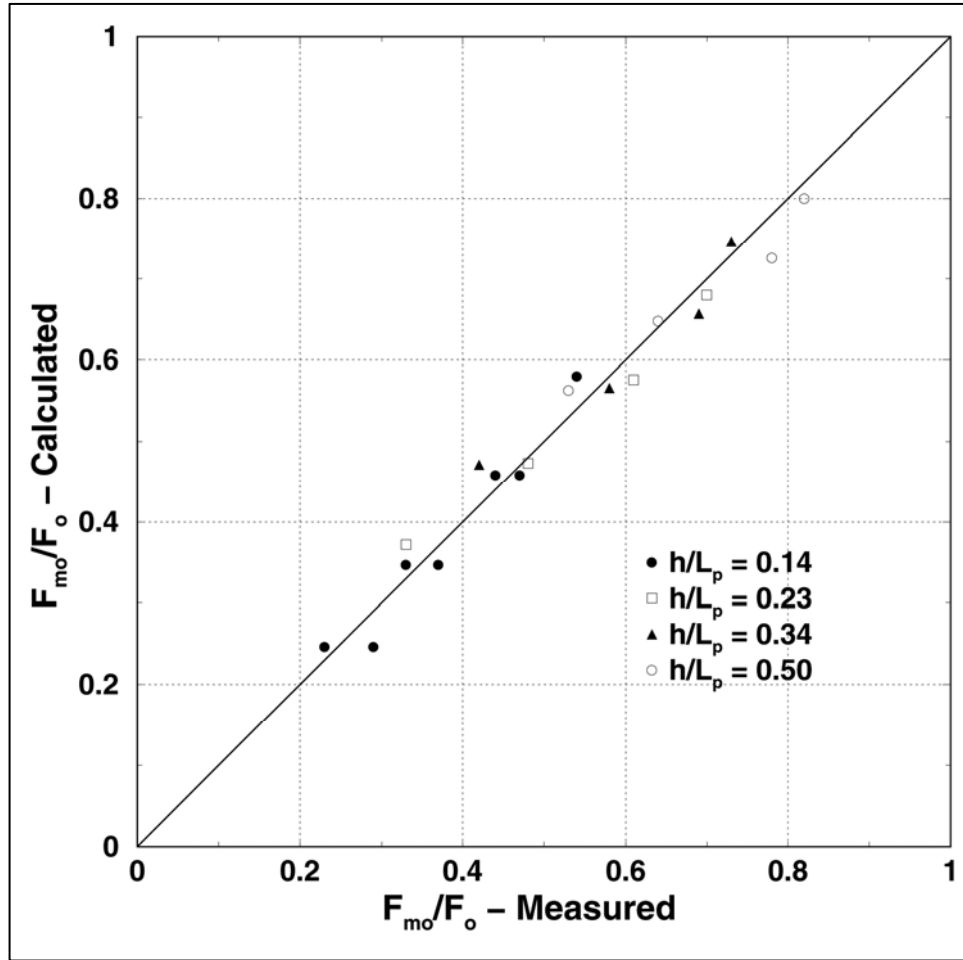


Figure VI-5-64. Comparison of Equation VI-5-139 to data used in empirical curve fits

(i) Use of Equation VI-5-164 should be limited to the range $0.4 < w/h < 0.7$ and $0.14 < h/L_p < 0.5$; however, estimates slightly outside the strict bound of the laboratory data are probably reasonable.

(j) The design force load on the vertical barrier should be the load corresponding to the design wave height, $H_{design} = 1.8 H_s$ as recommended by Goda (1985). For Rayleigh distributed waves, $H_{design} = H_{1/250}$; and by linear superposition, we can assume that force amplitudes will also be Rayleigh distributed. Thus, the design force load is determined as

$$F_{design} = 1.8F_{mo} \tag{VI-5-165}$$

(3) Structure length and alignment effects on wave height.

(a) Diffraction at the head of a structure creates variations in wave heights along the structure. For a semi-infinite, fully reflecting structure exposed to nonbreaking long-crested regular waves, Ito, Tanimoto, and Yamamoto (1972) calculated the ratio of the wave height along the structure, H , to the incident wave height, H_I , as

$$\frac{H}{H_1} = \sqrt{(C + S + 1)^2 + (C - S)^2} \quad (\text{VI-5-166})$$

where

$$C = \partial_0'' \cos\left(\frac{\pi}{2} t^2\right) dt, \quad S = \partial_0'' \sin\left(\frac{\pi}{2} t^2\right) dt, \quad u = 2\sqrt{\frac{2x}{L}} \sin\left(\frac{\alpha}{2}\right) \quad (\text{VI-5-167})$$

and x is the distance from the tip of the structure, L is the wavelength and α is the angle between the direction of wave propagation and the front alignment of the structure.

(b) Figure VI-5-65 shows an example of the wave height variation for regular head-on waves of period $T = 10$ s. Shown with the dotted line is the wave height variation calculated for nonbreaking long-crested irregular (random) waves (Bretschneider-Mitsuyasu spectrum, $T_{1/3} = 10$ s). The smoothing effect of random seas is clearly seen. At some locations the wave height exceeds twice the incident wave height expected for infinitely long vertical wall structures.

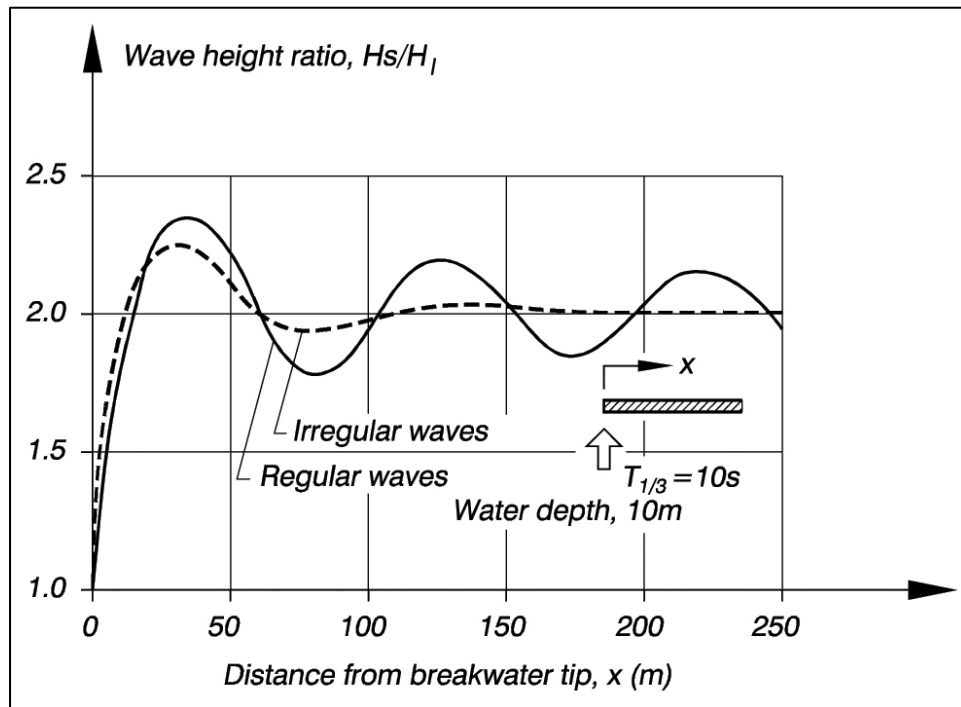


Figure VI-5-65. Variation of wave height along a semi-infinite, fully reflecting breakwater exposed to head-on, long-crested waves (from Goda 1985)

(c) For short-length breakwaters, the diffraction from both ends of the structure influences the wave height variation (see Goda 1985). Also note that experiments indicate that the theoretical assumption of complete reflection of waves from smooth vertical walls appears not fulfilled, because reflection coefficients on the order of 0.95 have been measured. (However, the methods for measuring reflection are less than perfect, as well.) Oblique waves create wave height variations different from those created by head-on waves. Concave and convex corners also affect the wave height variation along the structure (see Part VI-5-4e).

(4) Horizontal wave force reduction for nonbreaking waves.

(a) The effect of incident wave angle on the horizontal wave force exerted on a caisson is twofold. One effect is a force reduction, compared to head-on waves, due to the reduction of point pressure on the caisson, referred to as point-pressure force reduction. The second effect is a force reduction due to the fact that peak pressures do not occur simultaneously along the caisson, referred to as peak-delay force reduction. These two-force reduction effects will be present in short-crested waves because of spreading of the wave energy over a range of incident angles. Model test results Franco, van der Meer, and Franco (1996) with long-crested waves indicate that the point-pressure reduction can be estimated by the Goda formula.

(b) The peak-delay force reduction for oblique nonbreaking regular waves can be predicted by the Battjes formula (Battjes 1982)

$$r_F(L, \theta) = \frac{\text{max. force, wave incident angle } \theta}{\text{max. force, head-on wave } (\theta = 0^\circ)} = \frac{\sin\left(\frac{\pi L_s}{L} \sin \theta\right)}{\frac{\pi L_s}{L} \sin \theta} \quad (\text{VI-5-168})$$

where L and L_s are the wavelength and the structure length, respectively, and θ is the wave incident angle. Equation VI-5-168 is depicted in Figure VI-5-66. (In the figure β is used instead of θ .)

(c) The peak-delay force reduction for oblique nonbreaking long-crested irregular waves can be estimated by the formula (Burcharth and Liu 1998)

$$r_F(L_p, \theta) = \frac{\text{characteristic wave force, wave incident angle } \theta}{\text{characteristic wave force, head-on wave } (\theta = 0^\circ)} = \left| \frac{\sin\left(\frac{\pi L_s}{L_p} \sin \theta\right)}{\frac{\pi L_s}{L_p} \sin \theta} \right| \quad (\text{VI-5-169})$$

where L_p is the wavelength corresponding to the peak frequency. For example, the characteristic wave force can be chosen as F_{max} , $F_{1/250}$, $F_{1 \text{ percent}}$, $F_{10 \text{ percent}}$, etc.

(d) In order to investigate the uncertainty and bias of Equation VI-5-169, a real-time calculation of the wave force on a caisson by nonbreaking long-crested irregular waves was performed by Burcharth and Liu (1998). The result is given in Figure VI-5-67.

(e) Figure VI-5-67 shows that Equation VI-5-169 gives a close estimate of the mean value of the peak-delay reduction. However, a large variation of the peak-delay force reduction factor corresponding to a low exceedence probability, e.g., $F_{1/250}$, was observed.

(f) The peak-delay force reduction for oblique nonbreaking short-crested waves can be estimated by the formula (Burcharth and Liu 1998)

$$r_F(\sigma, \theta_m) = \frac{\text{characteristic wave force, short-crested wave}}{\text{characteristic wave force, head-on long-crested wave}} \approx \left(\int_{-\pi}^{\pi} r_F(L_p, \theta) D(\sigma, \theta_m) d\theta \right)^{1/2} \quad (\text{VI-5-170})$$

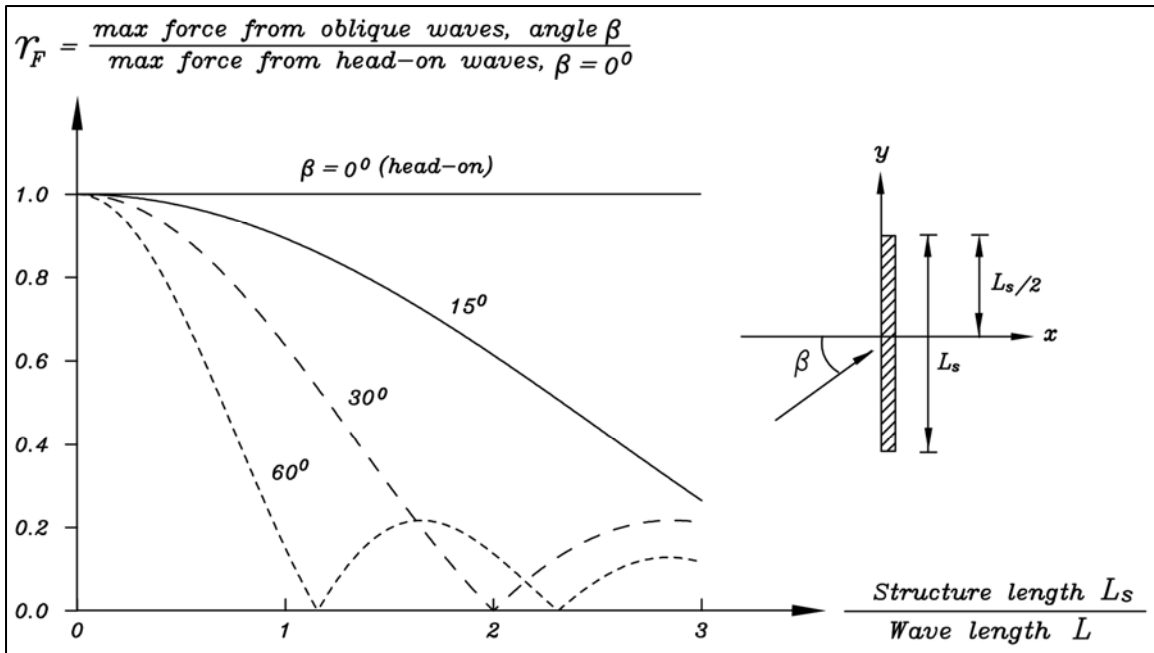


Figure VI-5-66. Peak-delay force reduction for oblique regular waves (Burcharth and Liu 1998)

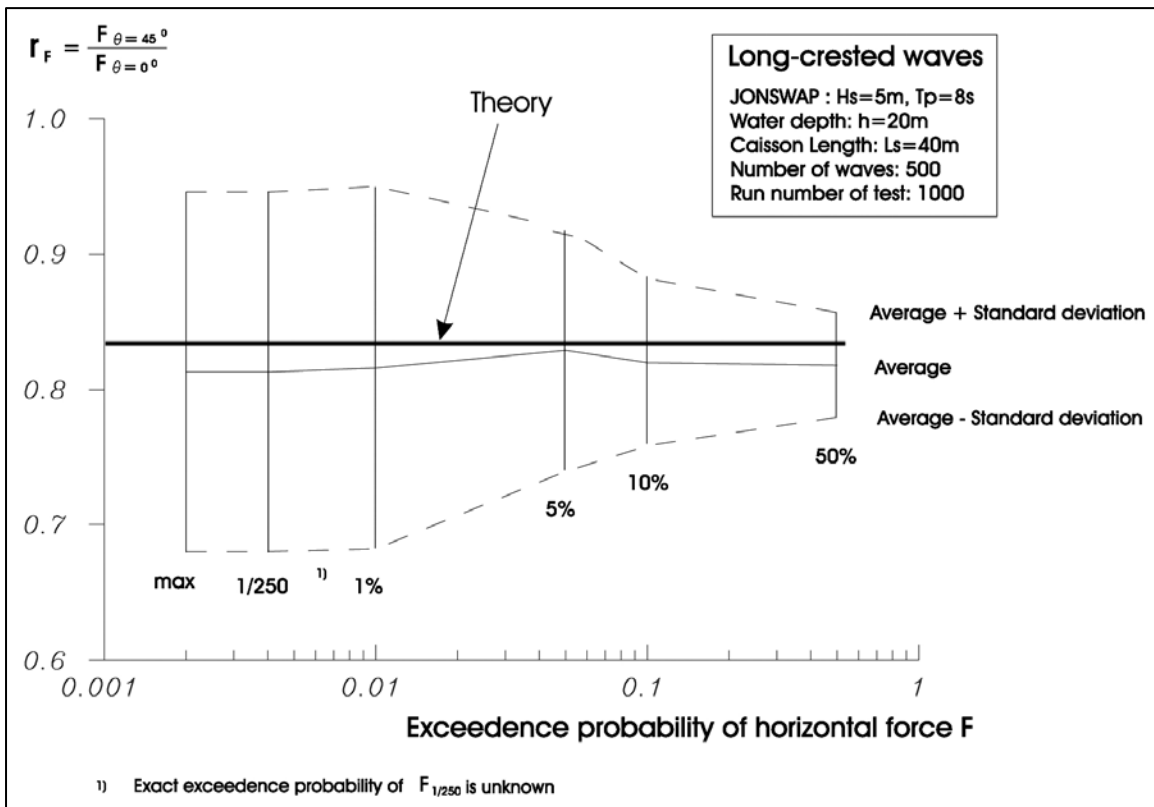


Figure VI-5-67. Numerical simulation of peak-delay reduction, long-crested waves. Examples of uncertainty calculation for wave train with 500 waves (Burcharth and Liu 1998)

where $r_F(L_p, \theta)$ is given by Equation VI-5-169 and $D(\sigma, \theta_m)$ is the wave directional spreading function with the wave energy spreading angle σ and the mean wave incident direction θ_m . An example of Equation VI-5-170 is depicted in Figure VI-5-68.

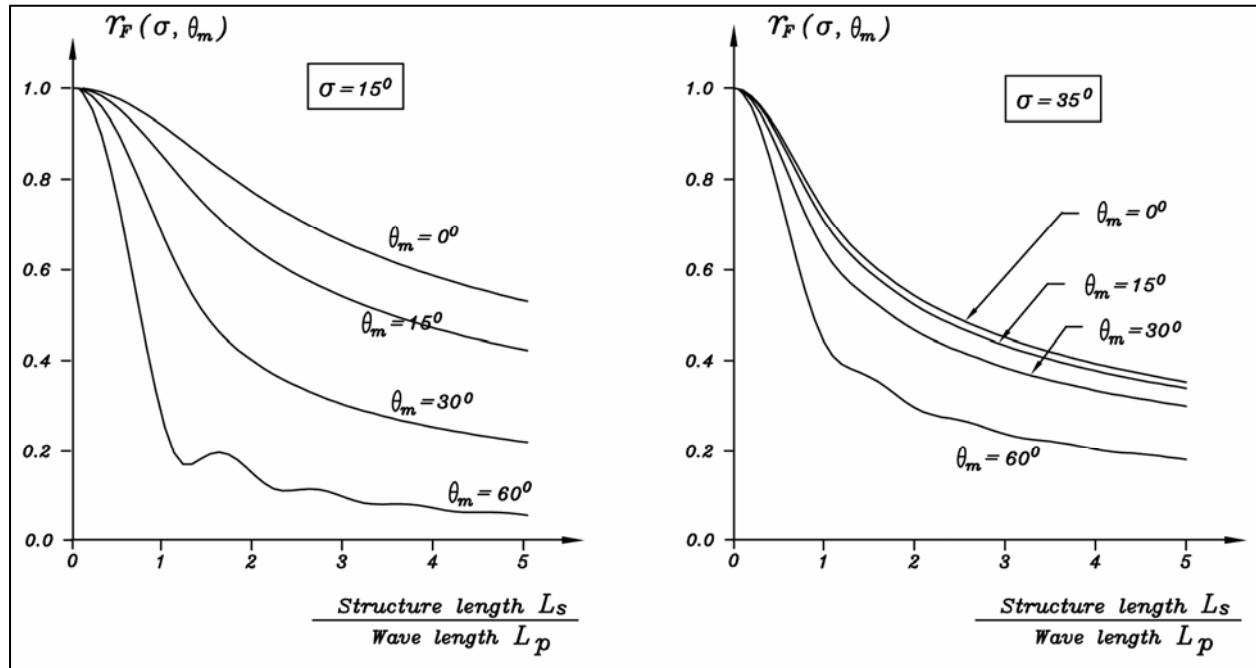


Figure VI-5-68. Example of peak-delay force reduction for short-crested waves (Burcharth and Liu 1998)

(5) Horizontal turning moment for nonbreaking waves.

(a) Oblique wave attack generates resultant wave forces acting eccentrically on the caisson front. The horizontal turning moment around the caisson center caused by oblique regular waves can be estimated by the formula (Burcharth 1998)

$$r_M = \frac{\text{max. moment, wave incident angle } \theta}{(\text{head-on max. force}) \times (\text{structure length})}$$

$$= \frac{1}{2} \left| \frac{\cos\left(\frac{\pi L_s}{L} \sin \theta\right)}{\frac{\pi L_s}{L} \sin \theta} - \frac{\sin\left(\frac{\pi L_s}{L} \sin \theta\right)}{\left(\frac{\pi L_s}{L} \sin \theta\right)} \right| \quad \text{(VI-5-171)}$$

Equation VI-5-171 is depicted in Figure VI-5-69. The maximum horizontally turning moment around caisson center under arbitrary wave incident angle is

$$M_{\text{max}} = 0.22 F_{\theta=0^\circ} L_s \quad \text{(VI-5-172)}$$

where $F_{\theta=0^\circ}$ is the maximum head-on wave force.

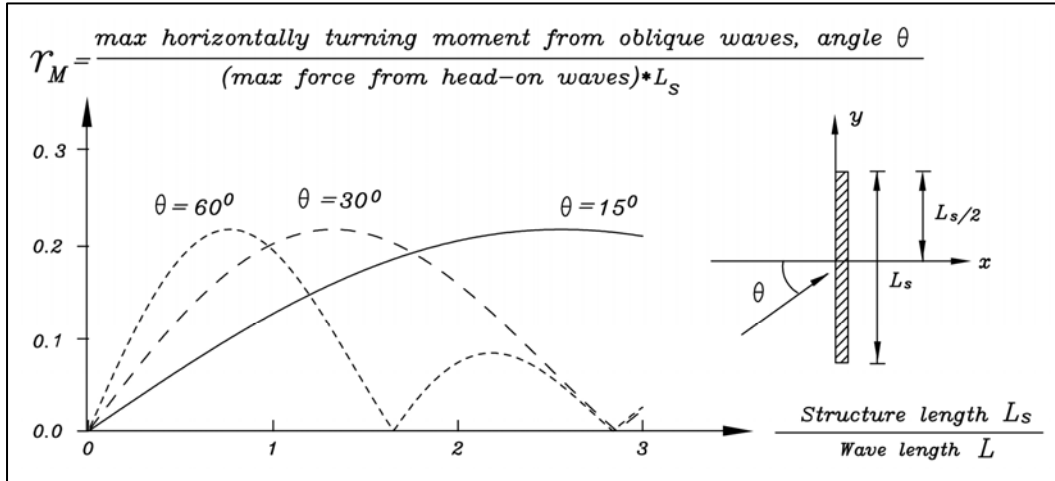


Figure VI-5-69. Nondimensional amplitude of horizontal turning moment around the center of the caisson exposed to oblique nonbreaking regular waves

(6) Horizontal wave force reduction for breaking waves.

(a) Short-crested waves break in a limited area and not simultaneously along the whole caisson, which results in an even larger force reduction in comparison with nonbreaking waves. Figure VI-5-70 shows an example of force reduction from model tests with short-crested, breaking, head-on waves, where the force reduction r_F is defined as

$$r_F = \frac{F_{1/250}, \text{ short-crested wave, mean wave incident angle } \theta_m}{F_{1/250}, \text{ long-crested head-on wave}} \quad (\text{VI-5-173})$$

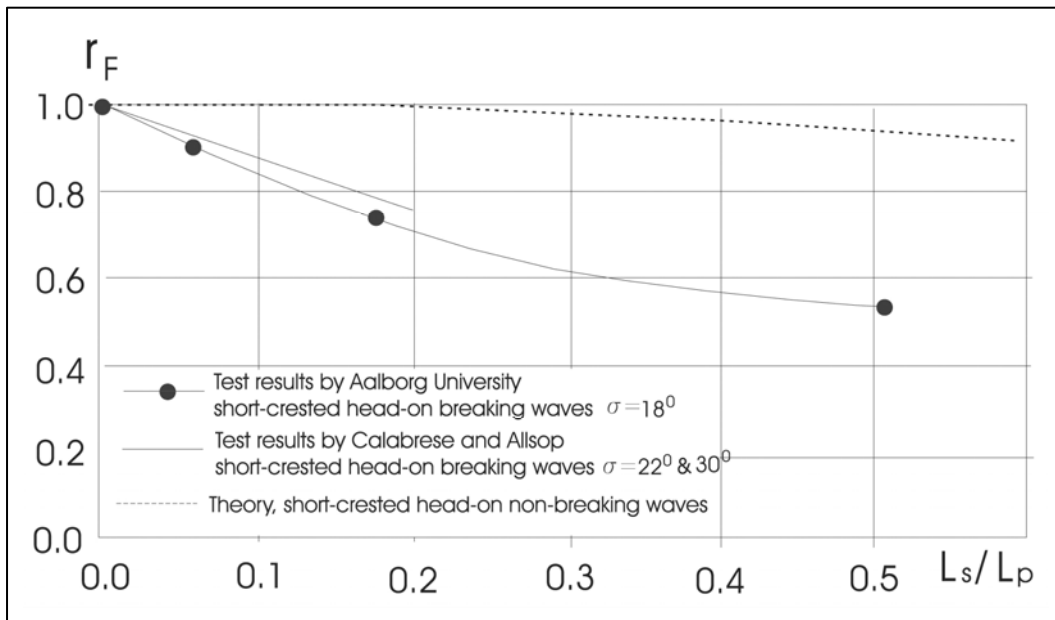


Figure VI-5-70. Example of force reduction from model tests with short-crested breaking waves (Burcharth 1998, Calabrese and Allsop 1997)

(7) Broken wave forces.

(a) Shore structures may be located where they are only subjected to broken waves under the most severe storm and tide condition. Detailed studies relating broken wave forces to incident wave parameters and beach slope are lacking; thus simplifying assumptions are used to estimate design loads. Critical designs should be confirmed with physical model tests.

(b) Model tests have shown approximately 78 percent of the breaking wave height ($0.78 H_b$) is above the still-water line when waves break on a sloping beach (Wiegel 1964). The broken wave is assumed to decay linearly from the breakpoint to the intersection of the swl with the beach slope, where the wave height is reduced to a height of $H_{swl} = 0.2 H_b$ for beach slopes in the range $0.01 \leq \tan \beta \leq 0.1$ (Camfield 1991). The water mass in the broken wave is assumed to move shoreward with velocity equal to the breaking wave celerity by linear theory, i.e., $C = (gh_b)^{1/2}$.

- Vertical wall seaward of the shoreline. Vertical walls situated seaward of the SWL/beach intersection are subjected to wave pressures composed of dynamic and hydrostatic pressures as illustrated in the sketch of Figure VI-5-71. The wave height at the wall, H_w , is determined by similar triangles to be

$$H_w = \left(0.2 + 0.58 \frac{h_s}{h_b} \right) H_b \quad (\text{VI-5-174})$$

where h_s is the water depth at the wall, and h_b is the water depth at wave breaking.

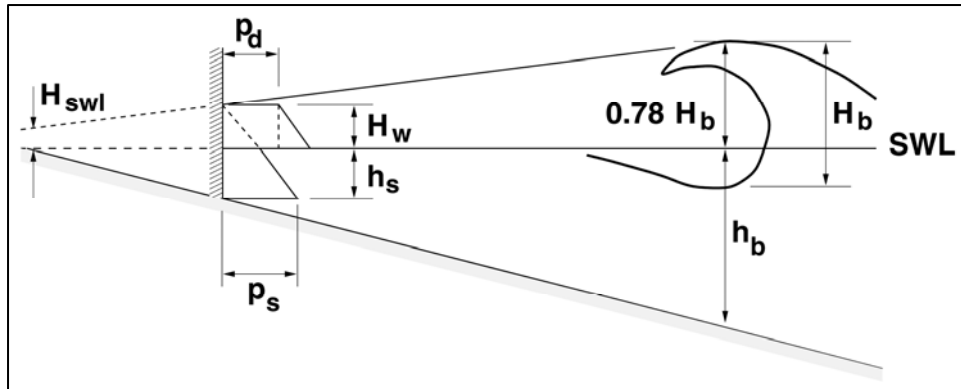


Figure VI-5-71. Nondimensional amplitude of horizontal turning moment around the center of the caisson exposed to oblique nonbreaking regular waves

- Above the swl, the dynamic component of the pressure is given as

$$p_d = \frac{1}{2} \rho C^2 = \frac{1}{2} \rho g h_b \quad (\text{VI-5-175})$$

and the corresponding force per unit horizontal length of the wall is

$$R_d = p_d H_w = \frac{\rho g h_b H_w}{2} \quad (\text{VI-5-176})$$

where ρ is the density of water. The overturning moment per unit horizontal length about the toe of the wall due to the dynamic pressure is given by

$$M_d = R_d \left(h_s + \frac{H_w}{2} \right) \quad (\text{VI-5-177})$$

- The hydrostatic pressure varies from zero at a height H_w above the SWL to a maximum at the base of the wall given by

$$P_s = \rho g (h_s + H_w) \quad (\text{VI-5-178})$$

- The hydrostatic force per unit horizontal width of the wall is calculated as

$$R_s = \frac{\rho g}{2} (h_s + H_w)^2 \quad (\text{VI-5-179})$$

and the corresponding hydrostatic overturning moment per unit width is

$$M_s = R_s \left(\frac{h_s + H_w}{3} \right) = \frac{\rho g}{6} (h_s + H_w)^3 \quad (\text{VI-5-180})$$

- The total force and moment per unit horizontal width of wall is the summation of dynamic and hydrostatic components, i.e.,

$$R_T = R_d + R_s \quad (\text{VI-5-181})$$

$$M_T = M_d + M_s \quad (\text{VI-5-182})$$

- Any backfilling with sand, soil or stone behind the wall will help resist the hydrodynamic forces and moments on the vertical wall.
- Vertical wall landward of the shoreline. Landward of the intersection of the SWL with the beach and in the absence of structures, the broken wave continues running up the beach slope until it reaches a maximum vertical runup height, R_a , that can be estimated using the procedures given in Part II-4-4, "Wave Runup on Beaches." If a vertical wall is located in the runup region, as shown in Figure VI-5-72, the surging runup will exert a force on the wall that is related to the height, H_w , of the surge at the wall.
- Camfield (1991) assumed a linear decrease in the runup surge over the distance X_2 shown in Figure VI-5-72 which yielded the following expression for surge height at the wall

$$H_w = H_{SWL} \left(1 - \frac{X_1}{X_2} \right) = 0.2H_b \left(1 - \frac{X_1 \tan \beta}{R_a} \right) \quad (\text{VI-5-183})$$

where $H_{SWL} \approx 0.2 H_b$ and β is the beach slope angle. The force of the surge per unit horizontal width of the vertical wall was approximated by Camfield (1991) based on the work of Cross (1967) to be

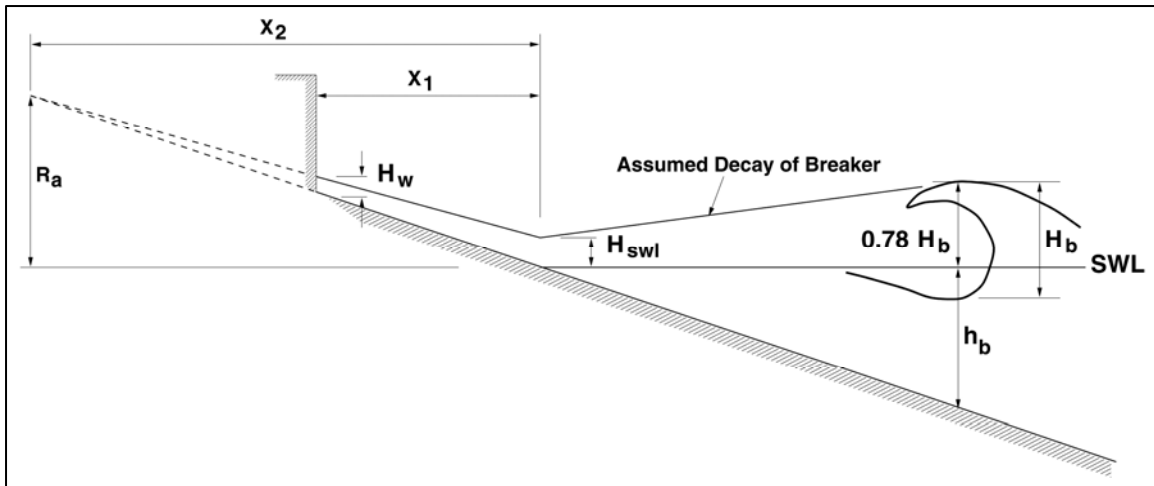


Figure VI-5-72. Broken wave forces on wall landwater of shoreline

$$F_{surge} \approx 4.5 \rho g H_w^2 \quad (\text{VI-5-184})$$

or when combined with Equation VI-5-158

$$F_{surge} \approx 0.18 \rho g H_b^2 \left(1 - \frac{X_1 \tan \beta}{R_a} \right)^2 \quad (\text{VI-5-185})$$

- This approximate method is intended for use on plane slopes in the range $0.01 \leq \tan \beta \leq 0.1$. The methodology does not apply to steeper slopes or composite slopes. No estimates are given for the pressure distribution or the resulting overturning moment on the vertical wall.

c. Wave-generated forces on concrete caps.

(1) Wave loads on concrete caps occur only if the runup reaches the wall. The load is very dependent, not only on the characteristics of the waves, but also on the geometry (including the porosity) of the seaward face of the structure.

(2) The wave forces on a monolithic superstructure exposed to irregular waves are of a stochastic nature. The pressure distributions and the related resultant forces at a given instant are schematized in Figure VI-5-73. Not included in the figure is the distribution of the effective stresses on the base plate.

(3) The wave-generated pressure, p_w , acting perpendicular to the front of the wall is the pressure that would be recorded by pressure transducers mounted on the front face. The distribution of p_w is greatly affected by very large vertical velocities and accelerations which often occur. F_w is the instantaneous resultant of the wave generated pressures.

(4) The instantaneous uplift pressure, p_b , acting perpendicular to the base plate is equal to the pore pressure in the soil immediately under the plate. The resultant force is F_b . At the front corner (point f) the uplift pressure p_b^f , equals the pressure on the front wall. At the rear corner (point r) the uplift pressure, p_b^r , equals the hydrostatic pressure at point r . The actual distribution of p_b between p_b^f and p_b^r depends on the wave-generated boundary pressure field and on the permeability and homogeneity of the soil.

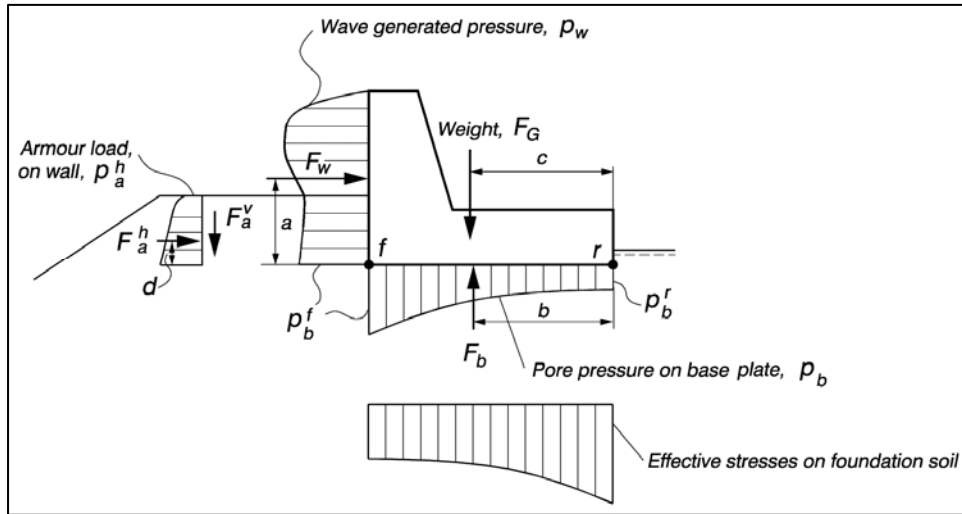


Figure VI-5-73. Illustration of forces on a superstructure

The distribution cannot be determined in normal wave flume scale tests because of strong scale effects related to porous flow. However, the corner pressures p_b^f and p_b^r can be measured or estimated, and in case of homogeneous and rather permeable soils and quasi-static conditions, a safe estimate on the most dangerous uplift can be found assuming a linear pressure distribution between a maximum value of p_b^f and a minimum value of p_b^r as shown in Figure VI-5-74a. If a blocking of the porous flow is introduced on the seaside of the base, the assumption of a linear distribution will be even safer as illustrated by Figure VI-5-74b. On the other hand a blockage under the rear end of the base plate might cause the linear assumption to be on the unsafe side as illustrated by Figure VI-5-74c. Note, that in case b and c the resultant of the base plate pressure is not vertical.

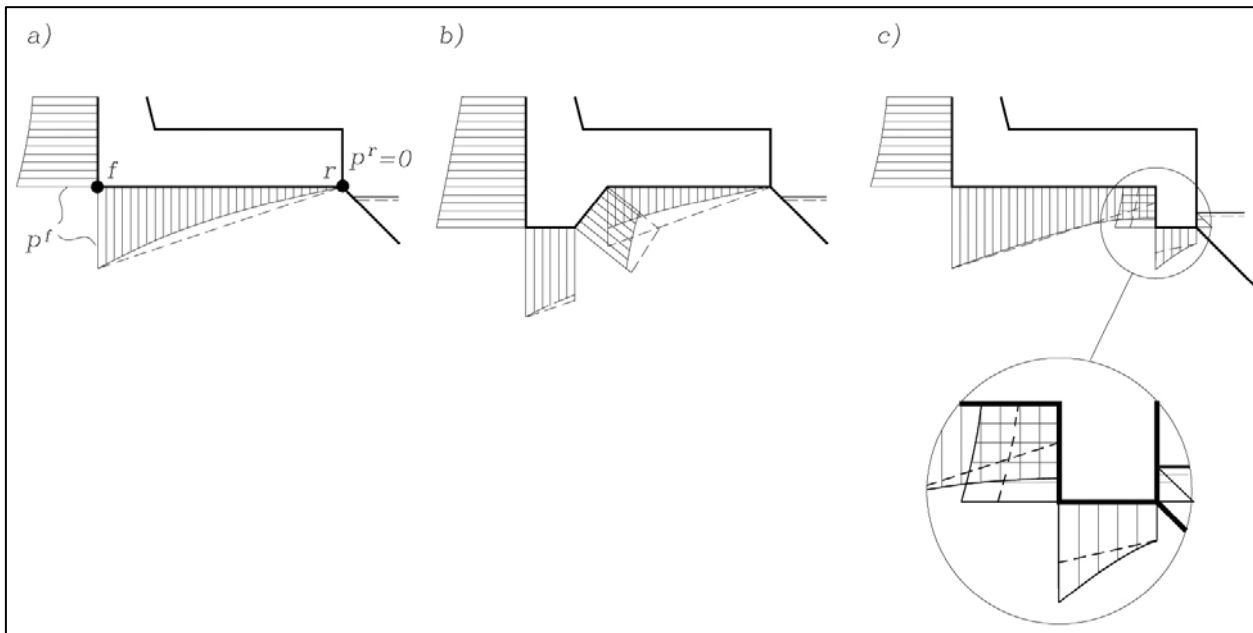


Figure VI-5-74. Illustration of comparison between base plate pore pressure distributions (under quasi-static porous flow conditions) and the approximated linear distribution

(5) Armor and filter stones resting against the front of the wave wall will introduce an armor load, p_a , on the front through the contact points. Both a normal soil mechanics load and a proportion of the dynamic wave loads on the armor contribute to p_a . The resultant force F_a is generally not perpendicular to the front wall due to friction between the soil and the wall, and must be split into the two orthogonal components F_a^h and F_a^v . In the case of high walls (low front berms) F_a is insignificant compared to the wave load, F_w .

(6) The load will in general be dynamic but is normally treated as quasi-static due to a rather smooth variation in time over a wave period. However, if wave breaking takes place directly on the wall face some short duration, but very large, slamming forces can occur, especially if the front face is almost vertical at the moment when the wave collides with the wall as shown in Figure VI-5-75. Such forces are also called impact or impulsive forces.

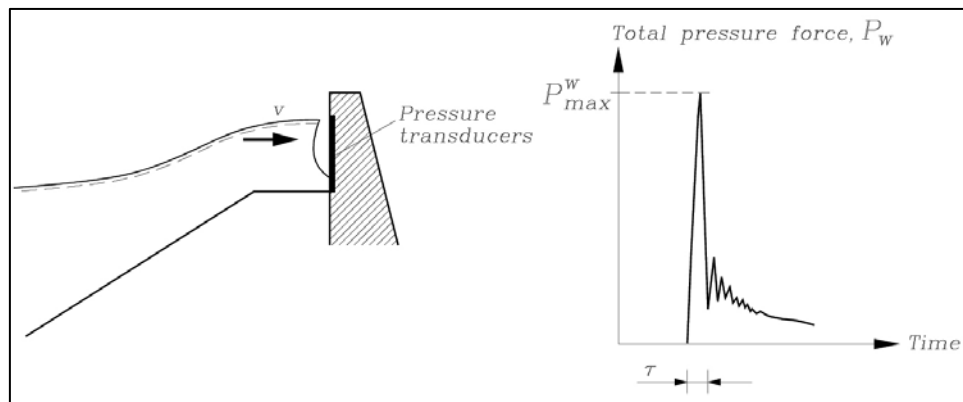


Figure VI-5-75. Impulsive pressure force caused by wave breaking on the wave wall

(7) Wave slamming on the wall can be avoided and the quasi-static wave loads reduced by increasing the crest level and/or the width of the front berm as shown by Figure VI-5-76. Wave slamming on the front of the wall will not occur in configurations *c* and *d*.

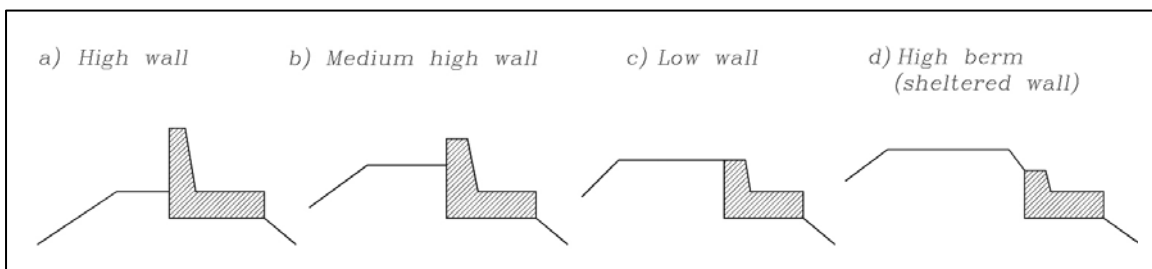


Figure VI-5-76. Typical crown wall configurations

(8) The wave loadings on a crown wall can be assessed only by physical model tests or by prototype recordings. However, no prototype results have been reported in the literature and most model test results are related to specific crown wall configurations.

(9) Table VI-5-60 shows an empirical formula for horizontal wave load given by Jensen (1984) and Bradbury et al. (1988). Table VI-5-61 shows empirical formulae for horizontal wave load, turning moment and uplift pressure presented by Pedersen (1996). The formulae are based on small scale model tests with head-on irregular waves. Predictions are compared to measurements in Figure VI-5-77.